

**A STUDY OF THE DRILLING OF  
ADVANCED CARBON FIBRE COMPOSITES**

**ZAFFAR M. KHAN, B.Eng., M.S.**

**THESIS SUBMITTED FOR THE DEGREE OF  
DOCTOR OF PHILOSOPHY**

**DEPARTMENT OF AERONAUTICAL AND MECHANICAL ENGINEERING  
UNIVERSITY OF SALFORD, ENGLAND**

**APRIL 1991**

TO MY DEAREST PARENTS WHO TAUGHT ME HOW TO READ AND WRITE  
AND TO MY LOVING WIFE FOR HER PATIENCE DURING THE COURSE  
OF PHD RESEARCH.

## CONTENTS

	PageNo
LIST OF FIGURES.....	II
LIST OF TABLES.....	XI
ACKNOWLEDGEMENTS.....	XIII
ABSTRACT.....	XV
1. CHAPTER ONE: INTRODUCTION.....	1
1.1 Research Objectives.....	3
1.2 Summary of Thesis.....	4
2. CHAPTER TWO: GENERAL SURVEY OF COMPOSITE MATERIALS.....	6
2.1 Evolution of Composite Materials.....	6
2.2 Structure of Composite Materials.....	7
2.2.1 The Epoxy Matrix.....	11
2.2.2 The Carbon Fibre.....	15
2.2.3 The Interphase.....	18
2.3 The Properties of Carbon Fibre Composites Relative to hole Generation.....	19
2.3.1 The Properties of Epoxy Matrix.....	20
2.3.2 The Properties of Carbon Fibre.....	22
2.4 The Fabrication of Composite Materials.....	24
2.5 The Drilling of Carbon Fibre Composites.....	25
2.5.1 Basic Aspects of Drilling of Carbon Fibre Composites.....	27
2.5.2 Drilling Defects in Carbon Fibre Composites.....	30
2.5.3 Failure Mechanism in Carbon Fibre Composites.....	31

2.6 Residual Stresses in Carbon Fibre	
Composites.....	33
2.7 Fractography of Carbon Fibre	
Composites.....	35
3. CHAPTER THREE: DRILL GEOMETRY, PERFORMANCE AND	
FAILURE CRITERIA.....	37
3.1 Review of Twist Drill Geometry.....	38
3.1.1 Drill Point.....	38
3.1.2 Body Profile.....	40
3.1.3 Drill Shank.....	42
3.2 Factors Affecting Drill Performance.....	43
3.2.1 Effect of Drill Geometry on Performance.....	43
3.2.2 Effect of Cutting Conditions on Drilling	
Performance.....	46
3.2.3 Effect of Workpiece Material on Performance..	47
3.2.4 Effect of Cutting Fluid on Performance.....	48
3.3 Drill Wear, Life and Failure Criteria.....	49
3.3.1 Drill Wear Classification.....	49
3.3.2 Drill Life and Failure criteria.....	51
3.4 Forces acting on the Drill.....	53
3.5 Tool Material; Cemented Carbides.....	55
3.6 State of the Art of CFC Drilling .....	57
3.6.1 Drilling Techniques.....	58
3.6.2 Technology Survey of Tungsten Carbide Drills.	61
4. CHAPTER FOUR: THE EXPERIMENTAL INVESTIGATIONS.....	67
4.1 Introduction.....	67
4.2 The Investigative Techniques.....	70

4.2.1 Travelling Microscopy.....	70
4.2.2 Scanning Electron Microscopy.....	71
4.2.3 Optical Microscopy.....	71
4.3 Experimental Procedure.....	72
4.4 The Drill Life Tests.....	75
4.4.1 Stage One-Preliminary Assessment of Drills.....	76
4.4.2 Stage Two-Detailed Drill Inspection.....	77
4.4.3 Stage Three-Drill Performance Characterisation.....	77
4.5 Fibre Pullout & Matrix Cracking.....	82
4.5.1 Effect of coolant on hole quality.....	82
4.5.2 Fractography of Damaged Fibres and Matrix....	83
4.6 Cemented Carbide Classification.....	83
4.6.1 The Lathe Test.....	86
4.6.2 The Machining Centre Test.....	87
4.6.3 The Pin-on-Disc Arrangement.....	88
5. CHAPTER FIVE: THE RESULTS.....	89
5.1 Drill Life Testing..	89
5.1.1 Stage One-Preliminary Drill Performance Evaluation.....	89
5.1.2 Stage Two-Detailed Drill Inspection.....	92
5.1.3 Stage Three-Drill Performance Characterisation.....	95
5.2 Fibre Pullout & Matrix Cracking.....	99
5.2.1 Effect of Coolant on Hole Quality.....	99
5.2.2 Fractography of Damaged Fibres and Matrix....	100
5.2.3 Summary of CFC Fractography.....	104

5.3 Material Properties of Cemented Carbides Used for the Sliding Test.....	105
6. CHAPTER SIX: DISCUSSION.....	108
6.1 Drill Performance in Drilling CFC.....	108
6.1.1 Drill Wear & Drill Life.....	108
6.1.2 Hole Quality.....	110
6.1.3 Photoelasticity.....	111
6.1.4 Cutting Forces.....	112
6.1.5 Structural Analysis.....	113
6.2 Fibre Pullout and Matrix Cracking.....	114
6.2.1 Effect of Coolant on Hole Quality.....	114
6.2.2 Damage Mechanism of Fibre and Matrix.....	115
6.2.3 The Mixed Mode; Pullout Initiated Internal Delamination.....	118
6.2.4 Identification of Factors Governing Drilling Defects.....	120
6.3 Material Classification.....	123
6.3.1 Wear Mechanism.....	123
6.3.2 Effect of Physical Parameters on Wear Properties.....	125
6.3.3 Wear Testing.....	127
7. CONCLUSIONS.....	128
8. RECOMMENDATIONS FOR FUTURE WORK.....	131
REFERENCES.....	133

**LIST OF FIGURES**

- Fig. (1): Graph showing the relative importance of engineering materials with respect to different ages [6].
- Fig. (2): Application of carbon fibre composites in military aircraft;
- (a) British Aerospace/McDonnell Douglas AV-8B.
- (b) British Aerospace, Experimental Aircraft Prototype (EAP)
- Fig. (3): Graph showing increasing use of carbon fibre composites in military aircraft [10].
- Fig. (4): The structure of carbon fibre [28].
- Fig. (5): Sketch showing fabrication route of carbon fibres [17].
- Fig. (6): The common weave styles of fibres used in composite materials.
- Fig. (7): The compressive stress/strain response of carbon fibre composite, T800/924C laminate [54].
- Fig. (8): Effect of temperature on compression failure of 1st generation CFC.
- Fig. (9): Sketch showing the pre-impregnation of carbon fibres with resin solution [17].
- Fig. (10): The curing cycle of the carbon fibre composite panels which have been drilled in the present study.
- Fig. (11): A typical wing box beam showing holes which act as stress concentrations on a stringer which is attached to the aircraft skin by rivets.
- Fig. (12): The interlaminar stresses in the composite

laminate [49].

Fig. (13): Variation of interlaminar stresses at the interface from the centre of a plate to the outer surface [49].

Fig. (14): Variation of 3-dimensional interlaminar shear stress around the CFC hole with respect to distance from the centre of hole and angular orientation of fibres [51].

Fig. (15): The strain distribution around a single hole in carbon fibre composite, T800/924C laminate [55].

Fig. (16): Drawing showing fibre microbuckling.

Fig. (17): Drawing showing fibre fractured in tension.

Fig. (18): The geometric features of a drill.

Fig. (19): The rake angle ( $\alpha$ ) and clearance angle ( $\beta$ ) of a drill.

Fig. (20): The main factors which determine drilling performance in CFC.

Fig. (21): The effect of large point angle (top) and small point angle (bottom) on the potential for creating burrs at drill breakthrough.

Fig. (22): Drawing showing deformation of fibres (solid lines) during CFC drilling using tools having positive rake angle (a), neutral rake angle (b) & negative rake angle (c).

Fig. (23): Vector diagram showing the effect of rake angle on the direction and magnitude of the cutting forces at a cutting speed of 0.2 m/sec. and various depths of cut [67].

Fig. (24): The effect of rake angle on outer corner wear of a HSS cutting tool when cutting rigid PVC resin at a

cutting speed of 440 m/min and cutting depth of 0.1 mm [67].

Fig. (25): Effect of web thickness of a 6mm dia. HSS drill on thrust and torque when drilling SK7 steel [68].

Fig. (26): Effect of varying relief angle on cutting forces when machining CFC, using a cemented carbide tool with a rake angle of  $+15^\circ$  at a speed of 0.6 m/sec. and cutting depth of 0.1mm [69].

Fig. (27): Effect of cutting speed on cutting temperature when machining a glass fibre reinforced material at a feed of 0.16mm/rev. and a rake angle of  $0^\circ$  [70].

Fig. (28): Sketch showing various types of drill wear [73].

Fig. (29): The nonlinear relations between drill wear at the outer corner of a carbide drill and penetration distance in CFC [74].

Fig. (30): Effect of percentage of cobalt on the hardness, transverse rupture strength and compression strength of tungsten carbide-cobalt alloy [78].

Fig. (31): The experimental arrangement during the drill life tests.

Fig. (32): Sketch of the drill showing the plane of sectioning (AA'BB') and the position of outer corner wear.

Fig. (33): Photograph showing the method of holding the drill in the specimen stage of the scanning electron microscope.

Fig. (34): The British Aerospace drill specification, PTS: 62.01.07 (see over for further details of drill geometry).

Fig. (35): Photograph showing, from left to right, the Solid Carbide, Precision, Gandtrack and Klenk drills.

Fig. (36): Chart showing the Talyrond trace of the 6.035mm plug gauge.

Fig. (37): Photograph of the Wadkin Mill/Drill machine showing associated instrumentation.

Fig. (38): Block diagram describing the equipment used for the dynamometer tests.

Fig. (39): Illustration of the experimental arrangement for the second phase of dynamometer tests.

Fig. (40): Drawing showing the sequence of sectioning for removing a hole specimen from CFC panel for examination in the scanning electron microscope.

Fig. (41): Sketch showing the lathe wear test arrangement.

Fig. (42): Sketch showing the wear test arrangement in the Kearney and Trecker Machining centre.

Fig. (43): Photograph showing the machining centre test.

Fig. (44): Close-up view of the CFC disc rubbing against the carbide rod in the holder on the machining centre test.

Fig. (45): Sketch showing the Denison Pin-on-Disc wear test arrangement.

Fig. (46): Photograph showing the Denison Pin-on-Disc test.

Fig. (47): Scanning electron micrograph showing a typical flank wear pattern of a Gandtrack drill where the flank wear increased toward the periphery of the drill.

Fig. (48): The average outer corner wear width of the Klenk ( $\nabla$ ), Gandtrack (\*), Precision ( $\Delta$ ) and Solid Carbide ( $\times$ ) drills.

Fig. (49): SEM micrographs of the two flanks at the outer corner measured after 40 holes of the Gandtrack (left) and Precision (right) drills showing non-symmetric wear in the case of the Gandtrack drill.

Fig. (50): SEM micrograph of the margin wear of Precision (top) and Gandtrack (bottom) drills.

Fig. (51): SEM micrograph of the chisel edge wear of the Precision (left) and Gandtrack (right) drills.

Fig. (52): SEM micrograph showing the damage development of the Precision (top) and Gandtrack (bottom) drills at or close to the brazed region between the cemented carbide and the HSS shank.

Fig. (53): The outer corner wear of the flanks A (×) and B (Δ) of the Precision drill in the second stage of drill testing.

Fig. (54): The outer corner wear of the flanks A (×) and B (Δ) of the Gandtrack drill in the second stage of drill testing.

Fig. (55): The comparison of the Precision and the Gandtrack drill in terms of total penetration distance.

Fig. (56): The drill body profiles of Gandtrack (top left), Precision (top right), Klenk (bottom left) and Carbide (bottom right) drills.

Fig. (57): Micrograph showing the magnified (103 times) view of the outer corner of the Klenk (top) and the Precision (bottom) drills.

Fig. (58): The variation of thrust force during the three stages of drilling.

Fig. (59): A typical drill torque (top) and thrust (bottom) response.

Fig. (60): The dynamometer torque and thrust response at the drilling speed of 2800 RPM and varying feed rates.

Fig. (61): The maximum thrust response for Klenk (×), Gandtrack (Δ), Precision (\*) and Carbide (∇) drills at a speed of 2800 RPM and various feed rates.

Fig. (62): The maximum torque response for Klenk (×), Gandtrack (Δ), Precision (\*) and Carbide (∇) drills at a speed of 2800 RPM and various feed rates.

Fig. (63): The maximum thrust and torque response for Klenk, Gandtrack, Precision and Solid carbide drills at a speed of 2800 RPM and feed of 0.05mm/rev.

Fig. (64): The thrust response of Klenk (×), Gandtrack (Δ), Precision (\*) and Carbide (∇) drills against penetration distance at a speed of 2800 RPM and feed of 0.05mm/Rev.

Fig. (65): The torque response of Klenk (×), Gandtrack (Δ), Precision (\*) and Carbide (∇) drills against penetration distance at a speed of 2800 RPM and feed of 0.05mm/Rev.

Fig. (66): The outer corner wear of Klenk (×), Gandtrack (Δ), Precision (\*) and Carbide (∇) drills against penetration distance at a speed of 2800 RPM and feed of 0.05mm/Rev.

Fig. (67): The pattern of the isochromatic fringes on the bottom ply of the CFC holes for Klenk (top left), Precision (top right), Gandtrack (bottom left) and Carbide (bottom right) drills at a speed of 2800 RPM & feed of 0.05mm/rev.

Fig. (68): Graph showing the distribution of residual strains at the bottom ply of the CFC hole at a speed of 2800 RPM and feed of 0.05mm/rev.

Fig.(69): SEM Micrographs showing a comparison between 20th and 100th wet and dry holes drilled by the Precision drill.

Fig. (70): The hole quality (dry) of the 30th CFC hole drilled by Klenk (top left), Carbide (top right), Precision (bottom left) and Gandtrack (bottom right) drills at a speed of 2800 RPM and feed of 0.05mm/rev.

Fig. (71): SEM micrograph showing softened matrix on the hole surface.

Fig. (72): The periodicity of damage scars in the holes drilled by Precision drills.

Fig. (73): SEM micrograph showing close-up view of the damage scar on the CFC hole boundaries.

Fig. (74): The geometrical features of the damage scar observed on CFC hole boundaries.

Fig. (75): The relative orientation of  $-45^\circ$  (top left),  $+45^\circ$  (top right),  $0^\circ$  (bottom left),  $90^\circ$  (bottom right) carbon fibres with respect to the cutting edge of the drill.

Fig. (76): SEM micrograph showing the  $-45^\circ$  fibres protruding against  $0^\circ$  fibres in the damage scar.

Fig. (77): SEM micrograph showing the microbuckled and kinked carbon fibres around the damage scar.

Fig. (78): SEM micrograph showing the  $-45^\circ$  fibres protruding in a series of steps in the damage scar.

Fig. (79): SEM micrograph showing the bi-modal failure of fibres in the damage scar.

Fig. (80): SEM micrograph showing the outcrop of pulled out fibres fractured in tension.

Fig. (81): SEM micrograph showing a typical pulled out fibre.

Fig. (82): SEM micrograph showing radials on the fractured surface of the pulled out fibres indicating the origin of fracture.

Fig. (83): SEM micrograph showing the  $0^\circ$  fibres on the CFC hole boundaries.

Fig. (84): SEM micrograph showing the interlaminar shear failure of the  $0^\circ$  fibres.

Fig. (85): SEM micrograph showing the obliteration of a  $90^\circ$  fibre by the cutting action of the drill.

Fig. (86): SEM micrograph showing the delamination at the interlayer region of the CFC hole boundaries.

Fig. (87): Optical micrograph showing the resin rich region in the interlayer.

Fig. (88): Scanning electron micrograph showing all the four fibre failure modes and internal delamination;

(a)  $0^\circ$  fibres failed by interlaminar shear.

(b)  $90^\circ$  fibres chopped away and smeared epoxy on surface.

(c)  $-45^\circ$  fibres microbuckled and formed pits.

(d)  $+45^\circ$  fibres failed in tension.

(e) Internal delamination at a  $-45^\circ/90^\circ$  interlayer.

Fig. (89): SEM micrographs showing the microstructure of the Krupps (top), Sandvik (middle) and Kennametal (bottom) specimens.

Fig. (90): SEM micrographs showing the microstructure of cemented carbide used in Precision (top left), Gandtrack (top right), Klenk (bottom left) and Solid Carbide (bottom right) drills.

Fig. (91): Graph showing variation of crack length with applied load using the Palmqvist fracture resistance test on Krupp THR (x), Sandvik H10F ( $\Delta$ ) and Kennametal F285 (\*) carbides.

Fig. (92): Photograph showing comparison between a new CFC disc (left) and the delaminated CFC disk (right) after the Kearney and Trecker dry wear test.

Fig. (93): Graph showing the wear scar diameter on Krupp THR/Sandvik H10F (x) and Kennametal F285 ( $\Delta$ ) specimens as a function of sliding distance in the pin-on-disc sliding test.

Fig. (94): The incidence of cracks on the Krupp THR specimen developed during the pin-on-disc sliding test.

Fig. (95): SEM micrographs showing the worn specimens of Krupp THR (top), Sandvik H10F (middle) and Kennametal F285 (bottom) cemented carbides after the pin-on-disc test.

Fig.(96): Drawing showing the mechanism of bimodal failure of microbuckled  $-45^\circ$  carbon fibres in CFC holes.

**LIST OF TABLES**

Table (1): A comparison of the properties of various composite materials and metals in terms of specific strength and modulus [15].

Table (2): A summary of the major advantages, disadvantages and typical applications of carbon, kevlar and glass fibres.

Table (3): Important physical and mechanical properties of 1st generation (Ciba Geigy XA-S/914C) and 2nd generation CFC (Ciba Geigy T800/924C) [17,19,20].

Table (4): Important physical and mechanical properties of Ciba Geigy 924C epoxy matrix [19,20].

Table (5): Important physical and mechanical properties of T-300, T-700 and T-800 carbon fibres [20,40].

Table (6): The specifications and related details about the four types of drills used in the present study.

Table (7): Summary of drill evaluation, phase-1 test results.

Table (8): Summary of drill evaluation, phase-2 test results.

Table (9): Thrust force (N) and torque measurements (N-cm) for Klenk drills over a range of speeds and feeds.

Table (10): Thrust force (N) and torque measurements (N-cm) for Gandtrack drills over a range of speeds and feeds.

Table (11): Thrust force (N) and torque measurement (N-cm) for Carbide drills over a range of speeds and feeds.

Table (12): Thrust force (N) and torque measurement (N-cm) for Precision drills over a range of speeds and feeds.

Table (13): The residual strains and stresses generated by drilling during the birefringent photoelasticity test.

Table (14) Results of the structural analysis of the drills.

Table (15): Summary of Drill Evaluation Test Results.

Table (16): Results of the Vickers hardness test on the cemented carbides.

Table (17): The crack lengths at the four corners of the diamond indentation made in the cemented carbide specimens in the Palmqvist test.

Table (18) Summary of Krupp THR, Sandvik H10F and Kennametal F-285 cemented carbide test results.

Table (19): Important physical and mechanical properties of Krupp THR, Sandvik H10F and Kennametal F-285 cemented carbides as reported in the literature [79].

**ACKNOWLEDGEMENTS**

The author expresses his deepest gratitude to his research supervisor, Professor B. Mills for his invaluable guidance, inspiring encouragement, continuing support throughout the research efforts and to Dr. A. Redford for countless fruitful discussions, help with the experiments and checking the manuscript of the thesis. Appreciation is extended to Professor T. R. Crossley, Head of Manufacturing Laboratories and Professor D. J. Sanger, Chairman of the Department for provision of Departmental facilities and continuous encouragement.

Profound thanks are due to the Aircraft Manufacturing Development Division, British Aerospace (Military Aircraft) PLC for providing tools, materials, special equipment and test facilities. The technical assistance extended by Mr. E. Hoggarth and Mr. P. Graham has indeed gone a long way towards completing this research within the specified time-frame.

Appreciation is expressed to Mr. B. North of Kennametal Corporation, USA for providing the cemented carbide test specimen and to Mr. A. Nowel of Strain Gauge Measurements, UK for assistance with photoelastic measurements in CFC. The research experience of Dr. C. Soutis at Cambridge University regarding T800/924C CFC proved to be very useful in interpreting the drilling induced failure modes.

The award of the Robert Blackburn Memorial Trust Award by the Royal Aeronautical Society, UK for enhancement of aviation safety by improving the CFC hole quality standards in aircraft structural joints is gratefully acknowledged. Many thank are due to the members of the departmental staff and in particular to Mr. G. France for assistance with SEM and many useful discussions, Mr. R. Gardner for help with the NC drill/mill machine, Mr. H. Pendelbury for photographic expertise and practical advice regarding routine problems.

The love, care and moral support extended by Dr. Naz, his wife, Dr. Evelyn and Dr. Zaman which greatly facilitated the conduct of research, shall always be remembered with sweet memories.

Penultimately, I would like to thank my parents for my upbringing, nourishment and development in a manner to be able to set out on this long march of academic excellence with teutonic dedication and missionary zeal. Last but by no means the least, I would like to thank my wife, Dr. Samina for helping me out in every possible way to complete this long march with a happy ending.

**ABSTRACT**

Carbon fibre composites are increasingly being used in aircraft structures due to their superior physical and mechanical properties. The process of drilling of carbon fibre composites in aircraft manufacture is economically important since the extremely abrasive nature of the fibres limits drill life. The hole quality produced by drilling in terms of fibre pullout and matrix cracking affects the notch sensitivity of the hole.

The present thesis describes an experimental and analytical study of drilling of the carbon fibre composites carried out with the support of British Aerospace (Military Aircraft Division). Full drill life testing was carried out using four low cost commercial cemented carbide drills, three of which had brazed inserts, and drill life was determined by measuring the outer drill corner wear. Hole quality was measured in terms of diametrical tolerance using accurate plug gauges. Drill forces were measured using a two component Kistler dynamometer and attempts were made to measure residual stress in the workpiece using the birefringent photoelastic technique. The hole quality was related to drill wear, cutting forces and heat generated during drilling.

Independent tasks were carried out to relate cemented carbide physical and mechanical properties to wear using several standard sliding wear experiments. Three different cemented carbide tool materials were investigated in terms

of cobalt layer thickness, carbide distribution and physical properties including hardness and fracture toughness. Independent sliding wear tests were performed using a Pin-on-Disc machine, lathe and machining centre. These tests allowed the materials to be ranked in terms of wear resistance when rubbing against carbon fibre composite. The fracture toughness was measured using the techniques developed by Palmqvist. The wear resistance was correlated to the physical and mechanical properties of the tool materials.

Hole quality was studied experimentally using scanning electron microscopy and fibre pullout shown to be primarily dependent on the fibre-matrix interface bond strength and the intrinsic strength of the fibres. The surface morphology of the fractured fibres in areas of fibre pullout showed multimode damage due to anisotropy of the carbon fibre composite and the dynamics of drilling. The degree and pattern of damage developed in the drilled holes was found to be highly directionally dependent. The experimental results and theoretical analysis showed that the degree of hole damage depends not only on drilling parameters but also on the material composition and the manufacturing process of the carbon fibre composite.

## Chapter One

### INTRODUCTION

In the brief history of the aerospace industry, a progressive evolution of new materials and design concepts has occurred. In the quest to fly faster with a greater load carrying capacity, stronger and lighter materials have been developed. These have ranged from wood, aluminum, titanium to advanced carbon fibre reinforced composite materials (CFC). As new composites with unique properties are being developed, the optimisation of their processing technology is eagerly being sought. Even if primary processing of a composite system is well established, quite often it is the secondary processing which determines the purchase price and the flight performance of the aircraft. One of the key secondary processes is drilling. Drilling has become a major cost factor because a fighter may have 250,000 to 400,000 holes and a bomber or transport aircraft 1,000,000 to 2,000,000 holes [1]. The drilling labour may account for as much as 50% of the total manufacturing cost of the airframe [2]. Billions of holes are drilled annually with a total cost, in the United States alone, estimated to be over 300 million dollars. If through advancement of the drilling processes the life of the drill could be extended by a modest 10%, the industry would not only save 30 million dollars but there are benefits in the sequential processes of reaming, boring and tapping [3].

The determination of the tool change time becomes important

for the automated drilling process. Frequent drill changing increases production cost and using the drill longer than it should be used produces substandard holes. Substandard hole quality accounts for as much as 60% of aircraft part rejection during final assembly [4]. The drilling induced defects in composite materials can be classified into two categories, the geometric and the non-geometric defects. The geometric defects are those defects ordinarily encountered in drilling metals i.e. hole taper quality, alignment and surface roughness. The non-geometric drilling defects are characteristically found in drilling CFC i.e. fibre pullout, matrix cracking and delamination. The presence and growth of such flaws have a highly detrimental effect on aircraft damage tolerance, survivability and reliability. It is important to take into account drilling defects when making allowances for possible manufacturing defects and in-service damage. These types of real-life machining defects are extremely difficult to comprehend due to the inherent material anisotropy and the complexity of drill geometry. Additionally fibre orientation, ply stacking sequence and the damage pattern in relation to the dynamics of the drill point make the problem even more intractable.

### **1.1 Research Objectives:**

The present research work is concerned with analysing and understanding the drilling of carbon fibre composites. The work follows the following logical sequence:

■ An investigation of the wear processes during drilling of four different types of cemented carbide drills including the determination of tool life after numerous regrinds.

■ A study of the hole quality in terms of fibre pullout and matrix cracking in relation to the micromechanics of drilling using scanning electron microscopy and to determine the fractography of failure modes, fracture pattern and fracture sequence.

■ A comparison of the wear rates of three different types of cemented carbides in terms of their physical properties i.e. microstructure, hardness and fracture toughness.

The present work was supported by British Aerospace (Military Aircraft Division) who supplied carbon fibre composite materials, drills and special equipment including a Kistler two component drill dynamometer. The drills were reground and the CFC panels/holes were sectioned at the Aircraft Manufacturing Division of British Aerospace PLC at Preston.

## **1.2 Summary of thesis:**

The origin, composition, fabrication, processing and applications of CFC in aircraft structures are presented and discussed in Chapter 2. The important properties of CFC's which influence the machining behaviour are also presented in this chapter.

The important geometric parameters of the drill and the effect of these parameters on the drill performance when drilling CFC are given in Chapter 3. This chapter presents the mechanism of drilling, drill wear and drill failure criteria. This chapter also includes the latest state of the art in drilling carbon fibre composites.

Chapter 4 presents the experimental investigation of drilling including the drilling tests, tool material classification and hole quality in terms of fibre pullout and matrix cracking.

The drilling tests were performed in three phases:

- Preliminary assessment of all the drills.
- Detailed investigation of the best two types of drills in terms of drill wear and drill failure.
- Determination of drilling forces, residual strains in CFC and structural analysis of the drills.

The results of the drilling tests, hole quality and material classification are discussed in Chapter 5. This

chapter includes the results of dynamometer tests, the birefringent photoelasticity measurements, structural analysis of the drills, effect of coolant on hole quality, fractography of carbon fibres, Vickers hardness tests, the Palmqvist fracture toughness measurements and the results of independent wear tests.

The main discussion of the experimental observations is presented in Chapter 6. The results are discussed in terms of appropriate theoretical models. The performance of the drills are ranked in terms of penetration distance and machining parameters. The manufacturing, machining and material aspects which promote the onset of fibre pullout and matrix cracking during drilling CFC are also discussed in this chapter. The tool materials are also discussed in terms of wear properties. The experimental results are discussed in terms of the appropriate theoretical models. Finally the conclusions are presented in chapter 7.

## Chapter Two

### GENERAL SURVEY OF COMPOSITE MATERIALS

The advent of CFC has heralded a new era of materials science to meet the challenging requirements of aerospace vehicle design. This relatively new material is however based on the ancient practice of combining several materials to evolve an integral material system which exhibits superior physical and mechanical properties than each of its constituents.

#### 2.1 Evolution of Composite Materials:

In early times (5000 B.C.) chopped straw was used to toughen mud bricks and Maya potteries to prevent them from cracking. Egyptian mummy cases were made of a composite material made from sheets of papyrus which were used as writing material in Egypt. Medieval swords were made of different layers Toledo and Damascus steel [5]. Around 1500 B.C., the consumption of bronze determined the world powers. Much later, around 1850, it would have been steel followed by the light alloys. The period between 1940 and 1960 saw maximum consumption of metals and alloys with respect to their relative importance to other materials in terms of their usage at that time as shown in Fig. (1) [6]. From this point on, the application of metals and alloys in the aerospace industry in particular has been, as a percentage of total material utilised, declining and production of composites has been expanding. The first

modern synthetic resin, Gordon Aerolite was developed by Aero Research Limited, UK, in the late 1930's [7]. A series of experiments at the Royal Aircraft Establishment, Farnborough England by Watt, Phillips and Johnson led to the manufacture of high strength, high stiffness carbon fibres and their composites in early 1964 [8]. At about the same time, Epoxy quickly established its superiority over other matrix materials for structural applications. Since then production of advanced composites has been increasing at a rate of 30 percent per year and is now a \$10 billion market. It is forecasted that the growth rate of composite materials is such that their usage will increase to 50 percent of the total for structural applications by the turn of the century [9].

Over more than a decade, the use of composites in aerospace industry has progressed from the simple beginning of access panels and cowling to secondary structural components of aircrafts as shown in Fig. (2). The current and future trends of composite application in military aircraft applications are given in Fig. (3). A detailed description of these applications is summarised in Appendix 'A' [10,11].

## **2.2 Structure of Composite Materials:**

Composite materials are defined as the combination of two or more mutually insoluble macro-constituents that differ in physical form and chemical composition [12]. Composite materials are superior to ordinary engineering materials

for a variety of reasons. Notably amongst these are their high strength to weight ratio and high modulus to weight ratio as shown in Table (1). The ability to tailor their strength properties to fit a particular structural situation and the flexibility of design in terms of reduced part count makes them even more attractive. Composite materials consist of three main elements, the matrix (resin), the structural reinforcement and the interphase. The matrix binds the reinforcement together to allow effective distribution of load, protects the notch sensitive reinforcement from self abrasion and externally induced scratches. The resin also protects the reinforcement from environmental moisture, chemical corrosion and oxidation. The shear, compression and transverse tensile properties and failure mechanism of a composite are resin dominated. The general thermo-mechanical behaviour of composites is dominated by the resin's heat resistance. Many types of thermoplastic and thermoset resins are being used in the fabrication of composite materials. Thermoplastic resins, cured by reversible chain extension chemical reaction can be melted repeatedly. Polyphenylene Sulphide (PPS), Polyvinylchloride (PVC) and Polyetheretherketone (PEEK) are some of the thermoplastic resins. Thermoset resins, once cured by an irreversible crosslinking chemical reaction, cannot become liquid again. Crosslinking is the chemical linkage between the molecular chains. This restricts movement between adjacent chains which results in greater dimensional

stability. Epoxies, polyimides and phenolics are some of the commonly used thermosetting resins. Epoxy based matrices have several attractive features for aerospace applications. The epoxy resin is compatible with fibres, thereby eliminating many of the interfacial problems that may be evident in other resin systems. They are also resistant to aircraft fluids such as jet fuel and hydraulic fluid. Finally large data bases and long flight histories exist for these systems both in military and commercial aircrafts [13].

There are four general categories of structural reinforcement in a matrix, particulate, flake, whisker and fibre. Particulate composites consist of particles of one or more material suspended in a matrix of another. The most common example of this type is concrete in which particles of sand and rock are bound together by a mixture of cement and water. Likewise a cobalt matrix is reinforced by tungsten carbide particles to produce tool materials. Such composites have good compression strength but have poor tensile properties. Flake reinforcement offers a number of advantages in composites due to their two dimensional geometry. Overlapping of flakes provides an effective barrier against solvent penetration but difficulties arise with their alignment in composites. Alumina matrix can be reinforced by silicon carbide whiskers to produce cutting tool materials but in spite of their high strengths, whiskers are not ideally suited for aerospace structural applications because of their short lengths. Long and

continuous fibres are more desirable in aircraft composites since they impart better structural properties, creep resistance and crack stopping properties. It is fibre reinforcement which primarily determines the tensile strength, flexural strength and stiffness of a composite system. The longitudinal mechanical properties and failure mechanism of a specific layup are determined by the type, stacking sequence and orientation of the fibres. The four types of commercially available fibres are Glass, Boron, Kevlar and Carbon fibres. The glass fibre reinforced plastics (GFRP) are easy and inexpensive to manufacture. They are widely used in the manufacture of various things such as kitchen sinks, bath room tubs and motor car bodies. However the higher specific gravity of glass fibres (2.5) and lower stiffness (72 GPa) as compared to other fibres do not suit high performance applications (Table 1). The higher stiffness property of boron fibres (420 GPa) made possible their early use in primary aircraft structures. However their high manufacturing cost, difficulty in handling and high specific gravity (2.5) have kept them from high volume applications. Kevlar fibres combine their extremely high toughness with good impact resistance. However, relatively poor compression strength and poor bonding characteristics to resin limit their applications. At a compressive load of about 20% of ultimate tensile load, a deviation from linearity occurs leading to internal buckling. Carbon fibres are the most widely used in aerospace applications because of the best balance of

properties. The best combination of highest specific strength and stiffness (0.95 GPa and 200 GPa respectively for type-I carbon fibre, 1.52 GPa and 118 GPa respectively for type-II carbon fibres) ratios as compared to other types of fibres (Table 1) makes them ideally suitable for high performance structural applications. The main advantages, disadvantages, applications and cost indices of carbon, kevlar and glass fibres are summarised in Table (2) [5,12].

#### **2.2.1 The Epoxy Matrix:**

The polyfunctional epoxy resin contains more than two epoxide groups ( $-\text{CH}-\underset{\text{O}}{\text{CH}}-$ ) per molecule in its pre-cured monomer form. Opening of the epoxide ring by the appropriate curing agent leads to crosslinking of the resin. The resin is very often modified by the addition of plasticisers, diluents and fillers to impart specific properties [14].

Besides specific strength and stiffness, damage tolerance and environmental durability are two key parameters which determine the structural performance of composite materials. The term 'Damage Tolerance' is used to describe a design philosophy whereby the structural integrity of an aircraft is maintained while a defect of a given size is present in the structure. The performance of an aircraft structure made of composite material is seriously affected by its operation in high temperature and humid environments. The 'hot/wet performance' of an aircraft is

attributed to its structural response in hot and wet environments. Different resin systems have varying performance in terms of fracture toughness and environmental stability [15].

**(a) First Generation Epoxy System:**

The first generation, Ciba Geigy 914 epoxy resin system has the following four major constituents.

(a) The tetraglycidyl derivative of 4 ' 4 '-diaminodiphenyl methane, TGDDM, (Ciba-Geigy nomenclature: MY 720): This is the basic prime epoxy component.

(b) The triglycidyl ether of para aminophenol, TGPAP, (Ciba-Geigy ERLA 0510): This increases the mean molecular weight of the epoxy polymer.

(c) Dicyandiamide, DICY: This is a heat activated catalyst and hardener used as a curing agent.

(d) Polyethersulphone, PES: This is a thermoplastic included to increase matrix viscosity during cure and provides a toughening mechanism. It decreases the shear modulus of the system.

The first generation, Ciba Geigy matrix system 914 could retain a higher degree of strength in hot and humid environments than the second generation epoxies but their inherent brittleness led to lower damage tolerance than the later. Some of the important properties of composite systems based on Ciba Geigy 914 matrix are given in Table (3) [16,17].

**(b) Second Generation Epoxy System:**

The second generation epoxy matrix system, Ciba Geigy 924C has been evolved by modification of the Ciba Geigy 914 system by the addition of carboxyl terminated butadiene acrylonitrile rubber (CTBN) which leads to phase separation during cure. The cured elastomer modified epoxy resin consists of finely dispersed rubber or thermoplastic rich domains (0.1-0.2  $\mu\text{m}$ ) chemically bonded to the epoxy matrix. This modification significantly improves the damage tolerance of the resin system by arresting crack propagation. However the relative increase in fracture toughness for the composite is not as high as in the case of bulk resin. It has been observed that the 25 fold increase in fracture energy of the resin will increase the interlaminar fracture energy of a woven composite by 4-8 fold. The rubber additives degrade the dimensional stability of the finished composite because of substantial increase in water pick up. The environmental stability of a system modified in this manner is drastically reduced making them of limited use in primary structures. Some of the important properties of composite systems based on Ciba Geigy 924C matrix are given in Table (3) [18,19,20]. The physical properties of Ciba Geigy 924C matrix system are given in Table (4).

**(c) Interleaved Systems:** In this concept, a composite within a composite (sandwich structure) is produced by interleaving the first generation epoxy, Ciba Geigy 914

with a discrete layer of a very high toughness and strength resin, Ciba Geigy R398 at critical locations i.e. holes. The interleaved matrix co-cures with the resin matrix as a discrete layer throughout the entire process. The interlayer acts to increase resistance to the compressive impact damage and the high temperature stability is provided by the first generation epoxy having better performance in high temperature environments. A localised adhesive interlayer of graphite epoxy composite significantly increases the mode-I fracture toughness (peel) by ten fold and mode-II fracture toughness (shear) by seven fold as compared with the fracture toughness of the non-interleaved counterpart. The combination of epoxy resins with novel interleaving materials has been shown to result in weight saving of over 40% as compared to 2024-T3 aluminum alloy [21,22,23,24].

**(d) Brominated Epoxy Systems:**

The heat resistance of the polymer can be increased by maximising the crosslinking density. The high dissociation energy of the well-bonded molecules imparts a high degree of thermal stability to the resin system. This strategy has been used to formulate heat resistant brominated epoxy systems. This has been evolved by physical mixing 10 parts of poly functional epoxy resin, TGDDM and from 6 to 12 parts of brominated diglycidyl additive and from 0.65 to 1.2 parts of an amine containing an epoxy curing agent. The brominated polymers also retain much higher shear strength

than does the material without such additives. An optimum combination of physical and mechanical properties is attainable with the combination of 38% bromine and 10% CTBN. Investigations at NASA Ames research centre, USA have confirmed that brominated-CTBN modified epoxy systems have better toughness, thermal stability, moisture resistance, environmental stability and ease of manufacture than the CTBN modified epoxies [25,26].

### **2.2.2 The Carbon Fibre:**

The sheets of covalently bonded carbon atoms arranged in a hexagonal pattern as in benzene ring are held together by much weaker Van-der-waal forces between aromatic planes which leads to the formation of the crystalline chains as shown in Fig.(4). Aromatic planes are the plane formed by the hydrocarbons containing one or more benzene rings which consist of six carbon rings (these benzene rings produce a characteristic aromatic smell) [27]. The formation and combination of longitudinally inter-twisted crystallite chains characterize carbon fibre. The degree of heat treatment to the polymer leads to rapid oxidation, an ordered arrangement of the surface layer and the formation of a surface 'sheath'. The relatively less oriented chains inside, form the 'core' of the carbon fibre [28]. The thin skin of circumferential layered planes and a core with random crystallites in carbon fibres are produced by the displacement of the aromatic component in the acrylonitrile monomer by a '-CN group' which operates as an ionic

initiator. Ionic initiators are synthetic resins containing chemically active groups which promote ionic reaction [27].

The carbon fibres are produced from the polymers in a process involving controlled pyrolysis of organic precursors as shown in Fig. (5) in the following discrete stages [17].

**(a) Oxidation:** Involves heating the organic precursor in an oxidising atmosphere at 200-250° C.

**(b) Carbonizing:** Heating in a non-oxidizing atmosphere at 1000° C or above which produces high strength fibres.

**(c) Graphitizing:** Heating in a non-oxidizing environment to promote the crystalline alignment optimized either for high strength at 1300-1500°C or high modulus at temperatures exceeding 2000°C.

There are three types of carbon fibres. The high tensile strength fibres (Type-1), high strength (Type-2) and moderate modulus/strength fibres (Type-3). The degree of heat treatment in the graphitizing stage determines the microfibrillar alignment and the modulus of the carbon fibre. The type-I carbon fibres are graphitised to give maximum stiffness (350-550 GPa) but have a relatively low strength (1.7-3.5 GPa). The type-II fibres are graphitised to produce maximum strength (2.8-4.0 GPa) but have a relatively lower modulus (230-250 GPa). The type-III fibres have intermediate values of strength and modulus [29].

Carbon fibres are made from Polyacrylonitrile (PAN) or

Pitch precursors. The PAN based fibres are generally selected for their high strength and efficient property translation into the composite. The pitch based fibres are not as strong as the PAN based fibres but their ease of processing and manufacturing cost make them attractive. The diameter of a single carbon fibre ranges from 5 to 10 microns. The carbon fibres are assembled in the form of unidirectional 'tows' usually containing between 1000 and 10,000 fibres. Tows are stitched into various weave patterns i.e. plain, satin and twill etc for subsequent resin impregnation. The weave style determines the handling of the fabric and controls the ability to conform to a contoured shape. In plain weave, each warp yarn is woven over one fill yarn and under the next repeatedly as shown in Fig. (6). Twill weaves have one or more warp yarns passing over and under two or more fill yarns in a regular pattern. In a satin weaves, one warp yarn repeatedly passes over several fill yarns then under one fill yarn. The fibre tows are layed at appropriate orientations to each other to achieve desirable structural properties. There is a family of laminates having four ply orientations spaced at  $45^\circ$  intervals that are symmetric with respect to the mid-plane and are called  $\pi/4$  laminates. The  $[0^\circ, -45^\circ, +45^\circ, 90^\circ]_s$  fibre composites, also categorized as quasi-isotropic laminates have the best combination of  $0^\circ$ ,  $90^\circ$  and  $\pm 45^\circ$  fibres for a variety of longitudinal, transverse and shear loads respectively and are usually the preferred choice in aerospace applications [30].

### 2.2.3 The Interphase:

The interphase is a separate constituent located between the resin and the structural reinforcement within the composite. It may result from the interaction of structural constituents or it may be a separate phase which improves the adhesion of the structural reinforcement to the resin system.

The interface acts as the coupling agent to provide adhesion between the resin and the structural reinforcement. The degree of adhesion between carbon fibres and a matrix material depends primarily on the quality and state of the carbon fibre surface. Carbon fibres have a highly active surface and readily absorb gases which affect the surface properties. A range of active functional groups  $[(-C-OH), (-C=O), (-CO_2H)]$  can be produced on the surface. The functional groups can form chemical bonds directly with unsaturated resins. The reactivity of the surface is a major contributor to the strong bonding associated with carbon fibres. An additional factor is the high specific surface area due to the large amount of surface microroughness. After graphitization, the carbon fibres are treated with a peroxide etch to promote good adhesion. This leads to the formation of carbonyl groups on the fibre surface which interact with epoxides. The production process is completed by coating with a 'size' of basic epoxy, MY-720, that is compatible with the required matrix resin. This prevents damage accumulation while handling. The interface has a marked influence on the transverse,

shear and flexural properties of the composite material. If the interface bond is weak, fibre pullout is responsible for rupture (cohesive failure). If the fibres are not matrix bound, they slide in their bedding and load transfer can no longer take place leading to tensile fracture or compression buckling. Strong interfacial bonding transfers the load to the fibre until the breakage point is reached (adhesive failure). In this case the failure is sudden and catastrophic. Fibres with a skin of greater microfibrillar alignment parallel to the surface (high modulus) are susceptible to cohesive failure rather than adhesive failure due to weaker bonding [31,32,33].

### **2.3 Properties of Carbon Fibres Composites Relative to Hole Generation:**

With any fibre, the material used for the resin must be chemically compatible with the fibres and must have complementary mechanical properties. The carbon-epoxy system is used for high performance aerospace applications because the highest specific stiffness and modulus of carbon fibres are physically and chemically compatible with an epoxy matrix. The epoxy matrix provides good chemical resistance, superior adhesive characteristics and dimensional stability as compared to other resin systems. The epoxy matrix can be formulated in a wide range of viscosities for different fabrication processes and cure schedules. They have long shelf life, provide relatively low cure shrinkage and are available in many thoroughly

characterised standard forms.

The properties of epoxy matrices and carbon fibres relative to drilling are given below.

### **2.3.1 The Properties of the Epoxy Matrix:**

The important properties of the resin which influence hole generation by drilling are given below. The available technical information about the Ciba Geigy 924 Epoxy system is given in Table (4) [19,20];

**(a) Heat Sensitivity:** The thermo-mechanical behaviour of a composite is dominated by the resin. The important drawback of the polymer resins is that they have a low heat distortion temperature e.g. the softening temperature of Ciba Geigy 924 is 210°C. The thermosets have better heat resistance as compared to thermoplastics. Despite the superior thermal properties of epoxy resin as compared to other thermoplastic materials, they do not have the desired degree of heat resistance. As the temperature increases, the matrix shear modulus and the fibre matrix bond strength decrease [20,34].

**(b) Brittleness:** A fundamental drawback of epoxies is their brittleness due to cross-linking of polymers and therefore poor resistance to crack propagation. The addition of rubber based tougheners decreases the brittleness, the shear strength and the temperature resistance of epoxies [18,24].

**(c) Hydrothermal (Hot/Wet) Response:** The transverse and shear properties of composites, which are very much

affected by the matrix properties, degrade upon absorption of moisture and exposure to elevated temperatures. The moisture penetration in CFC brings about dimensional changes. The hydrothermal response of composites is determined by exposing the test specimen to controlled temperature and moisture environments in an oven. The difference in the size and weight of the specimen before and after the test determines the hydrothermal absorption of the system. When exposed to humid environments for a length of time, carbon fibre reinforced composites containing up to 60% volume of fibres can absorb up to 2% by weight of water. The water absorption in Ciba Geigy-924 Epoxy system ranges between 0.1 to 0.4 % by weight when the specimen is exposed to 20°C for 24 hours [15,20,36,37].

**(d) Curing Stresses:** When an epoxy is being cured, a stress free state exists at the interface. The cure is not complete until the resin is post-cured to a higher temperature. This temperature difference leads to the generation of radially directed thermal stresses at the interface. When the composite is cooled down to room temperature, a significant drop of temperature leads to a secondary state of compressive stresses in the fibre that are of considerable magnitude. They lock onto the fibre and augment the shear strength of the fibre-matrix bond. The drilling heat relieves the radial clamping stresses exerted by the matrix over the fibre by an amount corresponding to the drilling temperature thereby promoting fibre pullout and re-ordering the residual stresses in the composite. The

higher the stress free curing temperature, the greater is the retention of radial stresses after drilling. Hence higher curing temperatures are advantageous from the view point of drilling [34,38,39].

### **2.3.2 The Properties of Carbon Fibre:**

Carbon fibres have the following properties which are influenced by drilling [20,40].

**(a) Abrasiveness:** The inherent abrasiveness of carbon fibres leads to excessive drill wear, limits drill life and leads to premature drill failure.

**(b) Elastic Modulus:** The elastic modulus of carbon fibres depends on the degree of heat treatment during carbon fibre manufacture. Higher processing temperatures lead to a greater degree of perfection of alignment along the fibre axis. This is accomplished by an increased axial ordering and decreased interfibrillar coupling. The T-800 carbon fibres have a tensile modulus of 295 GPa and a compression modulus of 267 GPa [41].

**(c) Compression Strength:** The carbon fibres have a compression strength of 8 GPa in monolithic form as indicated in Table (5). They have a tendency to recede within the matrix instead of being cut off in the drilling process. The compressive stress-strain response of CFC T800/924C is given in Fig. (7). The maximum attainable compressive strength of T800/924 laminate is about 1.5 GPa. There is rapid deterioration in the compressive strength of CFC laminate when it is exposed to heat. The compressive

strength response at different temperatures for 1st generation CFC is given in Fig. (8) [42]. It shows that the fibre failure mode above 100°C is governed by the microbuckling of fibres. It has been determined that 2nd generation CFC follows the same trend at temperatures exceeding 100°C and they also fail due to microbuckling at high temperatures under compressive load [54].

The compressive strength of the carbon fibres is determined by statistical imperfections in fibres and fibre misalignment. The local inhomogeneities lead to wide variations of compressive and tensile strength in the same type of fibres. In a single batch of type-I fibre, the strength varies between 0.5 and 4.3 GPa and Young's modulus varies between 270 and 580 GPa. The initial misalignment and curvature of the fibres which can easily arise during laying up pre-impregnated tapes may impose disproportionately high stresses in the composite system. For an XAS/914 carbon-epoxy system, a misalignment of only 0.25° reduces the predicted strength from 2720 MPa to 1850 MPa. At 3° this is reduced to 700 MPa [29,43].

**(d) Brittleness:** The flexibility of carbon fibre is inversely proportional to its elastic modulus when subjected to bending loads. The higher elastic modulus of the carbon fibres lead to a lower flexibility of the carbon fibres and a higher degree of brittleness. This results in limited drill grabbing and promotes brittle failure [29].

**(e) Fibre Orientation & Weaves:** The angular layers are easier to machine than the unidirectional ones and plain

weaves are easier to drill than satin weaves due to better distribution of drilling forces. Even within individual weaves, differences are found. Dense fabrics generate better hole quality than loose ones because of better load distribution [35].

**(f) High Temperature Resistance:** Carbon fibres can withstand high drilling temperatures as they have a high decomposition temperature (3600°C) but the composite cannot withstand these temperatures because of temperature limitations of matrix [34].

#### **2.4 The Fabrication of Composite Materials:**

Carbon fibre composites are fabricated in the following three stages [12,17].

##### **Stage-1: Pre-impregnation of Carbon Fibres**

Fabrication of a composite laminate starts with the fibres and a viscous matrix resin. The fibres are first impregnated with the resin and then wound with a backing sheet onto a mandrel in the form of a tape. The tape is passed through resin baths, rollers, ovens and combs in a continuous process as shown in Fig. (9). In this form the resin is dry enough to allow handling of the tape without excessive loss of resin but is still tacky and drapable. The tape has all the fibres oriented in the same direction; this process is called pre-impregnation of fibres and the pre-impregnated product is called 'prepreg'.

**Stage-2: Layup of CFC**

The prepregs are cut and stacked according to the desired structural shape and geometry over a mould. The layup is protected by various films and bagged. This provides an inert atmosphere for the curing reaction to take place.

**Stage-3; Curing of CFC**

The bag is cured in an autoclave by slowly heating and pressurising the autoclave for the specified time duration as shown in Fig. (10). The post curing cycle is followed by debagging and demoulding.

**2.5 The Drilling of Carbon Fibre Composites:**

Drilling is an important secondary process in the manufacture of CFC aerospace components. The high strength and stiffness capabilities of CFC make it suitable for use in airframe skins, panel stiffeners, web stiffeners, wing spans, floor beams, wing ribs and fuselage frames in a variety of cross-sections i.e. I's, C's, Z's and angles. If we consider an I-structure member of an aircraft, a titanium faced aluminium honeycomb core sandwich is normally used as a shear web. The compression strength of CFC is optimised by using high modulus epoxy resin in the compression (top) flange. A lower modulus epoxy resin is used in the tensile (bottom) flange to enhance the process by which the tensile strength of the carbon fibres is used. Numerous fasteners are used to attach the CFC flange firmly onto the shear web to ensure that the whole sandwich

structure behaves like a rigid body as shown in Fig. (11). Fasteners are generally not as adversely affected by thermal cycling or humidity as the bonded joints. They permit disassembly without destroying the substrate and are readily inspected for joint quality.

Slight dimensional inaccuracies in bolt tightening in metals that deform plastically seldom cause problems. The material around the hole can yield to distribute load to adjacent bolts. This is not true of advanced composites which have no yield point. If one bolt is tighter in its hole than others, the bearing stress at that hole remains higher. The brittleness of an epoxy/carbon fibre structural composite could cause ultimate failure of the material around a hole and the sudden distribution of its entire load to other holes; this may affect the safety, survivability and manufacturing cost of the entire aircraft [110]. The presence of drilling induced flaws changes the stress-strain behaviour, degrades the local material properties and reduces the failing strain in the fibre direction by causing a localised stress concentration in the hole. The plastic flow or failure of the matrix on the hole boundaries may lead to initiation of cracks in the laminate. The combination of longitudinal and transverse cracks are often termed 'Characteristic Damage State' in reinforced composites [32]. The characteristic damage state affects the values of important design parameters and introduces unexpected failure modes. High temperature environments result in a rapid deterioration of the matrix

shear modulus and a marked reduction of the compressive strength of the fibres. This affects the fibre damage mode and failure may occur at stresses far below the expected value. Many of these effects are likely to be aggravated by moisture penetration. Moisture is absorbed by cracks at a substantially greater rate than the normal equilibrium level for the matrix and the rapidly changing temperature might well subject the moisture to a freeze-boil-freeze cycle with consequent disastrous effects. High performance aircraft may experience 'thermal spikes' by cruising at high altitude (skin temperature may fall to  $-50^{\circ}\text{C}$ ) and then sprinting to supersonic speed (aerodynamic heating may raise skin temperature to well above  $100^{\circ}\text{C}$ ) Special care is required to ensure that moisture absorption in the hole boundaries does not degrade the high temperature performance of composites used in these situations [42].

#### **2.5.1 Basic Aspects of Drilling of Carbon Fibre Composites:**

The machining of carbon fibre composites differs from metal drilling in many respects. Carbon fibres are very hard, abrasive and quickly dull sharp tools. Worn tools tear up the filaments and ruin the surface of the CFC material. Dull drills apply high drilling forces which split, tear and pull out/push down of the fibres. Hence the reinforcement of abrasive carbon fibres in a heat sensitive epoxy matrix leads to a number of aspects of the drilling of CFC's which are different from the drilling of metals [34].

**(a) High Drill Cost:** One of the high cost elements identified in composites manufacturing is the cost of cutting, machining and drilling. Tighter hole tolerances are required when drilling composite materials. This requirement arises from the desire not to crush or delaminate the composite locally when inserting fasteners. The tighter hole tolerances for CFC requires lower drill feeds and longer times as compared to metal drilling. This increases drilling cost and affects the productivity.

Composite materials are particularly severe on drills and this leads to increase in wear rate. HSS drills produce poor hole quality and limited drill life [44]. Although carbide tipped drills are relatively more expensive than the HSS drills, they are preferred for their better hole quality and longer life as compared to later. The high initial cost of the carbide drill dictates that they be reground as least 3-4 times [45].

Hole quality defects accounted for 65% of all rejections during final assembly of CFC structural components of the A-7D attack aircraft: the majority of the defects were attributed to an improper drilling cycle and the use of drills longer than necessary produced substandard holes. On the other hand if frequent drill regrinding is used, it increases production cost [4].

**(b) Poor Dimensional Tolerance:** When a hole in a [0/90]<sub>s</sub> laminate cools from the drilling temperature to the room temperature, the 0° fibres expand in a longitudinal

direction by an amount,  $e_x$ , (coefficient of thermal expansion, CTE:  $-0.2 \times 10^{-6}$  m/m $^\circ$ K) and the 90 $^\circ$  fibres contract in transverse direction by an amount,  $e_y$ , (CTE:  $35 \times 10^{-6}$  m/m $^\circ$ K) on the same axis (Table (5)). This difference between CTE of 0 $^\circ$  and 90 $^\circ$  fibres leads to geometric mismatch between the 0 $^\circ$  and 90 $^\circ$  plies and for geometric compatibility residual stresses are set up in the material. This makes it difficult to attain a high degree of dimensional accuracy in CFC holes and the drilled holes have a smaller diameter than the diameter of the drill used [34,39].

**(c) Drilling Temperature:** Drilling of CFC is limited by the softening temperature of the matrix system. Though carbon fibres can withstand high temperatures (decomposition temperature 3600 $^\circ$ C), the cutting temperature must not exceed the softening temperature of the matrix [34].

**(d) Localized Heat Build-up:** The thermal conductivity of the CFC is determined by the resin matrix. The low thermal conductivity of epoxy matrix (0.2 W/m $^\circ$ K) favours localized heat build-up in the drilling zone (Table (4)). Since there is little heat dissipation into the material, the greater part of the heat has to be carried away either through the swarf or the drill; the latter leads to an increase in drill wear [34].

**(e) Safety:** Drilling of CFC's must be carried out under a controlled situation to prevent the inhalation of dust. A filtered vacuum collection system should be used although

face mask filter systems will reduce dust effects. Fine abrasive particles generated during machining of CFC can also be detrimental to equipment. Dust control measures must be taken to protect men and machines from carbon dust [44].

### **2.5.2 Drilling Defects in Carbon Fibre Composites:**

The defects in CFC arising from drilling can be categorized into the following two classes.

#### **2.5.2.1 Geometric Defects:**

These are commonly found when drilling metals. This category includes mislocated, oversized, misdrilled holes etc.

#### **2.5.2.2 Non-Geometric Defects:**

The non-geometric defects are characteristically induced whilst drilling in CFC. The various types of possible non-geometric drilling defects are as follows:

**(a) Drill Wear:** Abrasive drill wear is defined as the removal of solid particles from the tool face by the ploughing action of hard asperities on the opposing surface or by the hard particles trapped between the sliding surfaces. Machining of workpieces containing a hard phase generally leads to an abrasive wear mechanism which limits the tool life and increases production cost [46].

**(b) Delamination:** Separation of plies from the laminate when the drill enters or exits the workpiece is called

external delamination. Internal delamination takes place when the plies split or separate inside the hole as a result of improper drilling [47].

**(c) Fibre Pullout and Matrix Cracking :** The tearing away of the fibres or resin from the wall of the hole caused by drilling is called fibre pullout and matrix cracking [48].

### **2.5.3 Failure Mechanism in Carbon Fibre Composites:**

In the theory of laminates, only 2-dimensional stresses in the plane of the laminate ( $\sigma_x$ ,  $\sigma_y$ ,  $\tau_{xy}$ ) are considered and this does not take into account the out-of-plane interlaminar stresses ( $\sigma_z$ ,  $\tau_{zx}$ ,  $\tau_{zy}$ ) as shown in Fig.(12). For a high modulus carbon fibre composite panel whose width (2b) is four times the thickness; the distribution of stresses ( $\sigma_x$ ,  $\tau_{xy}$  and  $\tau_{xz}$ ) across the width of the laminate is shown in Fig. (13). As the free edge approaches,  $\sigma_x$  decreases and  $\tau_{xy}$  goes to zero. This simplification is not valid at the hole boundaries where a large out-of-plane stress ( $\tau_{xz}$ ) occurs to counterbalance the effect of decreasing stresses ( $\sigma_x$  and  $\tau_{xy}$ ). The out-of-plane stress components are the result of the ply interface load transfer mechanism. These stresses are localised and effectively reduce to zero beyond a distance approximately equal to the laminate thickness. These stresses at the free edge of the hole are considered to be instrumental in the generation of delamination and fibre pullout and matrix cracking. The magnitude of these stresses depends on the

elastic properties, orientation and stacking sequence of the fibres [5,49].

Standard laminate analysis of graphite epoxy, AS3501 having fibre orientations of  $[0^\circ, \pm 45^\circ, 90^\circ]_s$ , subjected to thermo-mechanical loading (1 kip axial load + thermal residual stresses) revealed that the maximum normal interlaminar stress existed between the  $-45^\circ/90^\circ$  interlayer. It was determined that if the magnitude of interlaminar stress is positive and large, it will cause delamination regardless of shear stress distribution. Hence the  $-45^\circ/90^\circ$  interlayer is the most sensitive region when a  $[0^\circ, \pm 45^\circ, 90^\circ]_s$  laminate is subjected to thermo-mechanical loading [50].

The three dimensional interlaminar shear stress distribution around a CFC hole can be explained by considering a hole having radius,  $R$ , in an orthotropic plate in polar coordinates  $(r, \theta, z)$  where  $r$  denotes the distance of any point from the centre of the hole,  $\theta$  is the angular position of the fibres and  $z$  represents the height of the hole from its base. The distribution of interlaminar shear ( $\tau_{r\theta}$ ) with respect to angular orientation and the distance from the centre of the hole is given in Fig. (14). It reveals that for the  $(r-R)/R$  value of 0.78 i.e.  $r = 1.78R$ , the interlaminar shear stress has the minimum value irrespective of the orientation of carbon fibres. The peak value of the interlaminar shear stress exists for the fibres oriented at  $45^\circ$  that are located at the distance of  $(r-R)/R = 0.05$  i.e.  $r = 1.05R$  from the hole boundaries [51].

## 2.6 Residual Stresses in Carbon Fibre Composites:

The residual stresses in composite materials are those stresses which are induced in the object without the application of external loads and result from primary or secondary processing such as curing or machining. The residual stresses have a detrimental effect on hole quality and it is difficult to obtain high dimensional accuracy under these conditions.

There are various techniques and methods to determine residual stresses around holes such as strain gauge and birefringent photoelastic techniques. The birefringent technique is superior to the strain gauge technique because of its higher sensitivity and its ability to display an entire strain field with the associated strain gradients. The birefringent strain field around a hole is given by the order and location of fringes according to the stress optic rule. The rule states that when the principal axes of the stress and the refractive index tensors coincide, the birefringence,  $\Delta n$  (difference in principle refractive indices) is proportional to the difference in the principal stresses [52,53];

$$\Delta n = (n_1 - n_2) = C_p (\sigma_1 - \sigma_2) \dots \dots \dots \text{Eqn. (1)}$$

Where  $C_p$  is the stress optic coefficient.

$\sigma_1$  and  $\sigma_2$  are the principle stresses in the direction parallel and perpendicular to the fibre.

Based on the stress-optic rule, the following empirical

relations have been evolved to determine the residual strains and stresses.

$$\text{Residual Strain} = (N f) \dots \dots \dots \text{Eqn. (2)}$$

and

$$\text{Residual Stress} = \frac{(N f E)}{(1+\nu)} \dots \dots \dots \text{Eqn. (3)}$$

Where N = Numerical Fringe Order = 0,1,2,3....

f = Fringe Value =  $\lambda / 2 t k$ .

$\lambda$  = Wavelength of white light =  $575 \times 10^{-9}$  m.

t = Thickness of coating.

k = Sensitivity factor.

E = Elastic Modulus

$\zeta$  = Poisson's Ratio

When an optically active transparent strip is subjected to strains, changes in optical properties in the film take place that are directly proportional to the stresses developed. These changes can be followed in a polariscope by observing the photoelastic colour sequences called isochromatic patterns. The order and location of fringes give the distribution of residual stresses around the hole according to the stress optic rule.

Various researchers have used other techniques to determine the stresses around holes under various load

configurations. Based on finite element analysis, a plot of the normal strain distribution ( $\epsilon_y$ ) as a function of far field compressive strain ( $\epsilon_a$ ) around a hole in a T800/924C specimen under compressive loading is given in Fig. (15) where 'x' denotes radial distance from the centre of the hole and 'R' is the radius of the hole. The graph indicates that the ratio of the compressive strain at the hole boundary to the strain at an infinite point on the plate reaches an optimum value at the hole boundaries (i.e.  $x = R$ ) and at a distance of about 3 times the hole radius, the strain ratio levels to a constant value of '1' [54,55].

### **2.7 Fractography of Carbon Fibre Composites:**

Unidirectional composites can fail in three different modes in compression. They can fracture along the fibre axis when loaded in compression. This may lead to the generation of transverse cracks in the matrix due to Poisson's ratio mismatch between the fibres and the matrix. The second failure mode of the composites is associated with the pure compression failure of the fibres in which the fractured surface is likely to be at  $45^\circ$  to the fibre axis. The third failure mode of composites, associated with fibre buckling and kinking initiated due to shear, is called shear buckling. Kinking is described as the transverse shear deformation of fibres parallel to their axes followed by the rotation of parallel laminae away from the original position as shown in Fig. (16). Macroscopically, shear crippling is initiated by the shear failure of fibres lying

at an angle to the direction of loading. Microscopic inspection indicates that shear crippling is frequently the result of buckling. The microbuckling may occur in various planes and indeed the overall fracture surface may consist of a series of steps, the height of each step being a multiple of half the buckling wavelength [55,56,57].

The clean fractured surfaces having a pattern of radiating lines from a point as shown in Fig. (17) characterise the tensile failure of carbon fibres. The discovery of these features, termed radials led to the concept of Directly Attributed Fibre Failure which makes it possible to trace the path of fracture over significant areas of failure.

For microscopic diagnosis of the compression surface, the most useful feature is the rough nature of the fractured surface and the large amount of debris. In fact the post failure movement of the mating surfaces destroys the features which characterise compressive failure. Maximum compressive strength is achieved when the failure occurs by compression of the fibres but the relatively low matrix modulus and weak fibre-matrix bond result in premature failure by microbuckling and kinking. If the matrix is ductile and the interface is strong, the fibre can fracture in bending which results in a bilateral structure; a tensile fracture structure and a compression fracture structure [58,59,60,61].

### Chapter Three

#### DRILL GEOMETRY, PERFORMANCE AND FAILURE CRITERIA

The origin of twist drills can be traced back to pre-historic times when bone drills were used to make holes in animal skin and flint drills were used to drill holes in wood. Twist drills in their present form were introduced about 2000 years ago. The first power drill was used by James Naysmyth in the U.K. during the 1840's in the Manchester area [2]. From 1860 onwards, the emphasis has shifted from the development of the machine tools and the know-how of production of the required shapes and accuracy, to the problems of machining new materials and the reduction of machining costs. The introduction of numerically controlled drilling machines in the last few decades has greatly improved the output per worker employed. The replacement of carbon tool steel by high speed steels and cemented carbides has allowed higher cutting speeds. A major evolution in drilling hard materials occurred with the introduction of carbide tipped twist drills. The carbide tipped twist drill combines the advantages of the lower material cost and higher toughness of the high speed steel shank with the enhanced cutting performance provided by the carbide tip. They resist wear better than high speed steel drills and are capable of drilling at high speeds and high rates of penetration. The performance of a twist drill is greatly influenced by the drill point geometry and the body profile which determine

its useful life, the penetration rate, the hole quality and the shelf price. These requirements are often interdependent on each other [62,63]. Their relationship is explained in three sections in this chapter. The first section explains the essential parts and geometry of twist drills. The second section describes the factors which affect the drill performance and the third section deals with drill wear, useful drill life and drill failure criteria.

### **3.1 Review of Twist Drill Geometry:**

A twist drill is defined as a rotary end cutting tool having one or more helical or straight flutes for the passage of chips and the admission of cutting fluid. The function a twist drill is to produce a hole. Drilling is done by revolving and simultaneously feeding the drill into the workpiece. The definition of the basic elements, angles and dimensions of the twist drill are given in B.S. 328, Part 1, 1986 which is presented in Appendix 'B'. There are three main portions of a twist drill i.e. the point, the body and the shank. These are briefly explained below together with a description of the interdependence of these geometric features.

#### **3.1.1 Drill Point:**

This is the entire cone shaped surface at the cutting end. It mainly consists of two cutting lips, the chisel edge and the flank. The cutting lips are conventional cutting edges

that shear the fibres. The chisel edge produces severe deformation in the workpiece. The drill flank is the surface at the back of the cutting lip. A proper clearance is provided on the surface so that only the cutting edges touch the workpiece. The point angle, the rake angle and the inclination angles have the following effects on the design features of drill geometry.

**(a) Point Angle:** The point angle is the included angle between the drill lips when projected on a plane parallel to both the cutting edges as shown in Fig. (18). One of the techniques for measuring point angle involves projection of the drill point on a shadow graph and measuring the included angle. The point angle ranges between  $90^{\circ}$ - $135^{\circ}$  but a common point angle is  $118^{\circ}$  at which angle the cutting edges form a straight line due to the shape of the flutes. The cutting edges will be convex or concave if the angle is decreased or increased from the angle which produces straight lips.

**(b) Chisel Edge Angle:** The chisel edge angle is the included angle between the chisel edge and the cutting lip as shown in Fig. (18). The chisel edge angle ranges between  $120^{\circ}$  to  $135^{\circ}$ . Large chisel edge angles result in long chisel edges whilst small chisel edge angles results in inadequate clearances.

**(c) Rake Angle:** The rake angle ( $\alpha$ ) is the angle between the deformed workpiece and the top of the cutting edge as shown in Fig. (19). The rake angle is largely determined by the

helix angle. The greater the helix angle, the greater is the rake angle. The rake angle of a twist drill varies from being equal to the helix angle (defined in Appendix 'A') at the outside diameter to zero or a negative angle at the centre.

**(d) Clearance Angle:** The lip clearance angle or relief angle, ( $\beta$ ), as shown in Fig. (19), increases from the periphery to the axis of the drill. It keeps the drill flank from rubbing with the workpiece. If the lip clearance angle is less than the feed angle, the drill cutting edge will rub against the bottom of the hole. A large clearance angle can improve tool life by reducing friction, but as the clearance angle increases, the strength of the tool decreases.

### **3.1.2 Body Profile:**

The section of the drill between the shank and the drill point is referred to as the body. This forms the core of the twist drill for it has a direct influence on the drilling process, the chip removal, the tool life, the torsional strength and the vibrations of the twist drill. A large cross sectional area for the body is able to withstand higher cutting forces but seriously restricts the chip flow space. It is said that for good torsional strength, the area of the cross section of the drills should be as large as possible and be distributed as far as possible, away from the cutting axis. The weight and bulk of longer drills add to the generation of undesirable

vibrations because of the large overhang from the drill spindle bearing and the physical problems caused by drill buckling [64].

The drill body comprises the flutes, the web, the land and the margin and their detailed description is given below.

**(a) Helix Angle and the Flutes:** The helix angle is the acute angle between the leading edge of a land (Section 3.1.2, para (c)) and the drill axis as shown in Fig. (18). It is given by  $\tan^{-1} (2\pi r/l)$  where 'r' is the radial distance and 'l' is the pitch length. A graphical method of determining helix angle consists of wrapping the drill in carbon paper and a sheet of plain paper. When the drill is rolled under even pressure, a series of lines are produced due to the impression of the lands. The ends of the lines are joined by a straight line. The angle between the straight line and the series of lines forms the helix angle.

Most twist drills are made in three basic helix angles i.e. high helix (typically 39°), medium helix (around 30°) and slow helix (typically 15°). High helix angles aid quick disposal of cutting debris and result in keener but weaker cutting edges. These contradictory requirements are balanced by compromising on the geometric features for the specific application. Typically a 15° helix angle with a small rake angle is used for cutting abrasive materials (Bakelite and plastics) where the edge strength is important [65].

The flutes are spiral grooves cut around the body. The

flutes determine the helix angle, allow cutting debris to escape and permit cutting fluids to reach the cutting edge.

**(b) Web Thickness:** The drill web is the central part of the drill body between the roots of the flutes as shown in Fig. (18). The most common web styles are parallel, standard increase and heavy increase. A major problem in resharpening increasing web tools is that the web thickens rapidly as the tool is ground back. The weakening of the cutting edge due to a high helix angle is partially overcome by having a thicker web. Increasing the web thickness is undesirable because of the increased thrust requirements. A thicker web increases drilling forces and produces bad hole quality. The web thickness is a compromise between minimising the axial thrust of the drill and the provision of sufficient rigidity for the drill. Optimum combinations are used in various drill designs to provide the required web strength at minimum thrust [66].

**(c) Land and Margin:** The drill lands are the peripheral portions of the drill body between adjacent flutes. A portion of the lands at the periphery is cut to provide clearance; the land determines the drill diameter. The remaining uncut portion forms the drill margins. The purpose of the margin is to hold the drill straight in the hole.

### **3.1.3 Drill Shank:**

The shank fits into the driving chuck or spindle. Drills are made with either a straight shank or a tapered shank.

The straight shank drill is held in a drill chuck and a tapered shank drill fits into a slot in a tapered sleeve.

### **3.2 Factors Affecting Drill Performance:**

For drilling, as for any metal cutting process, there is an optimum rate of metal removal for either maximum production or minimum cost since as metal removal rate increases, particularly as a result of increased cutting speed, the life of the cutting tool reduces. The drill life is influenced by many factors. For metal drilling, Galloway [68] has outlined five main elements for determining the optimum drilling performance which include the drill geometry, the cutting conditions, the work material, the drilling machine and the cutting fluid. The factors affecting CFC drilling performance as proposed by the author are outlined in Fig. (20).

#### **3.2.1 Effect of Drill Geometry on Performance:**

Drill performance is affected by changes in the drill geometry variables. These affect the drilling performance in terms of thrust, torque, life and hole quality in the following manner;

**(a) Point Angle:** An increase in point angle leads to an increase in thrust values and a slight decrease in torque values. A large point angle (more than  $118^\circ$ ) extrudes less material from the workpiece and reduces burring when the drill breaks out as shown in Fig. (21), 'a'. They have sharp and fragile cutting corners that tend to wear out

rapidly due to greater degree of applied thrust. Small point angles (less than  $118^\circ$ ) extrude more material from the workpiece but have more stable cutting edges as shown in Fig. (21/b). For every workpiece material there is an optimum point angle which best compromises drill thrust, wear and burring [65].

**(b) Rake Angle:** The cutting tool may be positively raked, neutrally raked or negatively raked. The positively raked tool pulls the reinforcing fibres away from their original position and shears or breaks them between the cutting edge and the uncut material as shown in Fig. (22/a). The original position of the fibres is shown by solid lines and the deformed position is given by dotted lines. The positively raked cutting edge facilitates chip flow, reduces the cutting forces, power consumption, improves the surface finish but weakens the cutting edge. The fragile and sensitive cutting edges of the positively raked tools leads to shorter drill life. Neutrally raked cutting edges tend to push the fibres out in front requiring a greater pressure to penetrate the workpiece as shown in Fig. (22/b). This pressure leads to generation of heat and this in turn causes hole quality deterioration. Negative rake is the worst geometric feature in drilling composite materials which results in the generation of maximum heat, poor hole quality and poor quality chips as shown in Fig. (22/c). When the chips formed during cutting are pushed in front of the cutting edge, they are forced into a pack that eventually blocks the flutes and hence the operation of the

tool. The rake angles determine the direction of strains during the cutting action as shown in Fig. (23). The amount of wear measured on several tools having varying rake angles for Polyvinyl Chloride (PVC) resin is given in Fig. (24). This shows that there exists an optimum value of rake angle for minimum wear [67].

**(c) Chisel Edge Length:** The chisel edge is responsible for almost two thirds of the thrust force generated during drilling. The cutting action under the chisel edge is partly cutting and partly extrusion. The chisel edge length is a function of chisel edge angle ( $\lambda$ ) the web thickness ( $2t$ ) and is given by  $(2t/\sin \lambda)$ . An increase in chisel edge angle tends to decrease the thrust values but the torque tends to stay constant [64].

**(d) Web Thickness:** Although an increase in web thickness strengthens the cutting edge, it raises the drill thrust needlessly very high. The effect of the web thickness on the drill thrust and torque forces is shown in Fig. (25). It can be seen from the figure that the thrust increases sharply with the web thickness while the torque value tends to stay the same [68].

The thrust force generated by a thicker web can be appreciably reduced by various thinning techniques which increase the active length of the cutting edge and reduce the specific pressure per unit length of the cutting edge. Web thinning also decreases the length of the chisel point and the lip angle at the web. These factors lead to a reduction in overall thrust force and increase in drill

life. Reducing the web thickness is thus an important design feature for reducing the drilling forces.

**(e) Helix Angle:** The helix angle has a pronounced influence on the drilling forces. An increase in helix angle reduces the thrust and torque forces. However it should be noted that an increase in helix angle tends to weaken the cutting edge and consequently shorten the drill life. An optimum value is selected to suit the material to be drilled.

**(f) Clearance Angle:** The orthogonal single point cutting tool machining of CFC revealed that increasing lip clearance (relief) angle leads to an almost unchanged horizontal force, but to a drastic drop of vertical force as shown in Fig. (26). This can be explained by the size of the contact area between the tool and the workpiece. This area is a function of the clearance angle in such a way that a decreasing angle results in a larger area and thus an increasing vertical force [69].

### **3.2.2 Effect of Cutting Conditions on Drilling Performance:**

The cutting conditions such as cutting speed and feed rate are important factors which affect drilling performance. The upper limit of cutting speed is limited not by the most effective tool life but by the risk of thermal damage to the CFC. This is ascribed to the drilling temperatures which exceed the softening temperature of the resin. Fig. (27) shows the relationship between the cutting temperature and the cutting speed in orthogonal cutting of glass fibre reinforced epoxy resin for which the rate of temperature

rise increases with an increase in cutting speed. The lower limit is defined by a quality decrease caused mainly by the receding of the individual fibres in front of the penetrating cutting edge. The optimum speed must be high enough to allow efficient cutting of fibres with minimum heat dissipation. The industrially accepted optimum speed in drilling CFC using carbide drills ranges between 50-100 m/min. The higher the feed rate, the greater the force required to penetrate the workpiece. Slower feed rates lead to heat intensive crushing of individual fibres and increased production time. Higher feed rates result in an increase in axial thrust and heat flux and are detrimental because they result in delamination. The industrially accepted optimum feed rate for CFC drilling using carbide tooling is 0.025-0.055 mm/Rev [70,71].

### **3.2.3 Effect of Workpiece Material on Drilling Performance:**

The workpiece hardness is one of the factors which has a significant effect on the drill life. Cook, N. H. carried out a number of experiments by drilling a number of holes in Meehanite cast iron specimens (Grade A, ASTM No. 25) of varying hardness values using HSS drills at 690 RPM to determine the relationship between workpiece hardness and tool life. One drill was used for each specimen having a particular hardness value until it failed at the end of its useful life (it would no longer cut effectively). It was found that the drill life is inversely proportional to the workpiece material hardness as expressed by the

relationship ( $T_l \propto H_b^{-16}$ ) where  $T_l$  is the tool life and  $H_b$  is the hardness of the workpiece i.e. the higher the hardness values of the workpiece, the shorter the drill life [72].

#### **3.2.4 Effect of Cutting Fluid on Drilling Performance:**

The primary function of the cutting fluid during drilling of composites is to act as a coolant. The secondary function of the cutting fluid is to minimize dust generation and flush away residue. When metal/composite combinations are encountered, the cutting fluid's primary function is to cool the epoxy matrix and prevent thermal damage; the hole quality in terms of surface roughness is increased by using coolant. Previous research by Grumman Aerospace Corporation and General Dynamics, USA in CFC drilling has revealed that the tool life of carbide drills used for machining carbon epoxy is not increased by using coolant. Generally the use of coolant when drilling epoxies is avoided due to its chemical affinity to water. This often leads to possible chemical material damage and water penetration. The water penetration results in detrimental radial swelling of CFC holes [44,74].

For drilling, water soluble oils are the most common coolant used. The general form of application for these is spray mist or flooding. In the current study, the effect of flood lubrication (cooling) on hole quality was investigated.

### 3.3 Drill Wear, Life and Failure Criteria:

The extent of wear on the tool determines whether a tool has reached the limit of its economical life.

#### 3.3.1 Drill Wear Classification:

There are seven common types of drill wear and these are shown in Fig. (28). These are outer corner wear, flank wear, margin wear, crater wear, chisel edge wear and lip chipping. Varying degrees of edge chipping and the formation of built-up edge have also been observed in drilling [73].

The types of drill wear are summarised below;

(a) **Outer Corner Wear:** 'W' in Fig. (28/a) indicates the extent of outer corner wear. This is determined using a travelling microscope to measure the distance,  $w_1$  and the distance of the other edge of the wear band,  $w_2$ . The outer corner wear,  $W$ , is then the difference between  $w_1$  and  $w_2$ . In practice, the drill is held so that the lip is perpendicular to the optical axis of the microscope and the image becomes parallel to a vertical reference line in the field of vision. The drill is then set so that the worn portion is clearly recognised and measured by adjusting the position of the illuminating lamp.

An extensive study on the tool wear mechanism for drilling composite materials conducted by Grumman Aerospace Corporation revealed non-linear relationships between the outer corner wear development and the linear distance

travelled by the carbide drill as shown in Fig. (29) [74]. It was noted that, generally, increases in the drill wear land in the initial phase are followed by a steady increase in the intermediate phase. This is again followed by a significant rise in wear development before the final failure of the drill.

**(b) Flank Wear:** The flank wear,  $W_f$ , is measured by noting the difference between corresponding flank wear readings using a travelling microscope as shown in Fig. (28/b).

**(c) Margin Wear:** The margin wear,  $W_m$ , shown in Fig. (28/c) is measured by placing the centreline of the drill perpendicular to the optical axis and parallel to the cross feed direction of the microscope and inspecting the wearland.

**(d) Crater Wear:** The symbol,  $W_k$ , shown in Fig. (28/d) represents the width of the crater wear. This is measured by turning the drill to a position such that its centre line become perpendicular to the optical axis and the image of the crater wear is parallel to the vertical reference in the field of vision. The position of the illumination lamp is adjusted to identify the crater profile.

**(e) Chisel Edge Wear:** The width and the depth of the chisel edge wear is represented by the symbols  $C_w$  and  $C_r$  as shown in Fig. (28/e). These parameters are measured by holding the drill such that its centre line is parallel to the optical axis of the microscope and the position of illuminating lamp is adjusted so that the worn portion of

the drill is clearly recognised.

**(f) Chipping of Cutting Edge:** The maximum width  $P_M$  and the maximum depth,  $P_T$  of the chipping that occurs along the drilling lip is shown in Fig. (28/f). If it occurs on the cutting edge, it is measured in the same manner as described for the outer corner wear section. If it occurs along the flute edge, it should be measured in the same manner as for the margin wear.

**(g) Built-up Edge (B.U.E.):**

Built-up edge results from severe deformation and convergent work-hardening of material flowing across the tool face in secondary deformation. This material is progressively built-up because its shear strength is greater than that of the main body of chip material.

The drilling operation can produce B.U.E's on the drill. These are significant on the drill lips, the chisel edges, the margins and the outer corners.

A seriously worn drill having significant flank wear, chisel edge wear and crater wear with chipped cutting edges can still be used for drilling as long as its outer corners and margins survive.

### **3.3.2 Drill Life & Failure Criteria:**

When a drill is removed and reground, this has a cost associated with it and regrinding too often results in higher than necessary cost. For this particular operation because regrinding is carried out every 30 holes, there is, potentially a significant loss of drilling machine

utilization as well. On the other hand if the cutting tool is allowed to become too dull, then unnecessary workpiece damage and greatly accelerated tool wear are incurred. Presently there are various strategies employed for changing the cutting tool. One of the most common methods is to replace the tool after drilling a predetermined number of holes. However the high initial cost of relatively expensive carbide tipped tooling and the solid carbide drills dictate that they are reground periodically and replaced after a few regrinding cycles. The number of regrinds possible is determined by outer corner wear which determines the hole diameter. The wide variation in tool life in industrial conditions makes it difficult to determine the regrind cycle and the tool life whilst maintaining the hole quality criterion. Commercially, drill life is determined by one or more of the following criteria [76];

**(a) Workpiece Dimensional Tolerance:** Sometimes a drill is removed from service whilst it is cutting perfectly well because the hole dimension is considered to be out of tolerance.

**(b) The Surface Finish of the Holes:** For some applications, the degradation of surface finish can indicate the useful life of the drill. The surface finish degradation can be determined by Talysurf and correlated with, for example, the number of holes drilled.

**(c) Drilling Sound Quality:** Tool failure is also indicated by the change in the drilling sound by the occurrence of 'screech'. This normally indicates inefficient cutting and, hence, wear.

**(d) Economic Considerations:** The high initial cost of carbide tipped twist drills dictate that they are reground periodically rather than discarded. This will sometimes occur before the tool is deemed to have failed because the hole produced is no longer acceptable. Premature failure of a drill will often result in either a 'spoiled' hole and/or a broken drill neither of which is acceptable. For carbide drilling, a broken drill has two disadvantages. It is expensive to remove and expensive to replace.

#### **3.4 Forces Acting on the Drill:**

The drill exert two types of forces on the hole boundaries, drilling thrust and torque. The greater the vertical thrust, the more the drill wear and the poorer the hole quality. Coincidentally, the drilling thrust determines the buckling stability of the drill which can affect the hole diameter. If a drill is slender, it may bend or deflect laterally which degrades the geometric hole quality. The buckling stability of a drill can be determined by Eulerian Buckling Theory. The theory states that when a column is loaded by a vertical load through the centroid of the cross section which is aligned with the longitudinal axis for the column that is fixed at the top and pinned at the bottom, the critical load for onset of buckling is given by [77];

$$(P)_{cr} = \frac{(\Pi^2 E I)}{(0.699 L)^2} \dots \dots \dots \text{Eqn. (4)}$$

Where  $(P)_{cr}$  is the critical vertical load.

$I$  is the minimum moment of inertia around  $x$  or  $y$  axis.

$L$  is the total length of the column.

$E$  is the modulus of elasticity of the column.

$G$  = Shear Modulus =  $E/(1+\nu)$ .

$\nu$  = Poisson's Ratio.

The torque exerted by the drill is limited by the torsional rigidity of the drill. The torsional rigidity of the drill is the product of polar moment of inertia and the shear modulus. The torsional rigidity, together with the applied drill torque and effective drill length determine the angular deflection of the drill according to the following relationship;

$$\Delta\theta = \frac{(L \times T)}{(J \times G)} \dots \dots \dots \text{Eqn. (5)}$$

Where  $\Delta\theta$  = Angular Deflection.

$T$  = Applied torque.

$L$  = Effective Drill Length.

$J$  = Polar Moment of Inertia.

$G$  = Shear Modulus.

The axial deflection of the drill can also be determined by using Hooke's law;

$$\Delta\zeta = \frac{(P L)}{(A E)} \dots\dots\dots \text{Eqn. (6)}$$

Where  $\Delta\zeta$  = Axial Deflection.

P = Drill thrust.

L = Effective drill length.

E = Elastic Modulus.

A = Cross-sectional area.

### 3.5 Tool Material, Cemented Carbide:

The combination of a high degree of hardness and compressive strength makes cemented tungsten carbide well suited for use as a tool material. Cemented carbides are produced by a powder metallurgy process which involves pressing the carbide and cobalt binder in powder form followed by sintering.

Tungsten carbide-cobalt possesses unique wear resistance due to the composite nature of its microstructure, which consists of hard carbide particles cemented by a tough cobalt binder phase. The desired degree of tool hardness, strength and toughness is achieved by tailoring the composition and microstructure of the constituents. As the cobalt content is raised, the hardness and compressive strength decreases and the transverse rupture strength increases for a given carbide grain size as shown in

Fig.(30) [78]. For maximum hardness, (HV), the tungsten carbide grains must be as small as possible, preferably below one micron. To attain optimum wear resistance, the carbide grains should be as small and as uniform as possible [79]. The abrasive wear resistance increases as the cobalt content is lowered for a given grain size provided that sufficient cobalt is present (1.5%) to ensure complete sintering. The amount of plastic deformation before fracture increases with the cobalt content. The hardness is balanced against the toughness by precise adjustment of the cobalt content so that the drill can be contoured to its complex geometry. The toughness of the cemented carbides can be determined by the Palmqvist test. The Palmqvist test provides a simple measure of fracture toughness by measuring the crack resistance of a brittle material at the four corners of a Vickers diamond indentation on a polished surface. The Palmqvist toughness parameter, ( $W_p$ ) is defined as the indentation load (P) divided by the sum of the crack lengths (L) measured at the indentation corners. For a specific material, the greater the parameter,  $W_p$ , the higher the fracture toughness. The Palmqvist parameter was used to calculate the bulk fracture toughness, ( $G_{IC}$ ) using the following relation [80,81];

$$G_{IC} = 174 \times 10^{-6} W_p + 15.00 \dots \dots \dots \text{Eqn. (7)}$$

The test provides a ranking of the cemented carbide grades in terms of toughness, which is expected to increase with increasing cobalt content. Abrasive materials are best machined with a grade that is as hard as possible to achieve maximum wear resistance with adequate toughness; this is achieved by carbide drills having 8-12% cobalt and a minimal (< 1 micron) and regular grain size. Typically, a grain size less than 0.7  $\mu\text{m}$  is rated as micrograin, 1  $\mu\text{m}$  as 'fine', 1.5-2.0  $\mu\text{m}$  as 'medium' and 3-4  $\mu\text{m}$  as 'coarse' grains [79,82,83].

It is usually uneconomical to make an entire tool of cemented carbide because it is about 20 times more expensive than steel (weight for weight) and no real improvement in terms of cutting performance is achieved. Usually the carbide cutting edge is attached mechanically or brazed onto a high speed steel shank depending on design requirements. There is an added benefit that the shank which is tougher is less prone to breakage [79]. Solid carbide drills are more difficult to fabricate. They would offer greater rigidity and less margin wear in deeper holes to abrasion from the cut surface.

### **3.6 State of the Art of CFC Drilling:**

This section consists of a literature survey regarding the state of the art of CFC drilling technology in two stages. The first is the systematic examination of the procedures which may be used for making holes in CFC. It reviews a number of alternate processes to conventional drilling. The

second part focuses on the improvements in tooling, material and processes made using conventional drilling techniques over the passage of time.

### **3.6.1 Drilling Techniques:**

**(a) High Pressure Water Jet:** Water jet drilling consists of drilling a hole by concentrating a small diameter water jet at a very high speed onto the workpiece. It is a widely used technique for drilling holes because thermal material damage is almost completely eliminated. In spite of its advantages, this technique has two major drawbacks.

■ The water jet has limited stability and therefore is easily distorted in a direction perpendicular to its own axis.

■ The cutting force which acts in the direction of fluid flow leads to delamination when the jet leaves the workpiece [34,84].

**(b) Pulsed Laser Drilling:** It is possible to drill holes in CFC using a laser by concentrating a pulse beam onto the workpiece. This technique is useful for drilling holes in otherwise inaccessible structural members. Only small mechanical forces are introduced in the workpiece but the matrix, which can tolerate limited temperature, tends to be destroyed and this leads to poor hole quality. This hole making technique results in high power consumption and costly processing gases which require huge capital investment and running expenses [34,85].

**(c) Ultrasonic Drilling:** Ultrasonic drilling consists of drilling a hole by means of vibrating abrasive particles in a slurry at high frequency (about 20,000 cps) by specially designed tools. Ultrasonic machining has advantages in both finish and accuracy as compared to other techniques. Unfortunately this method is slow which adversely affects productivity [34,86,90].

**(d) Electrochemical Spark Assisted Machining:**

In electrochemical machining, sparking takes place at the tool electrolyte interface above a certain value of applied voltage. The sparking occurs across the bubbles evolving at the cathode surface. If the sparking tool is brought in contact with the CFC, drilling would take place. This technique can be used for drilling of any nonconducting material i.e. composites. The material removal takes place primarily due to melting out but some vaporisation of matrix and fibres also take place. This technique is still in its infancy and requires many refinements before commercialisation can be realised [34,87].

**(e) Conventional Drilling Technology:** Conventional drilling involves hole making by feeding a rotating drill into the workpiece which results in acceptable holes but excessive drill wear. The drill wear can be reduced by improving drill point geometry and materials. In terms of materials, conventional drilling is carried out by using polycrystalline diamond (PCD) or tungsten carbide tooling for drilling CFC. Polycrystalline diamond consists of

micron sized diamonds bonded together in a polycrystalline structure that is of comparable hardness to monocrystalline diamond but more isotropic and, therefore, resistant to mechanical shock and impact without fracturing. The hole quality generated by PCD tipped drills is comparable to holes drilled ultrasonically. The special PCD drill may last 75 times longer than the carbide tipped drills. Such drill can be reconditioned two or three times giving a significant advantage in terms of drill life. The favoured PCD drill geometry for drilling composite materials include a  $62^\circ$  point angle, a  $32^\circ$  helix angle and a two flute point. More than 2700, 4.85 mm dia. holes were drilled in CFC using a PCD drill giving a much needed productivity improvement by reducing the number of tool changes required. These drills cost 20 times more than solid carbide drills and are exposed to damage and chipping. Even if the hole quality and tool life are good, they may not be suitable for manual drilling [88,89].

Exotic high pressure water jet, pulsed laser jet, ultrasonic, electro-chemical spark and PCD drilling techniques have their place but the capital investment and running costs are currently high. If lower cost and higher production is the goal within limited hole tolerance, hole quality and drill wear, then simple refinement of existing low cost technology using tungsten carbide tipped drills can produce good results.

### 3.6.2 Technology Survey of Tungsten Carbide Drills:

Conventional drilling techniques for drilling holes in CFC have been developed from well documented metal, wood and rock drilling techniques. A few early papers have discussed the peculiarities of drilling CFC. Friend et al., 1973, examined the technical and cost problems associated with machining CFC. He offered some solutions to machining problems and concluded that under certain conditions, conventional machining can be competitive with an advanced ultrasonic system [90].

Washington, W. L., outlined the optimum speed and feed conditions, types of carbide drills and drill motors used to drill various combinations of CFC/Aluminium [91].

Beall, R.T., 1979 suggested drilling deep holes in CFC with gun drilling technique for introducing coolant at the drill tip to cool and aid removal of CFC debris. The Lockheed Aerospace Corporation adapted such drills to portable equipment for drilling close tolerance holes in CFC [92].

Mackey, B., 1980 has offered practical solutions to the drilling problems in the CFC. Mackey provided qualitative recommendations regarding various factors affecting drill geometry, cutting conditions and noticed that improper geometric features of the drill lead to poor hole quality in terms of delamination at the exit plane of the drill [93]. In another paper he came up with a new tool geometry with an 'open flute exit' having extreme positive rake angle and minimum chisel edge [94].

Radhakrishnan, et. al., 1981 carried out dynamic

characterisation of drilling forces in CFC and related it to the surface roughness of the holes [95].

Two case studies in CFC drilling were performed by King, R.I., 1982. He evaluated various drill speeds, feed rates, drill configurations and presented optimised relationships for the drilling of various combinations of CFC and aluminium alloys [96].

Podder, R. K., carried out the evaluation of cutting forces, tool life and hole tolerance as a function of speed, feed, tool point geometry and coolant. Optimised drilling conditions and geometries were developed, tested and compared [71].

Koplev et. al., 1982 determined the effects of cutting forces for orthogonal machining of unidirectional CFC having fibre orientations perpendicular and parallel to the cutting edge. He discussed general aspects of machining CFC and provided observations on the damage caused to the hole in terms of cutting forces [69].

Sakuma, K., 1984 carried out investigations regarding the wear characteristics of drill materials in the drilling of glass fibre and carbon fibre composites. He found that wear of high speed steel drills is very much larger than that for carbide drills [97]. In an another paper, he determined the effects of the physical and mechanical properties of tool materials on wear in cutting CFC. He determined that an increase in the hardness will increase the wear resistance of the tool [98].

Major contributions in CFC drilling technology have been

made by Konig, et. al., 1985. Konig has made an extensive review of waterjet drilling, laser drilling and conventional drilling in terms of drilling forces, hole quality and manufacturing cost. He used a Talysurf machine to determine the surface roughness of holes. He established that the 45° fibres had maximum roughness at the hole boundaries but did not explain the underlaying mechanism. He concluded that mechanical techniques if performed well will give superior results if carbide or PCD tools with keen cutting edges are used [32,34,35]. In a later paper, he discussed the main parameters concerning surface roughness and material damage in drilling CFC . He found that the CFC drilling temperature is of the order of 300°C [100].

Chanani, J. P., 1985 suggested optimal methods for generating quality holes in composites and hybrids. He developed a spade drill for drilling and countersinking holes in CFC. He found that the spacematic gun drill was best for drilling deep holes in CFC/aluminium hybrids. He also developed a procedure for peck drilling deep holes in CFC/titanium hybrids [101]. In a later paper he supported the use of 8-facet point drills for drilling CFC holes [102].

Mesom et al, 1988 investigated the machining properties of advanced plastic and composite materials. He found that the drilling heat caused burning and gumming at most speeds using tungsten carbide drills [103].

Miller, J. A., 1987 tested seven drill bits having

different drill point geometries for CFC drilling and found that an 8 facet split point geometry produced the best overall results in terms of hole quality. He added that dramatic results in terms of greatly improved drill life and hole quality are expected from 8-facet PCD tipped drills and further research is in progress [104].

Malhotra, S. K., 1990 compared the results of drilling in carbon fibre and glass fibre composites. He attributed the high wear, thrust and torque in CFC drilling to the higher abrasiveness of carbon fibres compared with glass fibres [105].

Lauder, E., 1991 has recently evolved a double fluted router using a ceramic composite comprising an alumina matrix reinforced with silicon carbide whiskers for machining non-ferrous materials. He claims to have demonstrated that such routers can withstand the severe combination of compressive/tensile/shear stresses and repeated impact loading without failure at cutting conditions more severe than those for any material disclosed so far [106].

Many other papers have addressed drilling techniques in glass, Kevlar and boron fibre composites and provided useful information and a general insight into the drilling of CFC's. Petrof, R. C., 1986 found large dynamic variations in drilling forces due to changes in the relative orientation of cutting edges and fibre direction during the machining of glass fibre composites [107].

A systematic review of effective machining and tooling

techniques for Kevlar composite laminates was made by Doerr, R. et. al., 1982 in a 3-phased programme at Hughes Helicopters Inc. [108]. Similar approaches have been adopted during the present investigations regarding drilling problems in carbon fibre composites.

Sikorsky Aircraft Limited turned to punch drilling the holes in boron-epoxy to avoid delamination of holes drilled in UH-60A helicopter airframe in 1982 [109].

The literature survey revealed that most of the research in drilling CFC was done to suit specific technical requirements of an establishment i.e. Lockheed, Northrop or Sikorsky etc and was limited to first generation CFC's. With advancements particularly in workpiece material and to a lesser extent in drill materials, the nature of the drilling problem has changed and British Aerospace, now using second generation composites, required the problem areas to be evaluated; i.e. drill life, hole quality and drill material. For the work which has been done, there has been no systematic effort made so far to carry out a fractographic analysis of the pulled out and pushed down carbon fibres in CFC holes which determine its surface roughness.

This thesis gives the first systematic review of the damage modes of carbon fibres in CFC drilling and examination of these identifies the most critical damage mode. This information facilitates interpretation of the hole quality in terms of surface roughness which determines the extent

of reaming required on production floor. This research aims to investigate the above mentioned areas in modified, high performance CFCs using commercially available, low cost, conventional drilling techniques.

## Chapter Four

### EXPERIMENTAL INVESTIGATIONS

#### 4.1 Introduction:

A drill can normally fail in one of two ways: firstly, it can no longer cut effectively due to the amount of flank wear on the major cutting edge of the drill; secondly, the wear on the secondary cutting edges (flutes) is such that the hole produced by the drill is undersize. It has been found when drilling composite materials of the type used in this work that, starting with a drill on top hole tolerance and proceeding until the hole size has reduced to bottom hole tolerance, the drill can be reground several times to remove the worn flank before the hole it produces is too small. Standard practice at British Aerospace is to drill 30 holes between regrinds and to consider the drill life to be the product of the number of holes drilled and the penetration distance until the 'hole too small' criterion is reached. The cumulative penetration distance is the product of the total number of holes drilled and the distance drilled for each hole. For through holes, the distance drilled for each hole is the thickness of the plate. The measure of hole size is accepted to be the 'no go' of a suitable size of plug gauge. In the current tests, drill life in terms of the cumulative penetration distance, as defined above, for four commercially available drills was determined. The drills were chosen because they were currently being used at British Aerospace (Aircraft

Manufacturing Division).

The drilling tests were sub-divided into three major tasks i.e. preliminary drill testing, detailed drill investigation and drill performance characterisation.

The preliminary drill testing was carried out to determine the two most promising drills of the four types of commercially available drills. Five drills of each type were tested for drill life in this phase. The first two drills were tested to determine the cumulative penetration distance prior to plug gauge failure. These drills were only reground when the flank wear was such that the drill was considered to have failed due to flank wear development of about 0.2mm or when the drill started to screech. The remaining three drills of each type were reground after drilling 30 holes according to the standard practice at British Aerospace to determine the number of regrinds that could be achieved before ultimate hole size failure. After preliminary testing, two of the four commercial drills were chosen for further testing based on the previous results. The Klenk drills were rejected because they gave very inconsistent results which could be unacceptable in practice. The solid carbide drills proved to be the best, but British Aerospace indicated that these should be discounted on cost grounds. Consequently, for the detailed drill investigation and drill performance characterisation, the Gandtrack and Precision drills were used.

During the detailed drill investigation stage, one drill of each type was subjected to an extended drill test of 40

holes per regrind cycle and a maximum of 9 regrind cycles to determine the drill having maximum life in terms of cumulative penetration distance as defined above. For all this work, the standard test procedure was the same. A test panel was drilled with 20 holes per row as shown in Fig. (31) where the drilling sequence was 1-9, 10, 11-19, 20. With a hole inspection, as required, at 10 hole intervals, this procedure put the holes to be inspected (10 and 20) both together on the edge of the plate. This is practically useful when the holes have to be sectioned afterwards.

The drill performance characterisation tests were carried out to determine thrust and torque for a range of feeds and speeds for each of the test drills. The drill thrust was related to drill wear and drill torque was related to hole quality.

Some photoelastic work was also carried out to determine residual strains in the holes using birefringent technique. Structural analysis of the drills was carried out to predict their response to recommended drilling conditions. The axial and angular deflection, torsional rigidity and buckling stability of the drills were determined using structural analysis.

The hole quality was assessed by slicing through the holes, gold plating and examining the holes for fibre pull out/push down and matrix cracking using scanning electron microscopy. The surface morphology of the carbon fibres at  $+45^\circ$ ,  $-45^\circ$ ,  $90^\circ$  and  $0^\circ$  were systematically analysed and related to the drilling forces. The aim of this exercise

was to determine the most critical damage mode during CFC drilling and to identify all those factors which promote the damage mode.

Three different cemented carbides were tested for their microstructure, physical and mechanical properties. The microstructure was examined by C.C.T.V. studies of scanning electron micrographs. The hardness and fracture toughness were determined by Vickers hardness tests and Palmqvist tests respectively. The wear resistance of cemented carbides was assessed using sliding tests of various types. A lathe sliding test led to excessive vibration and a milling machine sliding test led to delamination. The Pin-on-Disc sliding test led to significant wear on the carbide specimens and produced acceptable results.

#### **4.2 The Investigative Techniques:**

The following investigative techniques were frequently performed during the present work.

##### **4.2.1 Travelling Microscopy:**

Travelling Microscopy was the standard optical technique used to measure the size of the wear land on the outer corner, the flank, the margin and the chisel edge of the drill according to procedure given in Section-3.3.1. (a). The outer corner wear was measured for ease, convenience and accuracy using a travelling microscope (Beck), having a magnification of 50 and a least count of 0.005 mm. The outer corner wear region is shown in Fig. (32).

#### **4.2.2 Scanning Electron Microscopy:**

A Cambridge, Stereoscan 600 scanning electron microscope (SEM) was used during the investigations to monitor the point wear, the margin wear and damage characteristics of the drills. Data were collected progressively after every drilling cycle using this technique. The drills were immersed in a beaker containing Genklene (1,1,1-Trichloroethane) produced by ICI. The beaker was placed in an ultrasonic cleaner for about 20 minutes to remove cutting debris. The drills were taken out, soaked in methanol for degreasing and dried. The drills were mounted on a support, vacuum degassed to a vacuum of 0.1 torr and coated with gold. The drills were held in the SEM stage as shown in Fig. (33) and different geometric features of the drills were inspected for wear at various magnifications and orientations.

This technique was also used to examine the cemented carbide specimen and carry out fractography of damaged fibres in the CFC holes.

#### **4.2.3 Optical Microscopy:**

An optical microscope (Reichert) was used to examine the body profile of the point geometries to determine the moment of inertia of the drills for use in the structural analysis. The cutting edge of the drills was also examined for side clearance at higher magnifications.

The drill body was sectioned in plane A-A'-B-B' (Fig. (32)) just beneath the point (with the drill facing upwards) by

a circular diamond saw which was rotated by a low speed wafering machine. The sectioned drill point profile was mounted in thermosetting resin. The mounted samples were polished down to a 1 micron diamond finish, thoroughly rinsed in methanol and then etched using Murakami's Reagent ( $K_3Fe(CN)_6$ : 10 grams, KOH: 10 grams and  $H_2O$ : 100 millilitre, used fresh).

This technique was also used to determine the resin rich areas in the laminate by polishing a CFC specimen measuring 20mm × 20mm × 10mm and examining the specimen for resin distribution in the interlayer, (on its side measuring 20mm × 10mm) when the optical axis of the microscope was aligned parallel to the centreline of the fibres.

Zetopan optical microscopy was used to determine the depth of the damage scar on the hole boundaries. The fine z-control was directly calibrated in microns. The top and bottom of the cavity was focused utilizing the limited depth of field of the lens which directly read off the depth of the damage scar.

#### **4.3 Experimental Procedure:**

The carbide tipped drills were custom-made for this work by Klenk, Gandtrack and the Precision drill manufacturing companies according to British Aerospace technical specification PTS: 62.01.07 as given in Fig. (34). The drills have been referred to by their manufacturer's name in this thesis. They had only nominal differences in their

geometry and had a diameter of 6.035 mm as given in Table (6) and shown in Fig. (35). The cemented carbide spade inserts were brazed onto HSS shanks. The solid carbide drills (diameter: 6.00 mm) having stock No: 2000600 were manufactured by Klenk as a catalogue item and have been designated as 'SOLID CARBIDE' in this thesis.

All the drills were inspected for their consistency by British Aerospace and were used from new during the drilling tests. The diametrical tolerance of the holes using 6.035 mm drills was checked using a 6.00 mm carbide plug gauge and the holes drilled by the 6.00 mm diameter drill were checked using a 5.965 mm gauge to give the same relative amount of diametral wear of 0.035 mm. The diameter and surface roughness of the plug gauges was checked using a Shadowgraph AP-6A and Talyrond-200 respectively as shown in Fig. (36).

The through holes were drilled vertically in the carbon fibre composite, T800/924C panels having fibre orientations of  $[90^\circ, +45^\circ, -45^\circ, 0^\circ]$  and fibre volume fraction of 0.65-0.69. All the plies were balanced and symmetric. This particular class of material and ply configurations were chosen in this study because they lead to maximum 'damage tolerance'; British Aerospace has selected this material for structural application in future aircraft. The CFC panels measured 372mm  $\times$  210mm and had a thickness of 10mm as shown in Fig. (31). The panels were supported along the two short edges such that through holes could be drilled. Four clamps were used as shown in Fig. (31) to hold the

laminate and preliminary testing indicated that even at the centre of the panel, with many holes already drilled, the deflection of the panel was insignificant.

A fixed bed Wadkin, Drill/Mill NC machine tool was used to drill the holes as shown in Fig. (37). A computer programme was developed to suit the drilling sequence and conditions. The listing, input and output of the computer programme are given in Appendix 'C/1', 'C/2' and 'C/3' respectively. The drills were mounted in a collet chuck and the holes were drilled at a drill speed of 2800 RPM and a feed of 0.05 mm/rev. during the drill assessment phase and the detailed drill investigation phase. The drilling speed and feed were varied during the drill performance characterisation phase. The drilling speed of 2800 RPM and the feed of 0.05 mm/rev. reproduced the standard drilling practice on the shop floor at British Aerospace. They regrind the drills after a CFC penetration distance of 300mm (30 holes in the test material) and the cumulative life of the drill depth before it loses its useful life is considered to be 2100 mm; i.e. 6 regrinding operations.

During the first phase of drilling, the drills were reground by the regrinding department of British Aerospace using a Brierley Zenith point regrinding system with the instructions to follow PTS 62.01.07 in every way; the drills were then inspected by the Manufacturing Development Division. All the angles were set on the digital control panel of the machine and set automatically i.e. the errors in inspectibility should have been zero as long as the

angles were set properly. The only source of error could have been due to wheel wear which was thought to be negligible and would have resulted in angle errors of less than  $0.25^\circ$ . The drills were inspected by the Manufacturing Development Division and were passed onto Salford University for drilling tests. The regrinding and inspection during the second stage of drilling was carried out by the Manufacturing Development Division themselves. A Christan 03-10 regrinding system was used which had a maximum error potential of less than  $0.25^\circ$  which was also fully dependent on machine setting.

Special safety precautions were observed for CFC drilling. A Nilfisk dust collector system, Type GS-80 with 5 micron filter was used to extract the drilling debris. A disposable paper gown and mask were worn at all times during the drilling operations to protect against airborne CFC particles. At the conclusion of drilling operations, hands and face were washed to remove any residual cutting debris. The CFC contaminated clothing was handed over to health and environmental agency of the University.

#### **4.4 The Drill Life Tests:**

Around 10,000 holes were drilled during the three stages of the experimental programme to determine the drill wear, life and the failure mechanism of the four commercially available drills in the following manner.

#### 4.4.1 Stage One-Preliminary Assessment of Drills:

The preliminary assessment of the drills was carried out to determine the performance, limitations and capabilities of the four types of drills in terms of their life. The outer corner wear of 0.2mm was the main criterion used for determining when regrinding was necessary. Alternatively, regrinding was considered necessary in some cases when the drill started to 'screech'. The plug gauge criterion was used to determine the cumulative penetration distance; i.e. the total hole length drilled for the drill to the point at which the hole was undersized.

Five new drills of each of the four types, a total of 20 drills, were subjected to preliminary drilling tests. The 1st and 2nd drill of each type drilled holes until the flank wear development and/or the 'screech' was significant enough to warrant regrinding. After wear development of about 0.2mm on the outer corner, the drills were taken to British Aerospace for regrinding, and inspection, to the original geometry.

The 3rd, 4th and 5th drill of each type were tested using a 30 holes per regrind cycle strategy. The outer corner wear was monitored using a travelling microscope and the hole diameter was checked using a carbide plug gauge after every tenth hole. In addition, a detailed inspection using scanning electron microscopy of the point wear, margin wear and damage characteristics was carried out at the end of every drilling cycle. These drills were also taken to British Aerospace for regrinding, and inspection, to the

original geometry. Inspection of the drills after the fourth regrinding operation by the Manufacturing Development Department revealed that they were not within the specified tolerance and further drilling tests using these drills were discontinued. These tests however revealed the two most promising drill point geometries in terms of drill life and these were selected for further tests and trials after discussion, agreement and approval of British Aerospace.

#### **4.4.2 Stage Two-Detailed Drill Inspection:**

Detailed drilling tests involving detailed inspection and a thorough examination of the two most promising point geometries i.e. Precision and Gandtrack were carried out. One new drill of each type was tested for the extended drill life of 40 holes per regrind cycle. The plug gauge criterion was used for determining the cumulative regrinds possible for each drill before it was no longer serviceable. Scanning electron microscopy was used for a detailed examination of the point wear, margin wear and damage characteristics after every drilling cycle. The drill body profile and the side clearance were also examined using optical microscopy during this stage.

#### **4.4.3 Stage Three-Drill Performance Characterisation:**

Three activities took place in drill performance characterisation

- Cutting forces were measured using a drill dynamometer
- An attempt was made to measure the residual strains using a birefringent photo-elasticity test
- The Structural analysis of the drills was carried out to determine the torsional rigidity, critical buckling load, axial and angular deflection of the drills.

(a) **The Cutting Forces:** A Kistler two component drill dynamometer type 9271A having a thrust sensitivity of 1.8 pC/N and a torque sensitivity of 1.5 pC/Ncm was used to assess the performance characteristics of the four types of drills. The dynamometer was connected to the Kistler charge amplifier type 5006, X-Y plotter and digital oscilloscope as shown in Fig. (38). After calibrating the dynamometer, the drilling torque and thrust response were determined with respect to the speed, feed and penetration distance in two stages. In the first stage, the drilling thrust and torque was determined at feeds of 0.01, 0.025, 0.035, 0.05, 0.075, 0.01 mm/rev. and speeds of 2250, 2500, 2800, 3000, 3250 RPM. The cutting force response was interpreted to determine the onset of delamination, fibre pullout and matrix cracking.

In the second stage the cutting force response was determined at a constant cutting speed of 2800 RPM and a feed of 0.05 mm/rev. for the 10th, 20th, 30th and 40th holes. Most of the holes were drilled on the main CFC panel that was mounted on the machine bed and every 10th test hole was drilled on the CFC strip that was clamped onto the

dynamometer by metallic strips as shown by arrows 'A' and 'B' respectively in Fig. (39). The CFC strip was made of the same material and had the same thickness i.e. 10mm as the main workpiece. The rectangular strips (measuring 185mm × 34mm and having thickness of 10mm) were cut so that they could be accommodated, held, clamped and moved easily on the dynamometer bed whenever required. Just before drilling the 10th hole on the CFC strip, the dynamometer was switched on to record the drilling forces. After drilling the tenth hole on the CFC strip, the machine was stopped and the drill was removed from the spindle chuck for the measurement of the outer corner wear. The CFC strip was moved to accommodate another test hole and the drill was replaced in the chuck to continue the drilling cycle. This novel test drilling arrangement, tried for the first time, ensured maximum economy in terms of material, labour, time and is now being practised by British Aerospace for their test drilling on CFC.

**(b) The Birefringent Photoelasticity:** The birefringent photoelastic technique was primarily used to establish a comparison of the residual strains in the bottom ply of CFC strip for the four types of drill used. The test was performed in accordance with the Measurement Group, Inc technical note TN-702. This consisted of bonding the manufacturer supplied optically transparent film, PS-1A onto the CFC strip using epoxy hardener, PC-1 bipax such that the bonded surface was reflective. The sensitivity of

the film was 0.15 and the thickness was 3.00 mm.

Three attempts were made to get a meaningful result for this test. To increase the accuracy of the results, it was necessary to minimize effects such as plate bending. To do this, rectangular strips measuring 50mm × 35mm and having thickness of 10mm were cut from the main work panel and the optically transparent film was attached. It was decided that a method of nullifying the effects of the drilling induced residual strains in the film would be by reaming 6.035 mm diameter holes through the film (the reamer would stop just short of piercing the CFC strip), record the residual strains, invert the plate/film assembly and drill another hole through the CFC strip using the test drill at exactly the same location. The subtraction of the residual strains generated by the film from the one due to CFC hole drilling was expected to lead to exact values of residual strains. The practical problem encountered was that of getting good alignment of the drilled hole in CFC plate and the reamed hole in the film. Misalignments which could not be removed gave misleading data.

In the second attempt, the film was glued on the top ply of the CFC plate and a hole was drilled at a speed of 2800 RPM and feed of 0.05 mm/Rev through the CFC plate/film. The isoclines were generated around the hole boundaries but were poorly defined. Because the bottom ply of the CFC strip was being subjected to maximum forces during the drill breakthrough, the plate/film were inverted and a hole was drilled through at the speed of 2800 RPM and feed of

0.05 mm/rev. The strains were transmitted to the coating and produced a clear pattern of isoclines. The patterns were examined by reflection polariscope, optical techniques and recorded by conventional photography for further analysis. The corresponding strains and stresses were determined for given film (Sensitivity = 0.15, Thickness = 3mm) CFC material (Quasi-isotropic Elastic Modulus =  $55 \times 10^9$  Pa, Poisson's Ratio = 0.34) and fringe order using equations (2) and (3) in Section 2.6.

Efforts were made to minimise interference from external sources. As the interference due to any other unavoidable reason would be common to all the tests, the results were therefore considered to be useful in establishing a relative comparison of the strains generated by the different drills.

**(c) Structural Analysis:**

Structural analysis comprised the determination of torsional rigidity, critical buckling load and axial and angular deflections of the drills at a speed of 2800 RPM and a feed of 0.05 mm/rev.

The polar moment of inertia is the summation of the moments of inertia of the drill cross-section around the x-axis and y-axis. The moment of inertia of the drills was determined by the best fit triangle or rectangle and using the appropriate equation as shown in Appendix 'D'. The values of drilling force at a drilling speed of 2800 RPM and a feed of 0.05 mm/rev. (determined in section 4.4.3 (a)) were

used to calculate different structural parameters.

The buckling stability of the drills was determined from the modulus of elasticity of the HSS drill shank (ignoring the carbide bit), the minimum moment of inertia of the drills (determined in Appendix 'D') and the effective drill length (protruding from the machine chuck). Remaining structural parameters required for the evaluation of torsional rigidity, axial deflection and angular deflection of the drills were determined and tabulated in Table (15).

#### **4.5 Fibre Pullout and Matrix Cracking:**

The holes were examined in two phases for hole quality in terms of fibre pullout and matrix cracking. In the first phase the effect of coolant on hole quality was determined and in the second phase detailed investigations regarding fibre pullout and matrix cracking were undertaken.

**4.5.1 Effect on Coolant on Hole Quality:** The British Aerospace coolant Clearcent G.B.A. was mixed with water in the ratio of 1:20 and was dispersed as a flood at the drill penetration region in the CFC. Holes were drilled wet using a Precision and a Gandtrack drill. Every hole was inspected for plug gauge failure. Hole numbers: 0, 20, 40, 100, 140, and 200 and the corresponding dry holes, drilled during the drill life investigation tests (Section 4.4), were sectioned using a diamond saw as shown in Fig. (40). Maximum care was taken to prevent internal damage and delamination in the hole. The test specimens were glued

onto a stub and examined visually by stereo optical microscopy. The mounted specimens were vacuum degassed to the pressure of 0.1 torr and gold plated. The wet holes were compared with their equivalent dry holes to determine the effect of coolant on hole quality.

**4.5.2 Fractography of Damaged Fibres:** In the second phase, surface morphology of the fractured fibres laying at various orientations ( $-45^\circ$ ,  $+45^\circ$ ,  $0^\circ$  and  $90^\circ$ ) in the dry test specimens were examined by using scanning electron microscopy. The micromechanics of fibre pullout and matrix cracking in terms of the interlaminar stresses were analyzed to predict the conditions under which fibre pullout and matrix cracking might occur. The 1st, 30th, 40th, 100th and 140th holes (drilled in section 4.4) were sectioned, gold plated and inspected in the same manner as before by the SEM for fibre pullout and matrix cracking. In the previous section, comparison of hole quality for 'wet' and 'dry' holes was carried out at relatively low magnification. In this section much more detailed examination of the surface morphology of damaged fibres was carried out at much higher magnification.

#### **4.6 Cemented Carbide Classification:**

Non-cutting, sliding wear tests were tried to determine which of three cemented carbides had the lowest wear rate when in contact with the carbon fibre composite. British Aerospace specified that all the drill manufacturers should

fabricate the drill tips from either Sandvik H10F or Krupp's THR cemented carbide. The Kennametal F285 cemented carbide was included in the study to broaden the scope of the investigation. Of the three manufacturers, only Klenk used one of the recommended grades (THR) for the tipped drill as indicated in Table (6).

The microstructure of Krupp's THR, Sandvik H10F and Kennametal F285 cemented carbide were examined using scanning electron microscopy (SEM) and their hardness was determined using a Vickers Hardness Tester at 50 Kg load. The fracture toughness of the cemented carbides was measured using the Palmqvist technique. Independent sliding tests of the cemented carbide specimen were carried out using a lathe test, a machining centre test and a pin-on-disk test to determine their wear resistance against carbon fibre composites.

The 'as received' specimens were polished, then etched using Murakami's reagent and examined for carbide grain uniformity. The SEM examination of the specimens enabled the cobalt and tungsten carbide regions to be clearly distinguished, cobalt areas being relatively bright. The complex shapes of the sectioned tungsten carbide grains made it difficult to distinguish a continuous cobalt network. However an approximate value of cobalt film thickness was obtained by measurements from the magnified images of the micrographs produced on a C.C.T.V. monitor screen. Film thickness was measured directly on the screen

at intersections with randomly oriented lines on the micrographs. A minimum of 100 measurements were made on each micrograph and the mean thickness calculated for each specimen. A similar technique was used to determine tungsten carbide grain size. The microstructure of drill tips was also examined and their grain size was analyzed for uniformity using SEM and CCTV.

The hardness of the cemented carbide was determined by taking the average value of the 5 readings of the width of diamond indentations in the carbide specimens at different locations in Vickers hardness tests. The Palmqvist fracture toughness of the cemented carbides were determined by conducting a number of Vickers hardness tests at applied loads of 20, 40, 60 and 80 Kg load. The crack lengths at the four corners of the indentation generated in each specimen were measured.

Technical information on microstructure and related physical properties including compressive strength, transverse rupture strength, thermal conductivity and the coefficient of thermal expansion were obtained from the manufacturers of the cemented carbides and Brook's Handbook of Hard Metals [79].

Independent sliding wear tests of the three grades of cemented carbide were carried out using the following three techniques.

#### 4.6.1 The Lathe Test:

The lathe sliding test was carried out on a Heidenreich & Harbeck Lathe, V3 by holding a CFC specimen (25mm × 45mm and thickness of 5mm) on the tool post as shown in Fig. (41). The stationary CFC specimen was rubbed against the 12 mm diameter rotating carbide. The carbide rods were rotated by the chuck at a speed of 500 RPM for 10 minutes with a load of 1 Newton on the weight arm of the lever. As the ratio of the length of the weight arm to force arm of the lever was 1:10, the application of 1 Newton load on the weight arm led to the application of a 10 Newton load by the CFC specimen onto the carbide rod. The rubbing action created a 60 mm deep cut in the two CFC specimens (30 mm in each CFC specimen) without causing any signs of wear on the cylindrical carbide rod. When the same test was repeated at a speed of 1000 RPM with a load of 2 Newtons on the weight arm for 7 minutes, the carbide rod cut through various CFC specimens diametrically a total distance of 115mm without having any sign of wear on its periphery.

It was decided to increase the severity of the rubbing action by machining a hexagonal cross-section out of the circular cross-section of the cemented carbide rods. Each side of the hexagon measured 5 mm. Rotation of the rod at a speed of 1000 RPM and the application of a 1 Newton force on the weight arm generated high amplitude vibrations in the lever which invalidated the results.

#### 4.6.2 The Machining Centre Test:

The test conditions were reversed on a Kearney & Trecker Machining Centre experimental arrangement by pressing the stationary carbide specimen held in the toolpost of the force arm against a rotating CFC disc as shown in Fig. (42). The carbide rods were machined down to a diameter of 10 mm to fit in the toolholder and the 120 mm CFC discs were rotated by a specially designed template that could fit in the chuck of the machining centre as shown in Fig. (43). The disc was rotated in a vertical plane at the speed of 142 RPM having 1 Newton load on the weight arm for 10 minutes as shown in Fig. (44). The sliding action generated heat which led to matrix softening and delamination of the CFC disc edges after 8 minutes. The Clearcent G.B.A. coolant, mixed with tap water in the ratio of 1:20, was used to flood the CFC-cemented carbide contact area to bring the rubbing temperature down and the test was performed with a 1 Newton load and times of 10 minutes, 20 minutes and 30 minutes at speed of 142 RPM. The same test was repeated for 2 Newton and 3 Newton loads for times of 20 minutes and 30 minutes. Detailed examination of the wear scar revealed that CFC rubbing using this technique merely polished the carbide surface and did not create the wear scar necessary for realistic comparison or classification.

#### 4.6.3 The Pin-on-Disc Arrangement:

Pin-on-Disc wear tests were carried out on a Denison Machine. Cemented carbide rods were precision machined to 9.8 mm diameter to fit in the holder of the force arm. The lower end of the rod was machined to a 6 mm radius hemisphere to reduce its contact area for rubbing on the CFC disc. The CFC disc was mounted horizontally on a specially fabricated fixture that was rotated in a horizontal plane as shown in Fig. (45). The load was successively increased to 10 Newtons on the weight arm to achieve the maximum possible wear rate without causing vibrations as shown in Fig. (46). As the ratio between the force arm and the weight arm was 1:1, application of a 10 Newton load on the weight arm resulted in the application of a 10 Newton load on the hemispherical end of the carbide rod in contact with the CFC disc. The CFC disc was rotated at a speed of 375 RPM in a circle having a diameter of 45mm. The diameter of the worn area on the end of the cemented carbide rod was measured by an in-built microscope after hourly intervals within which the pin covered a sliding distance of 3180 metres. This resulted in significant measurable wear. The microstructure of the worn region was examined to determine the wear mechanism by scanning electron microscopy after the test.

## Chapter Five

### RESULTS

The results of the drill life tests including the pullout studies and the measurements of material properties are given below.

**5.1 Drill Life tests:** The results of the drill life tests, performed in the three stages, are as follows:

**5.1.1 Stage One-Preliminary Drill Performance Evaluation:**

The flank wear width was found to increase from the drill centre to the periphery as shown in Fig. (47). The wear pattern of all the drills showed characteristic high wear during the early stage of drilling and a nearly linear lower wear rate in the secondary wear stage.

Three regrinding cycles were performed to determine the most promising drill types in terms of their life. Inspection of the drill points after the 4th regrinding operation revealed that the point angles were out of tolerance. Further drilling tests using these drills were discontinued and the regrinding process was reviewed and improved. It was found that the drilling performance and the wear rate were greatly influenced by the regrinding operation. Slight inaccuracies in attempting to regrind the drills to their original geometry would lead to a different flank wear rate and therefore different drilling performance.

Although there were nominal differences in the point geometries of the drills produced by the various manufacturers, the drills exhibited similar trend in flank wear and it was considered that these differences in geometry would produce, at most, a second order effect. However it was found that the average outer corner wear of the Klenk drills nearly 1.8 times, the Gandtrack drills nearly 1.6 times and the Precision drills nearly 1.3 times that of the solid carbide drills after drilling 200 holes as shown in Fig. (48). The performance of each drill is tabulated in Table (7) and is briefly described below.

**(a) Klenk Drills:** The Klenk-1 and Klenk-2 drills failed after a penetration distance of 7300 mm and 5600 mm respectively due to plug gauge failure. For these tests, the drills were reground when it was considered that the tool was due to fail because of flank wear (0.2mm/screech). The remaining three drills of each type were regrinded as per British Aerospace practice (every 30 holes). Although the Klenk-3 drill performed satisfactorily until the fourth regrind operation, the Klenk-4 and Klenk-5 drills failed after drilling 110 holes due to out of tolerance diameter (plug gauge failure). These drills had a maximum outer corner wear that was grossly non-symmetric on both flanks and the large differences between the tool life for drills 1 and 2 as compared with the drills 3 and 5 could be ascribed to different geometric features. The detailed results are given in Appendix 'E', Fig. (1) to Fig. (5).

**(b) Gandtrack Drills:** The Gandtrack-1 and Gandtrack-2 drills failed after a penetration distance of 5400 mm and 2200 mm respectively due to diametrical tolerance (plug gauge failure). The Gandtrack-3, Gandtrack-4 and Gandtrack-5 drills continued to drill satisfactorily until the fourth regrind operation (120 holes) as shown in Appendix 'E', Fig. (6) to Fig. (10).

**(c) Precision Drills:** The Precision-1 and Precision-2 drills failed after a penetration distance of 3390 mm and 5650 mm respectively due to diametrical tolerance (plug gauge failure). The Precision-3, Precision-4 and Precision-5 continued to drill satisfactorily until the fourth regrind operation (120 holes) as shown in Appendix 'E', Fig.(11) to Fig.(15).

**(d) Solid Carbide Drills:** The Carbide-1 and Carbide-2 drills failed after a penetration distance of 7100 mm and 7050 mm respectively. The Carbide-3, Carbide-4 and Carbide-5 drills continued to drill satisfactorily until the fourth regrind cycle (120 holes) as shown in Appendix 'E', Fig. (16) to Fig.(20). Excessive wear was recorded after the second regrind probably due to improper regrinding. These drills had minimum wear and maximum drill life but the feedback from British Aerospace revealed that these drills suffered serious handling problems on the shop floor, due to their inherent brittleness, and significant cost problems.

It was noted that the Klenk drills had maximum flank wear which as stated above was generally due to wear being non-

symmetric on the two flanks. The random and premature failure rate of the Klenk drills led to poor performance and also unpredictability of drill life. The results of stage one of drill testing indicated that the Precision and Gandtrack drills were the two most promising in terms of drill life, freedom from handling difficulties, initial cost and procurement efficiency. The average flank wear determined for the three Gandtrack and Precision drills (Serial No: 3,4 & 5) after drilling 30 holes over four drilling cycles was determined to be 0.077mm and 0.061mm which was consider to be very small. It was decided to carry out further tests at the extended drilling cycle of 40 holes for Precision and Gandtrack drills.

#### **5.1.2 Stage two-Detailed Drill Inspection:**

The second stage of the drill testing was confined to the extended drill life testing of the Precision and Gandtrack drills which were considered to be the most consistent drills after stage-1 testing. Moreover they had lower flank wear, drilling thrust (Section 5.1.3 (a)) and better structural stability (Section 5.1.3 (c)) as compared to Klenk drills. In most practical situations in metal cutting, tool users prefer consistency rather than occasional long life. The outer corner wear width, the margin wear width, the chisel point wear width, the diametrical tolerance and the damage characteristics of the Gandtrack and Precision drills were inspected in detail after a rigorous drilling sequence of 40 holes per regrind

cycle. Compared with the preliminary tests, outer corner wear consistency was improved by accurate drill regrinding as a similar wear width was recorded for each corner after every drilling cycle. Nine regrinding operations were performed for the Precision drill before plug gauge failure whilst only six regrinding operations could be performed for the Gandtrack drill before the plug gauge failure. The performance of each drill is tabulated in Table (8). In terms of tool life, these results would suggest that the Precision drills were superior. However other parameters have importance such as hole quality and this will be discussed later.

A detailed comparison between outer corner wear, flank wear, margin wear, chisel edge wear, damage characteristics, dimensional tolerance and drill body profile is described as follows.

**(a) Outer Corner Wear:** The outer corner wear width of the flanks of both the Precision and Gandtrack drills were examined by scanning electron microscopy at the end of every drilling cycle (40 holes). The Precision drills had an almost symmetrical wear of  $60 \mu\text{m}$  on both the outer corners and the Gandtrack drills had asymmetrical wear of  $70 \mu\text{m}$  and  $30 \mu\text{m}$  on the outer corners as shown in Fig. (49). Whilst not of great importance, this was considered to be due to basic drill geometry asymmetry.

**(b) Flank Wear:** The asymmetric difference in the outer corner wear of the Precision and Gandtrack drills was also found to be present for the flank wear in the same

proportions.

**(c) Margin Wear:** The drill margin wear was difficult to examine. It was inspected by precise adjustment of the image intensity, the image contrast, the drill angle and by minimising specimen charging in the scanning electron microscope. A close-up micrograph of margin wear of Precision and Gandtrack drills, given in Fig. (50). indicates machining marks on the Gandtrack drill and evidence of wear which has removed the machining marks. For the Precision drill there is no evidence of machining marks but there is some indication of more general rubbing of the margin.

**(d) Chisel Edge Wear:** The chisel edge wear on the Gandtrack drill was of the same order as the Precision drills as shown in the scanning electron micrograph of Fig. (51). This indicated that the vertical thrust forces applied by the Gandtrack and Precision drills were of the same order.

**(e) Damage Characteristics:** Overall inspection of the Gandtrack and Precision drills using the SEM revealed deposition of carbon fibres and epoxy in the braze porosities of the carbide tips of Gandtrack and Precision drills as shown in Fig. (52). Most of the porosity was observed in the non-critical areas of the drill as shown in Fig. (47). It was observed that the size of the pores did not change with the penetration distance due to their location in the noncritical region of the drill which was not exposed to direct drilling forces.

**(f) Diametrical Tolerance:** The hole diameter was checked for tolerance using a carbide plug gauge after every 10 holes. The Precision drills failed after 10 drilling cycles, 9 regrinding cycles (40 holes/cycle) and covered a total penetration distance of 4000 mm as shown in Fig.(53). The Gandtrack drills failed after 7 drilling cycles, 6 regrinding cycles (40 holes/cycle) and covered a total penetration distance of 2800 mm as shown in Fig. (54). A comparison of the Precision and Gandtrack drill life is made in Fig. (55).

**(g) Body Profile:** The drill body profiles of all the drill points were examined by optical microscopy as shown in Fig. (56). The cross-sectional area of the drill point determined the torsional rigidity and together with length determined the buckling stability of the drill. Higher magnification of the drill profile at the outer corner revealed that the Klenk drills had a maximum side-clearance angle and the Precision drills had minimum side-clearance as shown in Fig. (57). The lower the side-clearance angle, the larger the contact area between the tool and the workpiece and the greater is the drill rubbing effect against the hole boundaries which results in higher torque.

### **5.1.3 Stage Three-Drill Performance Characterisation:**

#### **(a) The Dynamometer Tests:**

A drilling operation can be divided into 3 stages: increasing thrust in stage-1, reasonably constant thrust in stage-2 and reducing thrust in stage-3 as shown in Fig.

(58). The first stage commences as the drill tip touched the workpiece and finishes when the whole drill tip contacts the workpiece. The second stage lasts until the drill tip is just about to break through the workpiece. The third stage is completed when the drill lip completely breaks through the workpiece. At each of the three stages, different defects are generated in the workpiece. Delamination appears as an impulsive response in the first and third phase when the drill enters or breaks through the laminate. Fibre pullout and matrix cracking are attributed to the second phase of drilling when the drill is actually drilling the hole.

The maximum value of the drilling torque was observed when the drill exited from the workpiece as shown in Fig. (59/a). The magnitude of drilling torque tended to stay high even though the thrust force went to zero at the point of drill exit. The magnitude of this residual torque was seen to gradually approach a value of zero with additional time. The peak value of the drilling thrust force was observed when the drill entered the workpiece as shown in Fig. (59/b). No breakthrough transients were observed when the drill emerged from the bottom surface of the laminate. The frequency transients in the drilling forces were found to be higher than normally found in metal cutting due to the composite nature of the workpiece.

The dynamic response of all the types of drills in terms of peak values of thrust and torque at speeds of 2250, 2500, 2800, 3000 and 3250 RPM and feeds of 0.01, 0.025,

0.035, 0.05, 0.75 and 0.1mm/rev. were recorded and are tabulated in Table (9), Table (10), Table (11) and Table (12). The thrust and torque response of all the drills at a speed of 2800 RPM and for varying values of feed are given in Fig. (60). The maximum values of thrust and torque output at a speed of 2800 mm/Rev and varying values of feeds are shown in Fig. (61) and Fig. (62), respectively. The maximum values of thrust and torque response at the speed of 2800 RPM and feed of 0.05 mm/rev. for all the drills are given in Fig. (63). The maximum drilling thrust force was found for Klenk drills. Little difference was found in the thrust response for Gandtrack, Precision and Carbide drills. The minimum drilling torque was found for the Klenk drills. Generally the variation of thrust force with drilling distance was found to be much greater than the variation of torque with drilling distance for a given drill geometry. It was noted that the changes in the cutting speed did not have a profound effect on the thrust forces whereas the torque rose significantly with an increase in feed rate. This is consistent with general metal cutting observations. The maximum thrust, torque and outer corner wear with respect to the penetration distance (40 holes) for all the types of drills are shown in Fig. (64), Fig. (65) and Fig. (66) respectively.

**(b) Birefringent Photoelasticity:**

The patterns of the residual strains generated in the bottom ply of the CFC holes for each type of drill are

shown by isochromatic fringes in Fig. (67). The sequence of fringes is black, yellow, red, blue, green, yellow and red etc in increasing order of the residual strains towards the hole boundaries. The values of the residual strains were calculated using equation (2) and (3) for the given film and tabulated in Table (13). Graphical differentiation of the fringe order versus location gave the strains along the horizontal axis as shown in Fig. (68). Away from the hole, the strains were fairly linear but non-linearity existed close to the hole boundaries. When the results were analyzed, it was found that the magnitude of the residual strains are fairly realistic at the boundaries ( $1261 \mu\text{m/m}$  for Precision drill) but the corresponding stresses were found to be unexpectedly high (51.75 MPa). The relative comparison of the isoclines pattern revealed that the Precision drills led to generation of maximum residual strains and the Klenk drills generated minimum residual strain. The residual strains generated by other types of drill were intermediate.

**(c) Structural Analysis:**

The cross-sectional areas of the drill body profile in Fig. (56) were determined using a standard geometric technique. The area was divided into best fit combinations of rectangles and triangles and the polar moment of inertia was calculated by using the standard formulae as shown in Appendix 'D'. The values of the polar moment of inertia for the Klenk, Gandtrack, Precision and Carbide drills were

found to be  $36.66 \text{ mm}^4$ ,  $47.93 \text{ mm}^4$ ,  $53.17 \text{ mm}^4$  and  $64.48 \text{ mm}^4$ . The torsional rigidity, axial deflection, angular deflection, critical buckling loads of the drills at a speed of 2800 rpm and feed of 0.05 mm/rev. were determined and tabulated in Table (14). The results showed that for the given load conditions, Klenk drills had a torsional rigidity of  $3512 \text{ kN-mm}_2$ , a buckling stability of 6471N and were subjected to an axial strain of about  $5.36 \mu\text{m}$ . The torsional rigidity and the buckling stability of Gandtrack/Precision drills was about 1.4 times and 4 times the Klenk drill. The Solid Carbide drill had maximum overall structural stability.

A brief summary of the performance of Klenk, Gandtrack, Precision and Solid Carbide drills in terms of drill life, outer corner wear, hole quality, side clearance, residual strains, thrust and torque is tabulated in Table (15).

## **5.2 Fibre Pullout and Matrix Cracking:**

**5.2.1 Effect of Coolant on Hole Quality:** Scanning Electron microscopy of the holes drilled by the Gandtrack and Precision drills using coolant revealed that the quality of the holes drilled wet was superior to that for the holes drilled dry; this is shown in Fig. (69). When the plug gauge was used to check the diametrical tolerance of the holes drilled wet by the new Precision and Gandtrack drills, it was found the plug gauge failed to go through the 6th, 7th, 9th, 12th, 14th holes in quite a random manner. This unexpected observation was demonstrated to

British Aerospace team during their visit at Salford University.

### **5.2.2 Fractography of Damaged Fibres and Matrix:**

The extent, pattern and the failure modes of the damage caused by drilling in terms of fibre pullout and matrix cracking were examined in detail macroscopically and microscopically. The macroscopic examination of the holes drilled by the four types of drills revealed varying degrees of damage. The holes drilled by Precision drills showed maximum damage, followed by Carbide, Gandtrack and Klenk drills in the decreasing order of severity as shown in Fig. (70). Clearly the hole surfaces were composed of softened matrix material which had smeared over the hole boundaries due to the heat generated during drilling as shown in Fig. (71). The damage scars produced by the Precision drill were most pronounced and were observed to be regularly periodic in nature as compared to the other drills. They were spaced apart at  $45^\circ$  as shown in Fig. (72). The depth of the damage scar was found to be increasing from the apex toward the base of the triangle as shown in Fig. (73). The damage was mostly characterised by the right angled triangular shaped pits measuring about 1 mm in length and 0.2 mm base with its apex facing the direction of the drill rotation as shown in Fig. (74). The maximum depth of the pit for various drills was found to be as shown on the next page;

S/No	DRILL TYPE	DEPTH OF PIT, mm
1.	Precision	0.18
2.	Solid Carbide	0.15
3.	Gandtrack	0.12
4.	Klenk	0.1

For a specific drill, the severity of damage increased with total penetration distance of the drill. For a particular hole, the damage was found to be more pronounced in the lower portion of the hole, close to the drill exit plane. The microscopic examination of the fractured fibres showed multi-mode damage development due to the inherent anisotropy of carbon fibre composites and the complexity of the drilling dynamics. The surface morphology of the damaged fibres was studied to establish the failure mechanism. The extent and pattern of damage was found to be strongly dependent on the direction of cutting relative to the axis of the fibres lying at  $-45^\circ$ ,  $+45^\circ$ ,  $0^\circ$  and  $90^\circ$  orientations as shown in Fig. (75) a, b, c & d respectively.

**(a) Fibres at  $-45^\circ$  Orientation:** Fibres lying at a relative orientation  $-45^\circ$  degrees sustained maximum damage due to compressive forces imparted by the drill as shown in Fig.(76). Approximately 80 percent of the damaged region in the hole surface is attributed to this failure mode which determines the extent of the subsequent reaming operation. Damage appears to have started with fibre buckling and the introduction of buckling in a few fibres

in the cutting direction. The buckled fibres disrupted the stability of the neighbouring fibres in the hole having the same orientation and they in turn failed due to buckling. This damage mode propagated in the direction of drill rotation leading to the formation of deep triangular pits. The pits held bundles of micro-buckled fibres as shown in Fig. (77). The intact protruding fibres were found to be in a series of 'steps' that gave the fractured surface its terraced appearance as shown in Fig. (78). The post-failure diagnoses of the intact fibres in the pit showed a bi-modal fracture surface consisting of tensile and compression regions as shown in Fig. (79).

**(b) Fibres at +45° Orientation:** Microscopically the failure mode of +45° fibres was characterised by a fairly rough outcrop of fibres having a brush like appearance indicating that the fibres have been pulled out in tension as shown in Fig. (80). Microscopically the clean fractured surface of +45° fibres consisted of converging fanwise striations, termed radials, indicating the origin of fracture at 'O' as shown in Fig. (81). The network of convergence of radials in a number of fibres indicated the direction of origin of failure as shown in Fig. (82). The fibre failure surface was generally perpendicular to the fibre axis. Approximately 10 percent of the damaged surface area of the hole is attributed to this failure mechanism.

**(c) Fibres at 0° Orientation:** The fibres lying at a relative orientation of 0° to the cutting edge sustained minimum damage. They were stripped off their supporting epoxy matrix as shown in Fig. (83). This failure mode was characterised by the interlaminar shear failure of 0° fibres as shown in Fig. (84). This led to the formation of the smooth fibre and socket surfaces which are known as 'Cusps'. Minimum damage to the hole is attributed to this failure mechanism.

**(d) Fibres at 90° Orientation:** Fractographic analysis of the fibres lying at a 90° orientation was complicated by frequent obliteration of the original fracture by post-failure damage caused by the cutting edge as shown in Fig. (85). In addition, deposition of epoxy on the fractured surface of the fibre obscured the detailed structure. Despite these limitations, it was observed that generally most of the 90° fibres were chopped in shear during the cutting action. As the cutting edge was wearing out, its radius of curvature increased, leading to a significant superposition of bending forces which resulted in propagation of longitudinal cracks along the fibres. This led to the generation of relatively rough hole surfaces.

**(e) Internal Delamination:** The combination of bending forces with tensile/compressive forces and shear force of the drill leads to fibre flexure. This created three

dimensional interlaminar stresses at the free edge of the hole which consisted of a shear stress component and a normal stress component. Whereas the interlaminar shear stress was instrumental in fibre pullout and matrix cracking, the interlaminar normal stress led to internal delamination which was pronounced in the intervening region between the  $90^\circ$  and  $-45^\circ$  plies as shown by the diagonal crack in Fig. (86). Optical microscopy of the CFC specimen revealed a resin rich region between fibre interlayers as shown in Fig. (87). The interlayer region was found to be a potential site for promotion of internal delamination between  $-45^\circ$  and  $90^\circ$  plies.

**5.2.3 Summary of CFC Fractography:** The scanning micrograph shown in Fig. (88) presents a brief summary of all the failure modes in CFC drilling. The  $0^\circ$  were stripped of their supporting epoxy and they failed by interlaminar shear as shown by arrow 'A'. The  $90^\circ$  fibres were mostly covered by smeared epoxy as shown by arrow 'B'. The  $-45^\circ$  fibres were characterised by damage pits carrying microbuckled fibres as shown by arrow 'C'. The pulled out  $+45^\circ$  fibres are shown by arrow 'D'. Internal delamination can be seen in the interlayer region between the  $-45^\circ$  and  $90^\circ$  fibres, as shown by arrow 'E'. The most critical mode appears to be the shear crippling of  $-45^\circ$  fibres close to interlayer region with  $90^\circ$  fibres.

### 5.3 Material Properties of Cemented Carbides used for the Sliding Tests:

The Scanning Electron Microscopy revealed that the microstructures of Kennametal F285, Krupp THR and Sandvik H10F cemented carbides were quite different as shown in Fig. (89). The grains were uniformly distributed for Kennametal F285 and Sandvik H10F materials but were not uniformly distributed for the Krupp THR material. An examination of the magnified images of cemented carbide specimen on a C.C.T.V. monitor screen revealed that the interlayers between carbide grains were  $0.14 \mu\text{m}$  for the Kennametal cemented carbide, an intermediate thickness of  $0.16 \mu\text{m}$  for the Sandvik cemented carbide and  $0.17 \mu\text{m}$  for the Krupp cemented carbide. The observations also showed that the average carbide grain sizes for Kennametal, Sandvik and Krupp cemented carbides were  $0.83$ ,  $0.98$  and  $1.07 \mu\text{m}$  respectively. The microstructures of all the drill tips were found to be similar in terms of grain distribution as shown in Fig. (90). The grain sizes of Klenk, Gandtrack, Precision and Carbide drill tips were found to be  $1.04$ ,  $1.08$ ,  $1.04$ ,  $1.02 \mu\text{m}$  respectively indicating nominal differences.

The averaged Vickers hardness tests over five readings at different locations for the Kennametal F285, Krupp THR and Sandvik H10F cemented carbides specimen were found to be 1725, 1580 and 1665 HV respectively as shown in Table (16). For the Palmqvist test the indentations were made by a diamond indenter in the Vickers hardness tester at the

applied loads of 20, 30, 40 and 60 Kg. The crack lengths at the four corners of the diamond indenter were recorded in Table (17) and total values were plotted with respect to the indentation load as shown in Fig. (91). The Palmqvist fracture toughness parameter for the Kennametal material i.e. 681 KN/m was found to be lower than that of the averaged Krupp and Sandvik fracture toughness i.e. 1186 KN/m. The bulk fracture toughness was calculated by using equation (7) in Section (3.5). The average value turned out to be 133 J/m<sup>2</sup> for Kennametal specimen and 221 J/m<sup>2</sup> for Sandvik H10F and Krupp THR. The experimental data regarding grain size, cobalt layer thickness, hardness, Palmqvist fracture toughness and bulk fracture toughness are tabulated in Table (18). The data regarding the physical and mechanical properties of the cemented carbides found in the literature/provided by the manufacturers are given in Table (19).

Sliding tests were performed to determine independently of drilling, the effect of physical parameters on wear characteristics. The lathe tests led to formation of deep cuts in the CFC plate without a significant wear pattern on the carbide rod. Lathe wear tests of hexagonal cross section carbide rods with CFC generated excessive vibrations which led to inaccurate results.

The heat intensive rubbing of the CFC plate edges with the carbide rod led to delamination of the plate in the Kearney and Trecker wear test as shown in Fig. (92) and by the arrow in Fig. (44). Although delamination was controlled

by flooding the contact area with the coolant, it prevented the development of a prominent wear scar on the carbide specimen. In the third independent wear test, the pin-on-disk rubbing test, wear was detected on the hemispherical end of the carbide pin. The diameter of the worn region was measured by an optical microscope and was plotted against sliding distance as shown in Fig. (93). The pin-on-disc sliding wear test indicated that the Kennametal material had the minimum wear rate whilst the Krupp and Sandvik materials had similar higher wear rates. Macroscopic examination of Krupps material using SEM showed cracks and microfracture on the wear scar as shown in Fig. (94). Microscopic inspection of the worn regions on all the specimens indicated that sliding action of the cemented carbide surface over the CFC plate led to the preferential removal of cobalt in varying degrees as shown in Fig. (95). The uprooting of tungsten carbide grains was more prominent in the Krupp specimen as compared to the rest of the specimens as shown in Fig. (95/a). Irregular grain sizes can also be seen in the Krupp specimen. An example of typical cobalt removal is shown in Fig. (95/b). The Kennametal F285 specimen in Fig, (95/c) showed minimum signs of surface damage as compared to Sandvik H10F and Krupps THR specimens.

## Chapter six

### Discussion

#### 6.1 Drill Performance in Drilling CFC:

Experimental relationships have been determined between flank wear, drill life, hole quality and cutting forces for Klenk, Gandtrack, Precision and Carbide drills when drilling CFC.

##### 6.1.1 Drill Wear and Drill Life:

The width of the wear land on the flank surface has been found to be a maximum at the outer corner of the cutting edge. The outer corner is subjected to the maximum angular velocity, torque and abrasion upon impingement with the CFC hole boundary. Scanning electron microscopy revealed that the outer corner wear was characterised by the formation of a triangular wear pattern. The extent, form and shape of this pattern determined the severity of the cutting action of the drills. The drills having a pronounced triangular pattern had maximum outer corner wear and produced a good cutting action i.e. good quality holes but a relatively poor tool life. The drills having a less well defined triangular pattern and lower flank wear showed evidence of margin rubbing against the CFC hole boundaries i.e. poor performance of the drill in terms of the rubbing action on the fibres but better performance in terms of the drill life.

It would be reasonable to suppose that high flank wear

correlates with high margin wear i.e. a drill that requires regrinding more frequently is also likely to produce an undersized hole more quickly which, by definition causes a reduction in the useful life of the drill. Furthermore uneven flank wear will tend to lead to uneven margin wear due to uneven margin forces and that will probably tend to give unpredictable reduction in hole diameter and, hence, variable useful life for the drill. It was found that Klenk drills had the maximum flank wear and this was uneven. This led to unpredictable plug gauge failure which is a bad characteristic for any drill.

The structural analysis revealed that the lower buckling stability of the Klenk drills may have been the reason for non-uniform wear and unpredictable plug gauge failure. The comparative analysis of the amount of outer corner wear for the other three drill types showed decreasing wear and increasing drill life for Gandtrack, Precision and Carbide drills respectively. The thorough and repeated drilling tests of Gandtrack and Precision drills showed that the Gandtrack drill could be used for 7 drilling cycles and the Precision drills for 10 drilling cycles during the extended drill life testing of 40 holes per cycle. The Carbide drills were considered to be unsuitable for production use due to their high cost and inherent brittleness which with careless handling in a production environment would result in chipping.

### 6.1.2 Hole Quality:

The cutting efficiency of the drill determined the hole quality (non-geometric) in terms of fibre pullout and matrix cracking. The sharp cutting edges performed efficient cutting action, generated lower heat flux and good hole quality. The drills which rubbed most against the CFC hole walls and created maximum damage pattern wore the least. This can be explained as follows. A drill which has a good cutting action (low torque) will produce a good quality hole. However this type of drill will suffer most from outer corner wear because of local force and hence heat generation. This in turn leads to the major cutting edge producing an undersized hole and the remaining material has to be removed by the margins which results in margin wear. At the same time, tools which cut efficiently always exhibit more flank wear because of localized heating.

The hole quality deteriorated from the drill entry plane towards the drill exit plane due to accumulated drill wear which led to the generation of higher temperatures. As the drilling torque also increased towards the drill exit plane, this led to increased fibre pullout and matrix cracking. Maximum hole damage was observed for the fibres loaded compressively at an angle of 45°, 135°, 225° and 315°. At these angles, the tangential force and the torque reached maximum values and caused maximum damage.

### 6.1.3 Photoelasticity:

The birefringent photoelasticity results showed different levels of strains generated by the four types of drills which, as expected, tended to zero at a distance three times the hole radius from the hole boundaries and that this increased steadily towards the hole boundaries where the maximum values of strain were recorded. The strain values at the hole boundaries were found to be fairly realistic but the magnitude of the corresponding residual stresses were found to be of a very high magnitude and close to the hole boundaries a nonlinearity was observed. The nonlinearity may have been due to appreciable shear deformation of resin at the hole boundaries which affected the stress-strain relation and resulted in exaggerated values of corresponding stresses for a given value of strain. Moreover it appears that the shear deformation of resin affected the stress optic coefficient. Changes in stress optic coefficient ( $C_p$ ) due to the drilling temperature altered the refractive index of the film. This led to invalidation of the basic assumption regarding the constant value of stress optic coefficient and the elastic nature of the material which resulted in highly exaggerated magnitudes of residual stress for the given strain at the hole boundaries. This technique however showed that the strain distribution followed the same pattern that was found by C. Soutis around a CFC T800/924C hole at Cambridge University in 1990 as shown in Fig. (15) [54]. The test was therefore found to be useful in establishing a ranking of

the strains generated by the four types of drills. These results revealed that Klenk drills, which had the best cutting characteristics induced minimum strains in the outer CFC ply, gave the best hole quality but had a limited life. Although the Precision drills had the maximum life, their rubbing action, characterised by the deep pits on the hole boundaries led to maximum strain and poor hole quality. The Gandtrack drills gave an intermediate hole quality with a medium drill life.

#### **6.1.4 Cutting Forces:**

Although the drilling thrust force and torque are closely related, the magnitude of the thrust force was dominated by the amount of drill wear and the magnitude of the torque was influenced by the elastic/plastic point of contact of the outer drill corner with the carbon fibre. As the drill wears, the thrust force rises sharply with only a marginal increase in torque. The dynamic response of the drills revealed that the holes having superior hole quality were drilled with the lowest drilling torques. The Klenk drills had good hole quality because they exerted minimum torque on the fibres. Their higher thrust value led to generation of maximum flank wear. On the other hand, the Precision drills, having the lowest flank wear rate were drilled with relatively lower thrust forces but higher torques. The measured thrust forces and torques of the Gandtrack drills were intermediate between the Klenk and Precision drills. When the drill penetrated through the lower surface of the

workpiece, a large residual torque was observed on the drill and extensive fibre pullout and matrix cracking was observed in the CFC hole. The thermo-mechanical drill loading of the workpiece generated dynamic visco-elastic /plastic strains which led to the thermal swelling of the CFC hole. The inward radial force, that is primarily applied by the relief side of the drill in the first and second drilling phase, is applied by the drill lips and the margin in the third phase due to its cutting/rubbing action against the swollen CFC hole. After the third stage, the radial force appeared as a residual torque that fluctuated with the relative orientation of the tool to the carbon fibres.

#### **6.1.5 Structural Analysis:**

At the drilling speed of 2800 RPM and feed of 0.05 mm/rev., all the drills had sufficient margin of safety (critical buckling load/applied load). However the Klenk drills had the minimum margin of safety. For manual drilling with the possibility of high feed rates, and hence high thrust, the Klenk drills would be most liable to fail due to buckling. The lower degree of micro-torsional rigidity and buckling stability of Klenk drills as compared to other drills might have lead to its asymmetric drill wear and unpredictability in terms of drill life. Furthermore the poor structural stability of Klenk drills might have led to poor diametrical tolerance of the holes. The torsional rigidity and buckling stability of Gandtrack/Precision drills was

found to be greater than that of the Klenk drill primarily due to a higher polar moment of inertia. The solid carbide drill had maximum torsional rigidity and buckling stability due to its high polar moment of inertia, superior material properties and shorter drill length. The holes drilled by the Solid Carbide drills could be expected to be better in terms of dimensional tolerance.

## **6.2 Fibre Pullout and Resin Cracking:**

### **6.2.1 Effect of Coolant on Hole Quality:**

The thermal conductivity of CFC is  $4.19 \text{ W/m}^\circ\text{K}$ , of H.S.S. is around  $50 \text{ W/m}^\circ\text{K}$  and that of cemented carbide about twice that of H.S.S. As CFC's are poor conductors of heat, heat is built up in the hole. The accumulated heat is conducted by the drill to the machine spindle and the body. The application of water based coolant Clearcent G.B.A. in the drilling region took away the drilling heat and improved the hole quality in terms of fibre pullout and matrix cracking. This can be explained by reference to the effect of temperature on the epoxy. The higher the temperature, the softer the epoxy and subsequently the greater the fibre instability due to microbuckling.

The application of coolant lowered the drilling temperatures but increased the degree of water penetration which led to the dimensional changes of the hole and random plug gauge failures. It appeared that the addition of rubber additives in epoxy made it more sensitive to the effects of moisture absorption and high temperatures

generated during drilling. Wet machining of the composites having modified epoxy is therefore not favoured due to its influence on the material properties.

#### **6.2.2 Damage Mechanism of Fibres and Matrix:**

The drilling temperature in CFC has been reported by Konig to be around 300°C [100]. This drilling temperature by far exceed the softening temperature of epoxy-924 which has been reported to be 210°C [19]. This is supported by the evidence of the softened epoxy on the hole boundaries. Generation of drilling heat softened the matrix, reduced its shear modulus and relieved the radial stresses exerted over the fibres. The matrix was unable to transfer efficiently the local strain perturbations to the fibres and failed to provide sufficient stability to the fibres against the cutting action of the twist drill. This may have resulted in premature fibre debonding, slipping and fracture at some arbitrary distance when the applied drill load exceeded the ultimate strength of the fibre and the fibres fractured in compression, tension or shear depending on the relative orientation of the fibre with respect to the cutting edge of the drill.

**(a) Failure Modes of Fibres:** The outer corner of the drill exerted compressive loading on the -45° fibres and fractured them by pushing them down. The sequence of failure mechanism suggest that the first response of the fibre was to debond and slide in shear due to the impact

of the cutting edge. The presence of the drilling-induced heat resulted in a rapid deterioration of the matrix shear modulus and a marked reduction of the compression strength of the fibres. This changed the damage mode from interlaminar shear to the one governed by the fibre instability which follows the same trend as shown in Fig. (8) at a temperature exceeding 100°C. This damage mode is characterised by the microbuckled and kinked fibres lying on the base of the triangular shaped pits. The damaged area grew across the width and the height from a small nucleus of fractured fibres to a deep pit. Simultaneously the kink band rotated, tilted and realigned itself in the direction of the cutting force. This induced elastic and plastic strains in the epoxy matrix and appears to have generated cracks in the damage pit region. Deposition of softened epoxy on the holes made it difficult to examine the matrix cracks along the fibre interface. Formation of damage pits stopped when the drill loading was insufficient to cause buckling in the fibre due to its different relative orientation.

Fractographic analysis of the surface of intact fibres in the pit revealed bimodal failure, consisting of a tensile and a compression region separated by a neutral axis. The tensile portion of the fibre surface, characterised by the formation of 'radials' (a network of fanwise striations) suggest that the tensile crack was initiated at the outer surface that propagated inward as shown in Fig. (96). The portion of the fibre surface under compression initiated

the simultaneous propagation of kink bands inward in the opposite direction as shown in the same figure. When the propagating fronts of the tensile crack and the kink bands met, then a ridged fractured surface having different bilateral textures was formed; the region resulting from tensile fracture exhibited a smooth topography, while the compressive failure zone exhibited a rough topography. This type of fractured surface showed buckling failure of the fibres and suggests that the cutting edge exerted compressive load on the fibres.

Maximum damage to  $-45^\circ$  fibres which led to the generation of damage pits can also be explained in terms of three dimensional interlaminar shear stress around a hole that is subjected to compressive loading as shown in Fig. (14). The peak value of the shear stress is exerted on the  $\pm 45^\circ$  fibres at the distance of 0.05 radius from the hole boundaries. As the radius of the holes drilled is of the order of 3.00 mm, the peak value of shear stress occurs at the value of  $0.05R$  i.e. 0.15 mm. This corresponded to the depth of the hole pits (0.1 mm-0.2 mm) observed during the present experimental investigation.

The outer corner of the drill fractured the  $+45^\circ$  fibres by pulling them out. The tensile loading by the drill resulted in the outcrop of  $+45^\circ$  fibres. The interlaminar shear stresses between the fibres and the matrix led to the fibres debonding, sliding and fracture in tension. It appears from Table (3) that the tensile strength of carbon fibres is about 60-70% more their compressive strength. The

carbon fibres have superior tensile strength in the laminate (2.3-2.4 GPa) as compared to its compressive strength (1.5 GPa). The +45° fibres are subjected to a combination of tensile/bending loading and combination of compressive/bending loading is exerted on -45° fibres. Better tensile strength of carbon fibres might have led to occasional tensile failures of the +45° fibres which were subjected to tensile drill loading. Poor compressive strength of -45° fibres might have led to a more frequent compressive failures of -45° fibres which were subjected to compressive drill loading in the hole boundaries.

For cutting parallel to the fibres (0°), a surface with visible fibres, stripped of the supporting matrix was produced. It suggested that in case of 0° fibres, the matrix rather than the far more resistant fibres were cut. As the matrix requires lower cutting forces than the fibres, it appears that the lowest cutting forces must have occurred when fibres were cut parallel to their orientation.

### **6.2.3 The Mixed Mode; Pullout Initiated Delamination:**

In drilling, the thermal and mechanical loading affects the interlaminar stresses at the free edge of the hole boundaries. The magnitude and direction of interlaminar stresses determines the initiation of drilling defects in CFC; i.e. delamination, fibre pullout and matrix cracking. It was observed during the sectioning studies that drilling induced two types of damage mechanisms in the composite

laminate; i.e. the in-plane (X-Y axis) damage mechanism and the out-of-plane (Z axis) damage mechanism as shown in Fig. (40). The interlaminar normal stress in the out-of-plane direction led to separation of the +90° and -45° plies. Separation of plies was also found to be dominant in the region close to the drill exit plane. The tensile nature of the interlaminar normal force led to delamination resulting in mode-I (peel) fracture. The presence of microbuckled -45° fibres close to the resin rich interlayer may have weakened and promoted internal delamination between the -45° and +90° layers. This observation was found to be consistent with Reifsnider's [50], who determined that when a quasi-isotropic layup is subjected to thermomechanical loading, maximum normal interlaminar stresses exist at the -45°/90° interlayer.

The interlaminar shear stresses play an important role in pulling out or pushing down the fibres in the (x,y) plane. If the interlaminar shear stress is positive, the fibre is subjected to tensile stresses and is pulled out. If the interlaminar shear stress is negative, the fibres are subjected to compressive stress and are pushed down in the axial direction. The first response of the fibre to the compressive or tensile drill loading is to slide in shear resulting in mode-II (shear) fracture.

Mixed mode fracture took place as a result of a combination of mode-I fracture, due to delamination of -45°/90° interlayer, and the mode-II fracture due to the microbuckling of -45° fibres. The interlaminar normal

stress attributed to mode-I fracture (peel) and the interlaminar shear stress attributed to mode-II fracture (shear) determined the stability of the crack caused by microbuckled  $-45^\circ$  fibres at the  $-45^\circ/90^\circ$  interlayer.

#### **6.2.4 Identification of Factors Governing the Fibre Damage:**

Many factors are found to be important in the generation of delamination, fibre pullout and matrix cracking. Drills with higher axial thrust having greater point angles are considered to generate higher interlaminar normal stress and delamination. Drills having lower/negative rake angles generate higher drilling torques and lead to extensive fibre pullout and matrix cracking. Drill geometries which have a smaller point angle ( $60^\circ$ - $65^\circ$ ) and a high helix angle, ( $30^\circ$ ) have maximum cutting edge stability to withstand abrasive carbon fibres and are ideally suited for drilling quality holes in CFC. These drill geometries, however will drastically reduce the drill life of tungsten carbide tipped drills. This study revealed that good quality holes and maximum tool life are contradictory drilling requirements. The ideal combination of good hole quality with long tool life is possible with materials which can be contoured for high positive rake/helix angles and small point angles and at the same time having maximum abrasion resistance. The reason that these materials have so far not been used is that in a shop floor environment with less than perfect tool care they are easily damaged which with their high cost renders them uneconomical.

Maximum abrasion resistance and tight geometric features are possible with PCD tipped drills which can be contoured for complex geometric configurations. The ceramic composites comprising an alumina matrix reinforced with silicon carbide whiskers have also been very recently proposed (March, 1991) as a cutting material for CFC's [100].

In terms of workpiece materials, the thermal sensitivity of epoxies must be improved to sustain higher drilling temperatures without sacrificing toughness and damage tolerance. The CTBN modified epoxies are considered to be more sensitive to heat and more readily lose their dimensional tolerance than the unmodified epoxies. Improper resin modification to increase the temperature resistance of epoxy will make it overly brittle which is an undesirable feature in aircraft structures. It is possible to improve the temperature resistance of epoxies without sacrificing toughness by selectively interleaving unmodified epoxy (having greater temperature resistance) in discrete layers of high shear strength polymer at critical locations i.e. holes. This would cause significant manufacturing and cost problems and is unlikely to be commercially successful. Investigations at NASA Ames Research Centre [25,26] have shown that brominated CTBN modified epoxy systems have better overall performance in terms of toughness, thermal resistance and ease of manufacture than the CTBN modified epoxies; this possibility needs investigating.

Most of the damage to the hole boundaries occurred due to the poor buckling stability of the carbon fibres. T-800 carbon fibres have a high degree of compressive strength in monolithic form (8 GPa) as indicated in Table (3) but when they are impregnated with epoxy 924C resin, the compressive strength decreases to 1.5 GPa as given in Fig. (7). In a drilling situation, i.e. high temperature environments, there is drastic deterioration of the compressive strength of CFC as indicated in Fig. (8) which leads to premature microbuckling. Premature microbuckling of carbon fibres in CFC holes indicated that there was incomplete utilisation of the compressive strength of carbon fibres in the laminate and that the carbon fibres fractured much before their intrinsic compressive strength was realised. Furthermore, increased axial preferred alignment and reduced transverse interfibrillar coupling in high modulus T-800 carbon fibres seems to have initiated the microbuckling failure by a shear mechanism at the interface. The shear initiated microbuckling led to shear crippling of  $-45^\circ$  carbon fibres in CFC holes.

Any improvement in compressive strength of the carbon fibres is expected to lead to improvement in the hole quality but this, in turn, also increases the hardness of carbon fibres. The higher degree of hardness of carbon fibres limits drill life which is an undesired drilling requirement. Whilst past efforts in this area have resulted in improving the compressive strength of T-800 carbon fibres (8 GPa) in monolithic form by about 270% as compared

to T-300 carbon fibres (2.88 GPa), poor translation of the compressive strength of T-800 carbon fibres in the T800/924C laminate (1.5 GPa) led to deterioration of compression strength by more than 500% and caused microbuckling in CFC holes. Significant research efforts are therefore required in the area of better translation and retention of compressive strength of carbon fibres in epoxy matrix systems at high temperatures. Over the last decade, whilst much work has been done to improve the fracture toughness of epoxies, little advancement has been made to improve their temperature sensitivity; this area also needs to be looked at in greater detail.

### **6.3 Material Classification:**

The effects of microstructure and physical/mechanical properties on wear characteristics of Kennametal, Krupp and Sandvik cemented carbides were investigated. The following are the major findings about their wear resistance.

#### **6.3.1 Wear Mechanism:**

Scanning electron microscopy of the worn surfaces on the Krupp, Sandvik and Kennametal cemented carbide specimens rubbed against CFC during the pin-on-disc sliding test suggest that the wear process was the result of the interaction of a number of mechanisms. Interpretation was made difficult by what appeared to be a thin film of cobalt covering the surface, nevertheless it could be observed that both polishing and removal of tungsten carbide grains

had taken place.

The following sequence of events may be postulated: an initial high rate of wear due to the removal of damaged tungsten carbide produced by the final grinding process followed by a steady state process which involves the following mechanisms:

First, cobalt is removed from between the tungsten carbide grains to a limiting depth, governed by the cobalt film thickness. The exposed tungsten carbide grains would then be subjected to abrasion by both the CFC and any wear debris trapped in the contact area. The exposed tungsten carbide grains would have been subjected to high shear stresses which could have resulted in brittle fracture, the resulting debris contributing to the abrasion mechanism. At some stage depending on the shape, size and remaining cobalt contact area, tungsten carbide grains would be pulled out rather than completely abraded away.

The role of the removed cobalt is difficult to assess. In the metallic form, it could act as a lubricant but once oxidised it would have abrasive properties.

The rate of wear would be a complex interaction between the rate of cobalt removal, (dependent on cobalt film thickness) and those characteristics of the tungsten carbide grains which determine the rate of abrasion and brittle fracture.

### **6.3.2 Effect of Physical Parameters on Wear Properties:**

**(a) Microstructure:** The removal of cobalt from the test specimen is the result of an abrasion action by the carbon fibres in the CFC. The thinner the cobalt interlayer, the greater is the wear resistance of the cemented carbide. The abrasion resistance is thereby inversely proportional to the cobalt layer thickness. As the cobalt layer thickness of the Kennametal, Sandvik and Krupp materials is in an increasing order, their abrasion resistance would be expected to be in decreasing order. The removal of carbide particles was governed by tearing away of the carbide grains due to lack of support by the surrounding cobalt. The wear rate varied with the grain size. As the carbide grain size decreased, the thickness of cobalt layer decreased for a given value of cobalt. Hence the finer the grain size, the more is the surface area, the lesser the cobalt thickness and the greater is its wear resistance. The Kennametal carbide, having the finest and most uniform grain size had the maximum wear resistance followed by the Sandvik and Krupp carbides in increasing order of grain sizes and decreasing wear resistance respectively.

#### **(b) Hardness:**

In cemented carbides, hardness is principally determined by the grain size of tungsten carbide and the cobalt content. The finer grain size of the Kennametal cemented carbide can be used to explain its high hardness and wear resistance as compared to the Krupp and Sandvik cemented

carbides. The slightly reduced cobalt content in the Sandvik cemented carbide compared with other cemented carbide explains the intermediate hardness of this carbide. The Krupp cemented carbide had the minimum hardness for its relatively bigger and non-uniform grain size.

The experimentally determined results regarding the hardness of Kennametal F285, Sandvik H10F and Krupp THR cemented carbides (1725 HV, 1665 HV and 1580 HV respectively) revealed that they had higher magnitudes but followed the same sequence as the values reported in the literature or quoted by the manufacturers (1626 HV, 1550-1650 HV and 1450 HV). It indicated that the manufacturers of Kennametal and Krupp cemented carbides had quoted the lower values of hardness.

**(b) Toughness:**

From the Palmqvist toughness values, it can be seen that the toughness decreases with decreasing cobalt content and grain size. The lowest toughness values for the Kennametal cemented carbide is attributed to its finest grain size, resulting in a greater surface area for cobalt impregnation and a thinner cobalt interlayer. The effect of the reduced cobalt content of the Krupp cemented carbide is balanced by its larger grain size and the combined effect gave it the same toughness ranking as the Sandvik cemented carbide which had a relatively higher cobalt content and a smaller grain size as compared to the former.

### 6.3.3 Wear Testing:

The independent lathe wear test led to excessive vibrations and the machining centre test led to the delamination of the CFC plate. No meaningful results were obtained from these two tests. The Pin-on-Disc sliding test, however led to useful results. The Pin-on-Disc sliding tests, which were completely independent of the drilling tests revealed that the Kennametal F285 cemented carbide had superior performance in terms of wear rate. This is attributed to its fine and regular grain size which gave it high hardness and wear resistance. The wear rate of the Sandvik H10F cemented carbide was found to be almost of the same order as the Krupp THR cemented carbide. The Sandvik cemented carbide had a fine and regular grain size and had a higher hardness value compared to the Krupp cemented carbide. The non-uniform, irregular and bigger grain size combined with the relatively lower cobalt content of the Krupp cemented carbide led to the generation of cracks on the sliding surface which in a drilling situation could lead to catastrophic failure.

Of the cemented carbides tested, only Krupp was used for the Klenk drills. The other drill manufacturers used drill materials for which rubbing tests were not carried out. The bigger and nonuniform grain size of Krupp cemented carbide might have been the reason for maximum wear and unpredictable life of Klenk drills.

## Chapter Seven

### CONCLUSIONS

7.1. An extensive study has been carried out on the drill life testing of cemented carbide tipped and solid cemented carbide drills when drilling holes in carbon fibre composites. These studies have shown that drill machinability of carbon fibre composites can be described in terms of drill life and hole quality in terms of hole dimensions and fibre pullout/matrix cracking. On the basis of drill life, the Precision drills showed the best performance. On the basis of hole quality, Klenk drills showed minimum fibre pullout and matrix cracking but they had unpredictable drill life, poor torsional rigidity and buckling stability as compared to other drills. The Gandtrack drills, which were cheapest to buy and convenient to procure, showed a good compromise between the other two carbide tipped drills tested. The solid carbide drill showed the best drill life but from an economic viewpoint was too expensive and had poor handling qualities and was therefore not considered to be suitable for industrial applications.

7.2. The application of coolant was found to improve hole quality in terms of reduced fibre pullout and matrix cracking but was found to lead to more frequent plug gauge failure of CTBN modified epoxies due to dimensional changes of the hole caused by water absorption.

7.3. Measurements of drilling torque have shown that drilling torque is closely related to hole quality. Lower drilling torque leads to improved hole quality in terms of fibre pullout and matrix cracking.

7.4. Measurements of drilling force show that the thrust force is related to the extent of flank wear. Higher amounts of flank wear lead to higher thrust force values.

7.5. A study of the fibre pullout and matrix cracking on the hole surface of the carbon-epoxy T800/924C system has shown that the CFC failure mechanism is highly directional in nature. The major failure mechanism in CFC drilling is shear crippling of  $-45^\circ$  fibres due to microbuckling and delamination at the interlayer region close to the drill exit plane. The heat generated during drilling reduces the shear modulus of the matrix and the compressive strength of the carbon fibres which leads to their microbuckling. The microbuckling failure of the fibres is due to compressive stress exerted by the outer corner of the drill on the fibres. The high compressive strength of carbon fibres in monolithic form is not reflected in the laminate which is a prerequisite for drilling quality holes in this composite system. The improved toughness of the 924C resin has resulted in a sacrifice in the elevated temperature shear modulus which has had an adverse effect on the drilling performance.

7.6. The present work has shown that improved hole quality in terms of fibre pullout and matrix cracking can be achieved by optimising drill design and operating parameters, increasing the compressive strength of the carbon fibres in the laminate, improving fibre processing techniques and perhaps more importantly, improving the resin chemistry for high temperature resistance in drilling.

7.7. Independent wear tests have been carried out on three types of cemented carbides. The superior wear resistance of the Kennametal F285 compared to the Sandvik H10F and Krupp THR is due to the fine, high strength microstructure and associated high hardness. The Sandvik H10F had intermediate performance in term of hardness and microstructure. The Krupp THR was found to have an irregular microstructure and the lowest hardness which led to its poor wear resistance.

## Chapter Eight

### RECOMMENDATIONS FOR FUTURE WORK

8.1 From the present work carbide properties and drill geometry have been shown to affect drill life and hole quality. Work should now be carried out on combining the optimum carbide type with optimum drill geometry and configuration for improved performance.

8.2 It has been found that the drills which had longer life produced bad hole quality in terms of fibre pullout and matrix cracking. The drills with keen cutting edges produced good hole quality but had limited drill life. It is possible to achieve the optimum combination of good hole quality and longer drill life by drilling with harder materials optimised for CFC drilling i.e. PCD tipped drills. Further drilling tests and cost analysis per hole is recommended using PCD tooling.

8.3 The brominated CTBN modified epoxy systems have reported to result in a tremendous improvement in toughness while providing a good hot/wet compressive strength. This makes them a potential candidate for applications in the aircraft structural members and a material that is friendlier to manufacturing operations. It is recommended that drilling tests should be carried out on this material system to determine its suitability from the drilling point of view.

8.4 Preliminary attempts have been made to measure drilling induced residual stresses using birefringent photoelasticity. Further research efforts are needed to refine and develop this technique to measure residual stresses in CFC.

8.5 A single notch leads to a significant reduction of the compressive strength of a laminate. Drilling induced defects generate local stresses within stress concentrations which affect the notch sensitivity. It is important to take into account these defects when designing CFC structural components.

The effect of defects in isolated holes in toughened epoxies and their interaction with other holes under various load configurations need to be studied in order to evaluate their effect on design considerations and production processes.

## REFERENCES

- [1] Huber, J. and Micillo, C.; Innovated Manufacture for Automated Drilling Operation; Proceeding of Autofact West, Volume 2, p292-316, (1980).
- [2] Tipnis, V. A.; Influence of Metallurgy on Hole Making Operations; Pub. ASTM, (1978).
- [3] Kahng, C. H.; Increasing Hole Making Efficiency; The Carbide & Tool Journal, p10-15, May-Jun 1983.
- [4] Pimm, J. H.; Defects Experienced in the Production of Advanced Composites Outer Wings of A-7D Attack Aircraft; ICCM2, p1621-1635, (1978).
- [5] Jones, R. M.; Mechanics of Composite Materials; Pub. McGraw-Hill Book Company, (1975).
- [6] Ashby, M. F.; Advanced Materials and Predictive Design; Phil. Trans. R. Soc. London, A 322, p393-407, (1987).
- [7] Composite Materials in Aircraft Structures, Metals and Materials, June (1985).
- [8] Watts, W., Phillips, L. N. and Johnson W.; High Strength, High Modulus Carbon Fibres; The Engineer, p815-816, May (1966).
- [9] Simentz, R. F. ; The Influence of Aerospace Performance Requirements on Development of Advanced Structural Materials; Phil. Trans. R. Soc. London, A322, p323-333, (1987).
- [10] Aerospace Applications of Advanced Materials; The Royal Aeronautical Society Conference, London; March (1989).

- [11] Middleton, D. H.; Composite Materials in Aircraft Structures; Longman Scientific and Technical; (1990).
- [12] Departmental Handout, Course AE-650; Department of Aeronautical Engineering, Wichita State University, Kansas, USA; January (1987).
- [13] Evans, R. E. and Masters, J. E.; A New Generation of Epoxy Composites for Primary Structural Application: Materials and Mechanics; Toughened Composites; ASTM STP 937, p413-436, (1987)
- [14] Plastics for Aerospace Vehicles; Department of Defence Publication MIL-HDBK-17A, USA, September (1973).
- [15] Hoskin, B. C. and Baker, A. A.; Composite Materials for Aircraft Structures; AIAA Education Series; (1984)
- [16] Taylor, G.; Carbon Fibre Composite Research-Contents of Volatiles in Epoxy Resin; M.S. Thesis, University of Leicester, UK, October (1983).
- [17] Trewin E. M. & Turner, R. F.; Carbon Fibre Properties and Manufacture: Caurtaulds Ltd Technical File No: 76 & 77.
- [18] Sela, N. and Ishai, O.; Interlaminar Fracture Toughness and Toughening of Laminated Composite Materials: a Review; Composites, Volume 20, Number 5, p423-435, September (1989).
- [19] Ciba Geigy Technical Information Sheet No: FTA 159B
- [20] Personal Communication with Dr. C. Southis, University of Leicester; (1991)

- [21] Sela, N. et al; The Effect of Adhesive Thickness on Interlaminar Fracture Toughness of Interleaved CFRP Specimen; Composite, Volume 20, Number 3, p257-264 May (1989).
- [22] Chan, W. S.; Delamination Arrester-An Adhesive Inner Layer in Laminated Composite; ASTM STP 907, p176-196, (1986)
- [23] Bell Pushes for Broader Application of Composite to Helicopter Structures: Rotorcraft Technology Update, Aviation Week and Space Technology, p95-96, January (1987).
- [24] Hertzberg, P.E.; Methods of Making Delamination Resistant Composite; United States Patent No: 4,786,343, p1-12, November (1988)
- [25] Nir, Z.; Toughened Reinforced Epoxy Composite with Brominated Polymer Additive; United States Patent No: 4,550,129 , p1-14, October (1985)
- [26] Gilwee, W. J.; Modified Epoxy Composites; Pub. NASA Ames Research Centre, (1985).
- [27] Hawley, G. G.; The Condensed Chemical Dictionary; Von Nostrand Reinhold Limited (1986)
- [28] Hughes, J. D. H.; Fibre for Reinforcements; Metals and Materials; p365-368, June (1986).
- [29] Hull, D.; An investigation to Composite Materials; Pub. Cambridge University Press; (1981).
- [30] Chun, M. and Niu, Y.; Airframe Structural Design; Pub. Conmilit Press, (1988).

- [31] Ehrburgeral, P. and Donnet, J. B.; Interface in Composite Materials; Phil. Trans. R. Soc. London A294, p495-505, (1980).
- [32] King, J. E.; Failure in Composite Materials; Metals and Materials, p720-726, (1989).
- [33] Donnet, J. B. and Guilpain G.; Surface Characterisation of Carbon Fibre Composites; Composites, Volume 22, Number 1, p59-62, January (1991).
- [34] Konig, W. et al.; Machining of Fibre Reinforced Plastics; CIRP Ann 34, p537-548, (1985).
- [35] Konig, W. et al.; New Developments in Drilling and Contouring Composites Containing Kevlar; The Production Engineer, p56-61, September (1984).
- [36] Barker, A. J. and Balasundaram; Compression Testing of Carbon Fibre Reinforced Plastics Exposed to Humid Environments; Composite, Vol. 18, 3 (1987).
- [37] Clark, G. et al; Moisture Absorption in Graphite/Epoxy Laminates; Composite Science and Technology, 39, p355-375, (1990).
- [38] Woolstencroft D. H. and Curtis; Interface Stresses in Unidirectional Carbon Fibre Composites; British Aerospace Report (Warton) p1-27.
- [39] Tsai, S. W. and Hahn, H. T.; Introduction to Composite Materials; Technomic Publishing Company, (1980).
- [40] Personnel Communications with Toray Industries, Inc. London; Fax No. 01 872 8071, (1991).

- [41] Kumar, S. and Helminiak, T. E.; Compression Properties of High Performance Fibres; SAMPE Journal, p51-61, March-April (1990).
- [42] Ewins, P. D. and Potter, R. T.; Some Observations on the Nature of Fibre Reinforced Plastics and the Implications for Structural Design; Phil. Trans. R. Soc. London, A 294, p507-517, (1980).
- [43] Wisnom, M. R.; The Effect of Fibre Misalignment on the Compression Strength of Unidirectional Carbon Fibre/Epoxy; Composites, Volume 21, Number 5, p403-405, September (1990).
- [44] Handley, F. and Hardage, J. T.; Manufacturing Methods for machining processes for high modulus composites; General Dynamics/Convair Aerospace Report No: AFML-TR-73-124, May (1973).
- [45] Connolly, J. J.; and Foster, J. C.; Cost Driven Design Concerns; SME Technical Paper EM89-109, p1-17, (1989).
- [46] Eyres, T. S.; Friction and Wear Control in Industry; Metals and Materials, p143-148, March (1991).
- [47] Chanani, J. P.; Optimal Methods for Generating Holes in Advanced Composites and Hybrids; ASTM No: 8501-003, March (1985).
- [48] Pengra; J. J.; Study of the influence of hole quality on composite materials; NASA Langely Research Report No: 159257; February (1980).
- [49] Puppo, A. H. and Evensen H. A.; Interlaminar Shear in Laminated Composites under Generalised Plane Stress; Journal of Composite Materials; Vol. 4, p204-219, (1970).

[50] Reifsnider K. L. et al; Delamination in Quasi-isotropic Graphite Epoxy Laminates; ASTM STP 617, p93-105, (1977).

[51] Altus, E. and Dorogoy, A.; Three Dimensional Study of Delamination; Engineering Fracture Mechanics, Volume 33, Number 1, p1-19, (1989).

[52] Technical Note-702, Measurement Group, Inc (1981).

[53] Soutis, C., Fleck N. A. and Curtis, P. T.; Hole-hole interaction in Carbon Fibre/Epoxy Laminates under Uniaxial Compression; Composites; Volume 22, Number 1, p31-38, January (1991).

[54] Soutis, C. and Fleck, N. A.; Static Compression Failure of Carbon Fibre T800/924C Composite Plate with a Single Hole; Journal of Composite Materials, Volume 24, p536-557, May (1990).

[55] Evans, A. G. and Adler, W. F.; Kinking as a Mode of Structural Degradation in Carbon Fibre Composites; Acta Metallurgical, Volume 26, p725-738, (1978).

[56] Weaver, C. W. and Williams, J. G.; Deformation of Carbon Epoxy Composites Under Hydrostatic Pressure; Journal of Material Science, 10, p1323-1333, (1975).

[57] Da Silva, J. L. G. and Johnson, D. J.; Flexural Studies of Carbon Fibres; Journal of Material Science, 19, p1301-3210, (1984).

[58] Dobb, M. G., Johnson, D. G.; Park C. R.; Compression Behaviour of Carbon Fibres; Journal of Material Science, 25, p829-834, (1990).

- [59] Purslow, D.; Fractography of Fibre Reinforced Thermoplastics, Tensile, Compression and Flexural Failure; Composites; Volume 19, Number 5, p358-366, (1988).
- [60] Purslow, D.; Some Fundamental Aspects of Composites Fractography; Composites, p241-247, October (1981).
- [61] Grundy, J. D.; Characterisation of Four Simple Modes of Failure for Code 69-Type II Carbon Fibre; British Aerospace Report Number HSA-MSM-R-GEN-0343, June (1978).
- [62] DeVries M. F. et al.; Investigation of the Cutting of the New Point Drill, CIRP Annals, Volume 37, p73-78, (1988).
- [63] Oxford C. J.; Research on Twist Drills; The Engineer Digest, Volume 16, Number 5, p185-186, May (1955).
- [64] Spur, D. I. G. et al.; Drilling with Twist Drills of Different Cross Section Profiles; CIRP Annals, Volume 30, p31-35, (1981).
- [65] Skevington, E. Freeman, R.; The Truth about Twist Drills; Tooling and Production; Apr (1986).
- [66] Hickey, J. H.; Drilling Graphite Composites; Modern Machine Shop; p84-90 Mar (1987).
- [67] Encyclopedia of Polymer Science and Technology; Pub. John Willey and Sons; (1985).
- [68] D. F. Galloway and Mortan, I. S.; Practical Drilling Tests; The Institute of Production Engineers; (1946).
- [69] Koplev, A. et al; The Cutting Process, Chips, and Cutting Forces in Machining CFRP; Composites, Vol. 14, No. 4 (1983).

[70] Takeyama, H. and Lijima, N.; Machinability of Glass Fibre Reinforced Plastics and Application of Ultrasonic Machining; CIRP Annals, Volume 37, p93-96, (1988).

[71] Podders, R. K.; Hole Generation: Aircraft Assembly; Proceedings of the Eighth North American Manufacturing Research Conference; Society of Manufacturing Engineering (1980).

[72] Cook, N. H., and Subramaniam, K.; Sensing of Drill Wear and Prediction of Drill Life; Journal of Engineering for Industry, p295-301, May (1977).

[73] Kanai, M., Iwata, K., Fujii, S., and Kenda, Y.; Statistical Characterisation of Drill Wear and Drill Life for the Standard Performance Test; CIRP Annals, Vol: 27, p61-66, (1978).

[74] Warx, W. et al; Manufacturing Methods for Cutting, Machining and Drilling Composites; Grumman Aerospace Corporation Technical Report AFML-TR-78-103; Aug (1978).

[75] Tseng, M. M. and Noujaim, R. A.; On the Measurement and Propagation of Flank Wear in Cutting Tools; ASME Paper Number 78-WA/PROD-23, p1-7, Jul (1978).

[76] Cook, N. H.; Tool Wear and Tool Life; Journal for Engineering for Industry; Transactions of ASME; Paper No. 72-WA/Prod-19, p1-7, (1972).

[77] Gere, J. M. and Timoshenko, S. T.; Mechanics of Materials; Wadsworth International, (1985).

[78] Trend E. M.; Metal Cutting; Pub. Butterworths; (1984).

[79] Brook, K. J. A.; World Directory and Handbook of Hard Metals; Engineer's Digest Limited and International Carbide Data, (1982).

[80] Peters, C. T.; The Relationship between Palmqvist Indentation Toughness and Bulk Fracture Toughness for Some WC-Co Cemented Carbides; Journal of Material Sciences, Number 14, p1619-1623, (1979).

[81] Jack, D. H.; Cemented Carbides as an Engineering Material; Materials Engineering, p125-131, July (1984).

[82] Kalish, H. S.; Selecting the Optimum Cutting Tool Materials; Cutting Tool Engineering; Adams Carbide Corp. Report, p283-290.

[83] Basse, J. L. et al; Abrasive Wear of Tungsten Carbide-Cobalt Composites, Material Science and Engineering, Vol. 13, p83-91 (1974).

[84] Hashiash, M.; Machining of Advanced Composites with Abrasive Waterjet; ASME Publication: PD-Vol. 35, p1-17 (1988).

[85] Chryssolouris, G. et al; Three Dimensional Laser Machining of Composite Materials; ASME Publication: PD-Vol. 35, p19-37, (1988).

[86] Cusumano J. et al; Ultrasonic Drilling of Boron Fibre composites; Modern Plastics, Vol: 52, p88-90, Jan (1974).

[87] Jain, V. K. et al.; Experimental Investigations into Electrochemical Spark Machining of Composites; Journal of Engineering Industry (Trans. of ASME), 112 (2), May (1990)

[88] Stauffer N. R.; Diamond Tools Solve New Machining Problems; Manufacturing Engineering; p.54-56 (1979)

[89] Editorial Note; Special PCD tool last up to 75 times longer; American Machinist and Automated Manufacturing, p67, Jul (1987).

[90] Friend et. al.; Machining Graphite Composite Materials; Symposium on Composite Materials in Engineering Design, p.217-225, May (1972).

[91] Washington, W. L.; Drilling of Composites and Aluminium; Lockheed Missile and Space Company Inc. Report: MR76-268

[92] Beall, R. T.; Drilling Composites with Gun Drills; 11th National SAMPE technical Conference, Nov. (1979).

[93] Mackey, B. A. ; How to Drill Precision Holes in a Hurry; Plastics Engineer, p22-24, February (1980).

[94] Mackey, B. A.; A solution to the Problems of Drilling Reinforced Plastics; 35th Annual Technical Conference; The Society of Plastics Industry, Inc. (1980).

[95] Radhakrishnan, T. and Wu, S. M.; On-line Hole Quality Evaluation for Drilling Composite Material Using Dynamic Data; Journal of Engineering for Industry, Feb (1981).

[96] King, R. T.; High Speed Drilling of Aluminum Alloy and Aluminum Graphite Epoxy Sandwich Structures; North American Manufacturing Research Conference, (1982).

[97] Sakuma, Yoke and Seto.; Study on Drilling of GFRP and CFRP; Bulletin of Japanese Society of Mechanical Engineer, Vol. 27, p228, Jun, (1984).

[98] Sakuma, K.; Tool Wear in Cutting Carbon Fibre Reinforced Plastics; Bulletin of Japanese Society of Mechanical Engineering; Vol. 28, No. 245, Nov (1985).

- [100] Konig W.; Quality Definition and Assessment in Drilling of Fibre Reinforced Thermosets; CIRP Annals, Volume 38, p119-124, (1989).
- [101] Chanani, J. P.; Optimal Methods for Generating Holes in Advanced Composites and Hybrids; American Society of Metals Report No: 8501-003 (1985).
- [102] Chanani, J. P. and Boldt, J. A.; Solid-Tool Machining and Drilling; Composites, ASM International; Engineered Materials Handbook Vol. 1 (1987).
- [103] Masom S. E. and Chambers A. R.; Observations on the Machining of Advanced Plastics and Composites; First International Conference on Influence of Metallurgy on Machinability UK, Institute of Metals, (1988).
- [104] Miller, J. A.; Drilling Graphite Epoxy at Lockheed; American Machinist and Automated Manufacturing, p70-71, Oct (1987).
- [105] Malhotra, S. K.; Some Studies on Drilling of Fibrous Composites, Journal of Materials Processing Technology, Vol. 24; p291-300, (1990)
- [106] Lauder, E. A. and Greer, S. C.; Method for Cutting Nonmetallic Materials; US Patent No. 5,002,439, Mar (1991).
- [107] Petrof, R. C.; On the Dynamics of Drilling Glass Reinforced Plastic with Different Drill Point Geometries; SME Report No. EM86-363, (1986).
- [108] Doerr, R., US Army Research and Technology Laboratories Report (AVRADCOM), Jun (1982).
- [109] Schwartz, M. M.; 196 Holes per shot in boron-epoxy; American Machinist; Vol. 126, p130-131, Oct 1982.

[110] Toth I. J. et al.; Making a Product from Composites;  
Journal of Metals; Vol. 27; p37-42, (1972).

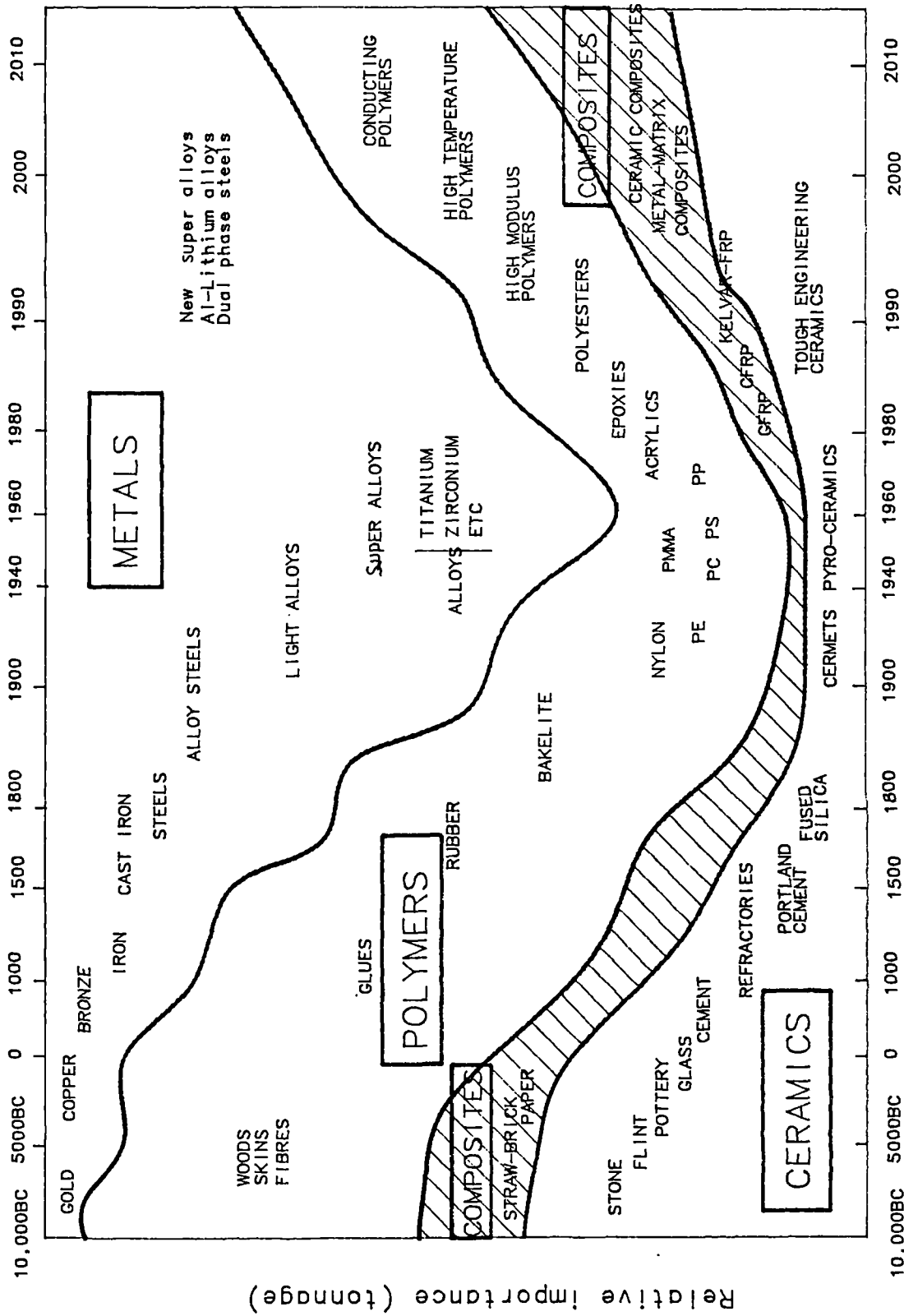
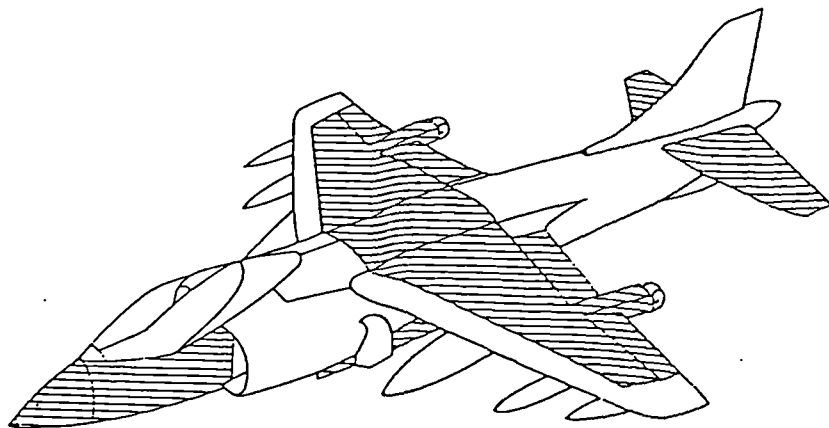
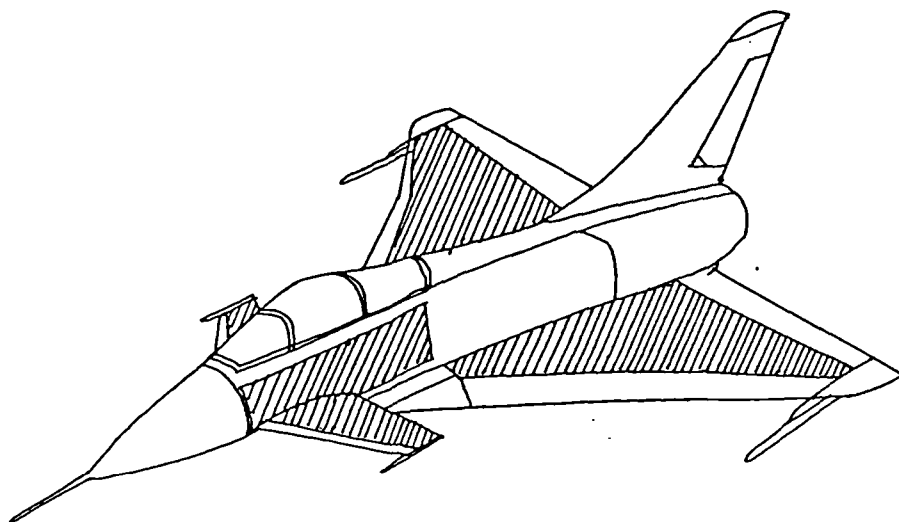


Fig. (1): Graph showing the relative importance of engineering materials with respect to different ages [6].



(a)



(b)

Fig. (2): Application of carbon fibre composites in military aircraft;

(a) British Aerospace/McDonnell Douglas AV-8B.

(b) British Aerospace, Experimental Aircraft Prototype (EAP)

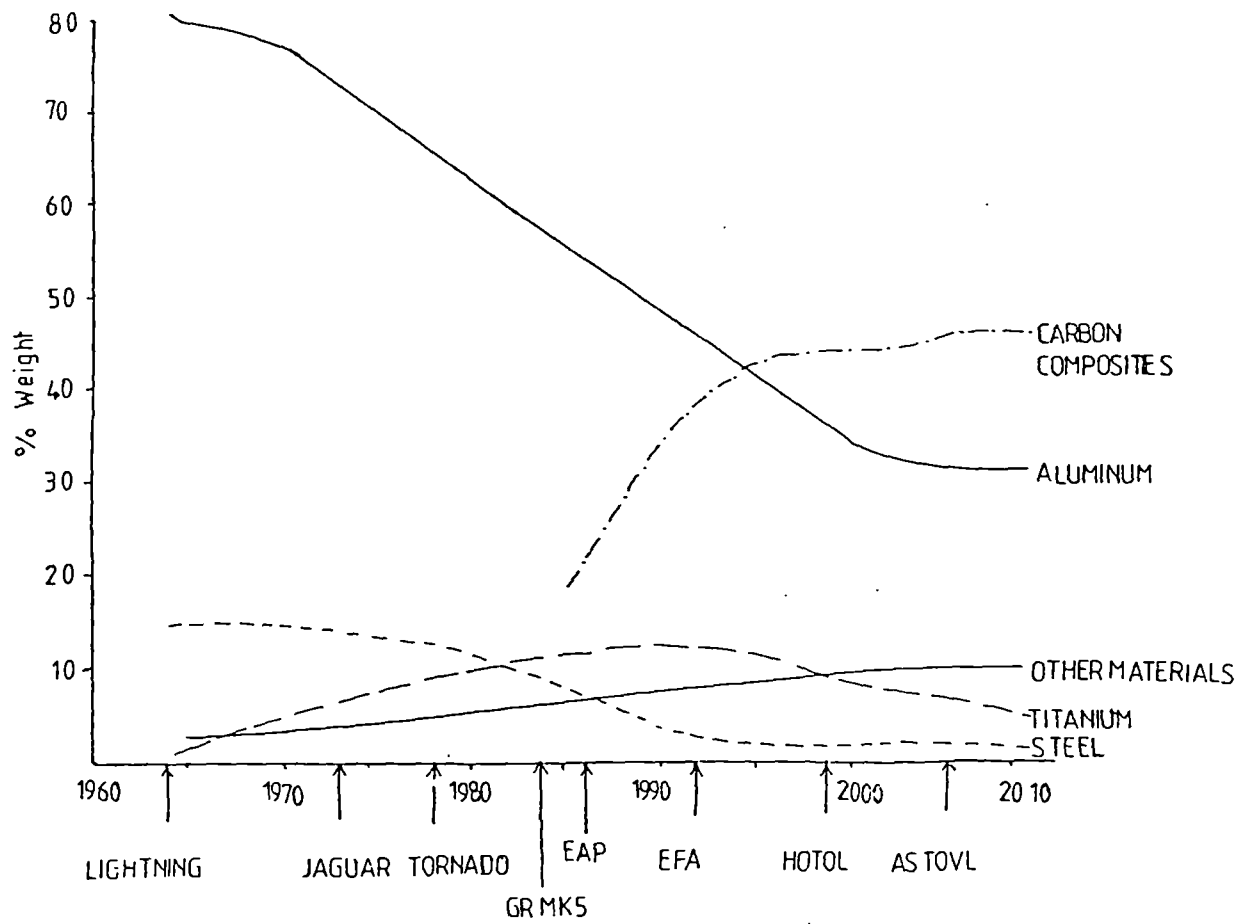


Fig. (3): Graph showing increasing use of carbon fibre composites in military aircraft [10].

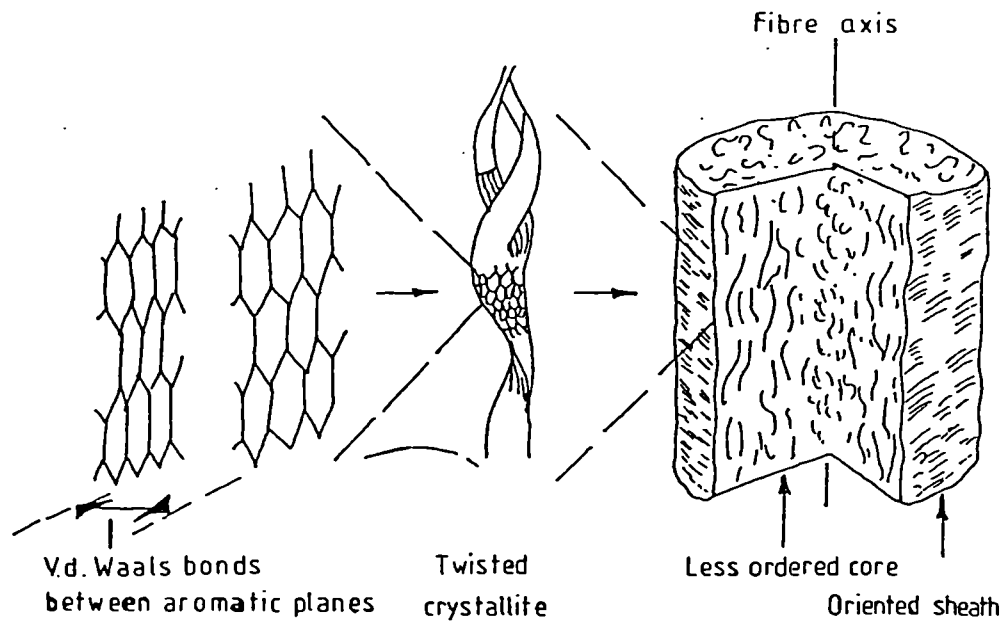


Fig. (4): The structure of carbon fibre [28].

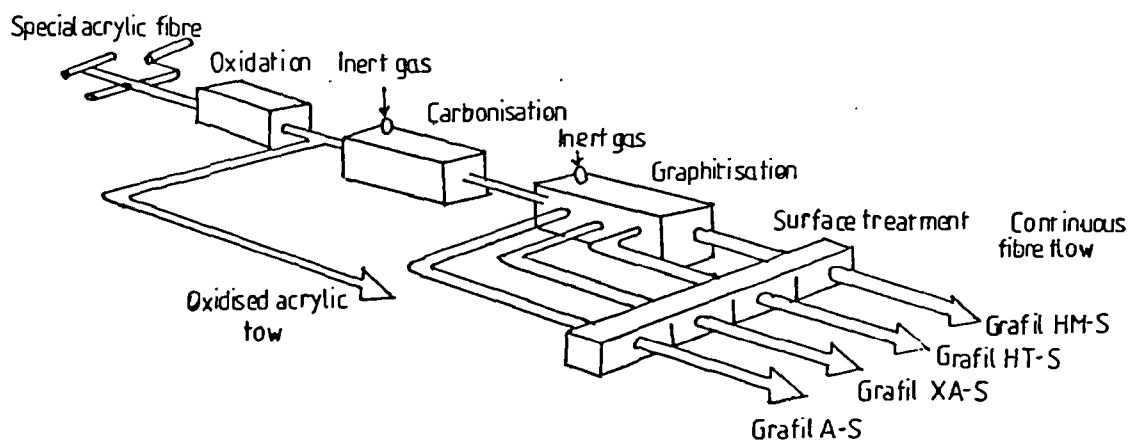


Fig. (5): Sketch showing fabrication route of carbon fibres [17].

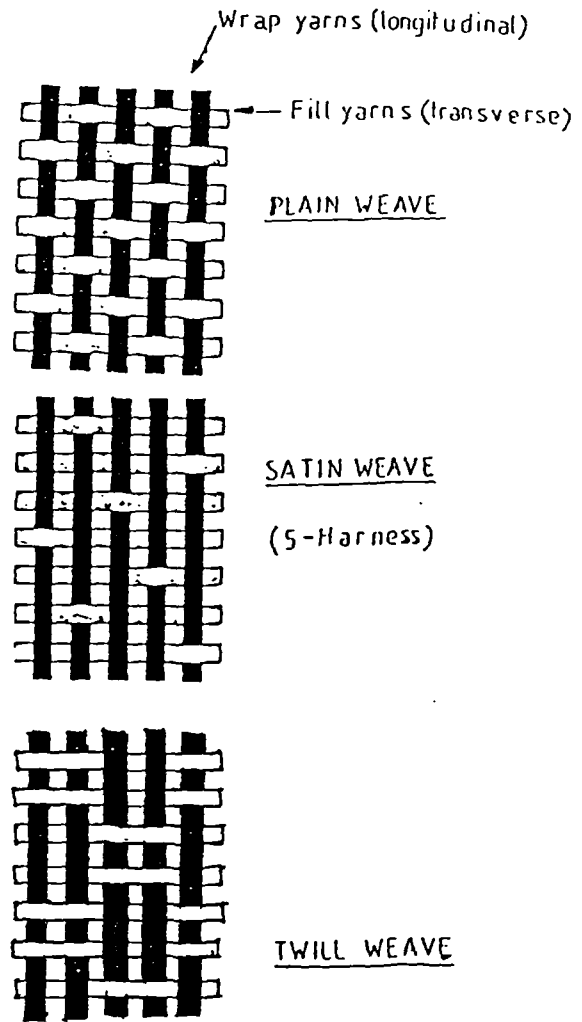


Fig. (6): The common weave styles of fibres used in composite materials.

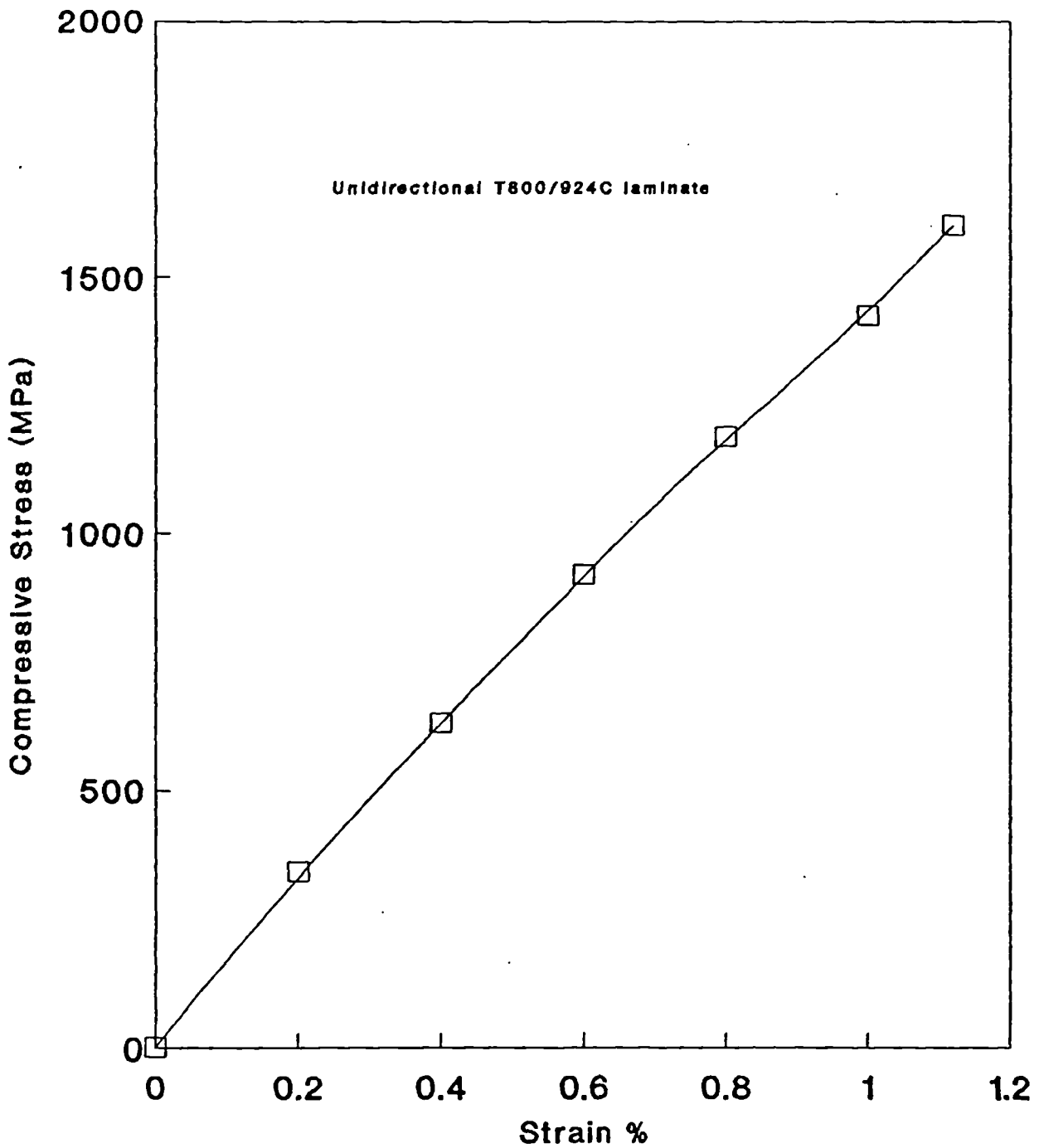


Fig. (7): The compressive stress/strain response of carbon fibre composite, T800/924C laminate [54].

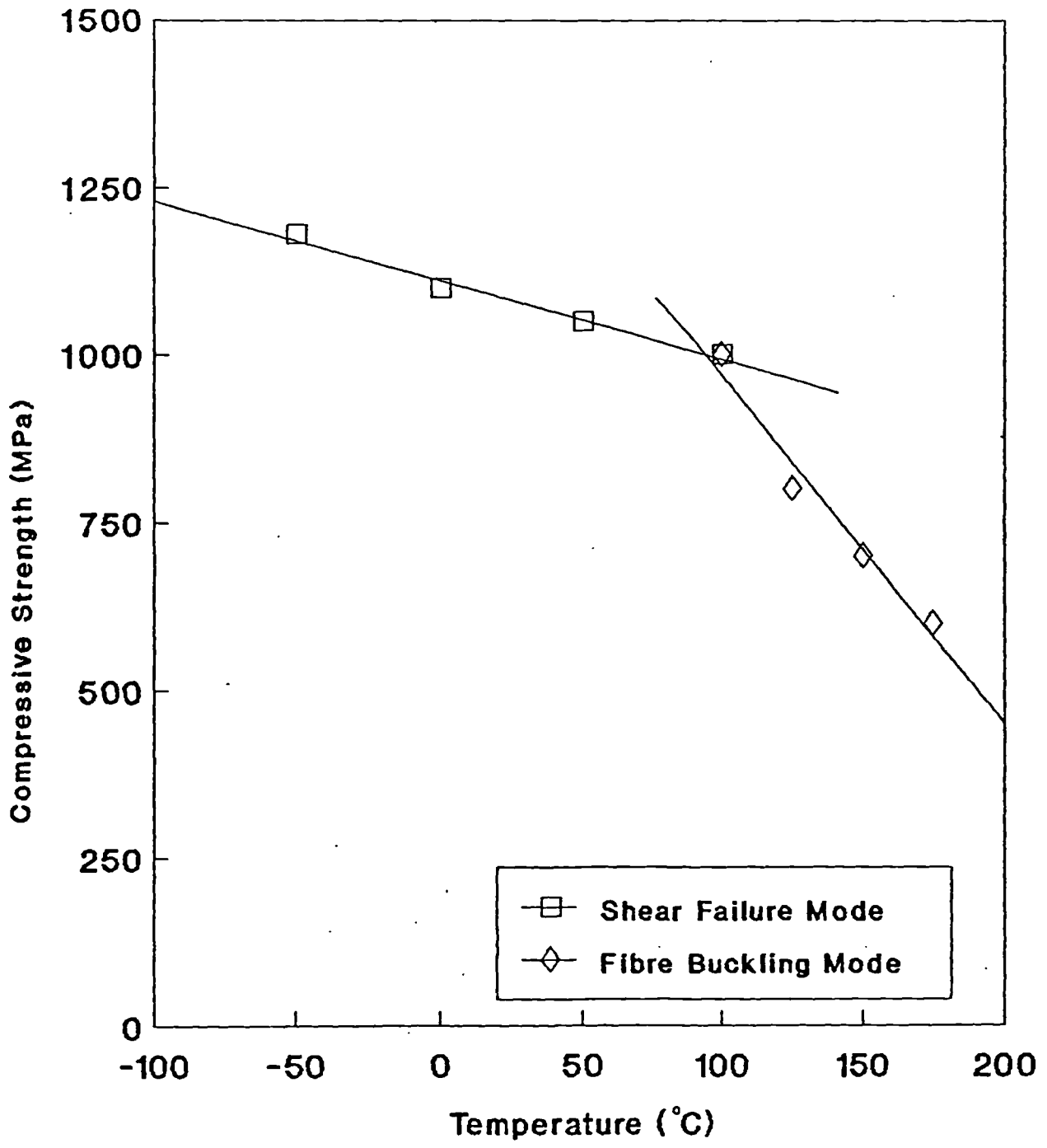


Fig. (8): Effect of temperature on compressive failure of 1st generation CFC [42].

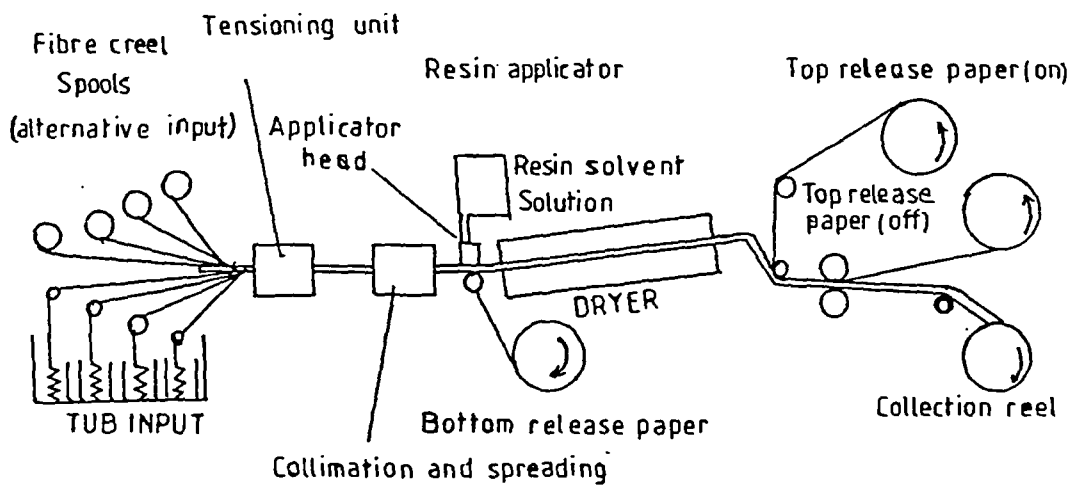


Fig. (9): Sketch showing the pre-impregnation of carbon fibre with resin solution [17].

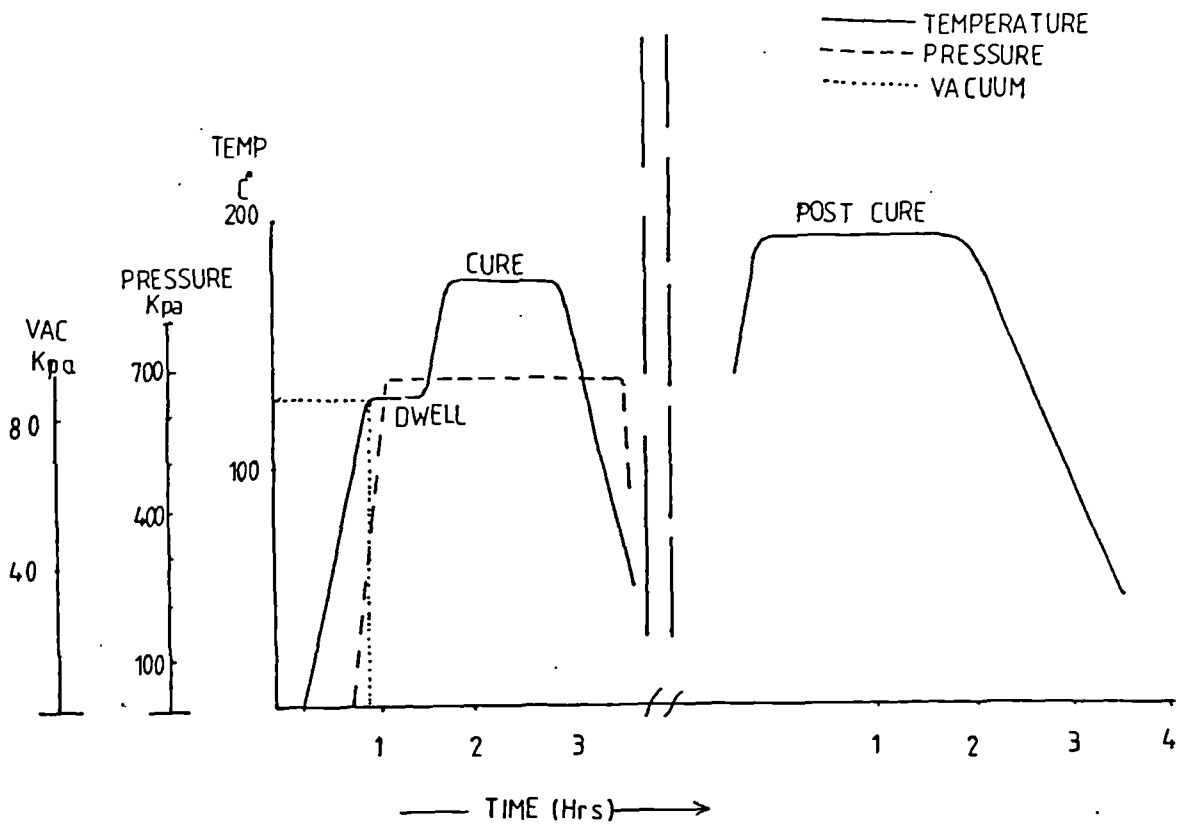


Fig. (10): The curing cycle of the carbon fibre composite panels which have been drilled in the present study.

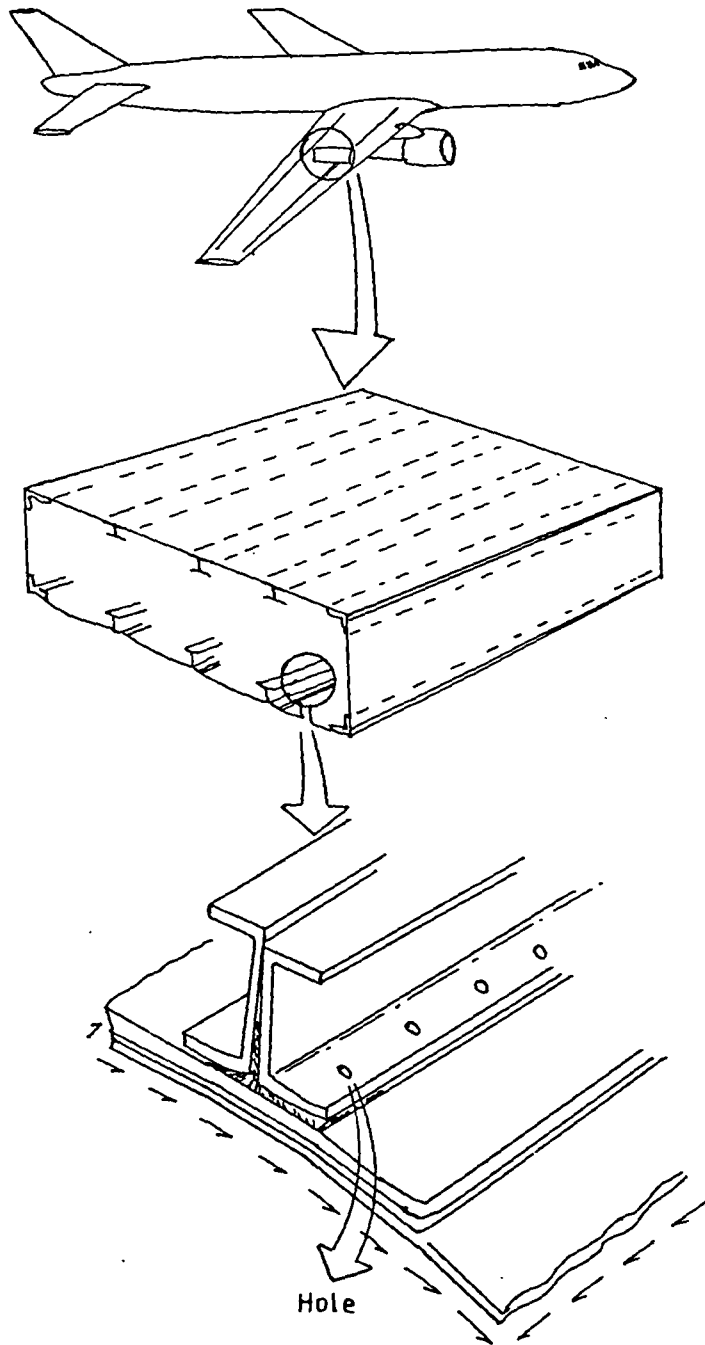


Fig. (11): A typical wing box beam showing holes which act as stress concentrations on a stringer which is attached to the aircraft skin by rivets.

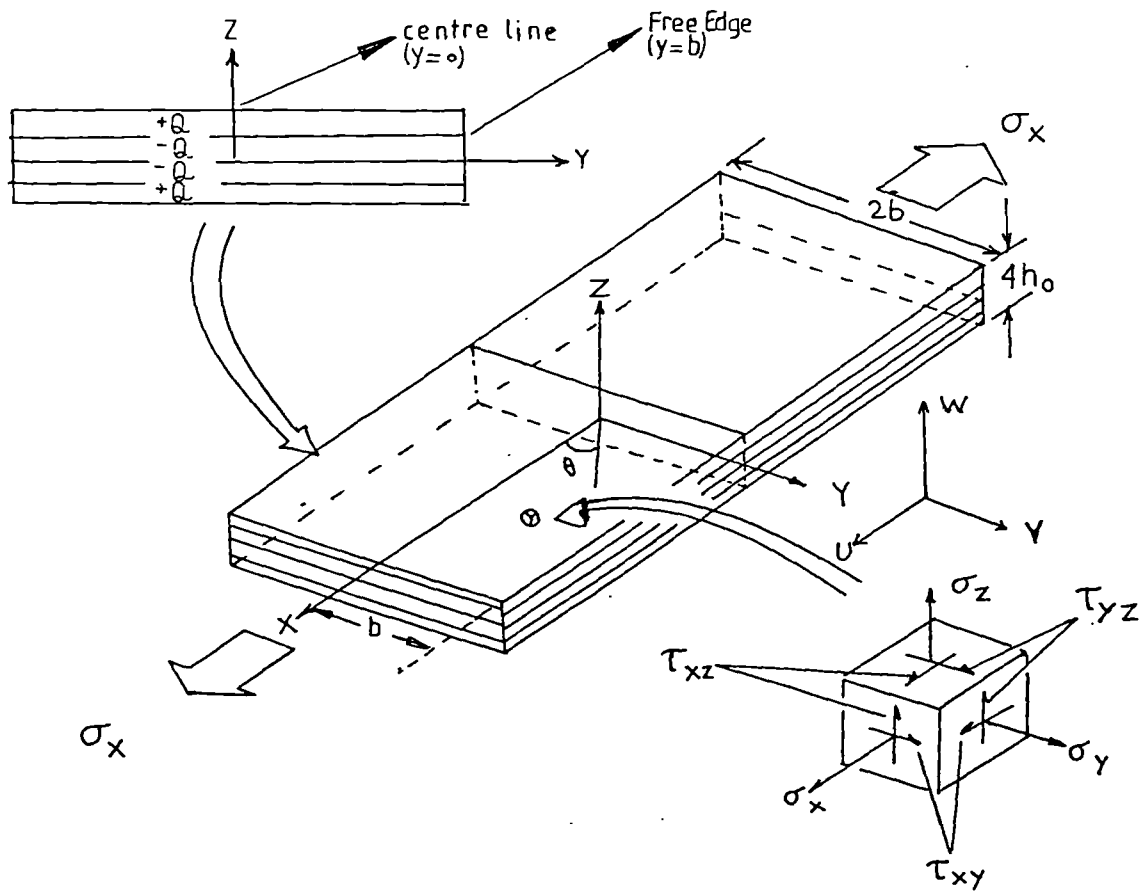


Fig. (12): The interlaminar stresses in the composite laminate [49].

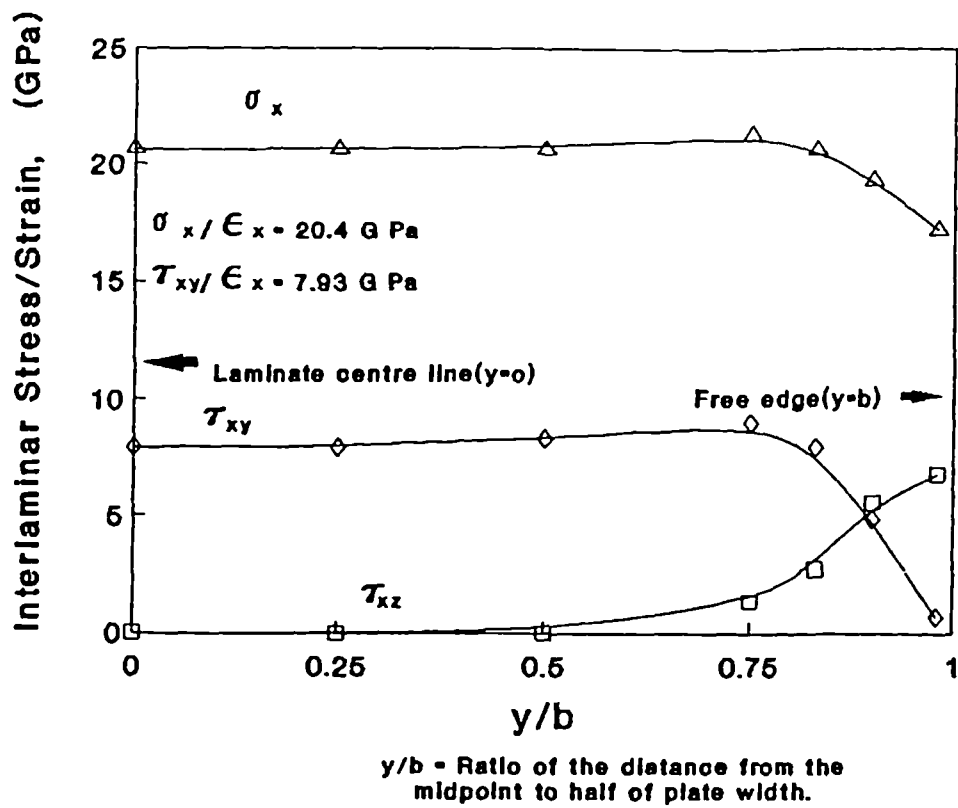


Fig. (13): Variation of interlaminar stresses at the interface from the centre of a plate to the outer surface [49].

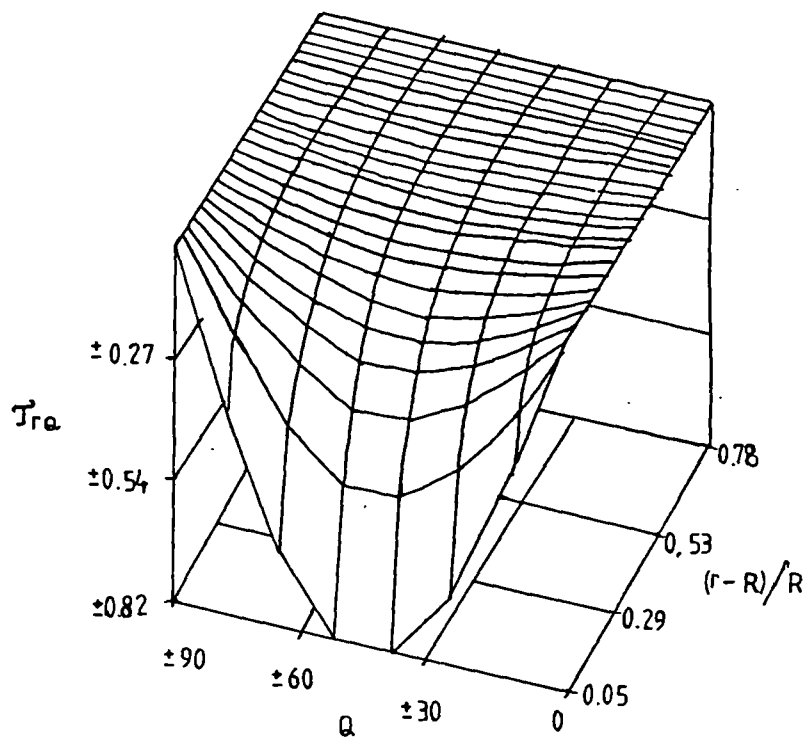
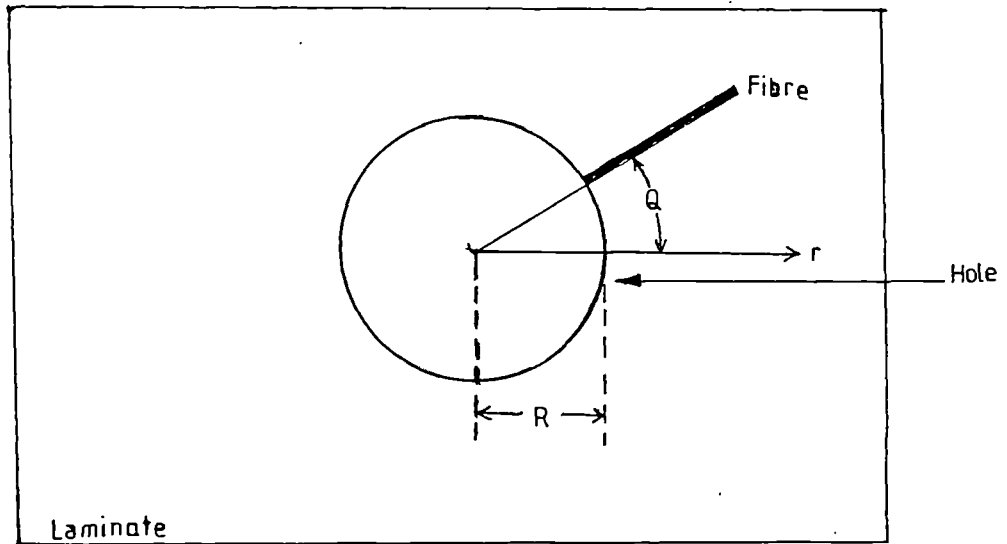


Fig. (14): Variation of 3-dimensional interlaminar shear stress around the CFC hole with respect to distance from the centre of hole and angular orientation of fibres [51].

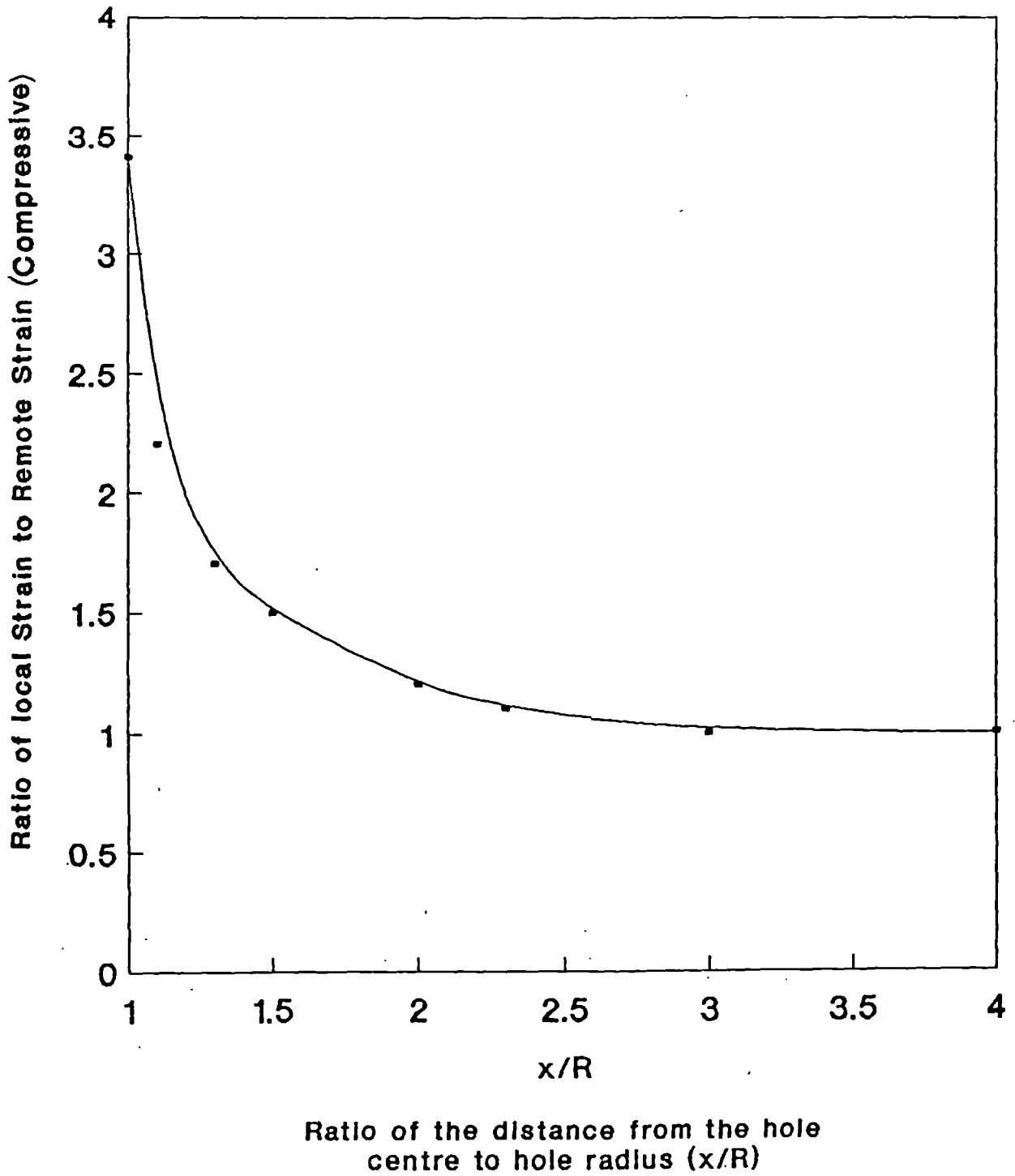


Fig. (15): The strain distribution around a single hole in carbon fibre composite, T800/924C laminate [55].

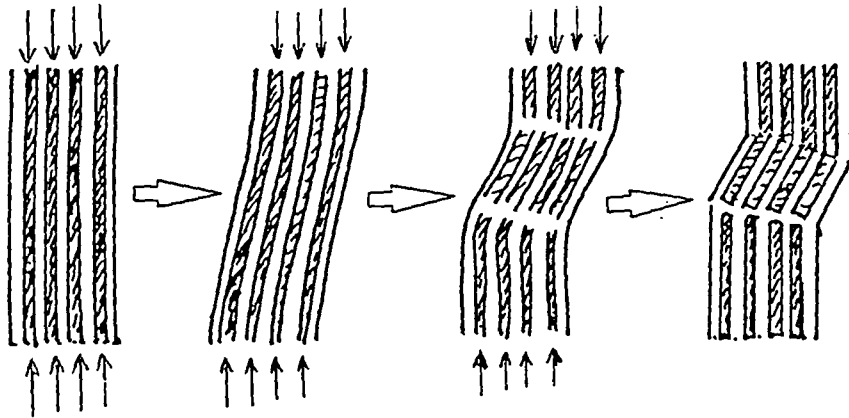


Fig. (16): Drawing showing fibre microbuckling.

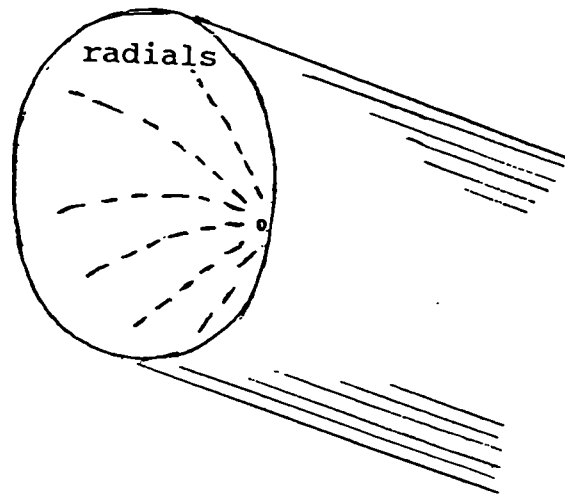


Fig. (17): Drawing showing fibre fractured in tension.

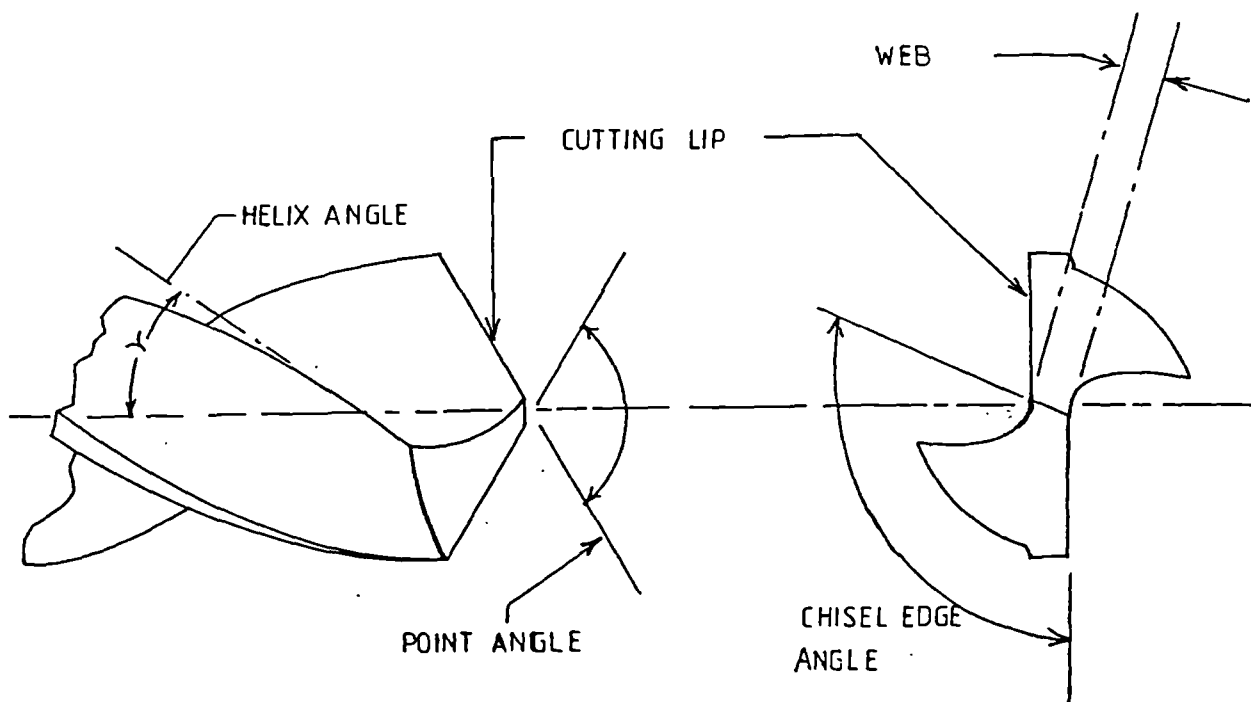


Fig. (18): The geometric features of a drill.

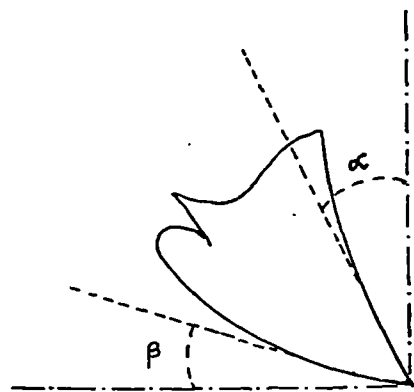
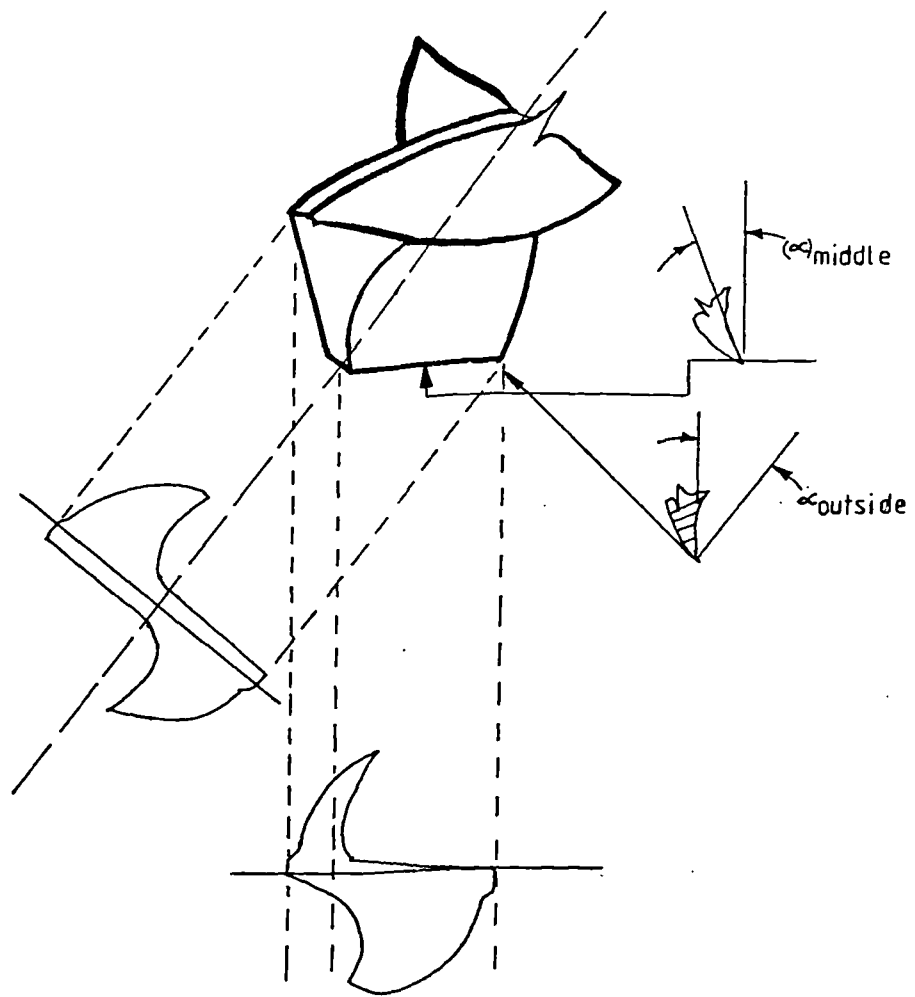


Fig. (19): The rake angle ( $\alpha$ ) and clearance angle ( $\beta$ ) of a drill.

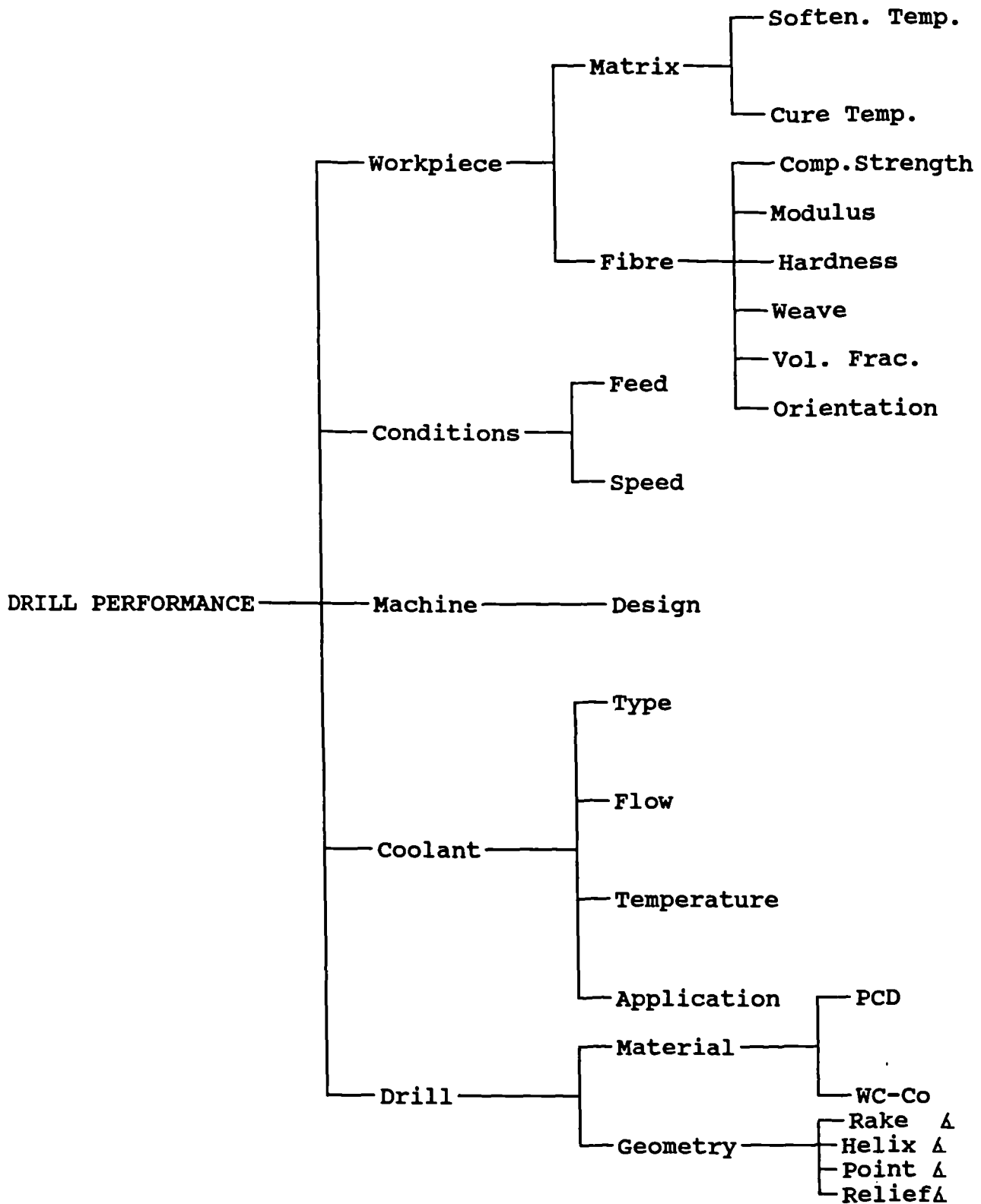


Fig. (20): The main factors which determine drilling performance in Composite materials.

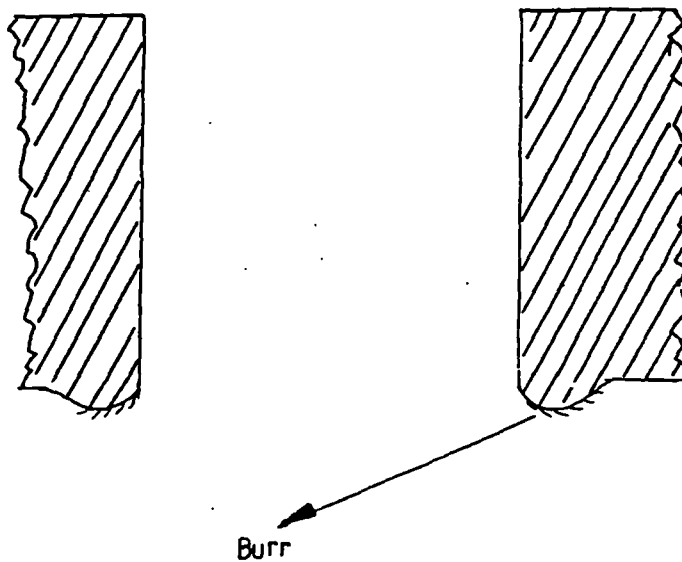
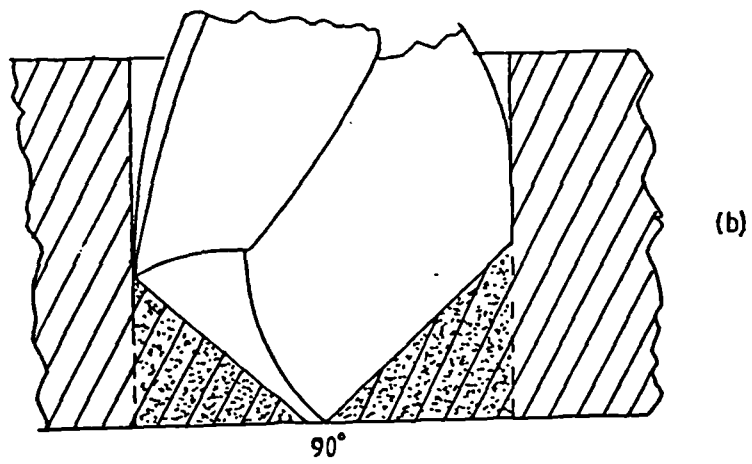
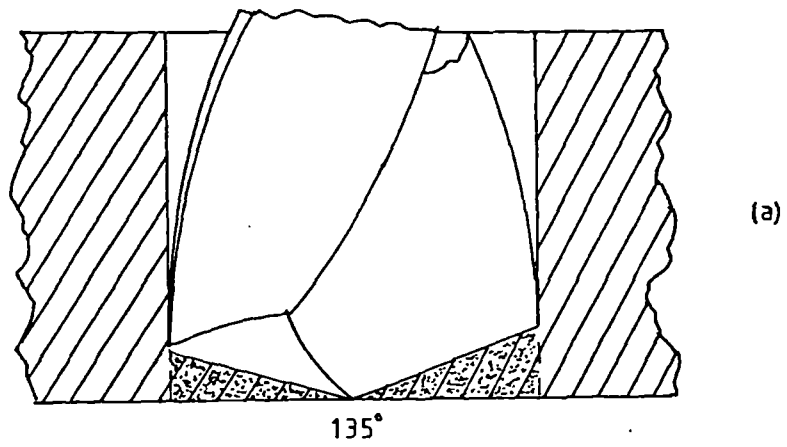
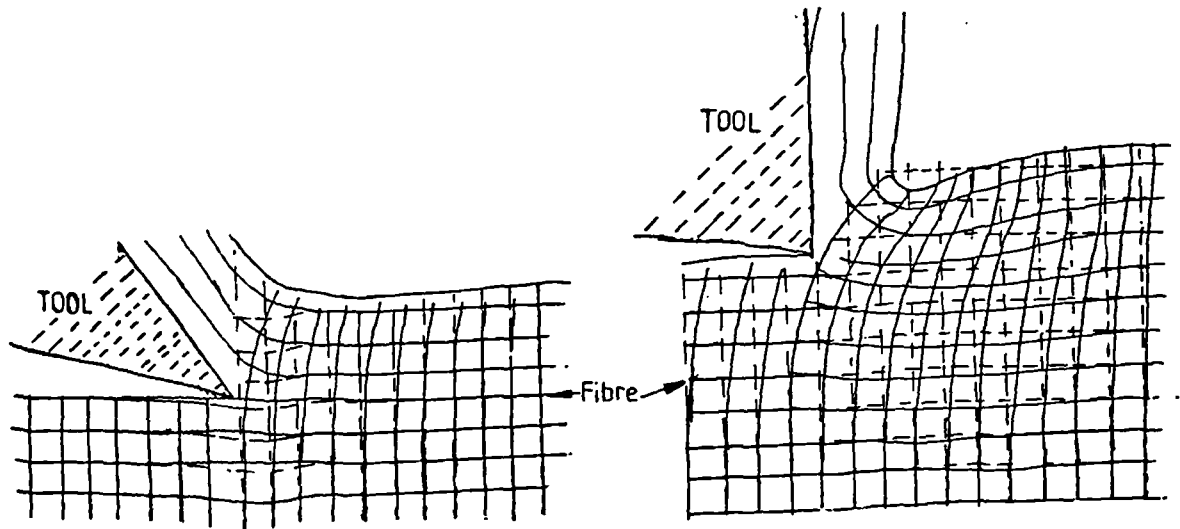
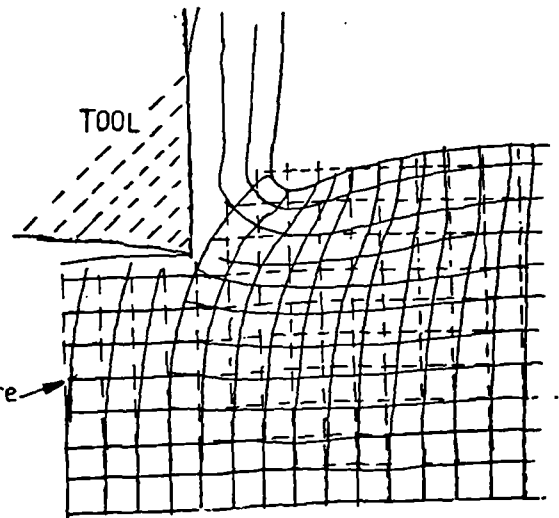


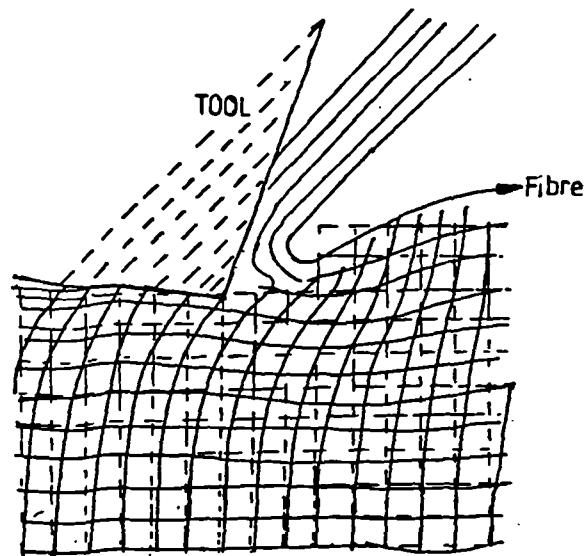
Fig. (21): The effect of large point angle (top) and small point angle (bottom) on the potential for creating burrs at drill breakthrough.



(a)

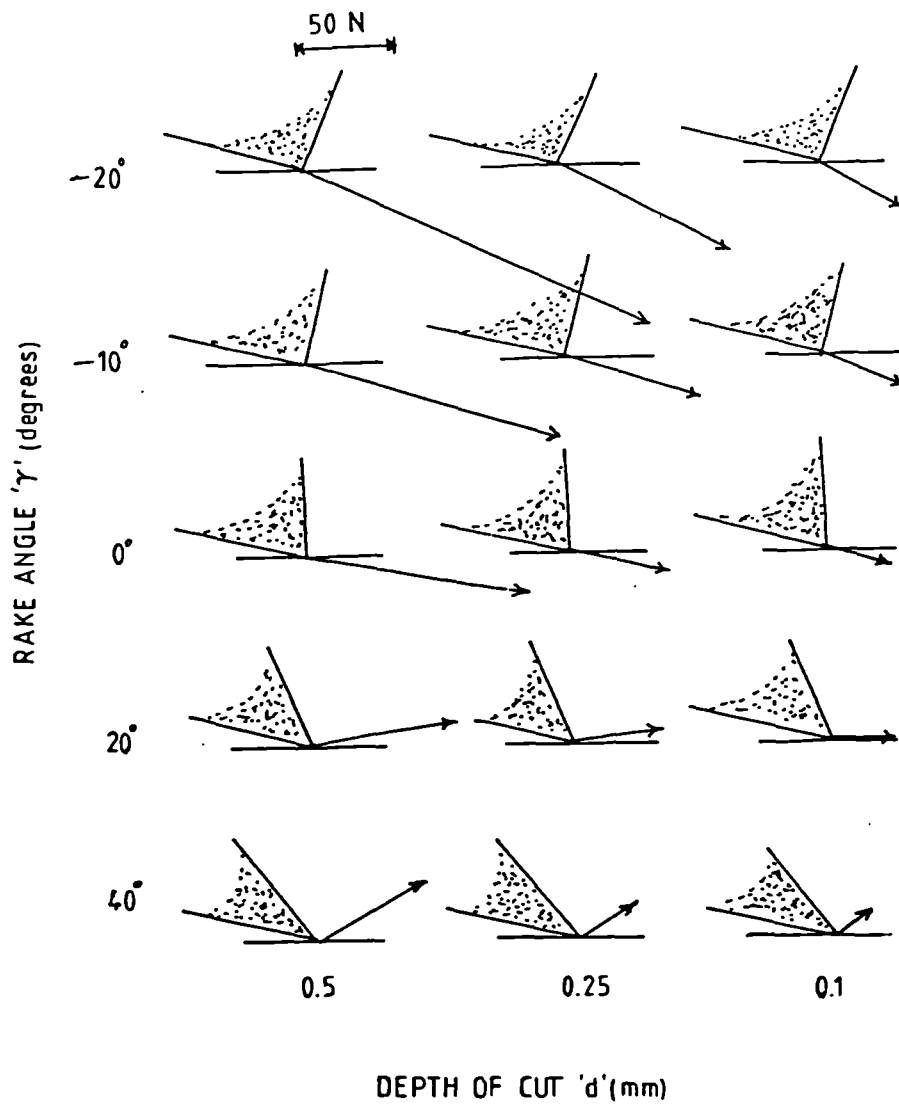


(b)



(c)

Fig. (22): Drawing showing deformation of fibres (solid lines) during CFC drilling using tools having positive rake angle (a), neutral rake angle (b) & negative rake angle(c).



Material used: Polystyrene (W/P)

**Fig. (23):** Vector diagram showing the effect of rake angle on the direction and magnitude of the cutting forces at a cutting speed of 0.2 m/sec. and various depths of cut [67].

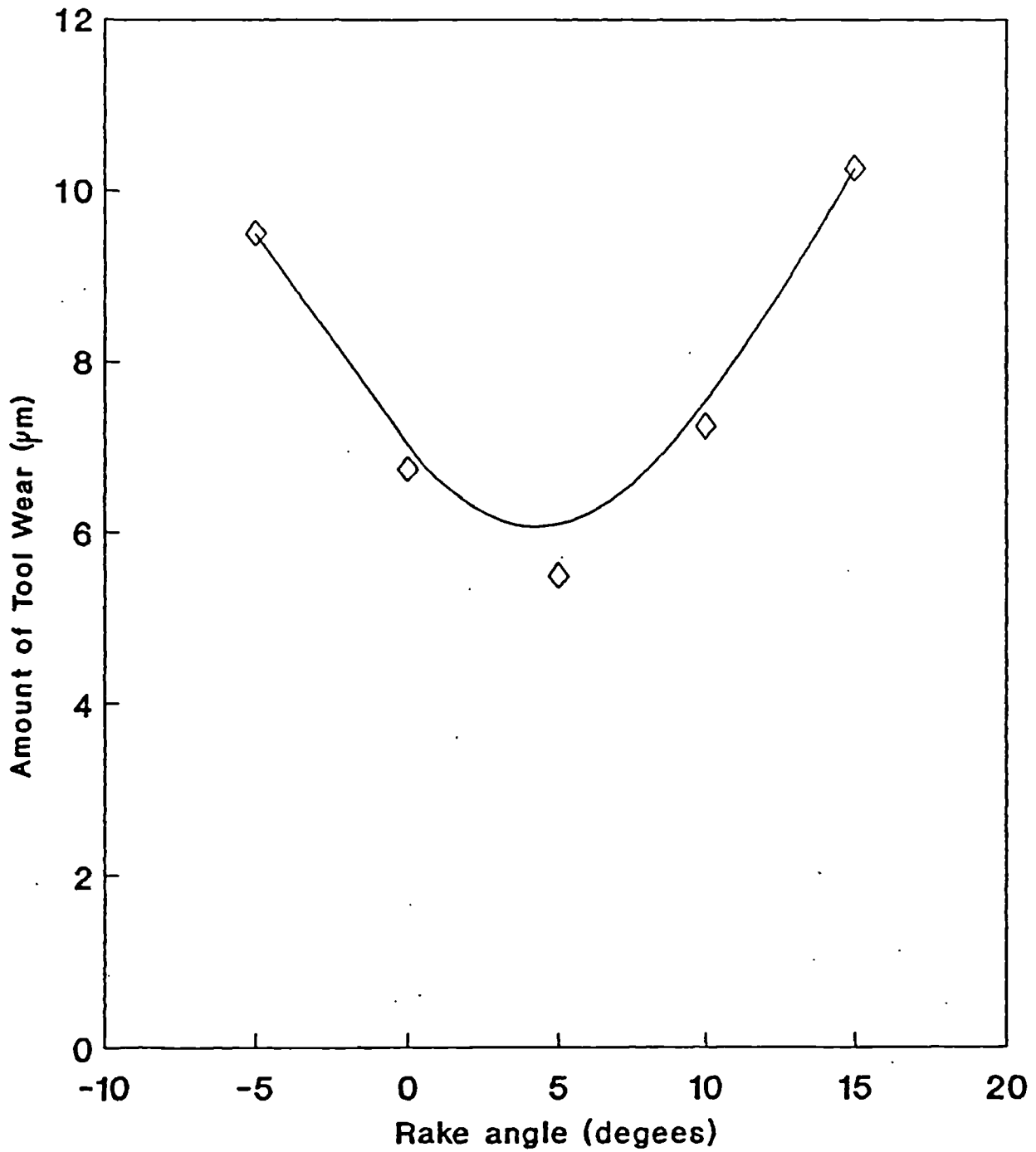


Fig. (24): The effect of rake angle on outer corner wear of a HSS cutting tool when cutting rigid PVC resin at a cutting speed of 440 m/min and cutting depth of 0.1 mm[67].

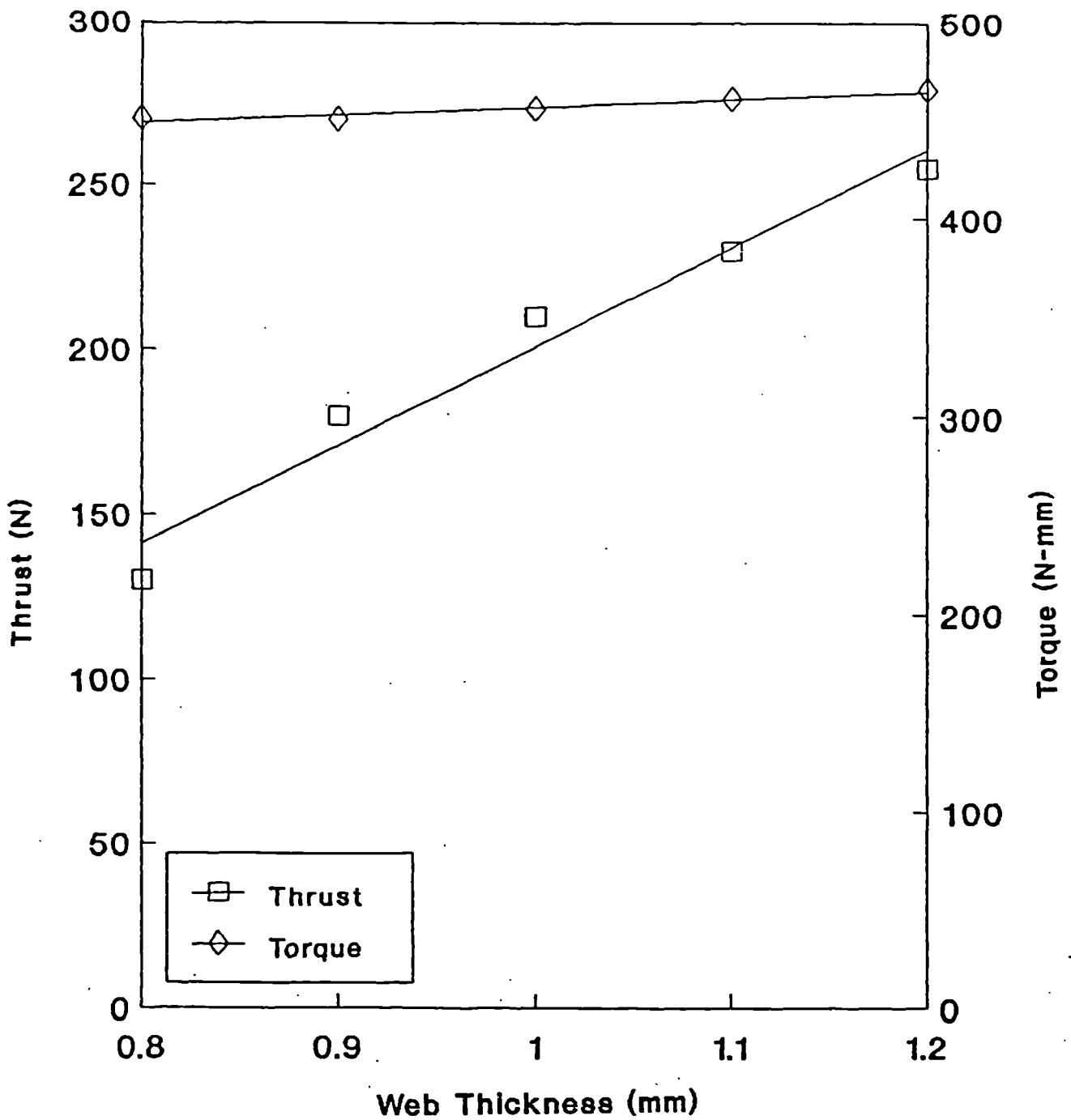


Fig. (25): Effect of web thickness of a 6mm dia. HSS drill on thrust and torque when drilling SK7 steel [68].

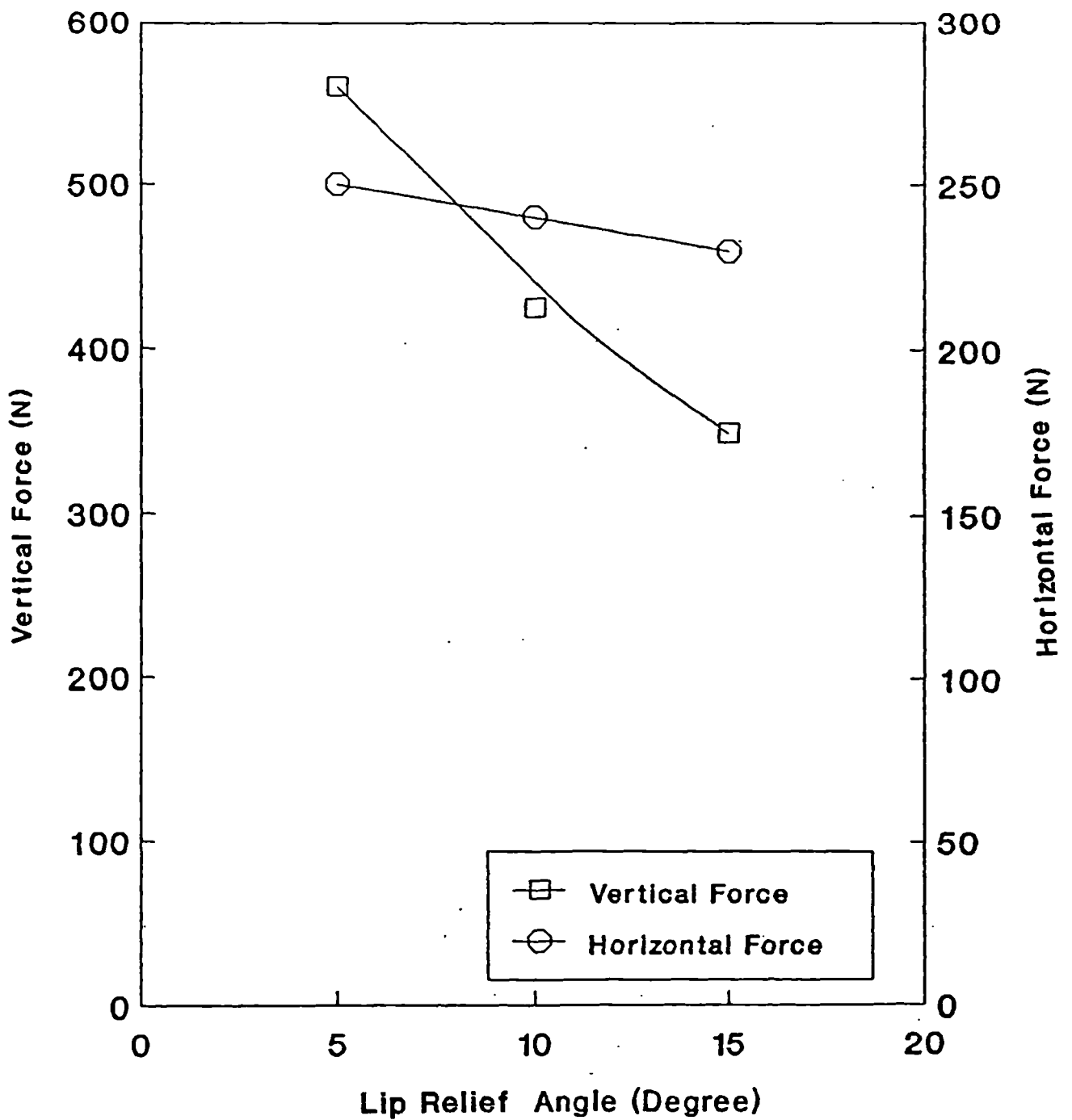


Fig. (26): Effect of varying relief angle on cutting forces when machining CFC using a cemented carbide tool with a rake angle of  $+15^\circ$  at a speed of 0.6 m/sec. and cutting depth of 0.1mm [69].

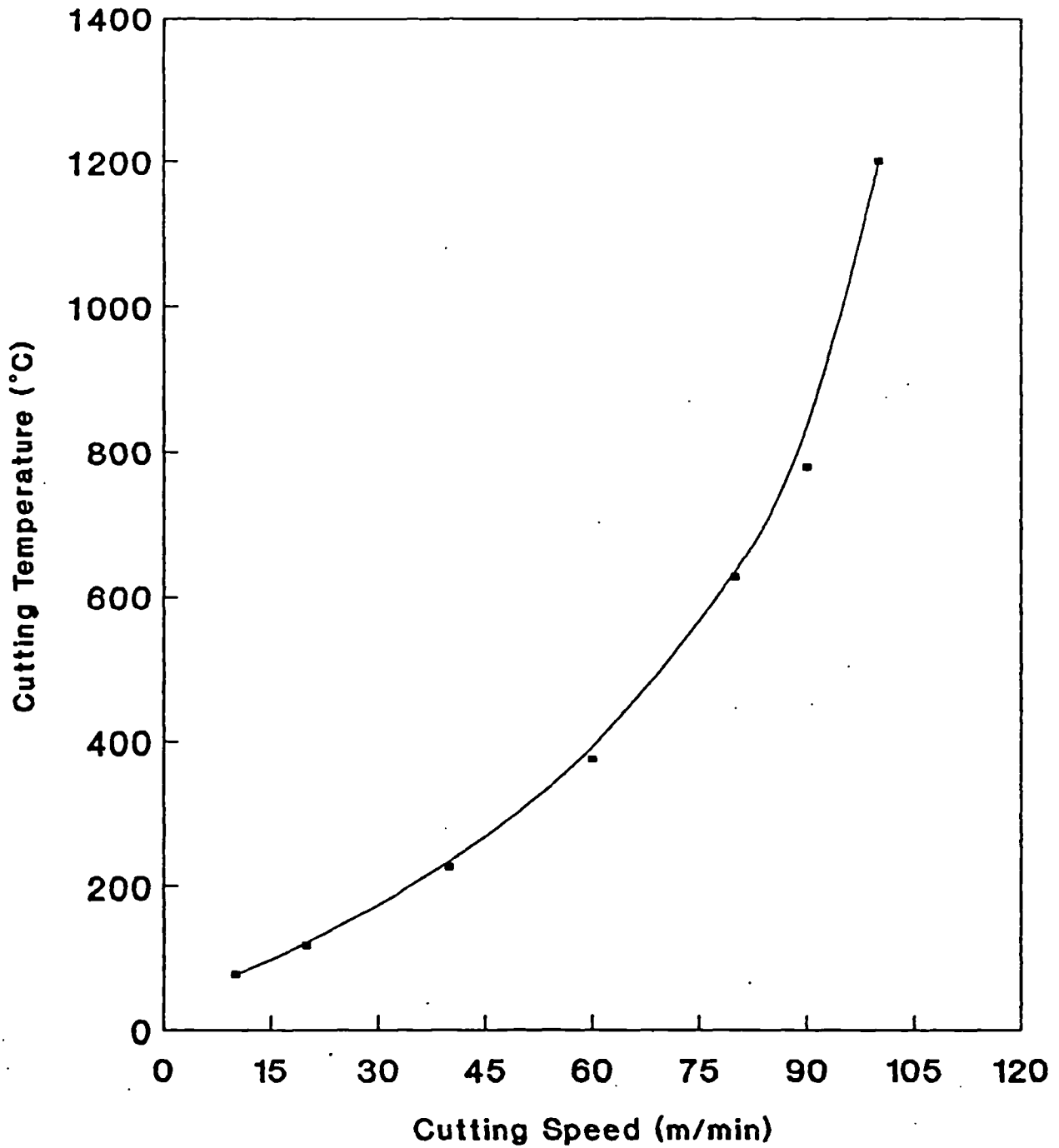
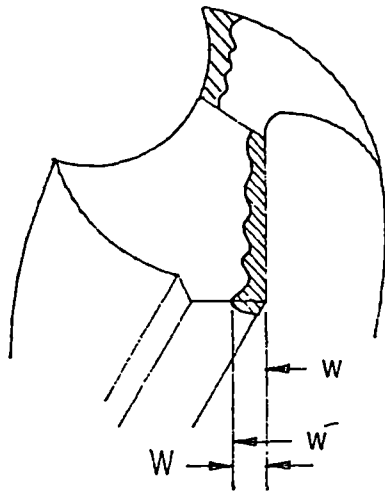
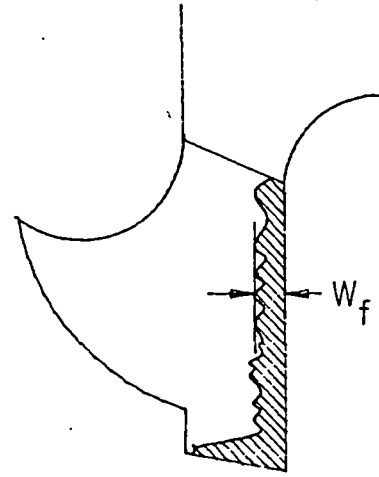


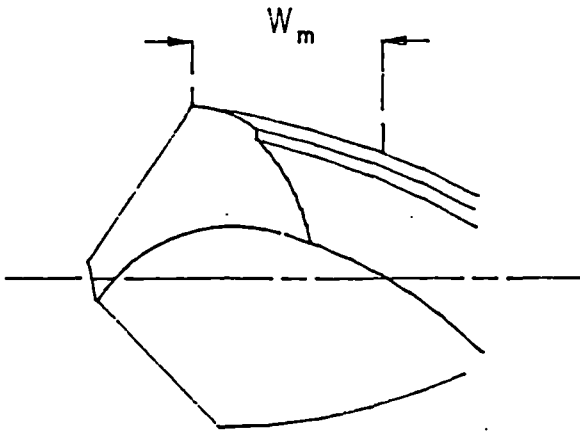
Fig. (27): Effect of cutting speed on cutting temperature when machining a glass fibre reinforced material at a feed of 0.16mm/rev. and a rake angle of 0° [70].



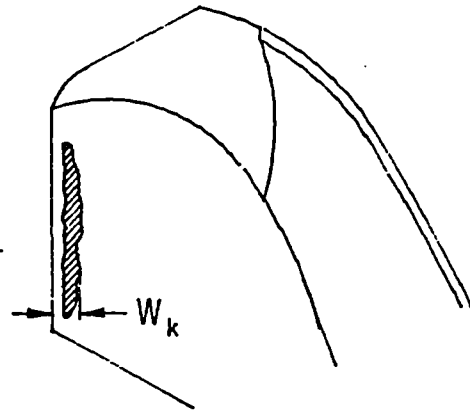
(a). Outer corner wear



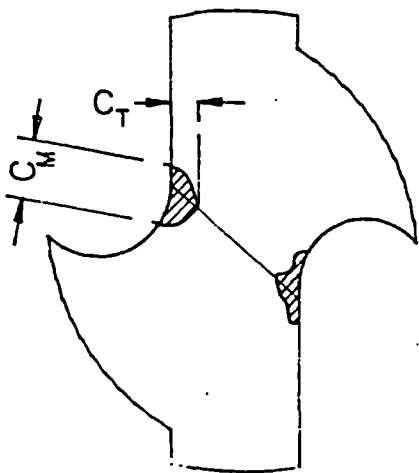
(b). Flank wear



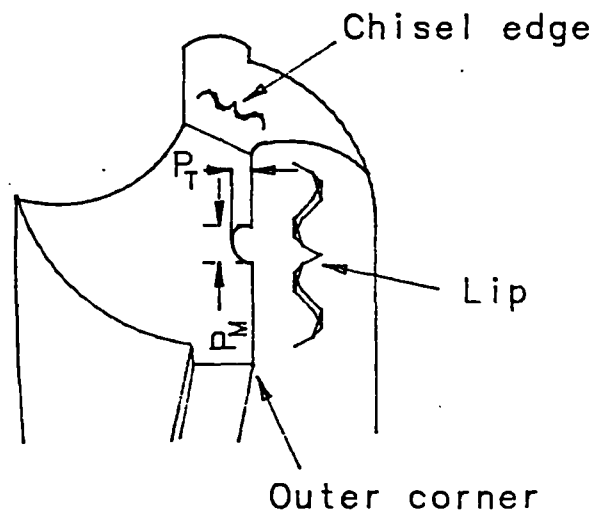
(c). Margin wear



(d). Crater wear



(e). Chisel edge wear



(f). Chipping at lip

Fig. (28): Sketch showing various types of drill wear [73].

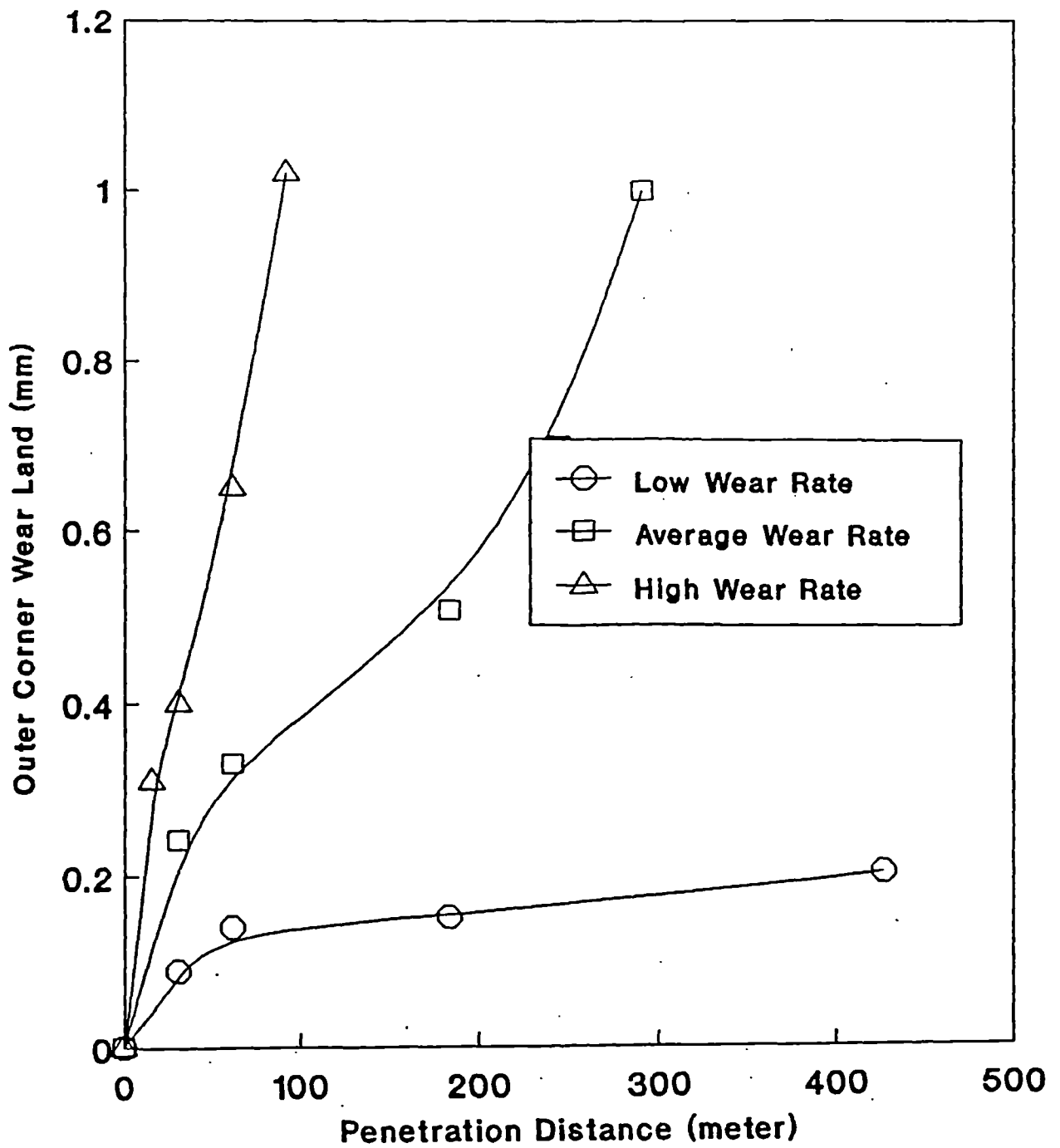


Fig. (29): The nonlinear relations between drill wear at the outer corner of a carbide drill and penetration distance in CFC [74].

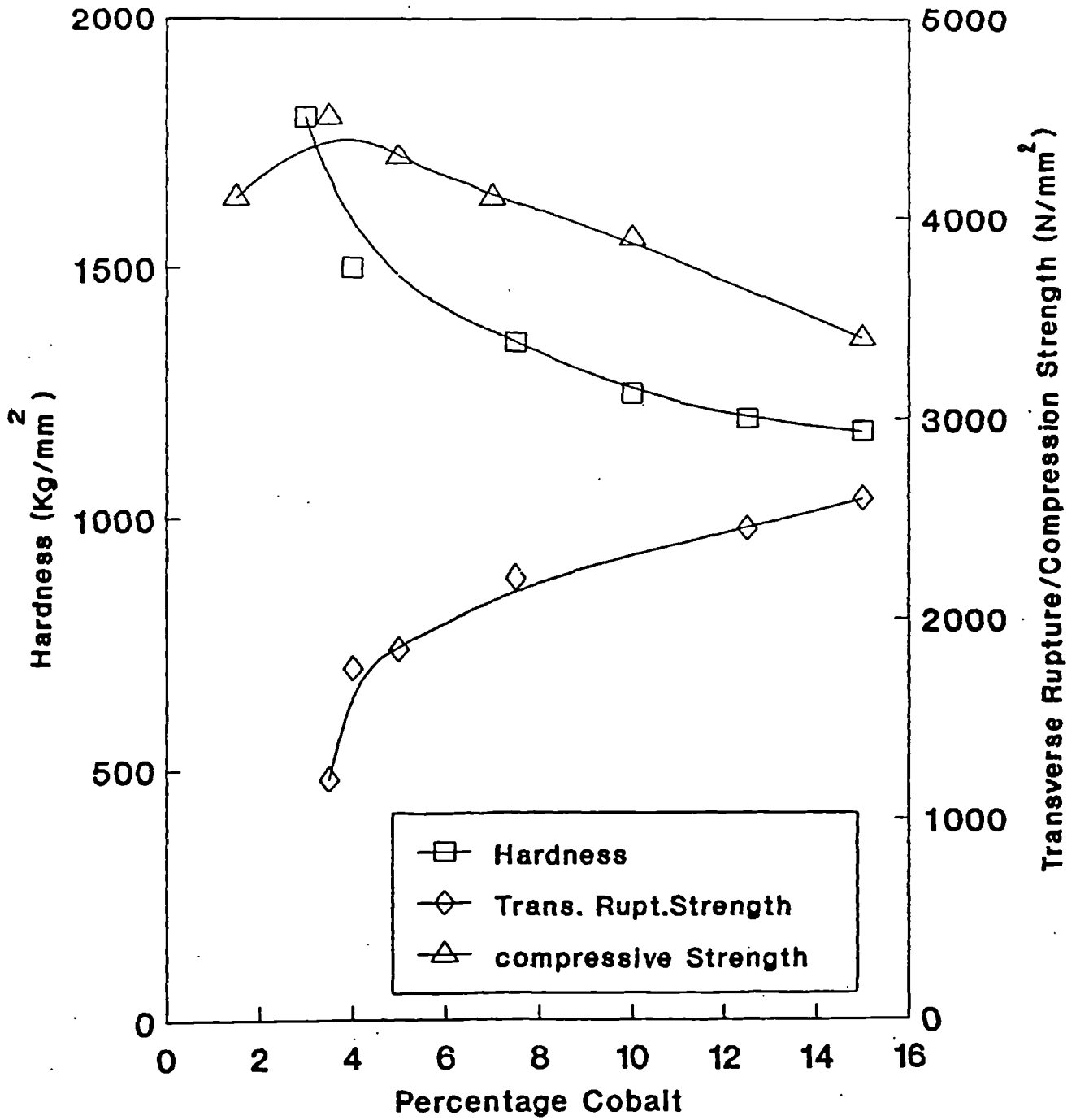
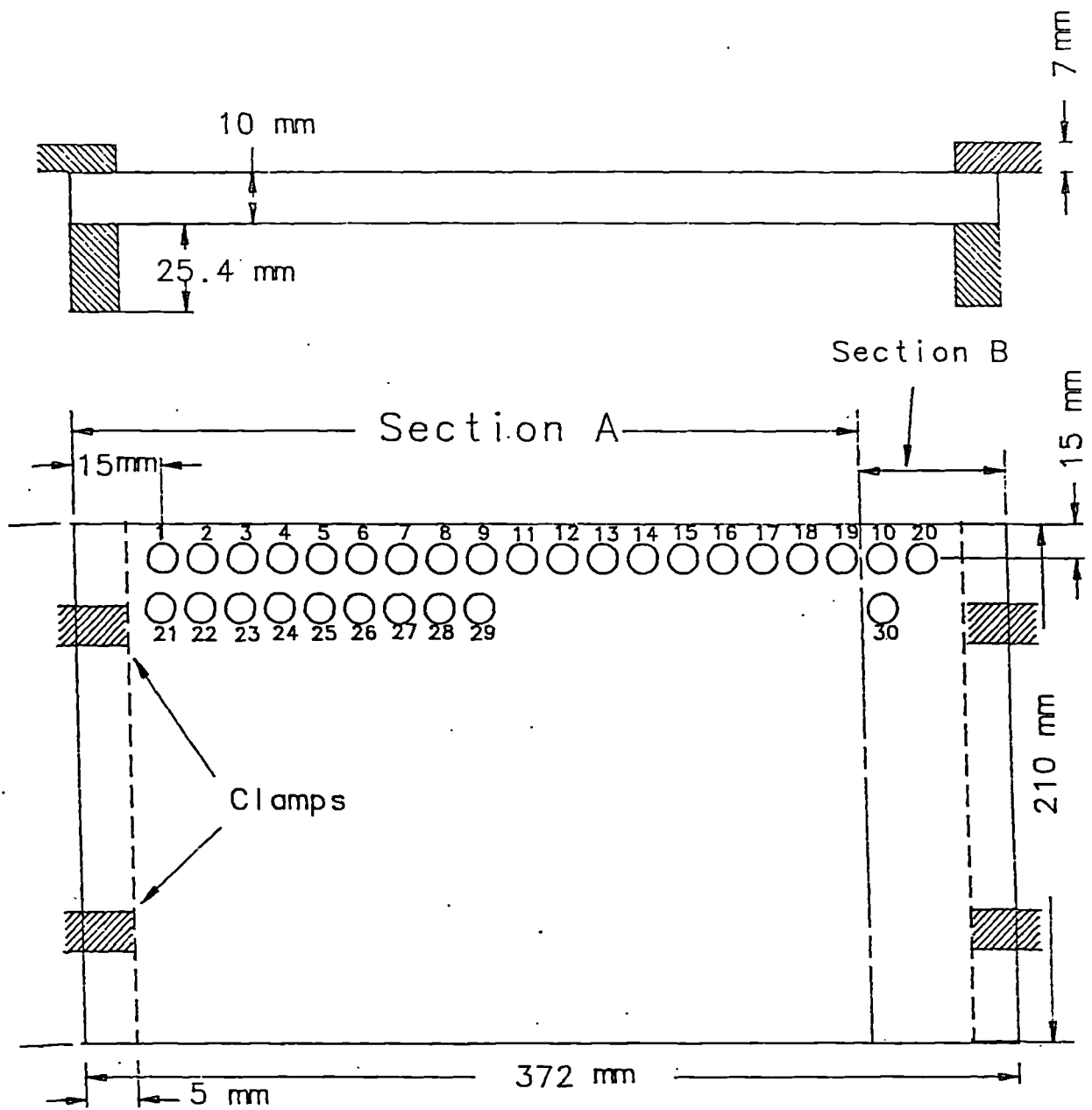


Fig. (30): Effect of percentage of cobalt on the hardness, transverse rupture strength and compression strength of tungsten carbide-cobalt alloy [78].



Hole Diameter 6mm

Hole Pitch 18 mm

Maximum Number of Rows in a Plate 11

Maximum Number of Columns in a Plate 20

Fig. (31): The experimental arrangement during the drill life tests.

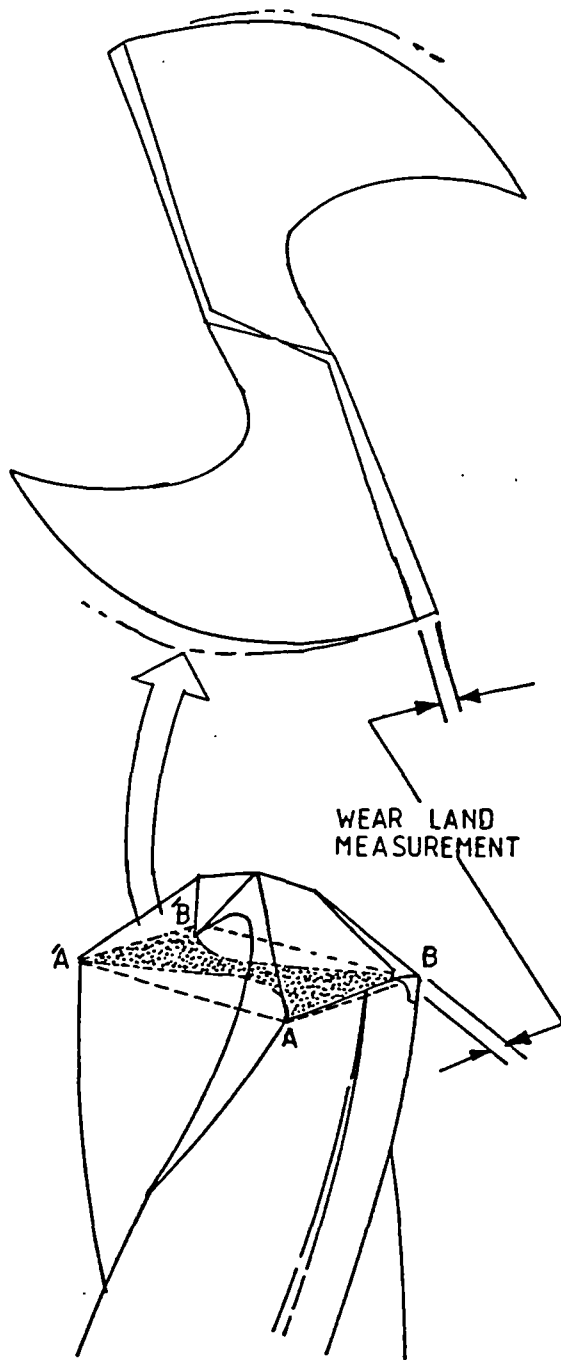


Fig. (32): Sketch of the drill showing the plane of sectioning (AA'BB') and the position of outer corner wear.

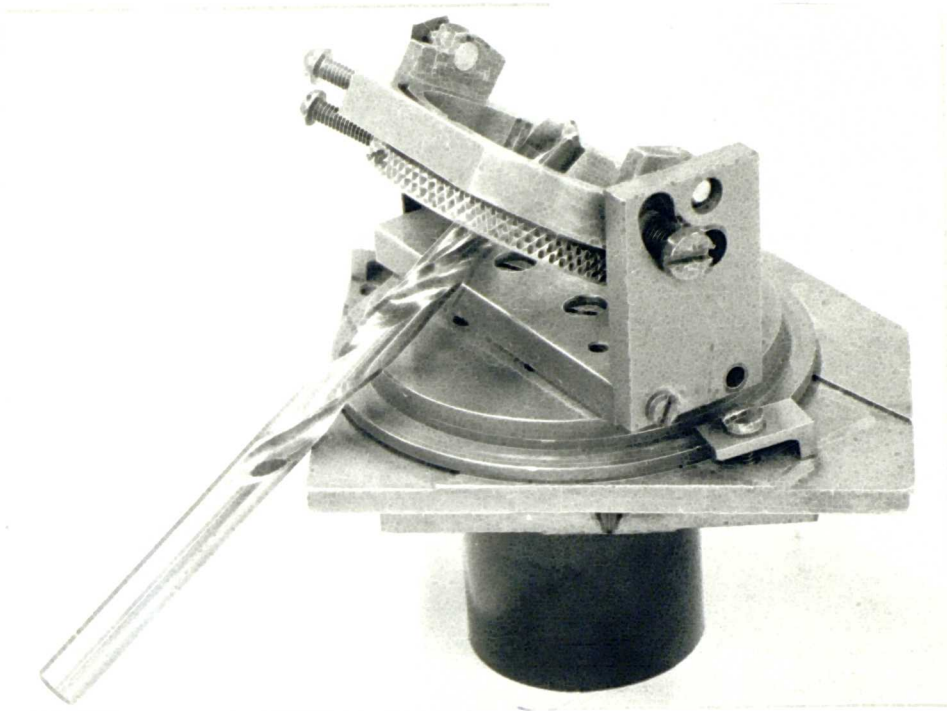
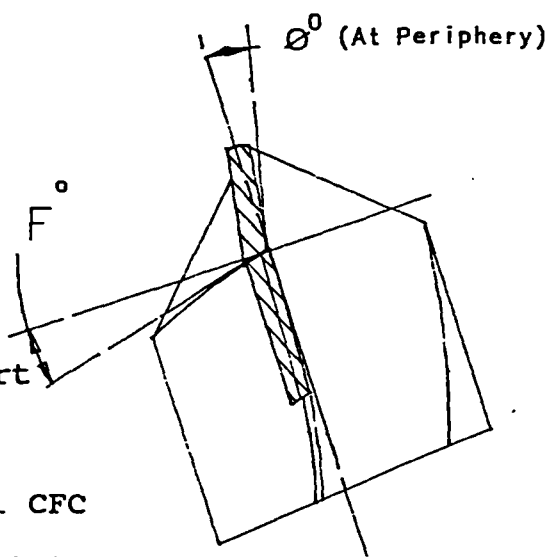
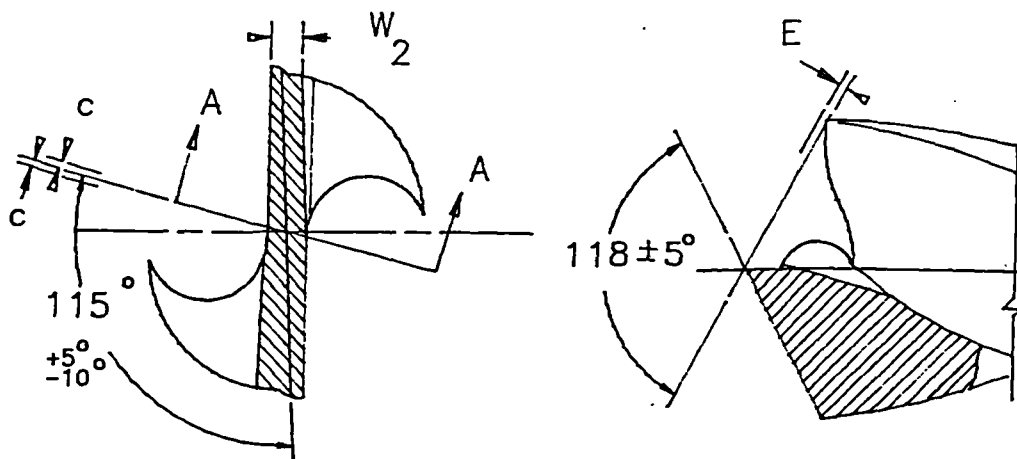
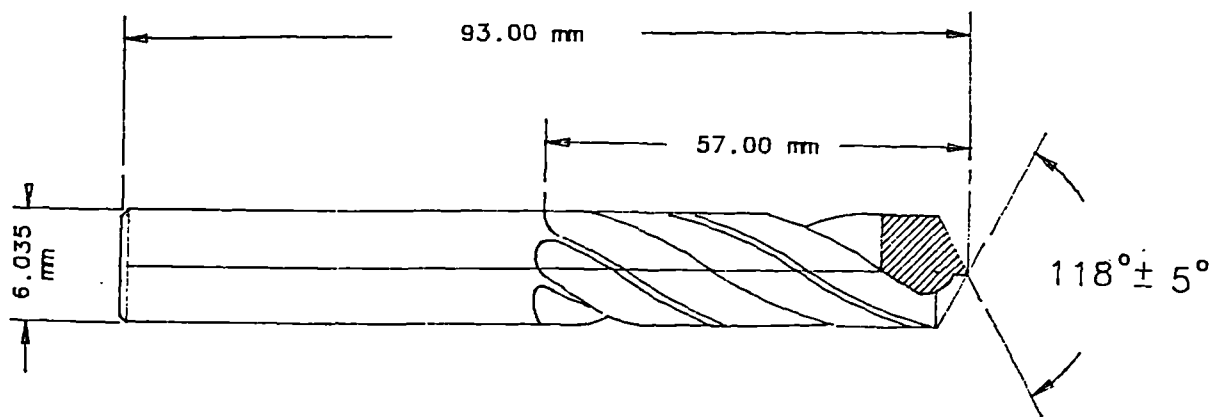


Fig. (33): Photograph showing the method of holding the drill in the specimen stage of the scanning electron microscope.



Material: Carbide Insert

HSS Shank

Used on: Unidirectional CFC

Epoxy 914/Aluminium Alloy Combination

Fig. (34): The British Aerospace drill specification, PTS: 62.01:07 (see over for further details of drill geometry).

Continued from Fig. (34).

1. Body helix angle  $20^{\circ} \pm 2^{\circ}$
2. Smooth transition from Tip helix to Body helix
3. Point thinning may be required to achieve  
     "W<sub>2</sub>" dimension

RANGE. (mm)	'F' Lip Relief	'E' Lip Height	'W2' Web After Thinning	$\emptyset^{\circ}$ Helix Through Tip (min)	'C' Chisel Edge Centra- lity
over 3.2 - 6.3	$14^{\circ} \pm 2^{\circ}$	0.050 TIR	.45-.88	$4^{\circ}$	0.080



Fig. (35): Photograph showing, from left to right, the Solid Carbide, Precision, Gandtrack and Klenk drills.

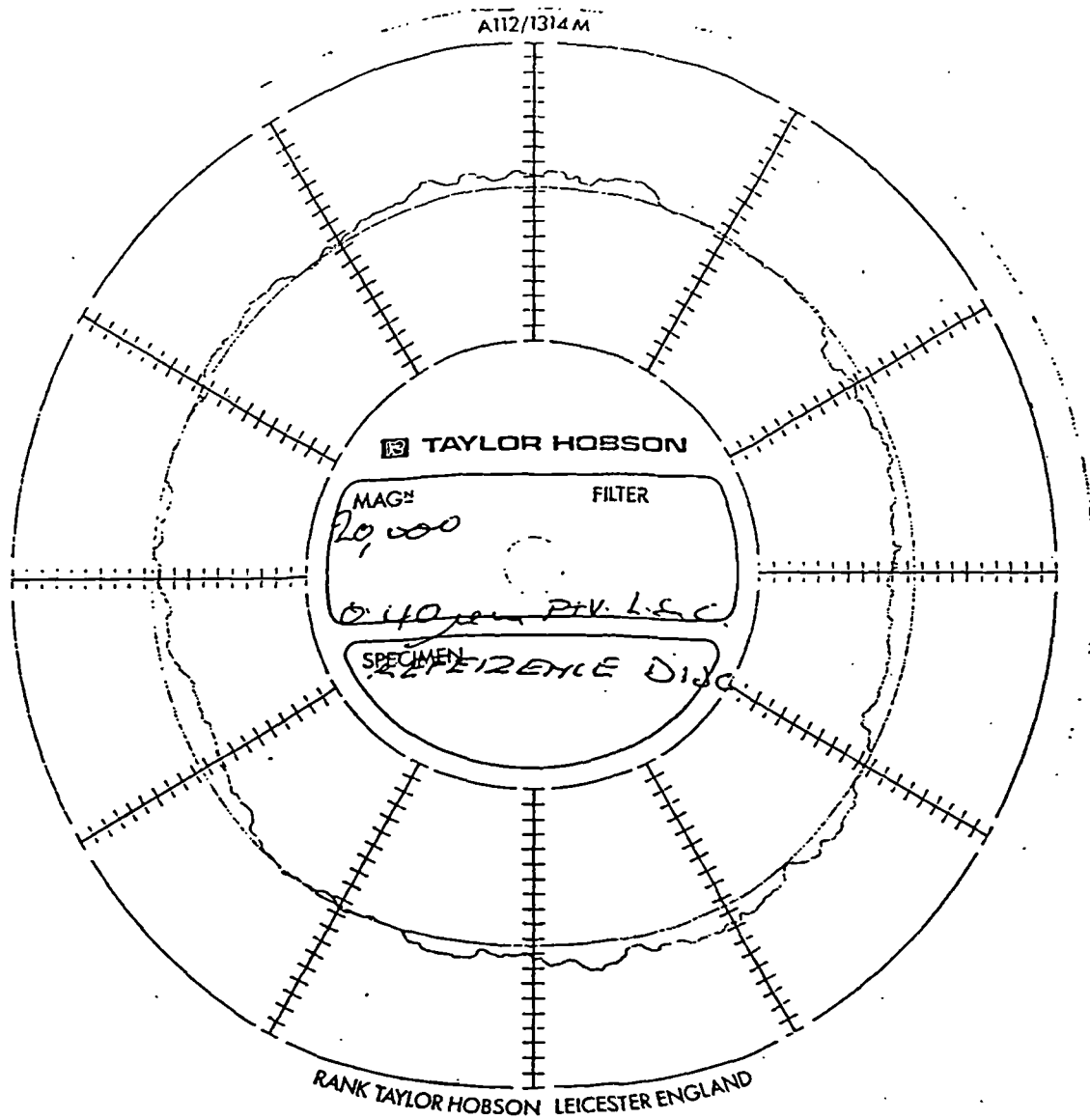
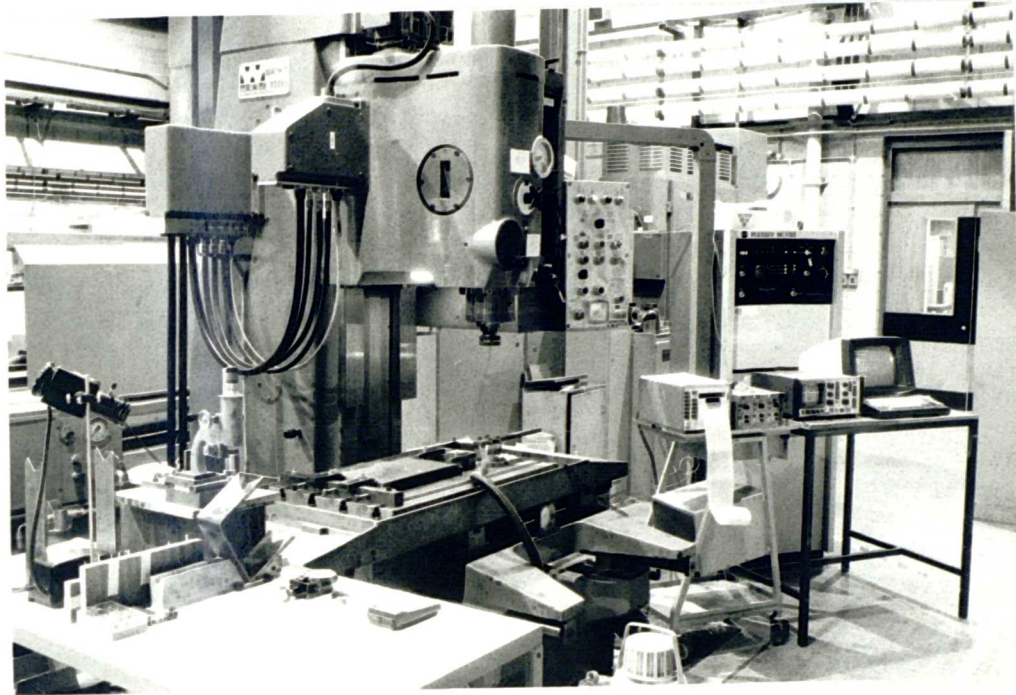


Fig. (36): Chart showing the Talyrond trace of the 6.035mm plug gauge.



**Fig. (37): Photograph of the Wadkin Mill/Drill machine showing associated instrumentation.**

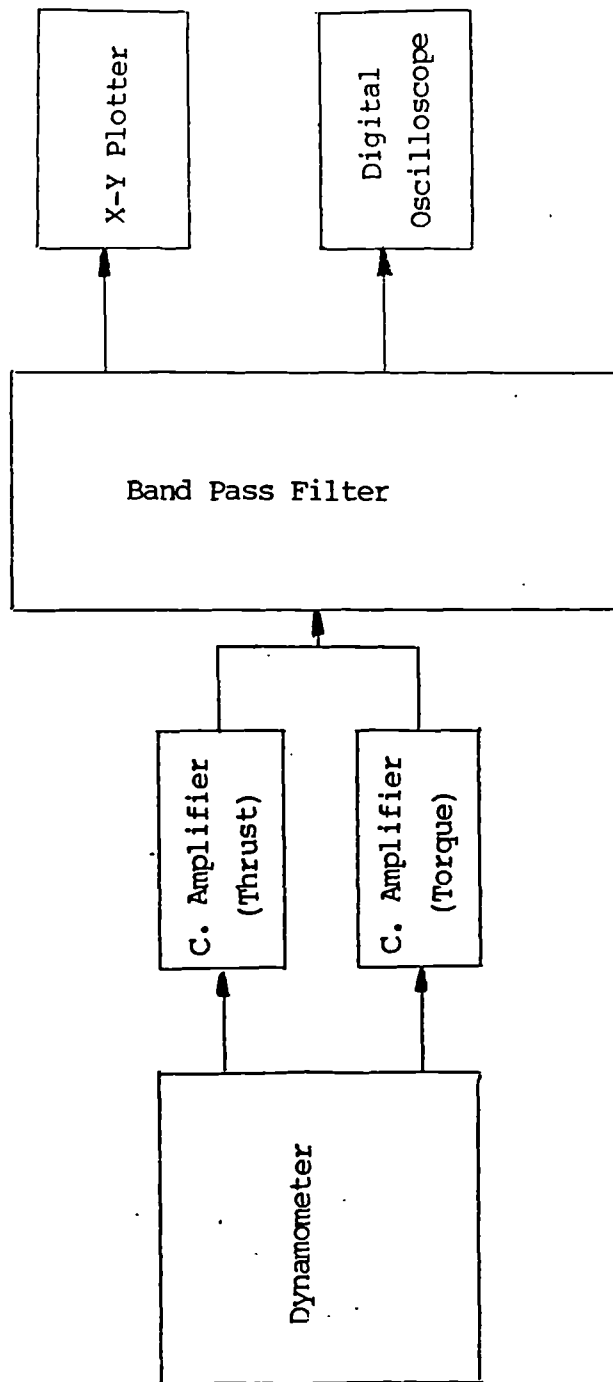


Fig. (38): Block diagram describing the equipment used for the dynamometer tests.

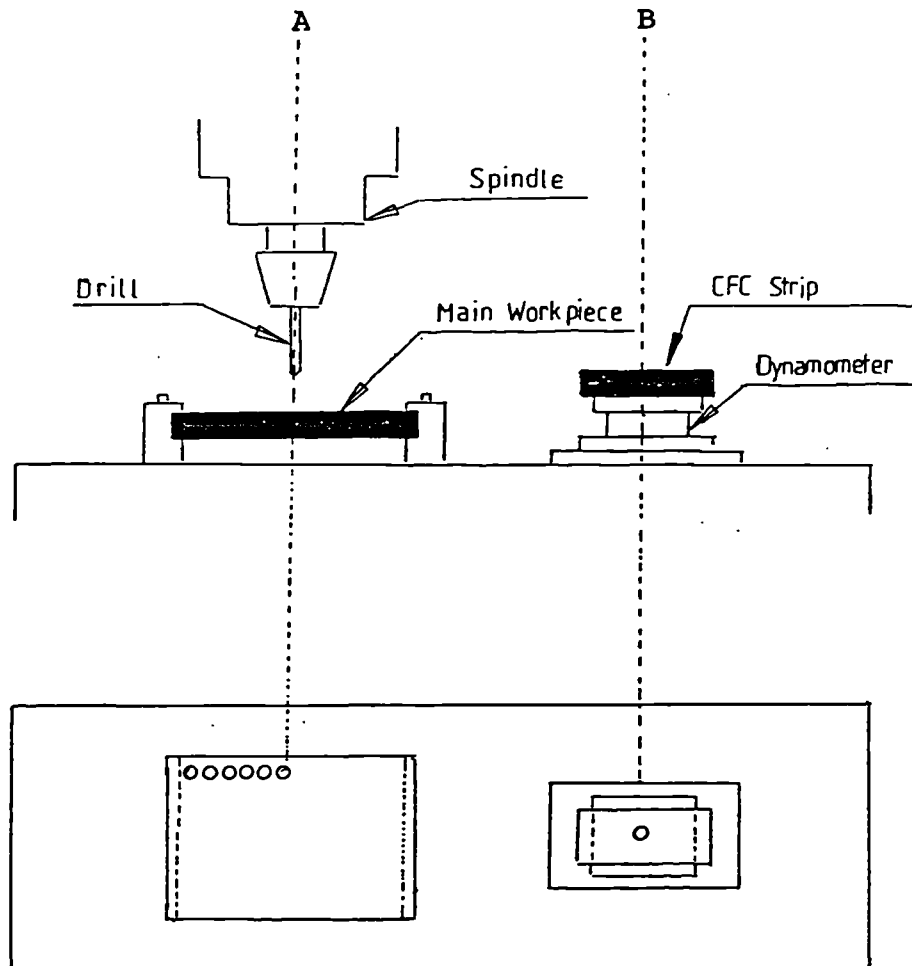
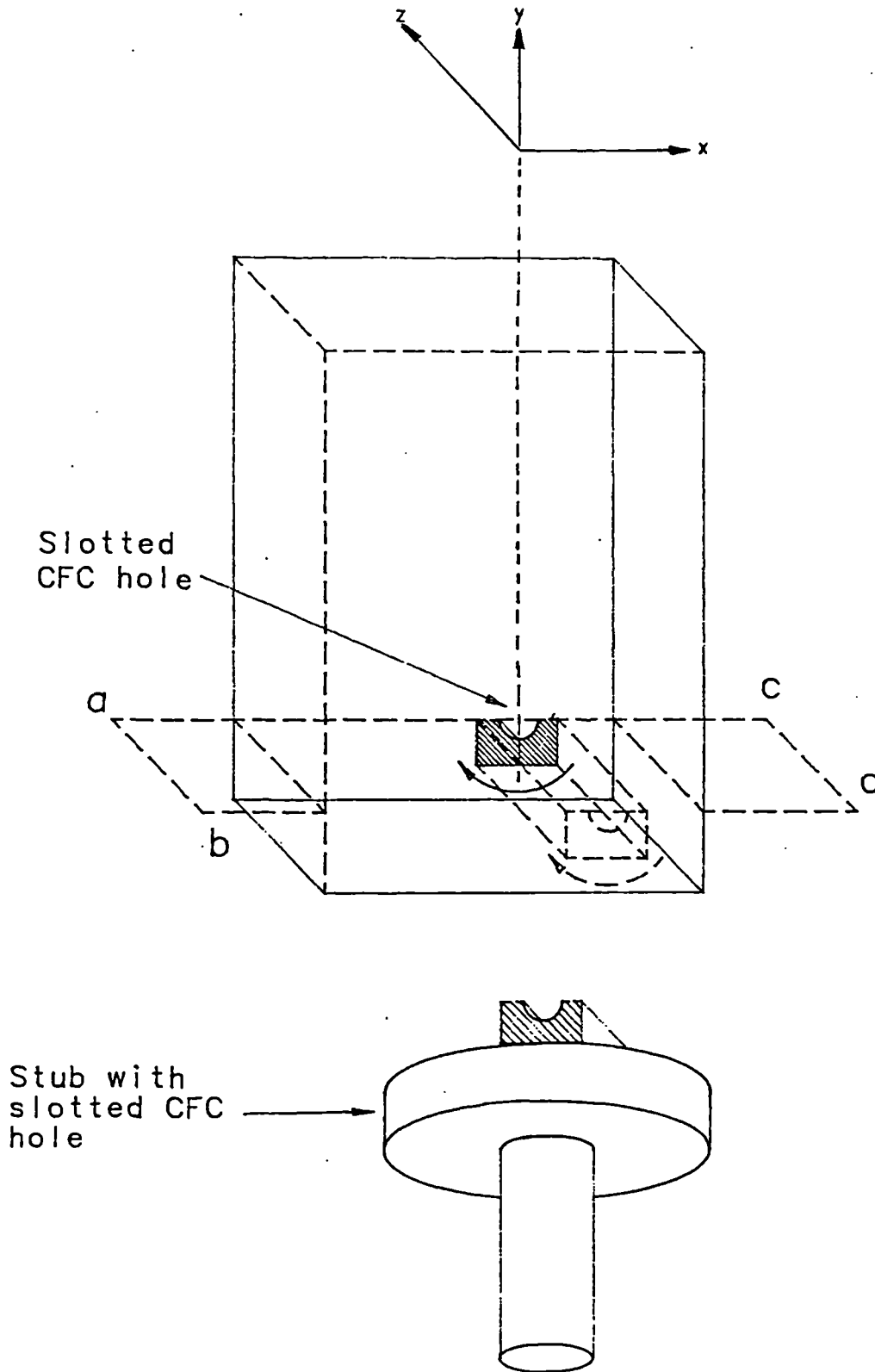


Fig. (39): Illustration of the experimental arrangement for the second phase of dynamometer tests.



a,b,c,d: Hole sectioning plane

Fig. (40): Drawing showing the sequence of sectioning for removing a hole specimen from CFC panel for examination in the scanning electron microscope.

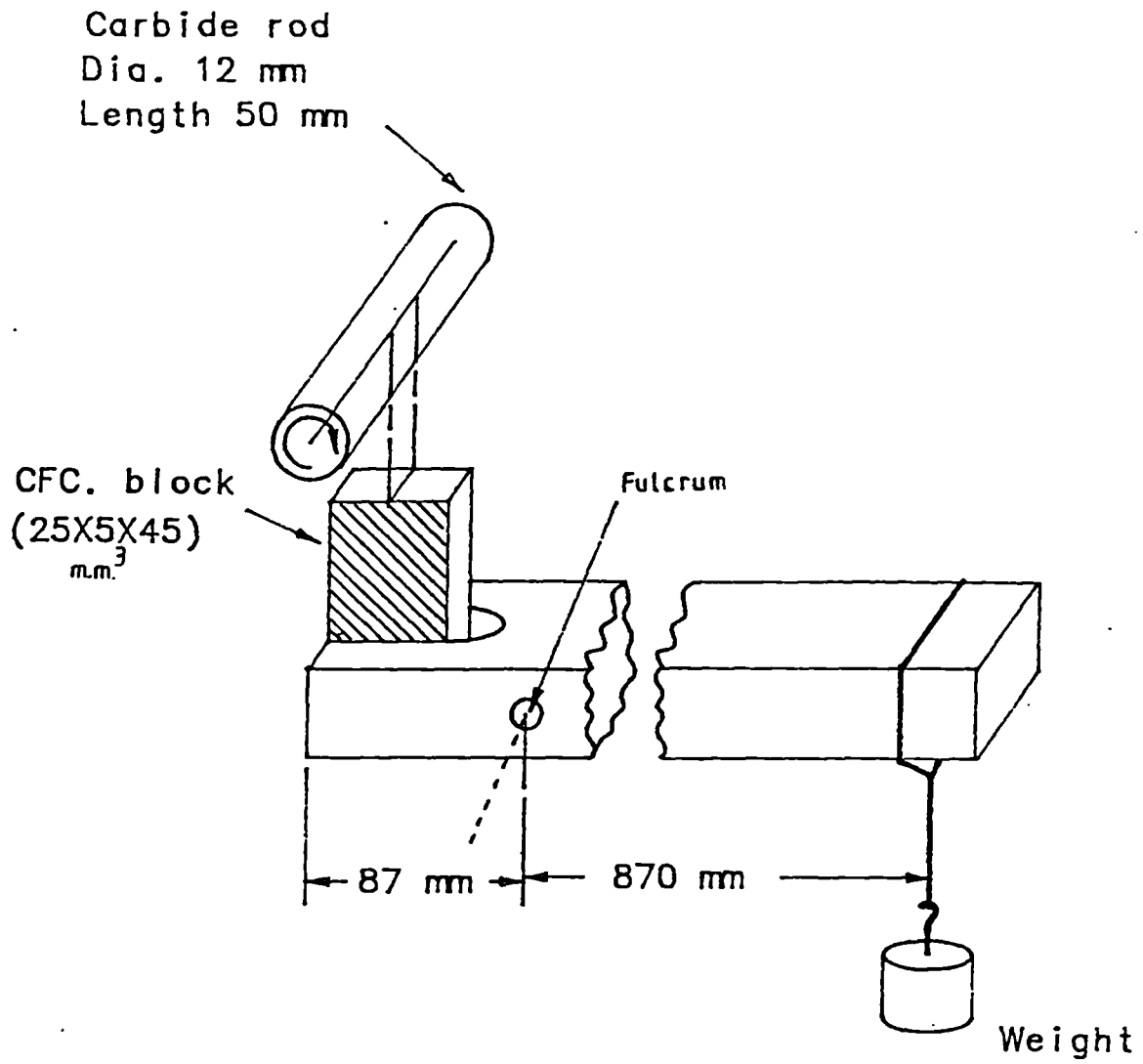


Fig. (41): Sketch showing the lathe wear test arrangement.

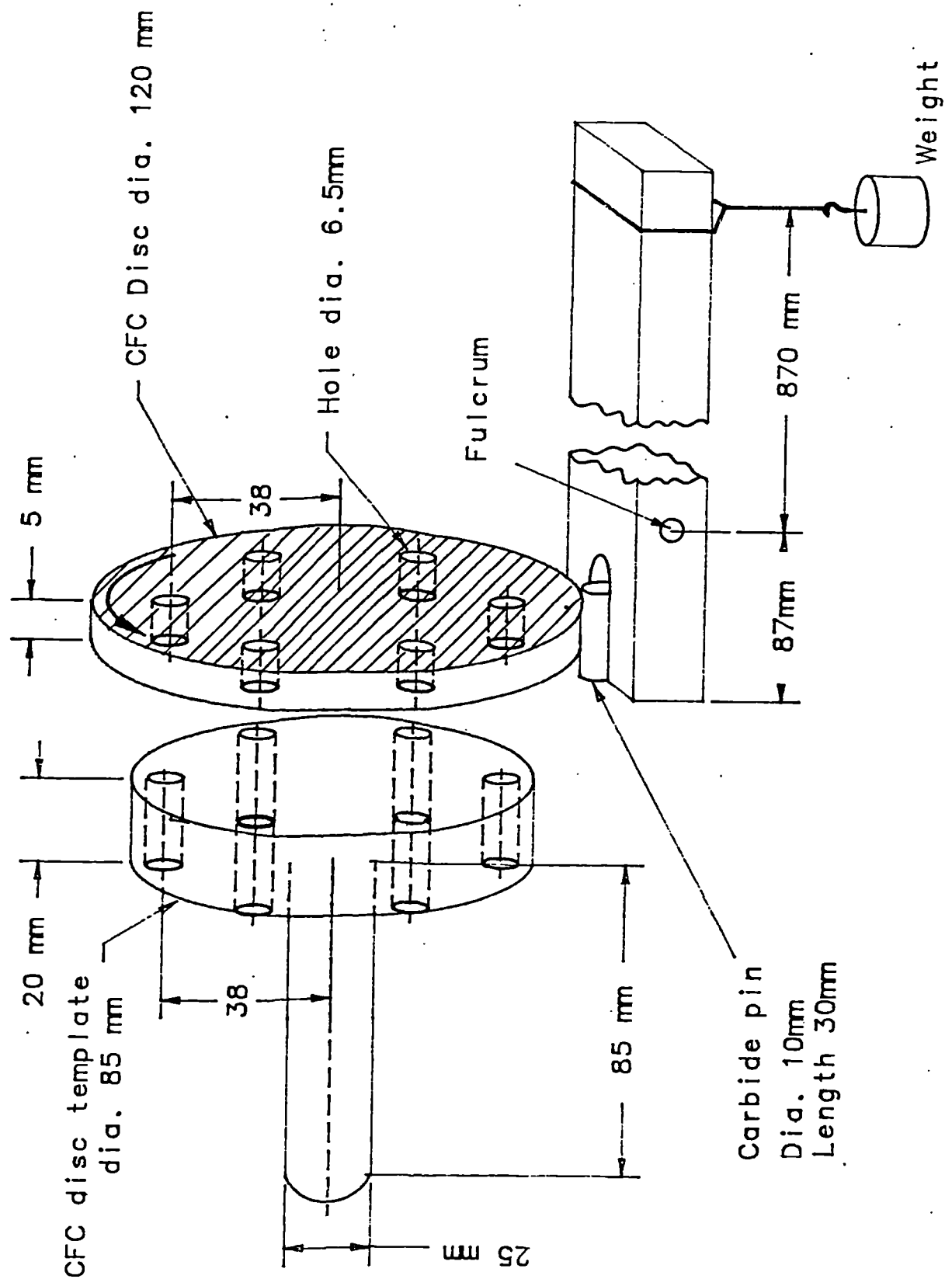
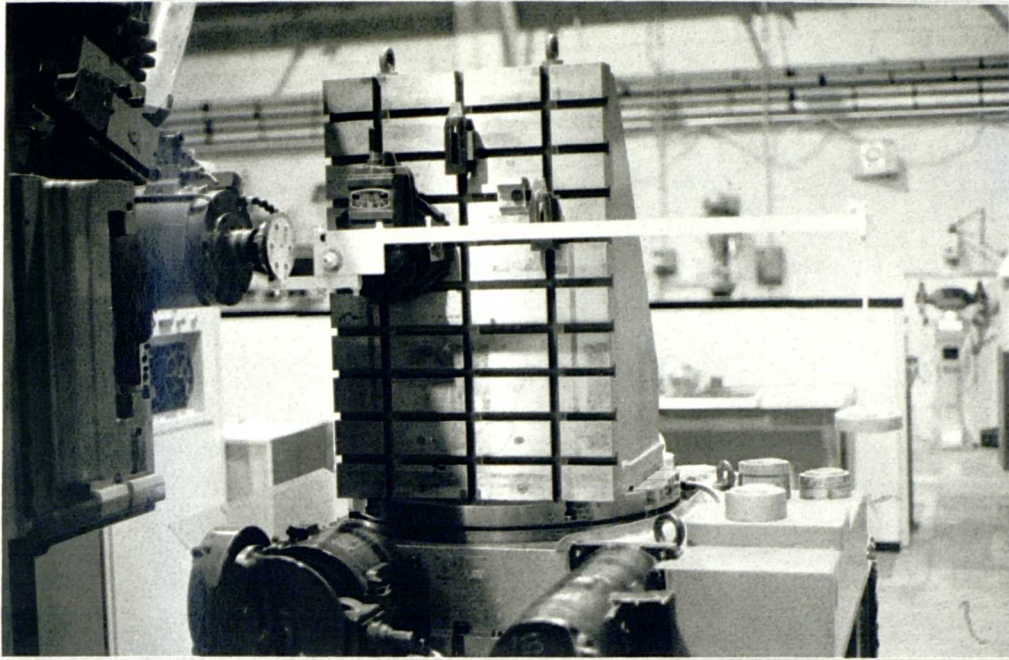
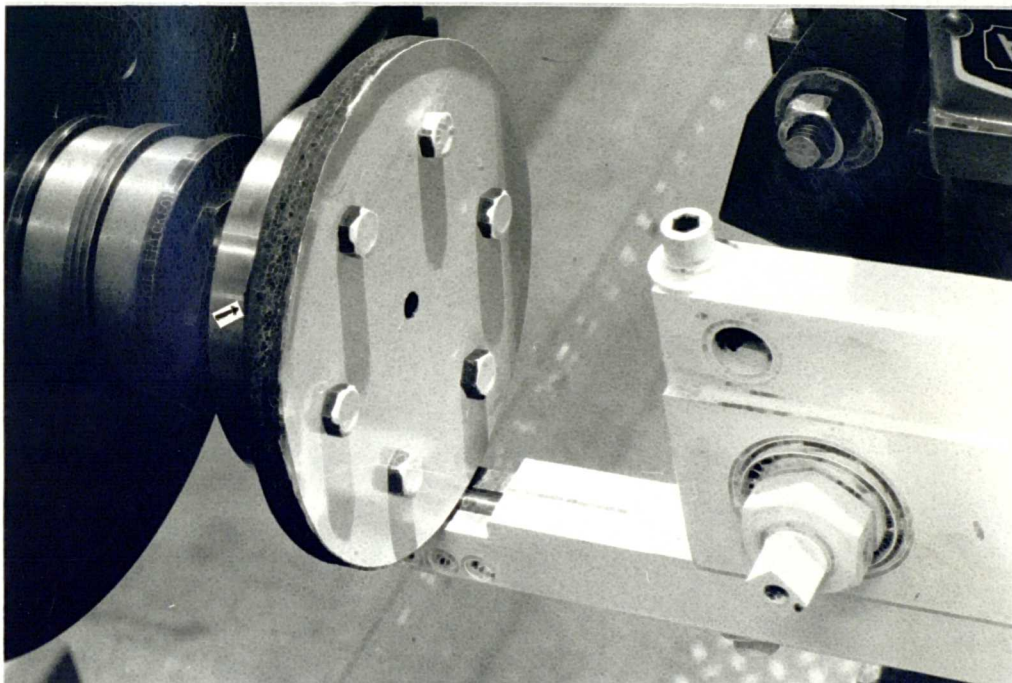


Fig. (42): Sketch showing the wear test arrangement in the Kearney and Trecker Machining centre.



**Fig. (43):** Photograph showing the machining centre test.



**Fig. (44):** Close-up view of the CFC disc rubbing against the carbide rod in the holder on the machining centre test.

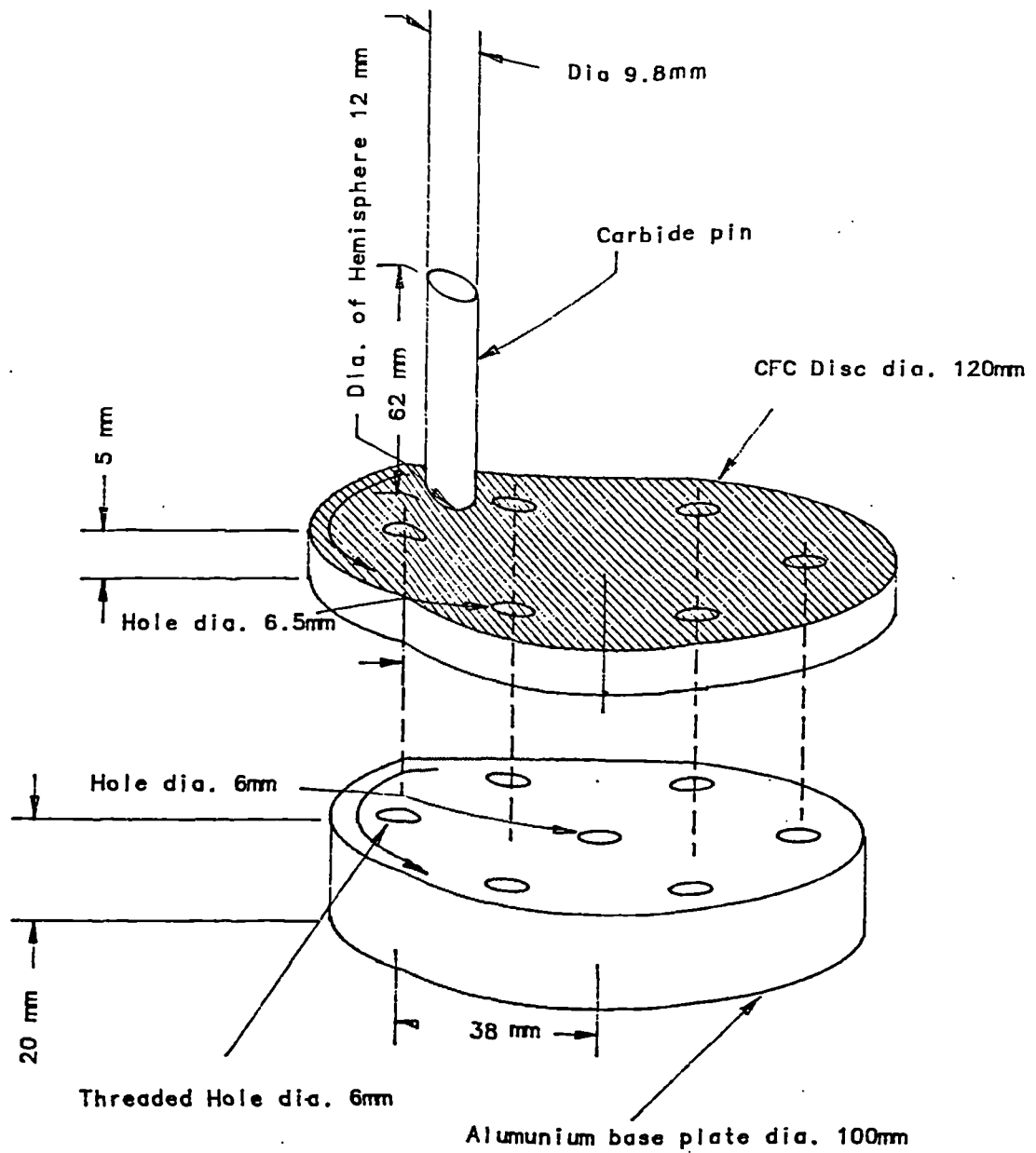


Fig. (45): Sketch showing the Denison Pin-on-Disc wear test arrangement.

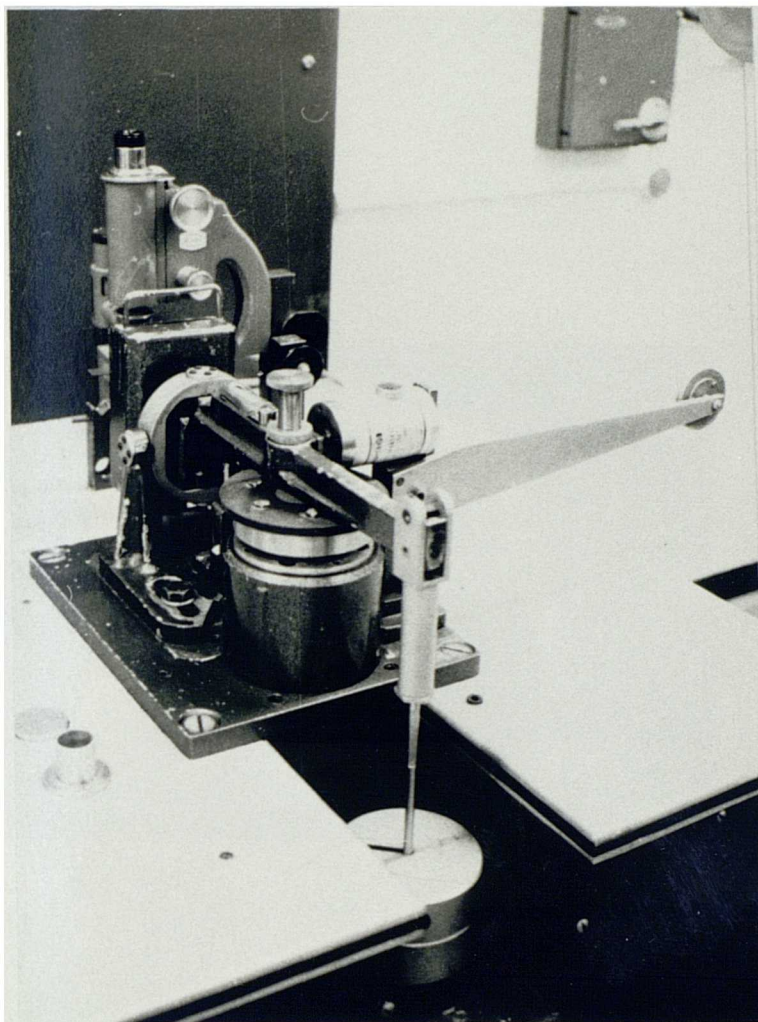


Fig. (46): Photograph showing the Denison Pin-on-Disc test.



**Fig. (47): Scanning electron micrograph showing a typical flank wear pattern of a Gandtrack drill where the flank wear increased toward the periphery of the drill.**

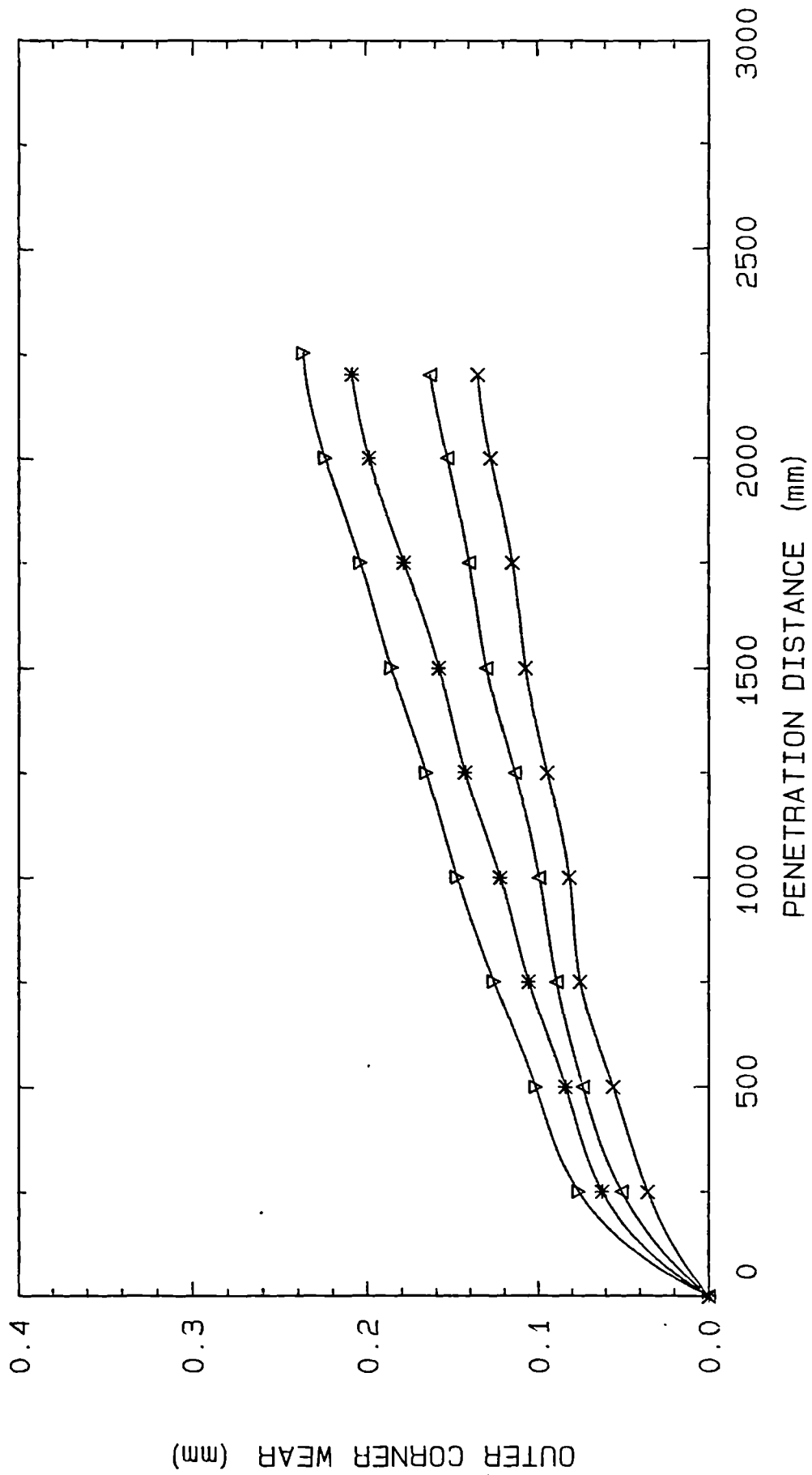


Fig. (48): The average outer corner wear width of the Klenk (v), Gandtrack (\*), Precision (Δ) and Solid Carbide (x) drills.

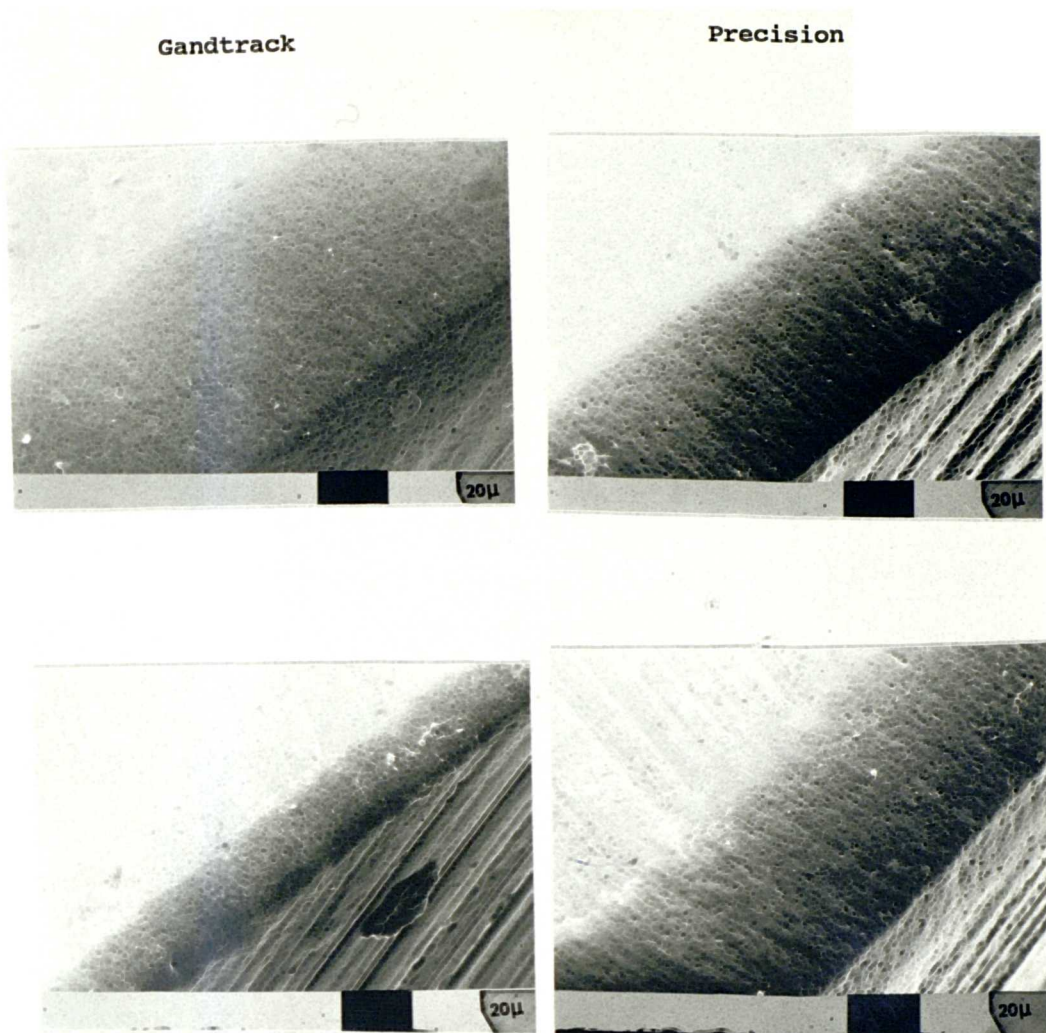
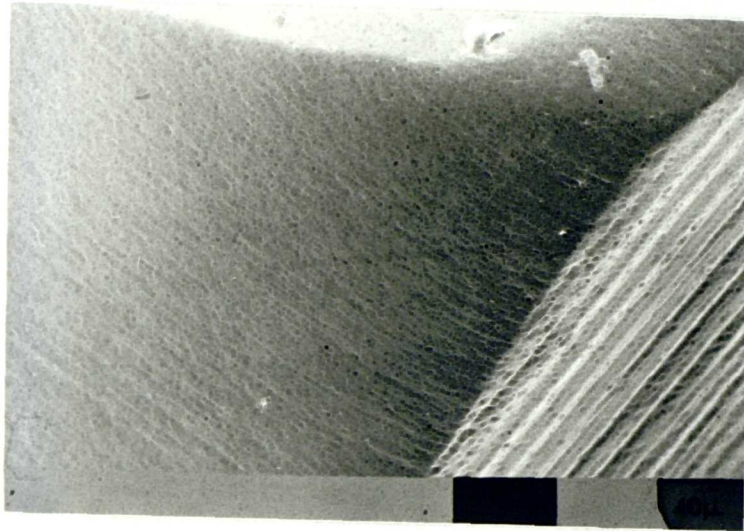


Fig. (49): SEM micrographs of the two flanks at the outer corner measured after 40 holes of the Gandtrack (left) and Precision (right) drills showing non-symmetric wear in the case of the Gandtrack drill.

Precision



Gandtrack

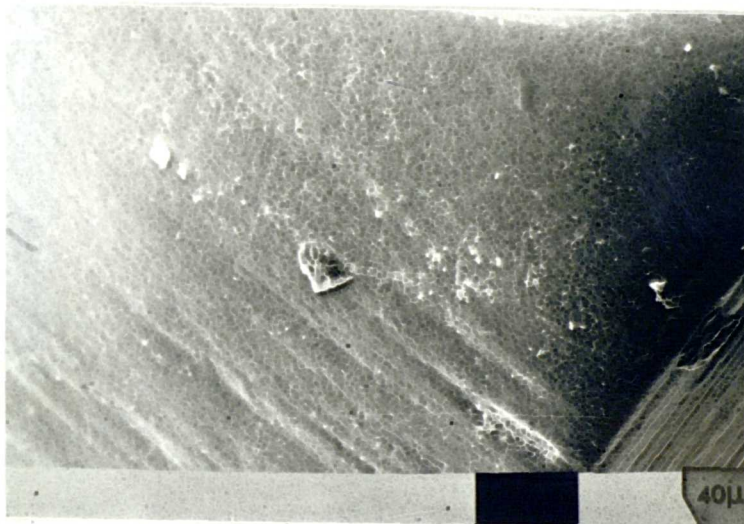


Fig. (50): SEM micrograph of the margin wear of Precision (top) and Gandtrack (bottom) drills.

Precision

Gandtrack

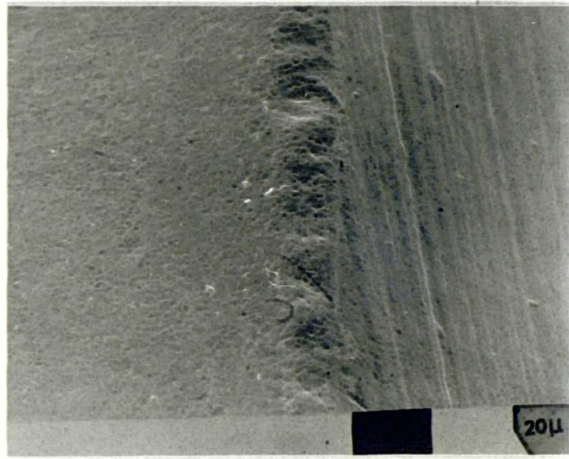
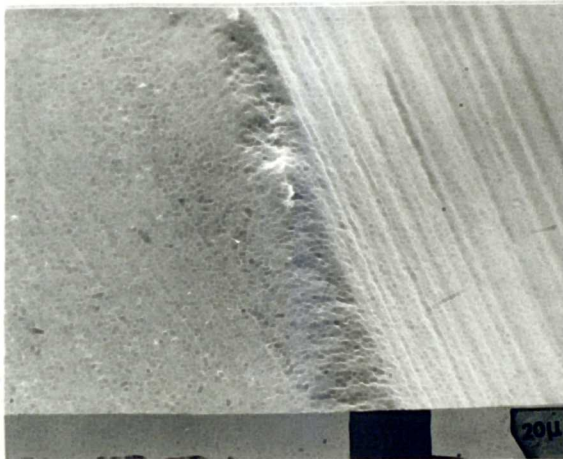
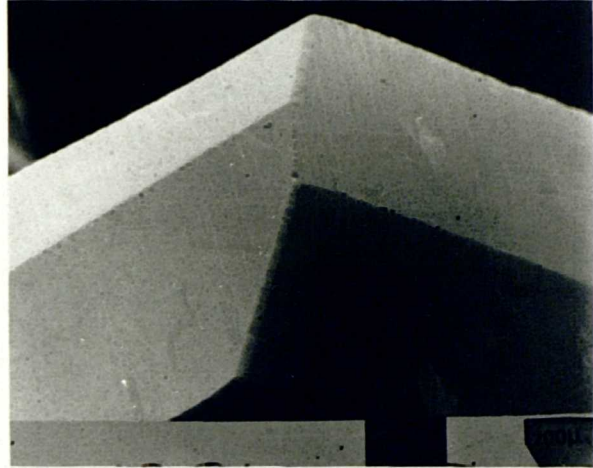
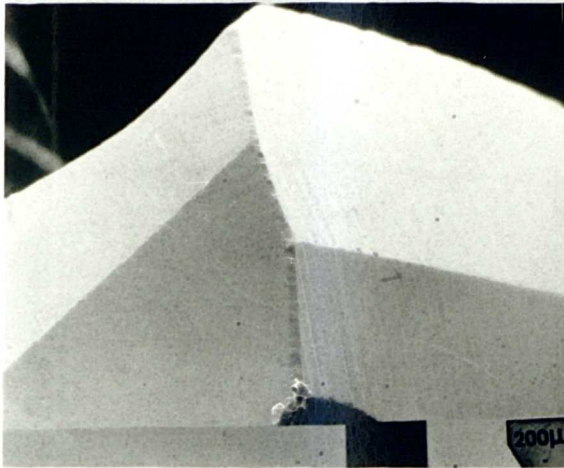


Fig. (51): SEM micrograph of the chisel edge wear of the Precision (left) and Gandtrack (right) drills.

Precision



Gandtrack

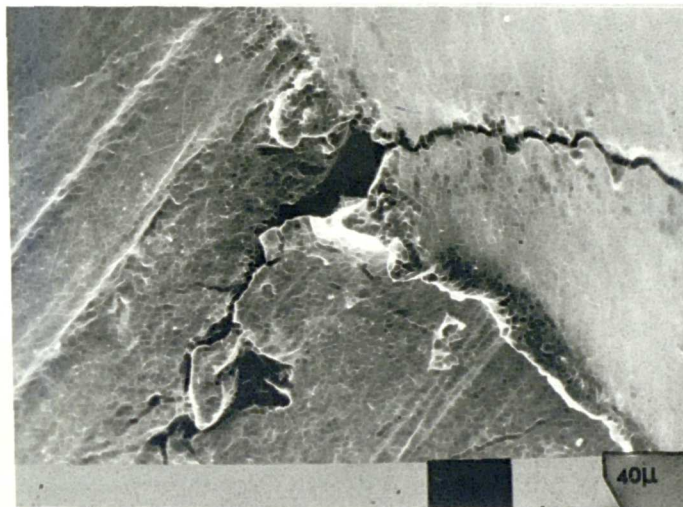


Fig. (52): SEM micrograph showing the damage development of the Precision (top) and Gandtrack (bottom) drills at or close to the brazed region between the cemented carbide and the HSS shank.

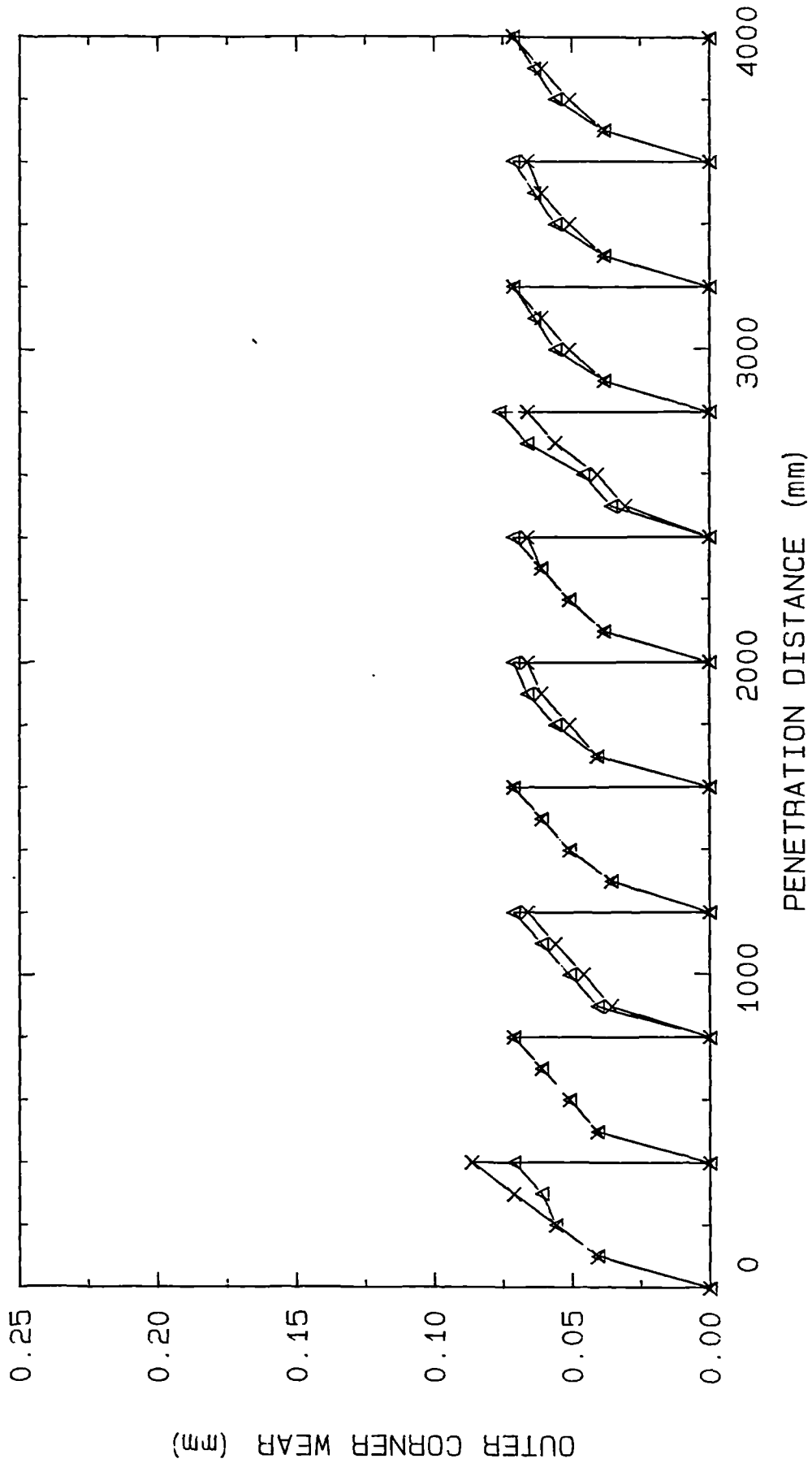


Fig. (53): The outer corner wear of the flanks A (x) and B (Δ) of the Precision drill in the second stage of drill testing.

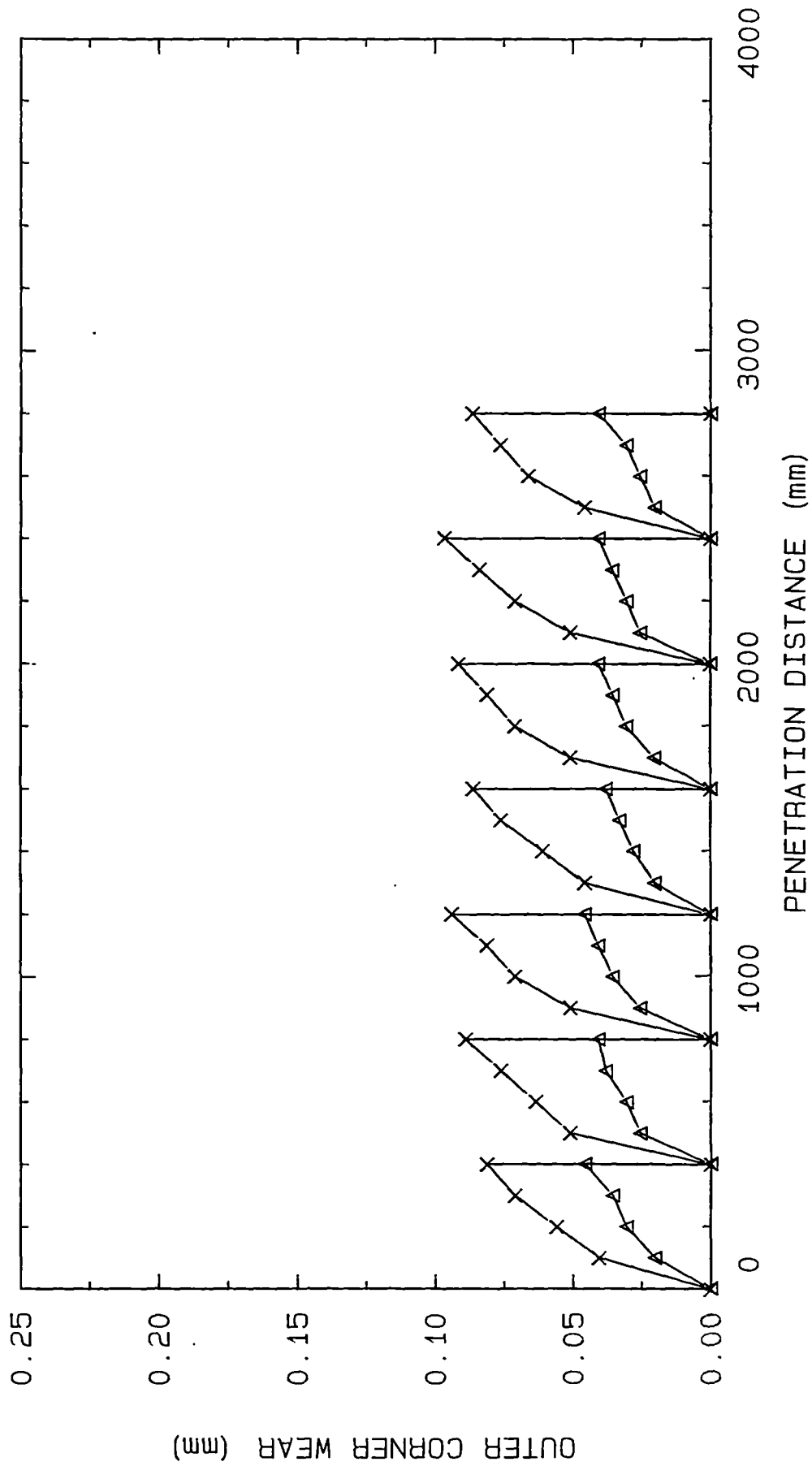


Fig. (54): The outer corner wear of the flanks A (x) and B (Δ) of the Gandtrack drill in the second stage of drill testing.

# Drill Life Test Result

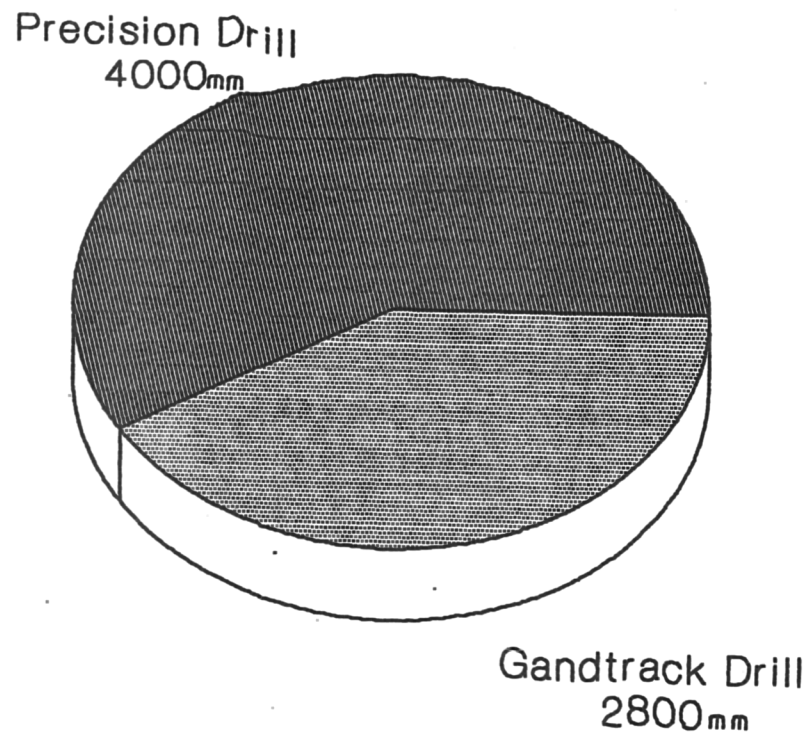
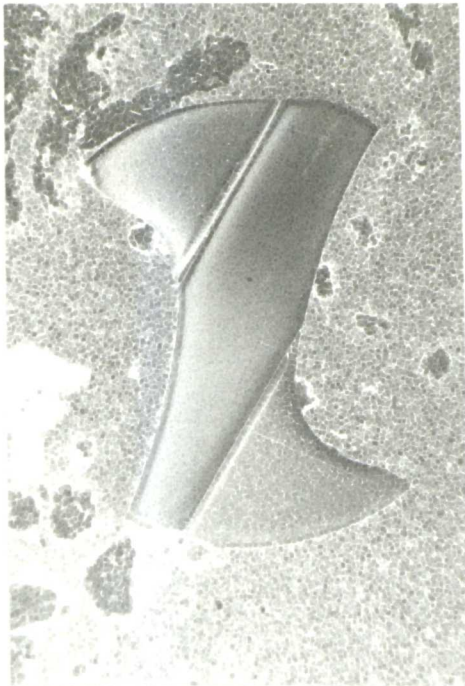
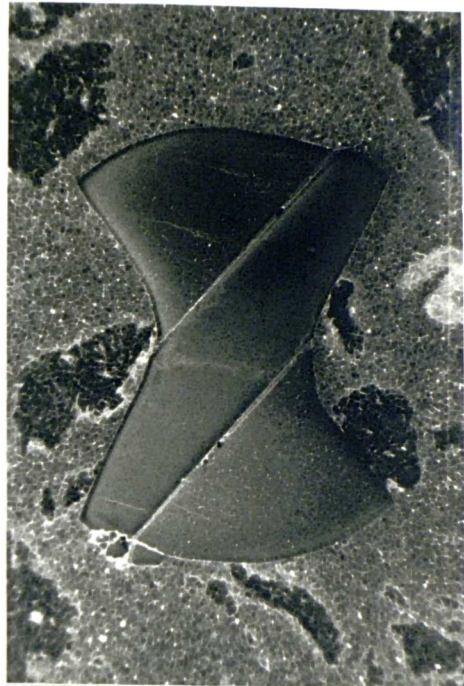


Fig. (55): The comparison of the Precision and the Gandtrack drill in terms of total penetration distance.

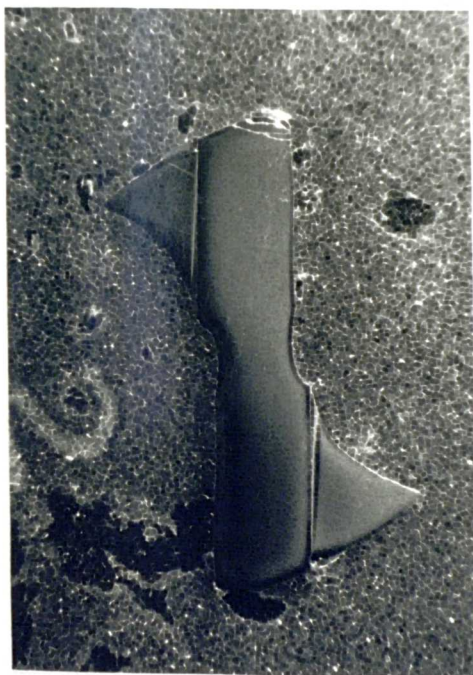
**Gandtrack**



**Precision**



**Klenk**

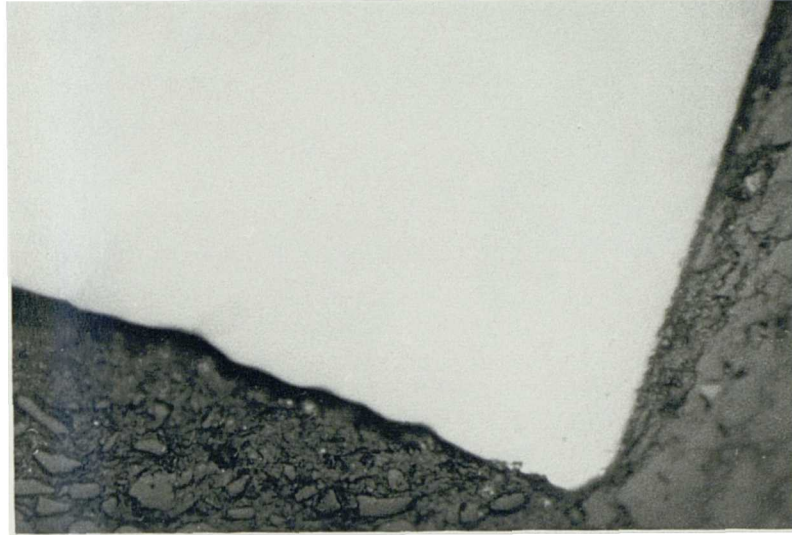


**Carbide**



Fig. (56): The drill body profiles of Gandtrack (top left), Precision (top right), Klenk (bottom left) and Carbide (bottom right) drills.

Klenk



Precision

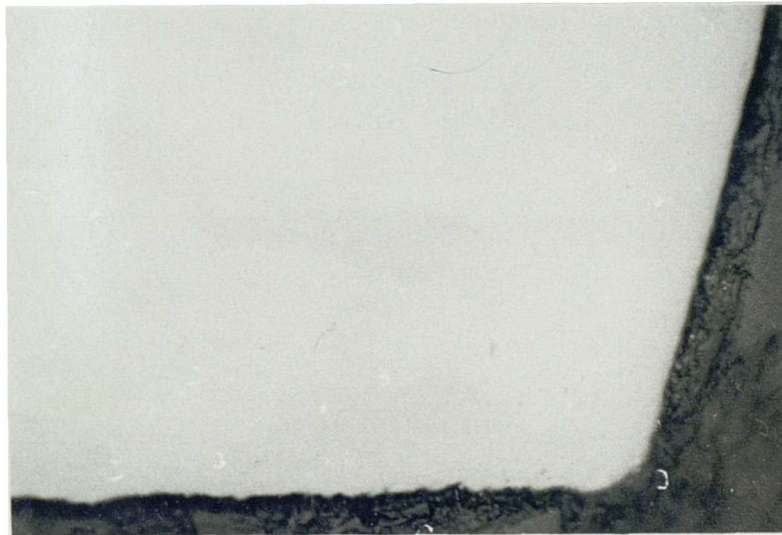


Fig. (57): Micrograph showing the magnified (103 times) view of the outer corner of the Klenk (top) and Precision (bottom) drills

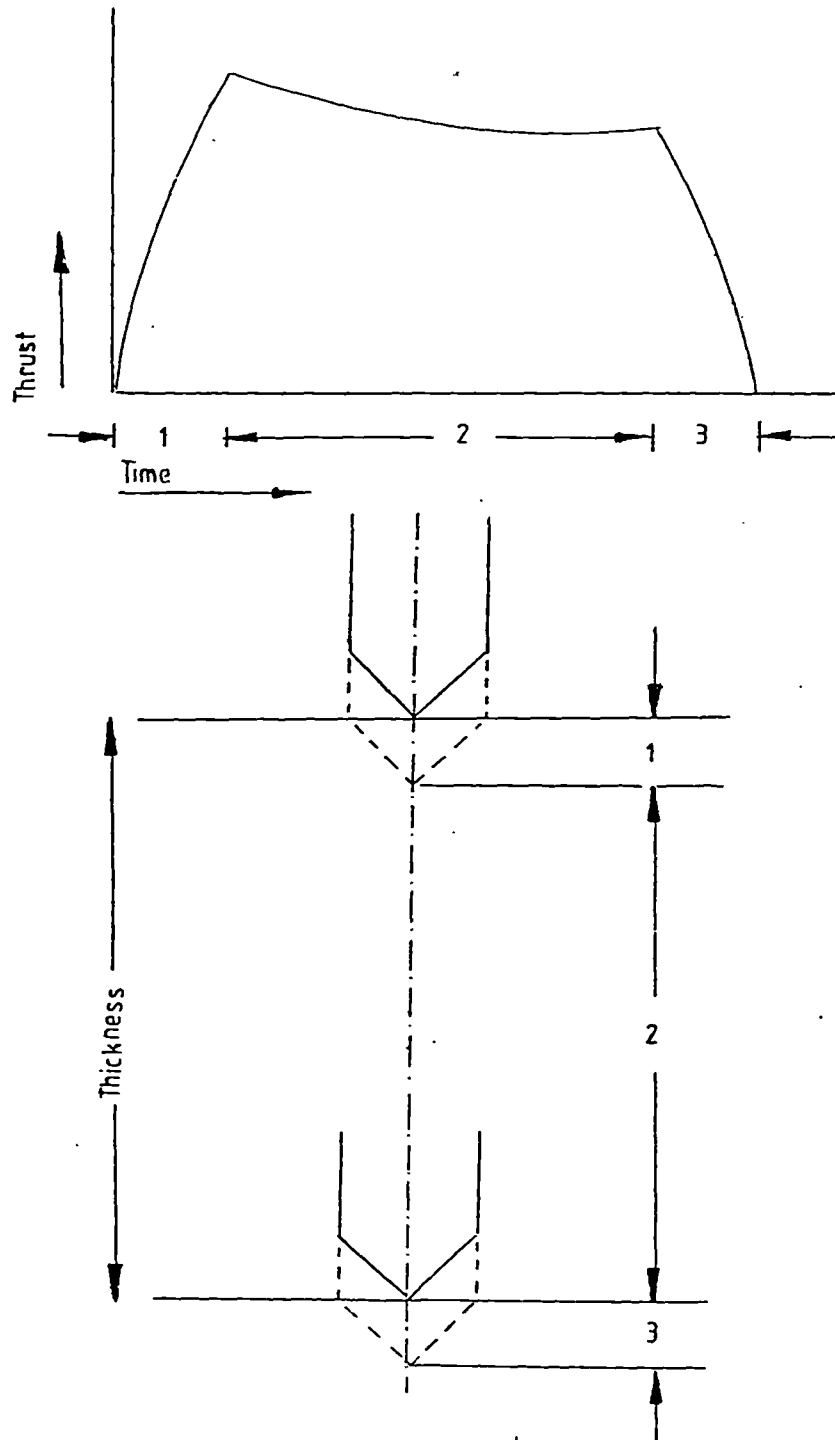


Fig. (58): The variation of thrust force during the three stages of drilling.

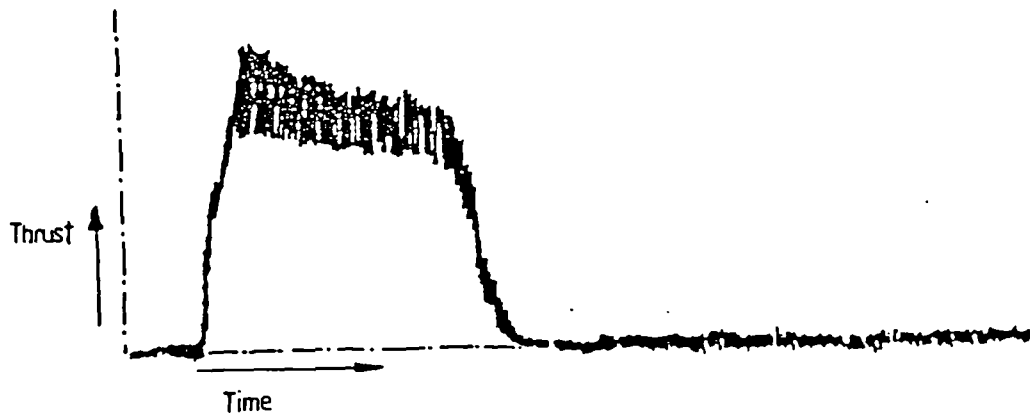
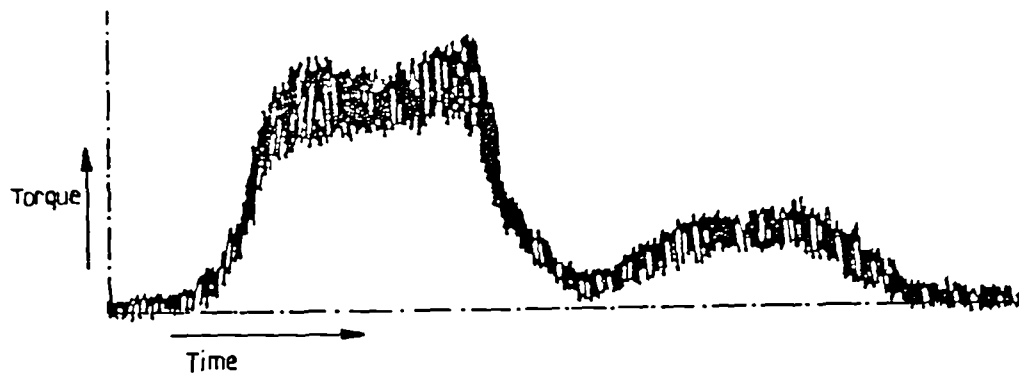


Fig. (59): A typical drill torque (top) and thrust (bottom) response.

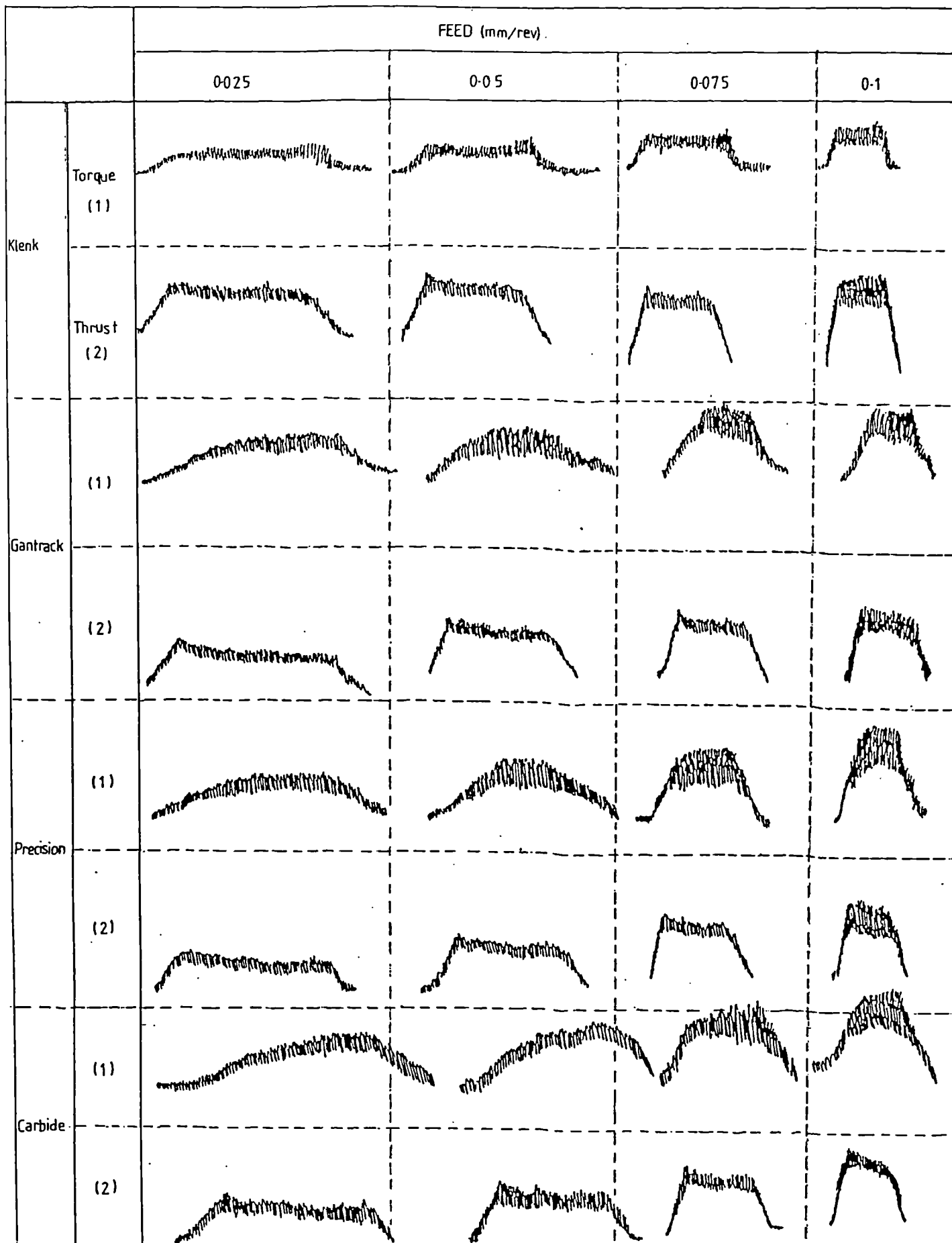
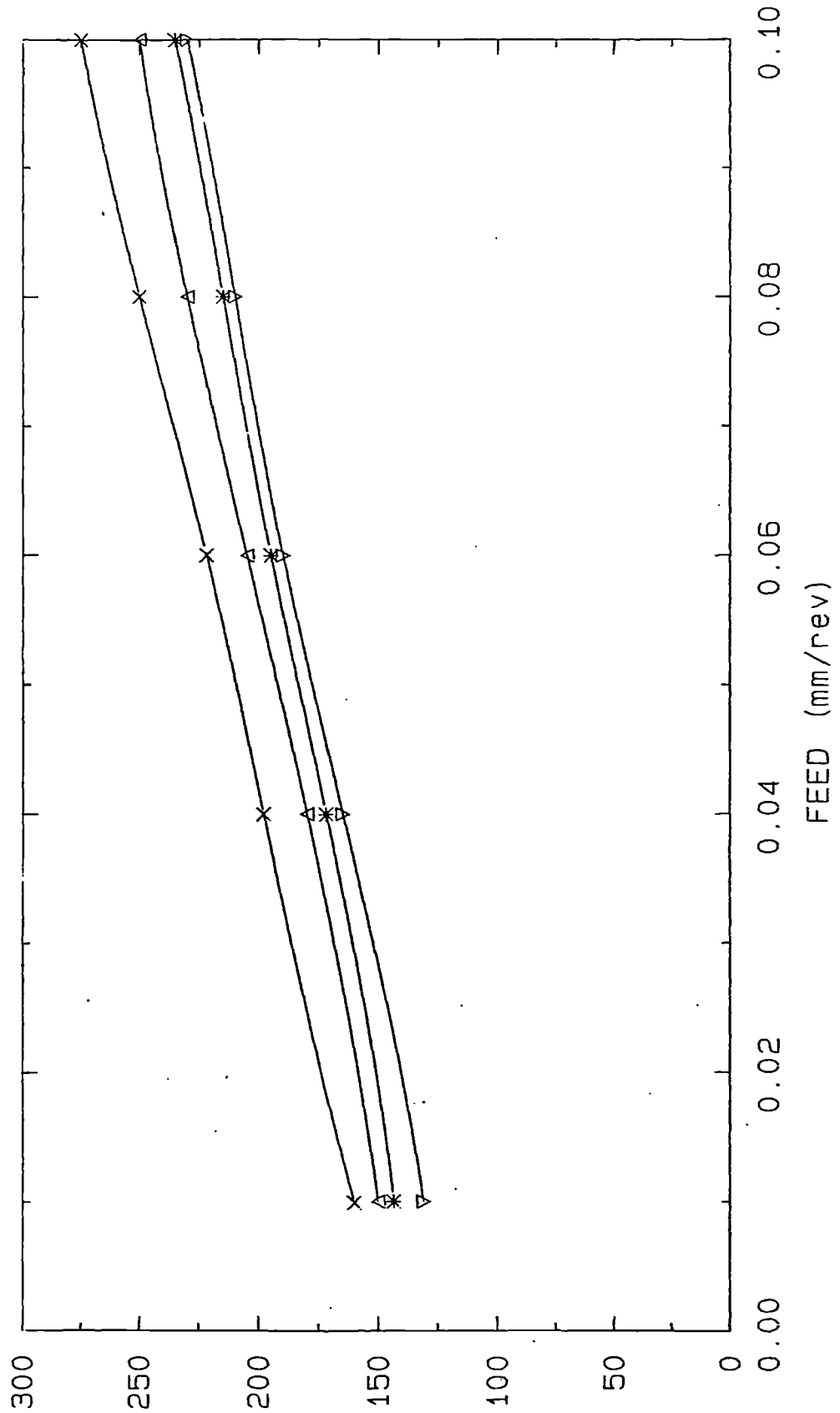


Fig. (60): The dynamometer torque and thrust response at the drilling speed of 2800 RPM and varying feed rates.



(N) THRUST

Fig. (61): The maximum thrust response for Klenk (x), Gandtrack (Δ), Precision (\*) and Carbide (∇) drills at a speed of 2800 RPM and various feed rates.

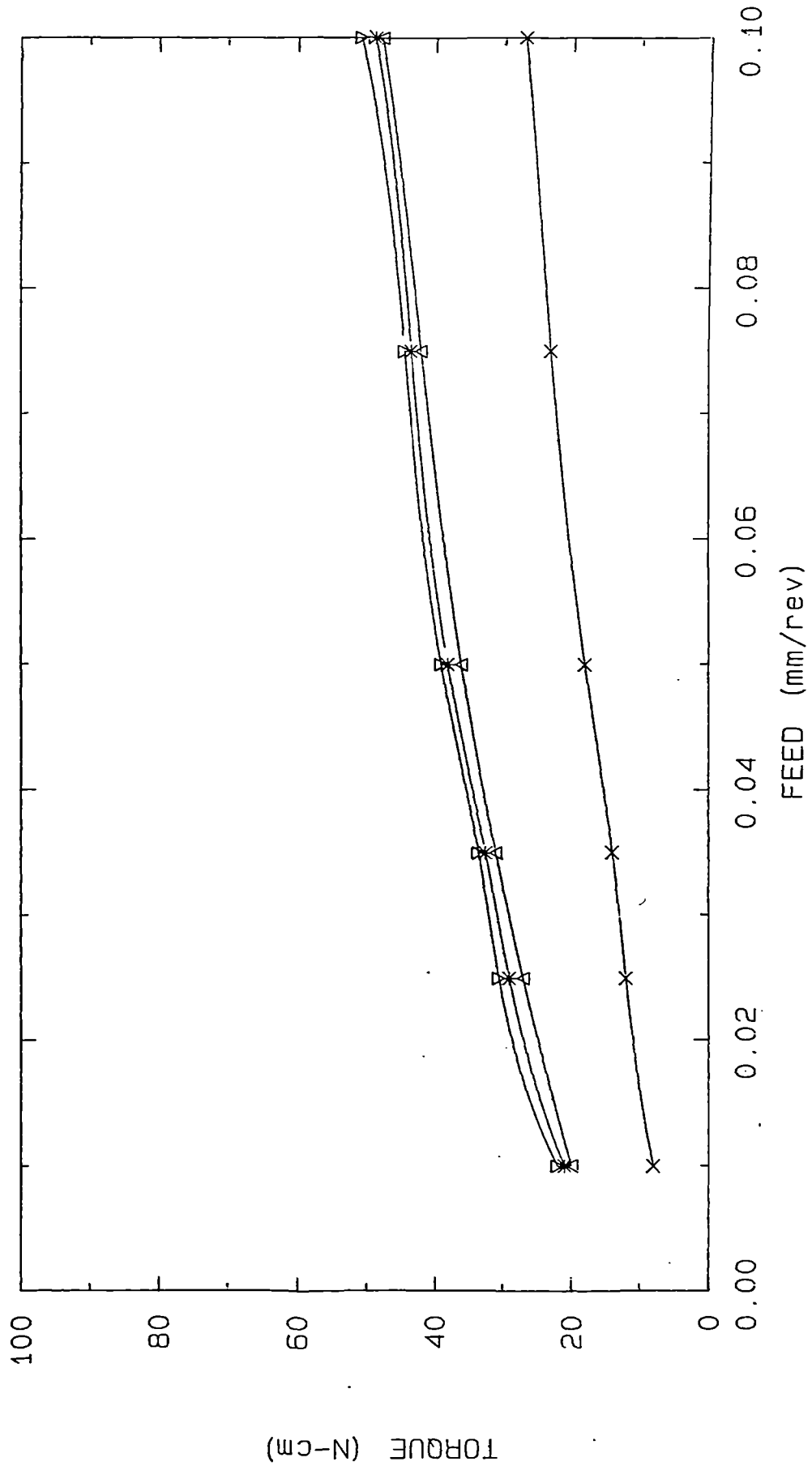


Fig. (62): The maximum torque response for Klenk (x), Gandtrack (Δ), Precision (\*) and Carbide (∇) drills at a speed of 2800 RPM and various feed rates.

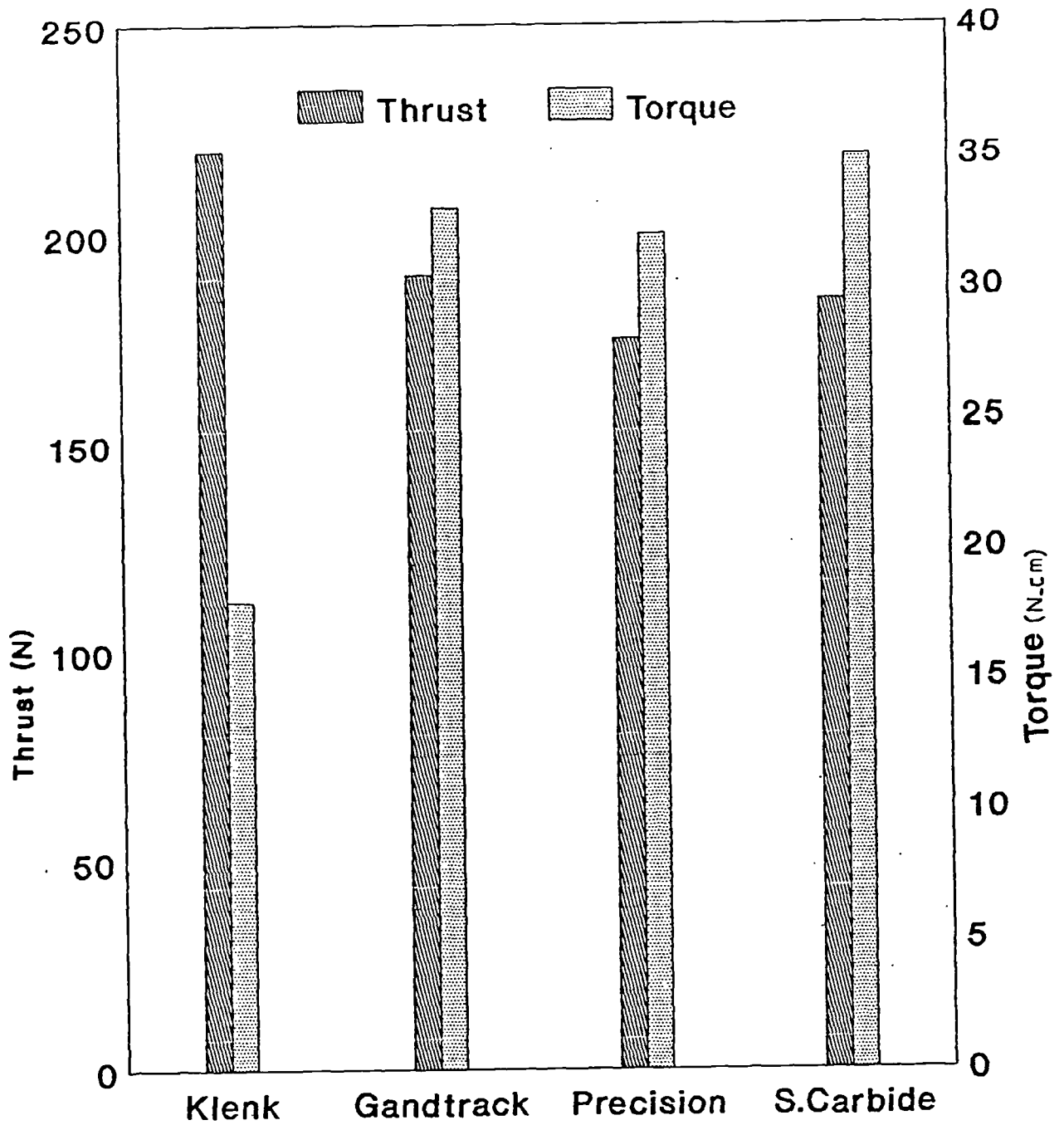
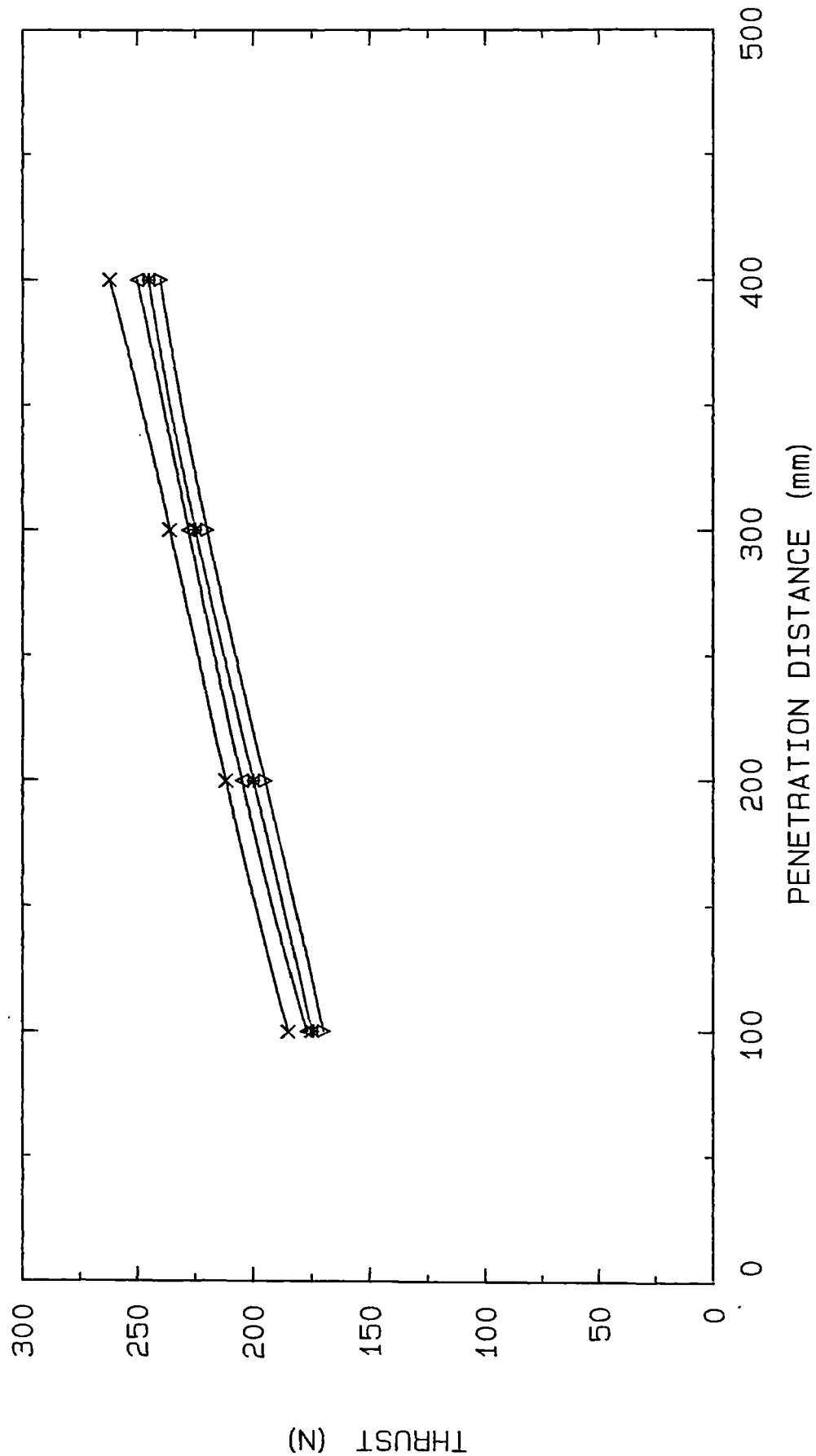


Fig. (63): The maximum thrust and torque response for Klenk, Gandtrack, Precision and Solid carbide drills at a speed of 2800 RPM and feed of 0.05mm/rev.



(N) THRUST

Fig. (64): The thrust response of Klenk (x), Gandtrack (Δ), Precision (\*) and Carbide (v) drills against penetration distance at a speed of 2800 RPM and feed of 0.05mm/Rev.

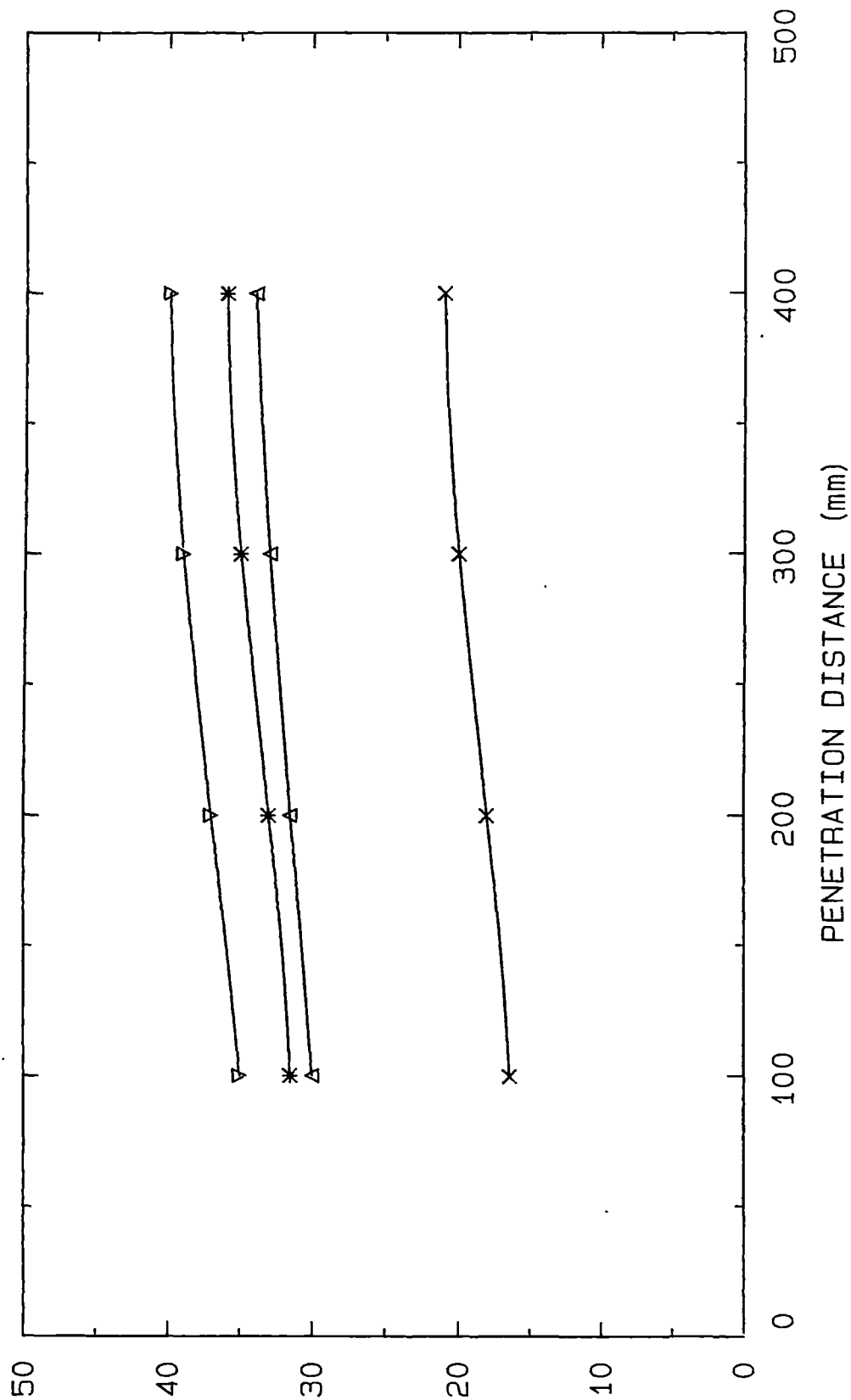


Fig. (65): The torque response of Klenk (x), Gandtrack (Δ), Precision (\*) and Carbide (∇) drills against penetration distance at a speed of 2800 RPM and feed of 0.05mm/Rev.

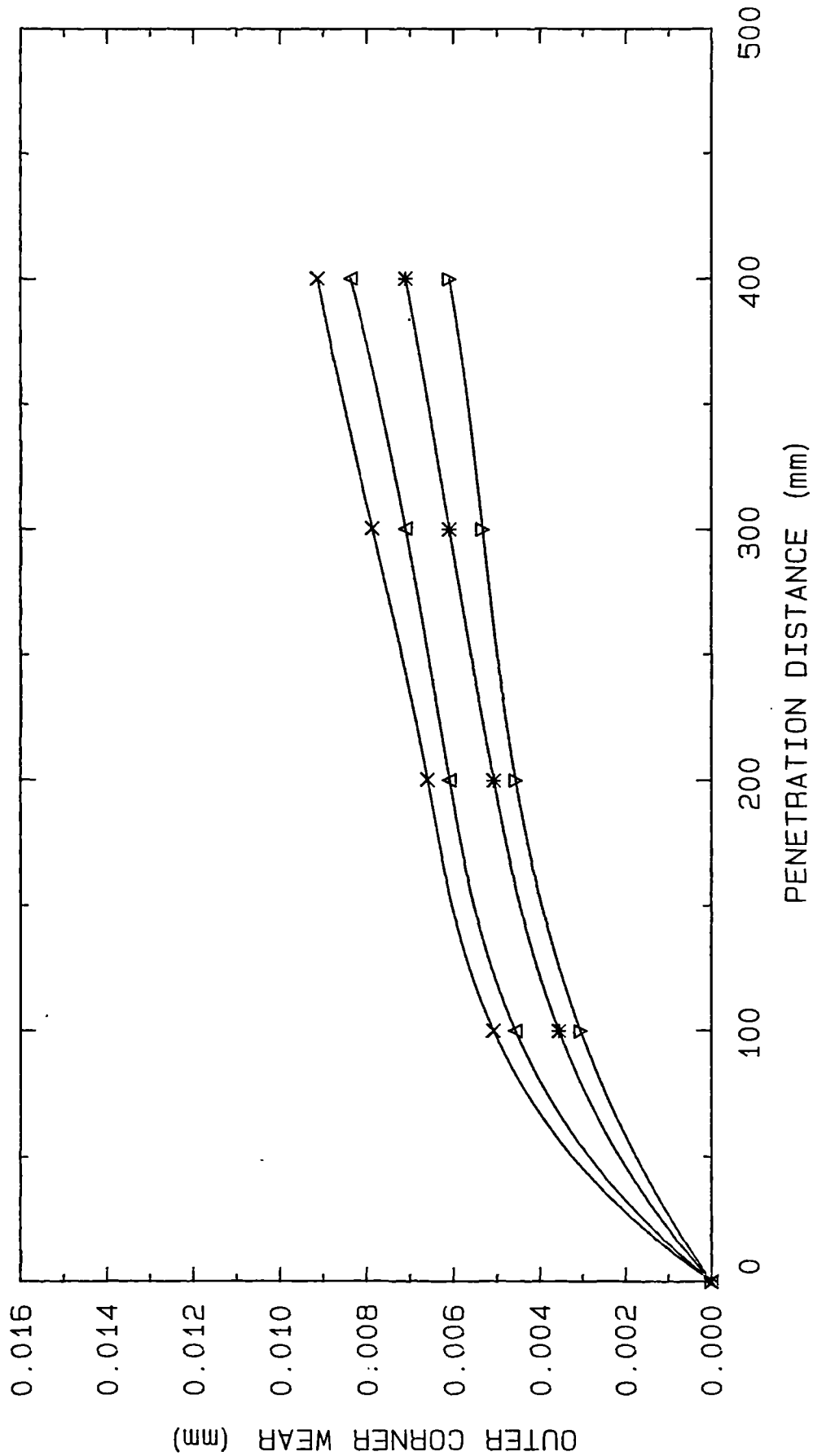
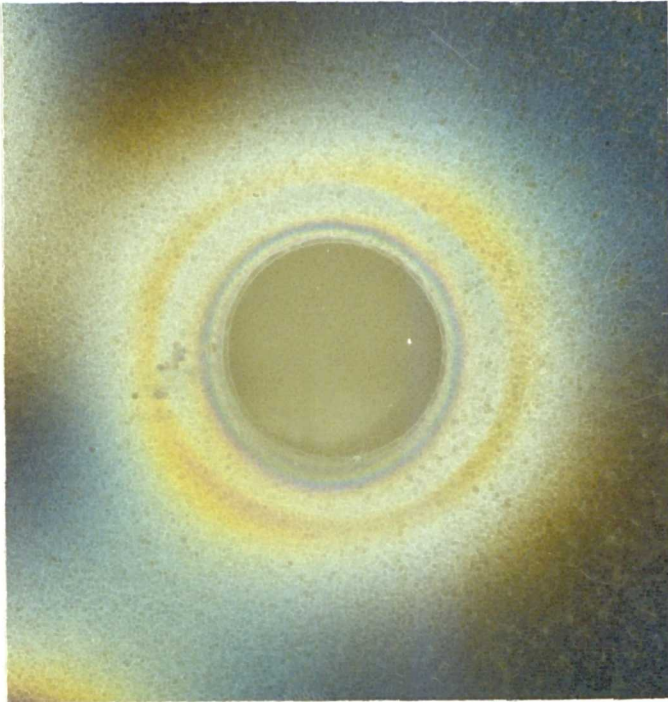
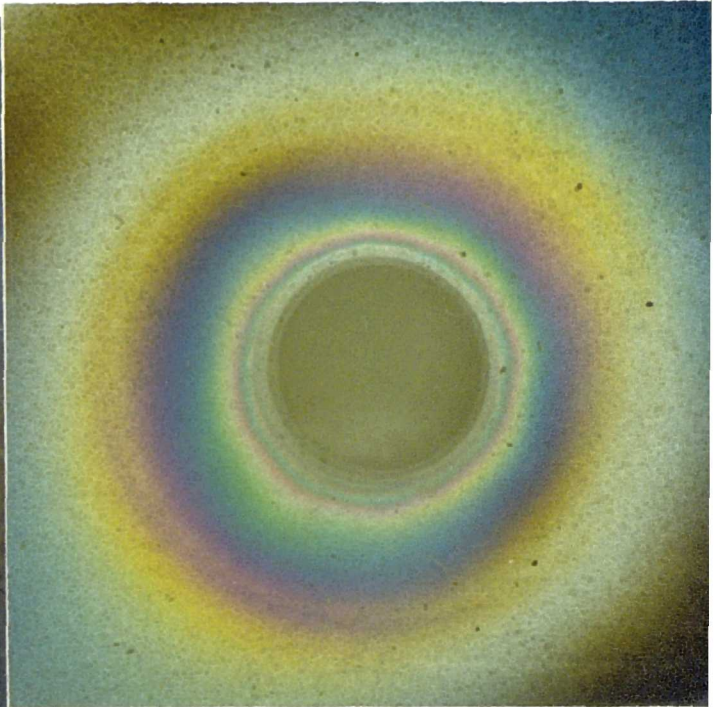


Fig. (66): The outer corner wear of Klenk (x), Gandtrack (Δ), Precision (\*) and Carbide (∇) drills against penetration distance at a speed of 2800 RPM and feed of 0.05mm/Rev.

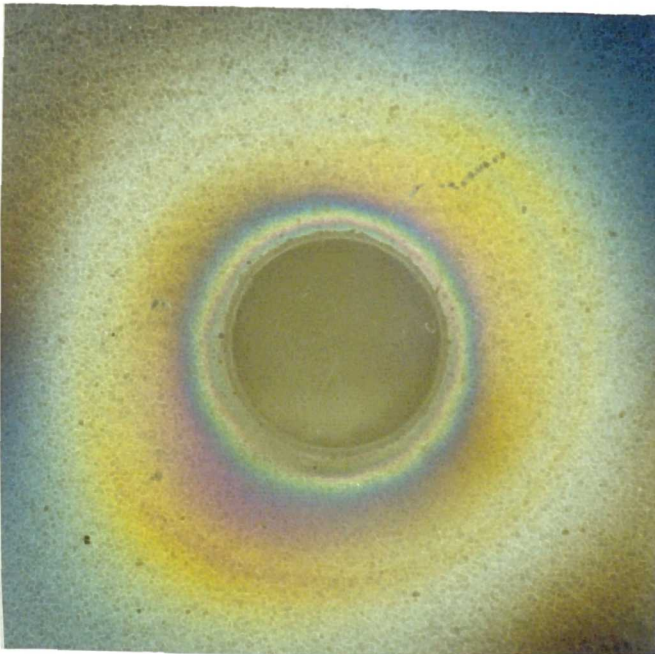
Klenk



Precision



Gandtrack



Carbide

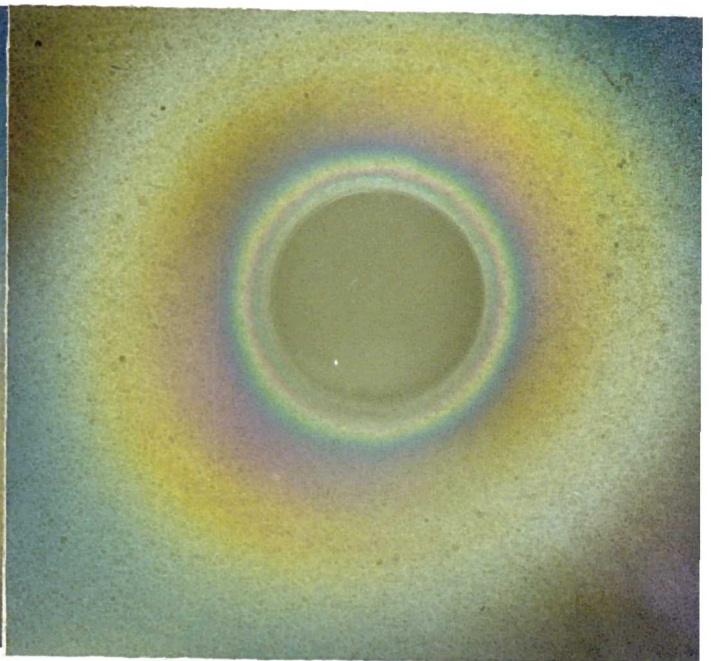


Fig. (67): The pattern of the isochromatic fringes on the bottom ply of the CFC holes for Klenk (top left), Precision (top right), Gandtrack (bottom left) and Carbide (bottom right) drills at a speed of 2800 RPM & feed of 0.05mm/rev.

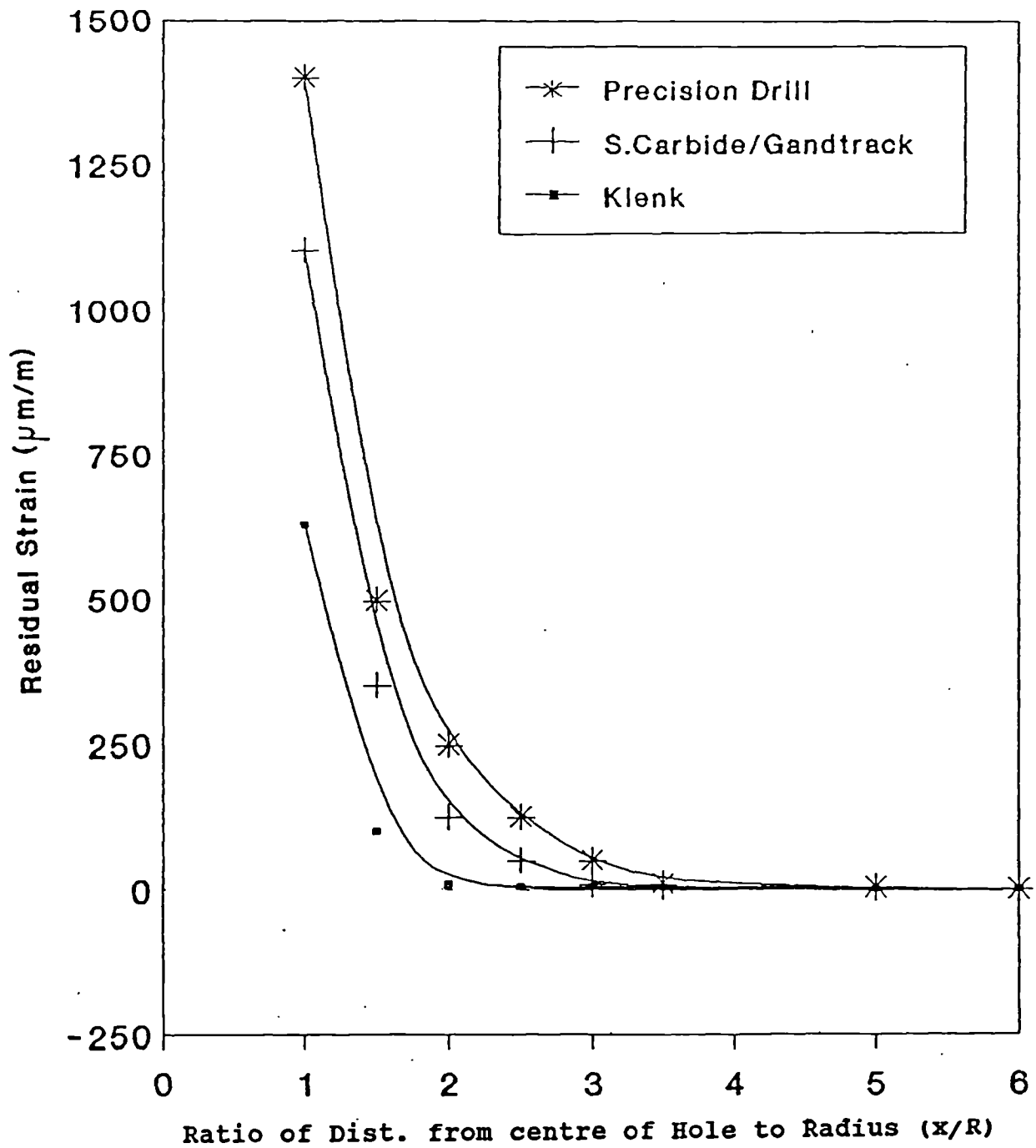


Fig. (68): Graph showing the distribution of residual strains at the bottom ply of the CFC hole at a speed of 2800 RPM and feed of 0.05mm/rev.

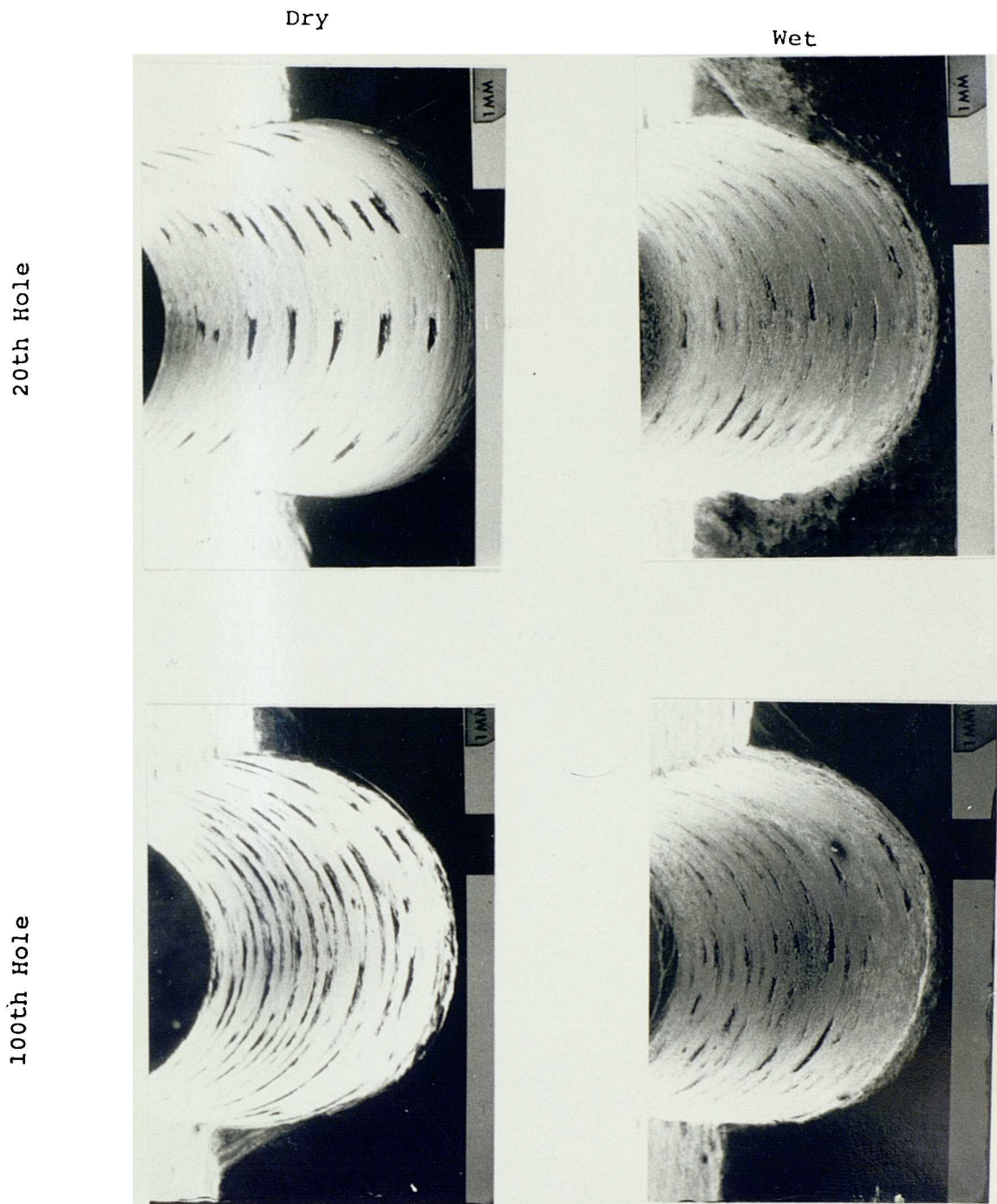


Fig. (69): SEM Micrographs showing a comparison between 20th and 100th wet and dry holes drilled by the Precision drill.

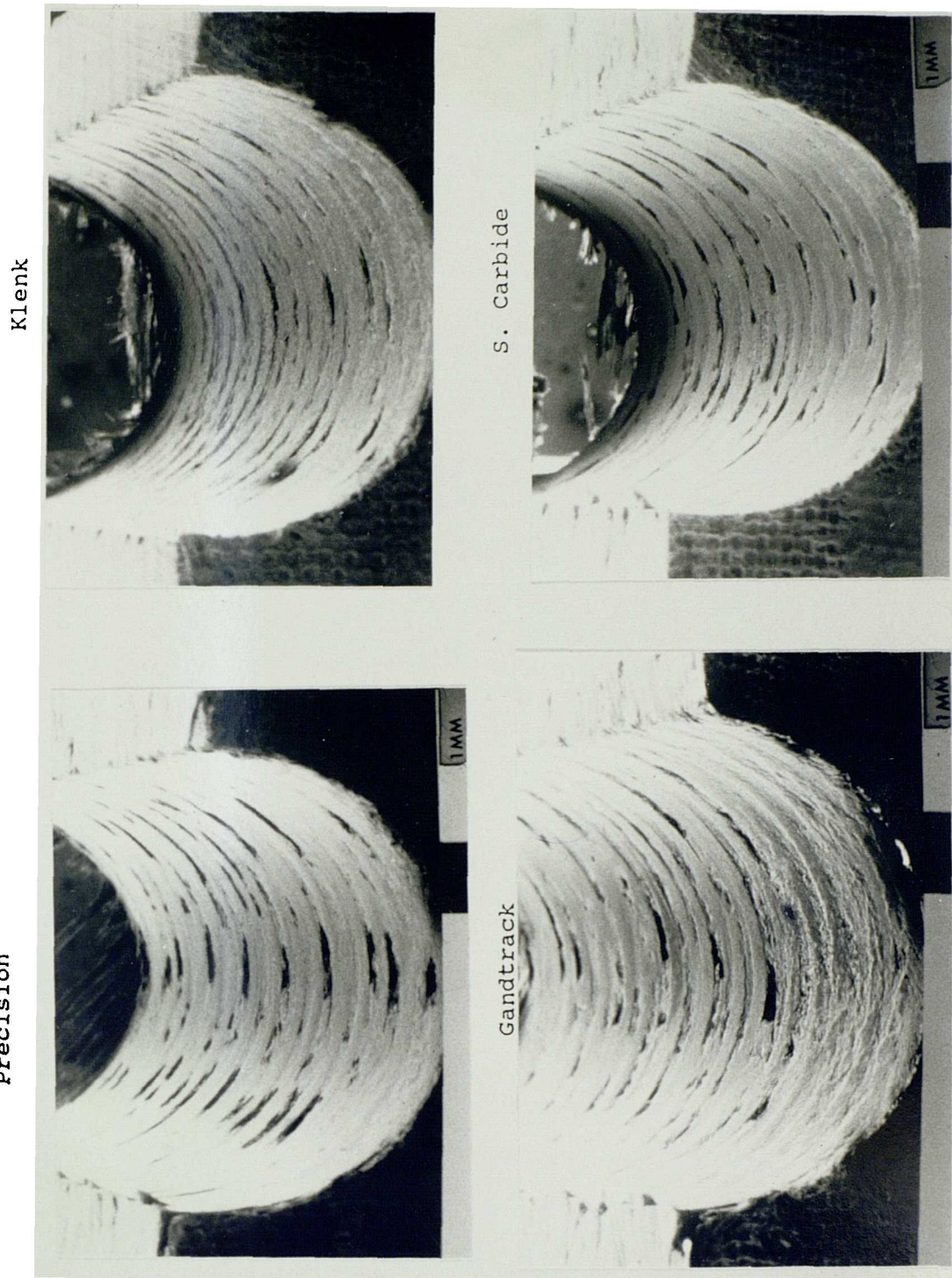


Fig. (70): The hole quality (dry) of the 30th CFC hole drilled by Klenk (top left), Carbide (top right), Precision (bottom left) and Gandtrack (bottom right) drills at a speed of 2800 RPM and feed of 0.05mm/rev.

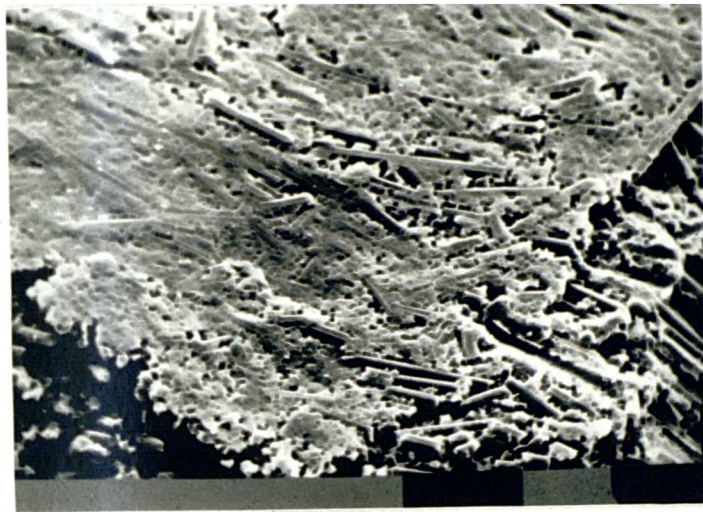


Fig. (71): SEM micrograph showing softened matrix on the hole surface.

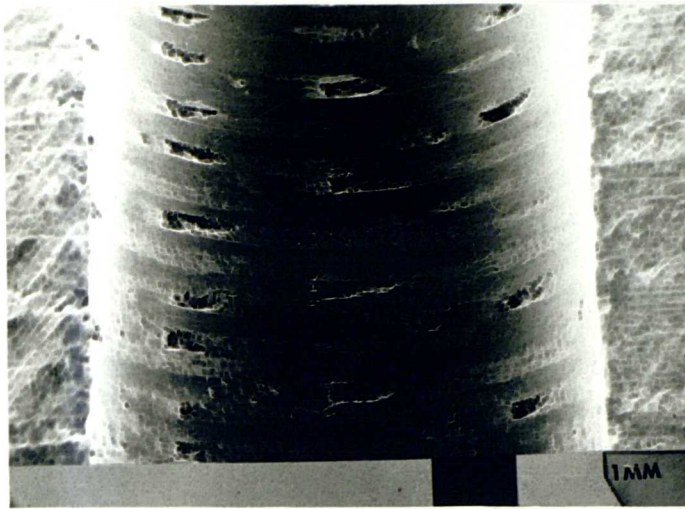


Fig. (72): The periodicity of damage scars in the holes drilled by Precision drills.

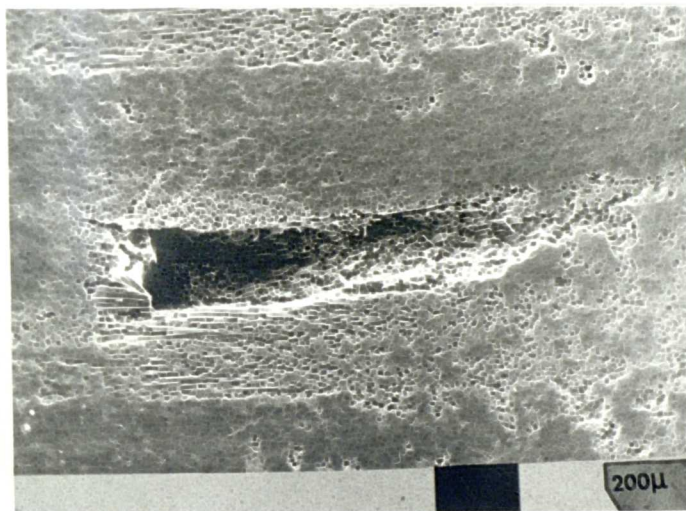


Fig. (73): SEM micrograph showing close-up view of the damage scar on the CFC hole boundaries.

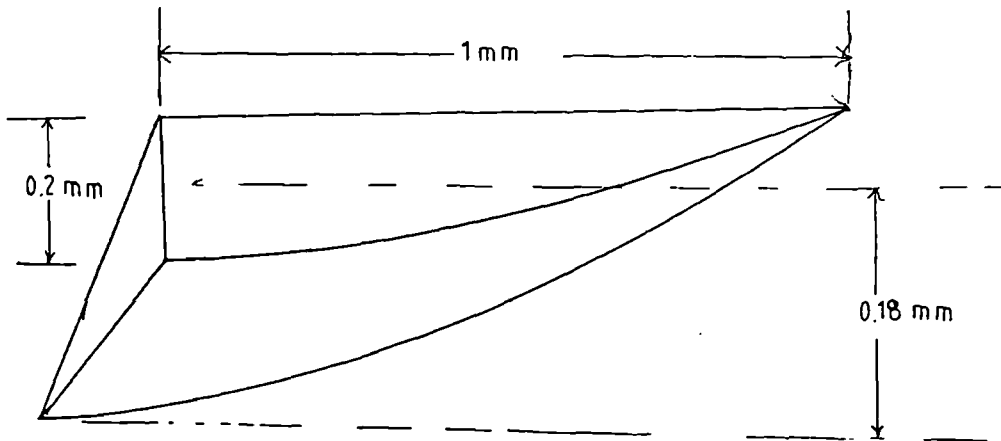


Fig. (74): The geometrical features of the damage scar observed on CFC hole boundaries.

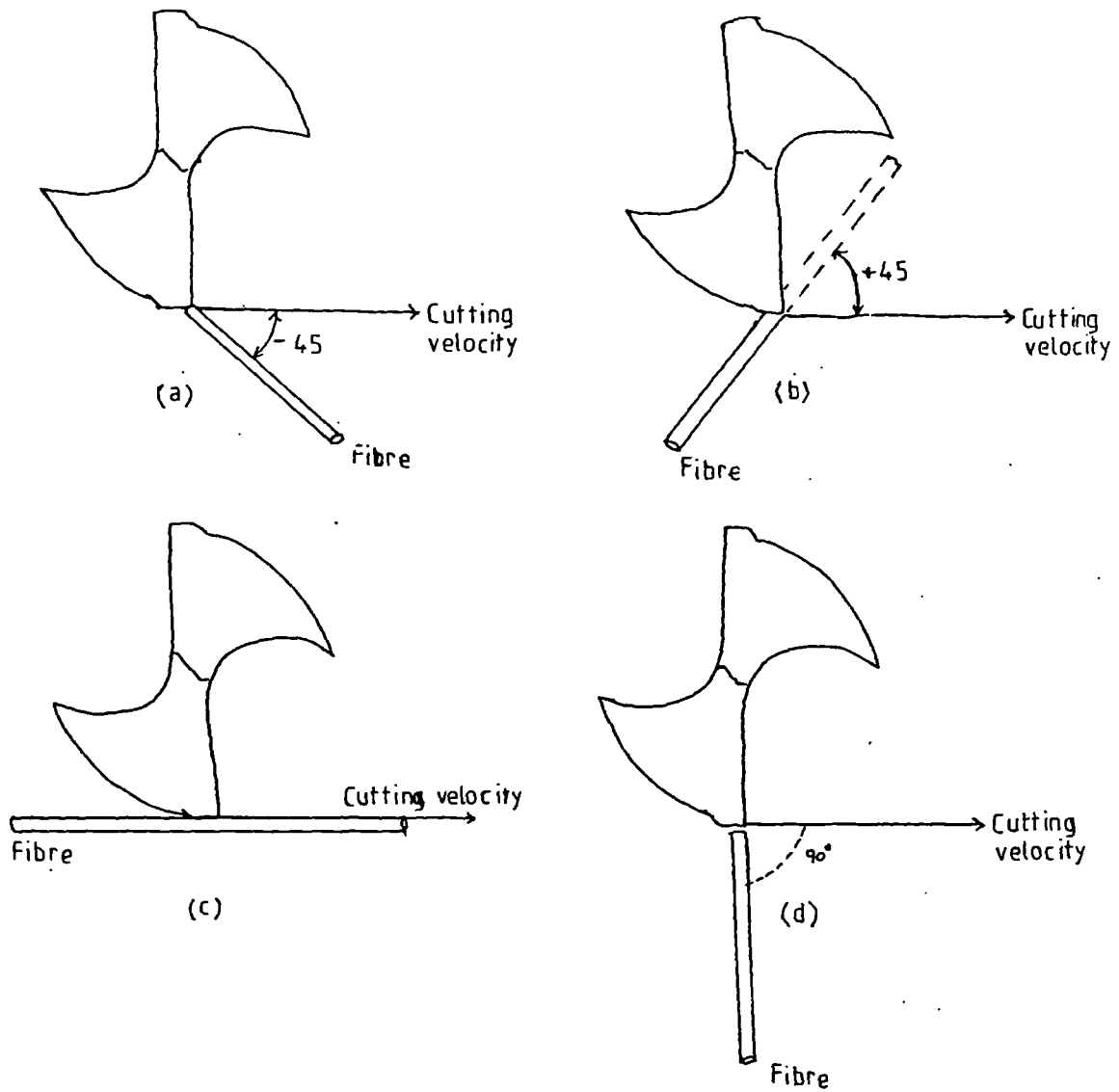


Fig. (75): The relative orientation of  $-45^\circ$  (top left),  $+45^\circ$  (top right),  $0^\circ$  (bottom left),  $90^\circ$  (bottom right) carbon fibres with respect to the cutting edge of the drill.

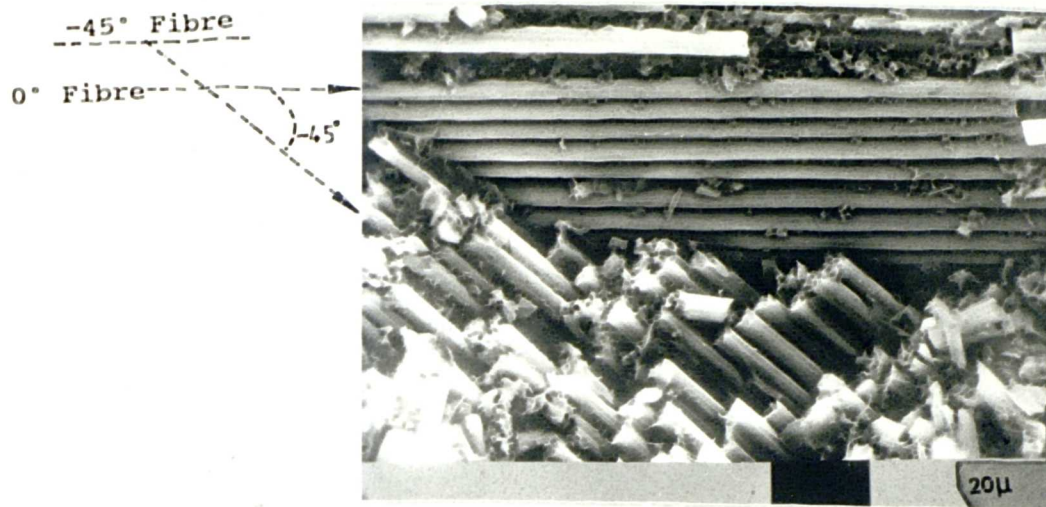


Fig. (76): SEM micrograph showing the  $-45^\circ$  fibres protruding against  $0^\circ$  fibres in the damage scar.

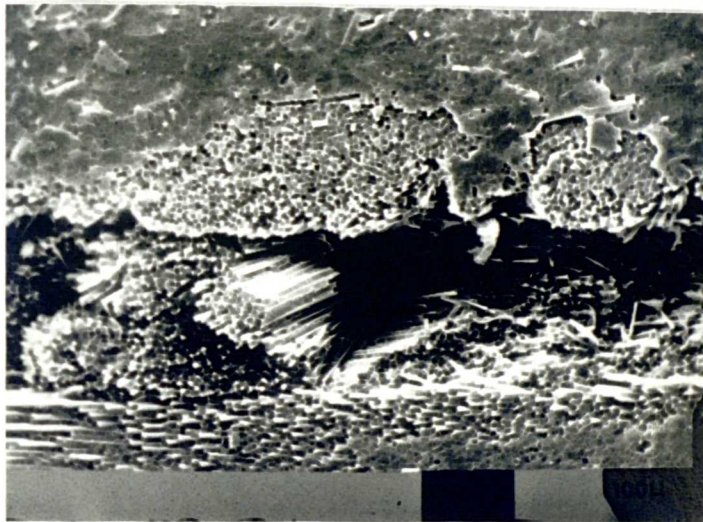


Fig. (77): SEM micrograph showing the microbuckled and kinked carbon fibres around the damage scar.

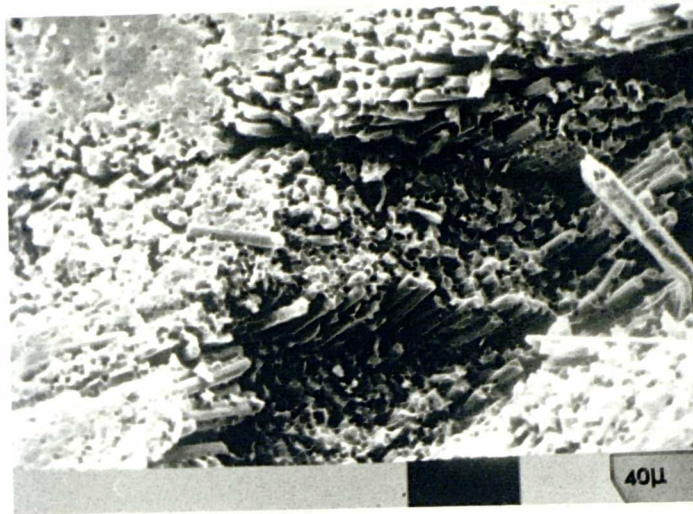


Fig. (78): SEM micrograph showing the  $-45^\circ$  fibres protruding in a series of steps in the damage scar.

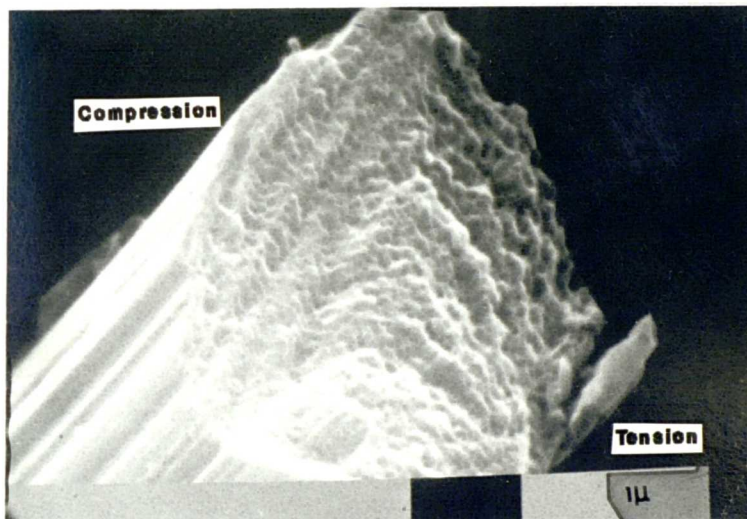


Fig. (79): SEM micrograph showing the bi-modal failure of fibres in the damage scar.



Fig. (80): SEM micrograph showing the outcrop of pulled out fibres fractured in tension.

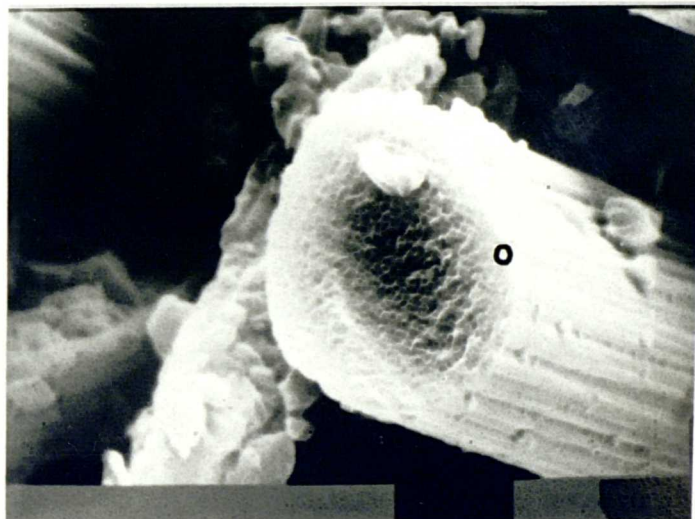


Fig. (81): SEM micrograph showing a typical pulled out fibre.



Origin of  
Fracture

Fig. (82): SEM micrograph showing radials on the fractured surface of the pulled out fibres indicating the origin of fracture.

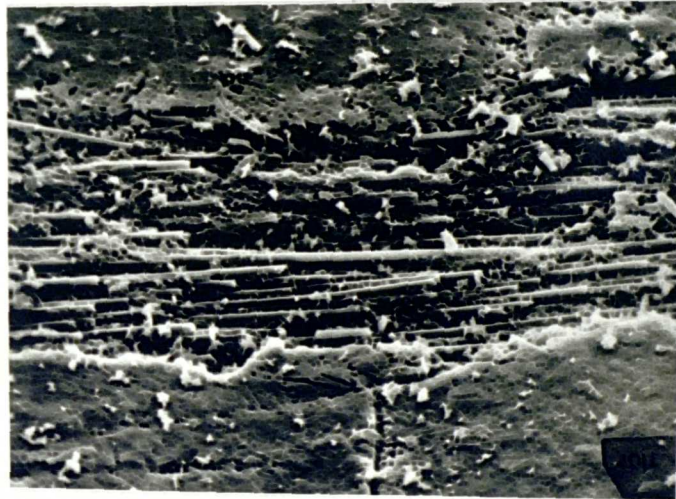


Fig. (83): SEM micrograph showing the 0° fibres on the CFC hole boundaries.

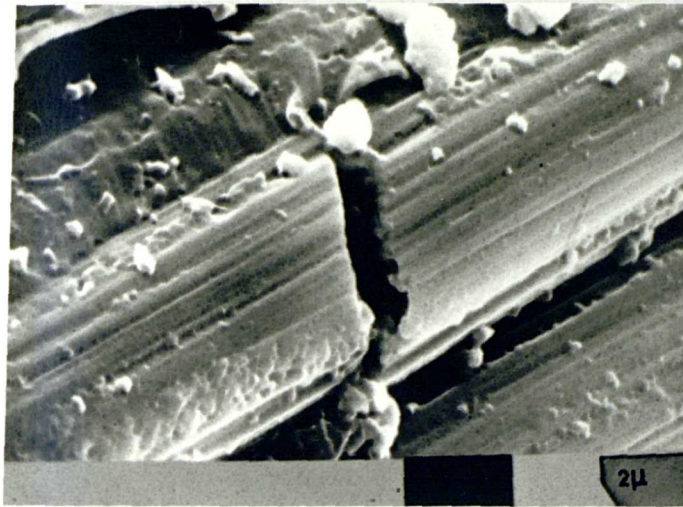


Fig. (84): SEM micrograph showing the interlaminar shear failure of the 0° fibres.

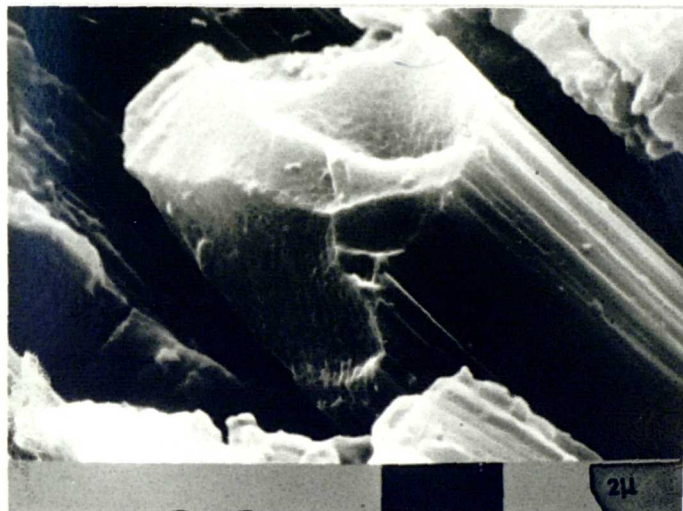


Fig. (85): SEM micrograph showing the obliteration of a 90° fibre by the cutting action of the drill.

Delamination

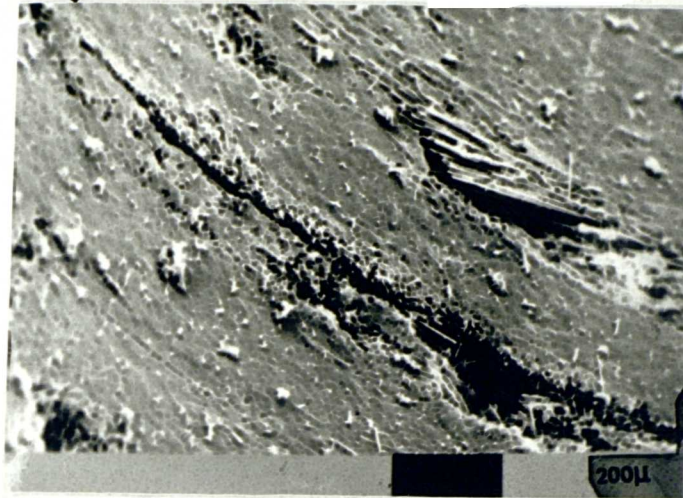


Fig. (86): SEM micrograph showing the delamination at the interlayer region of the CFC hole boundaries.

Resin Rich Interlayer →

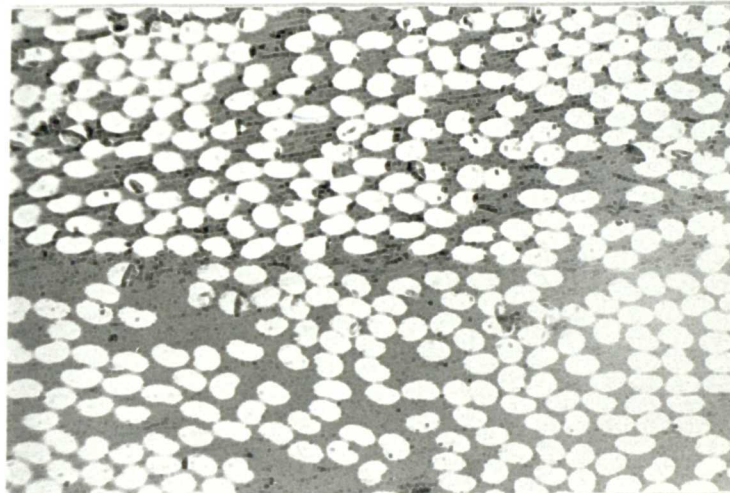
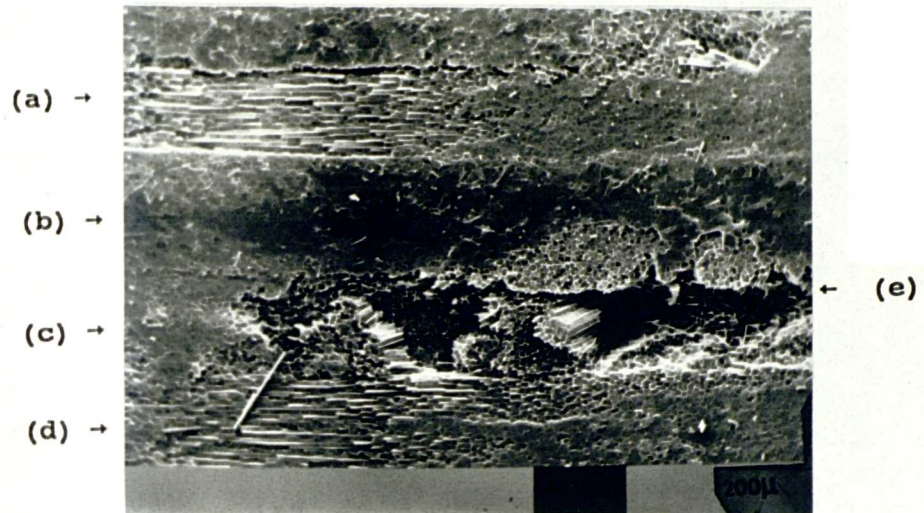


Fig. (87): Optical micrograph showing the resin rich region in the interlayers.



**Fig.(88):** Scanning electron micrograph showing all the four fibre failure modes and internal delamination;

(a)  $0^\circ$  fibres failed by interlaminar shear.

(b)  $90^\circ$  fibres chopped away and smeared epoxy on surface.

(c)  $-45^\circ$  fibres microbuckled and formed pits.

(d)  $+45^\circ$  fibres failed in tension.

(e) Internal delamination at a  $-45^\circ/90^\circ$  interlayer.

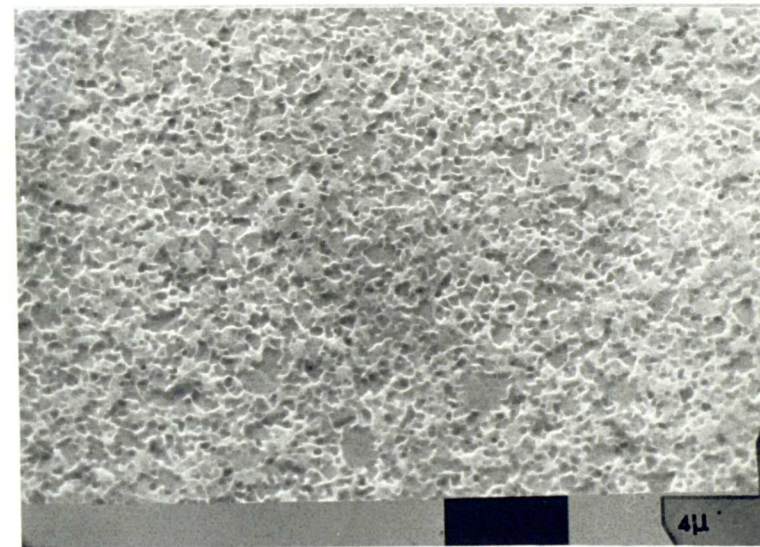
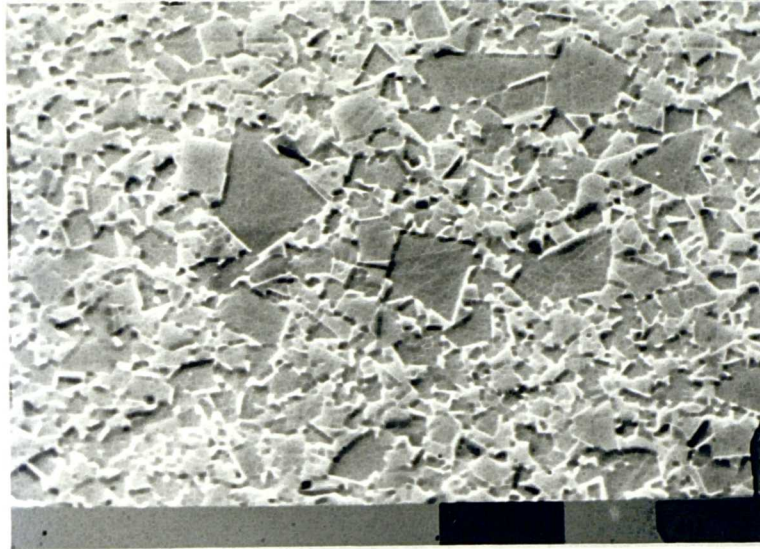


Fig. (89): SEM micrographs showing the microstructure of the Krupp (top), Sandvik (middle) and Kennametal (bottom) specimens.

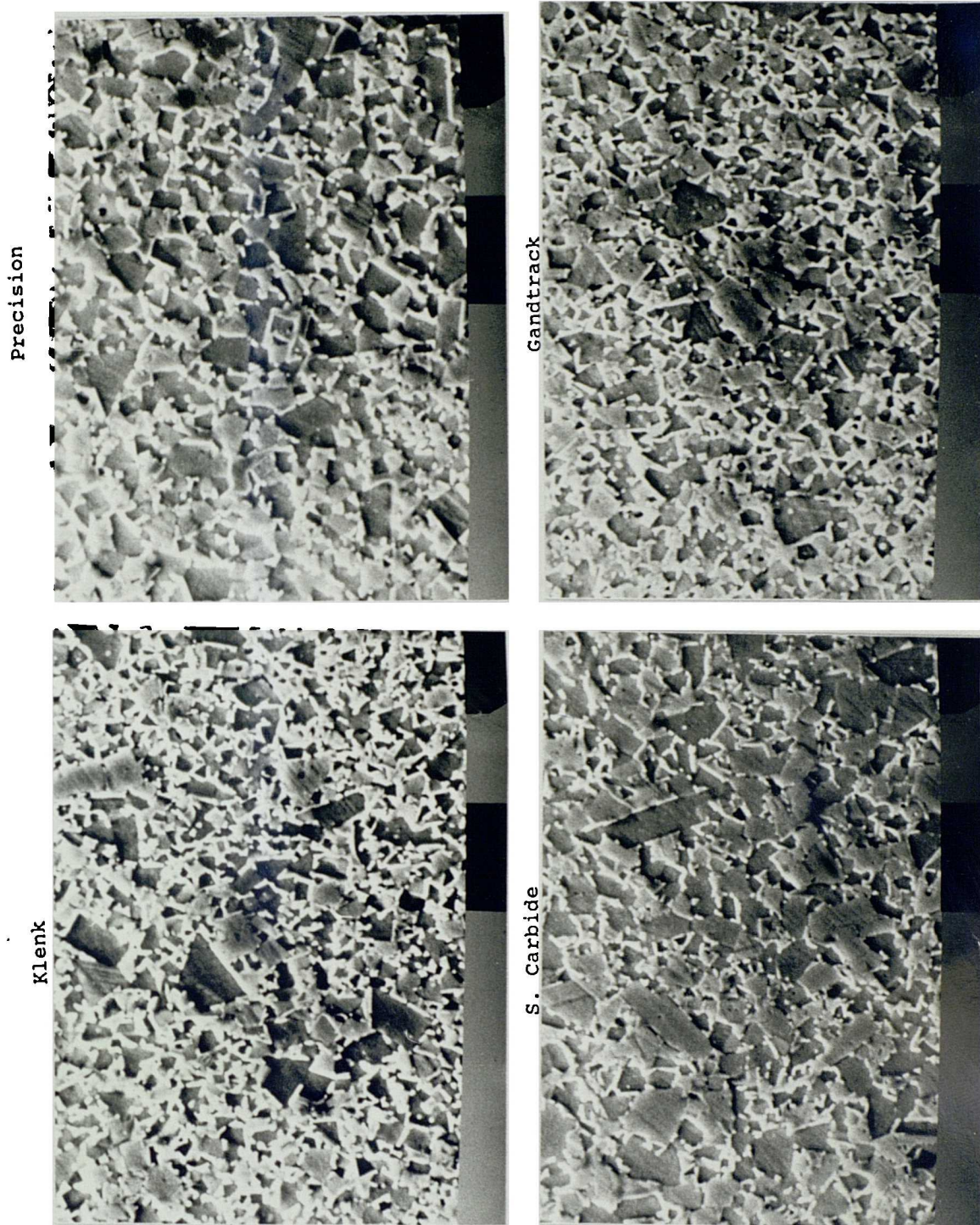


Fig. (90): SEM micrographs showing the microstructure of cemented carbide used in Precision (top left), Gandtrack (top right), Klenk (bottom left) and Solid Carbide (bottom right) drills.

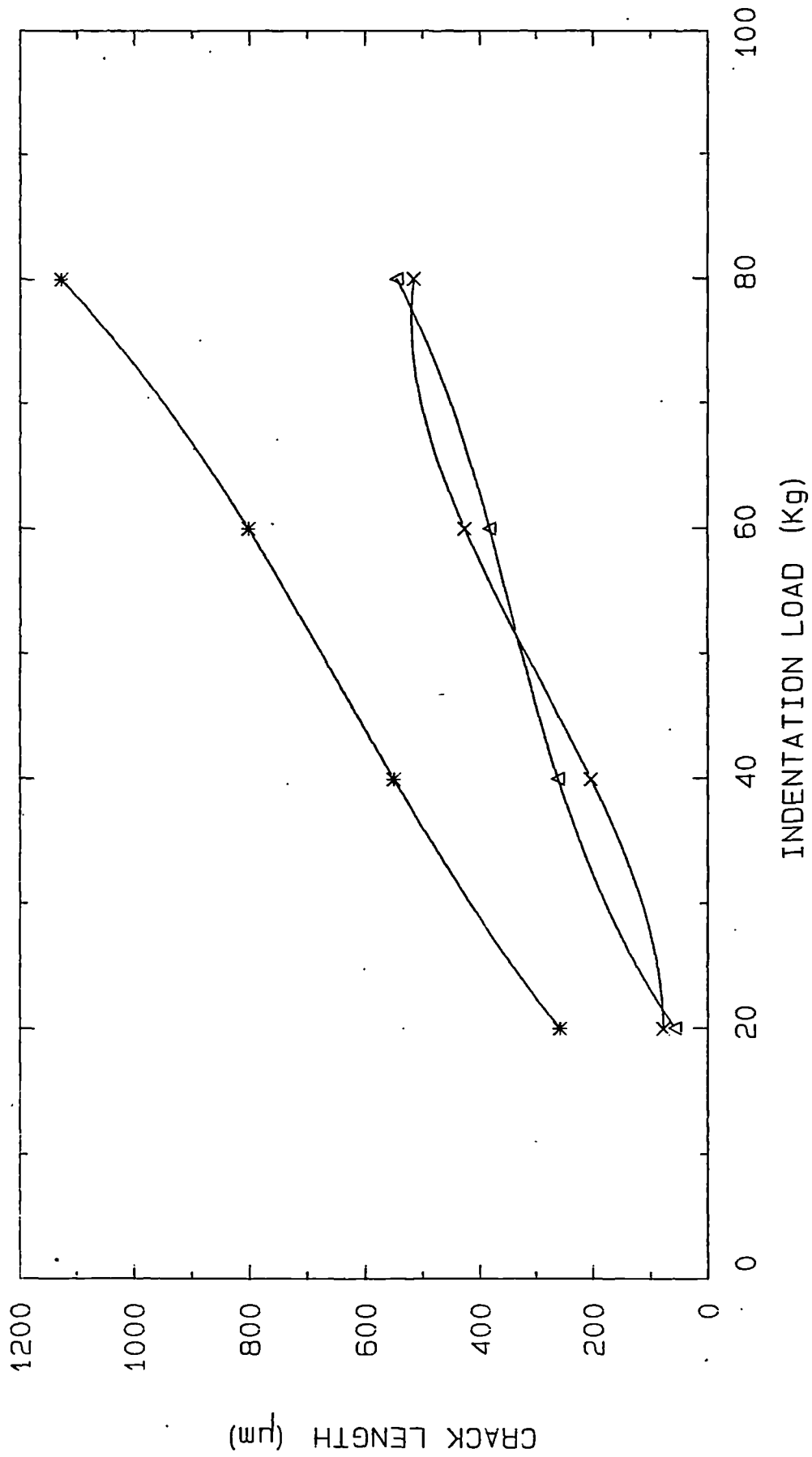


Fig. (91): Graph showing variation of crack length with applied load using the Palmqvist fracture resistance test on Krupp THR (x), Sandvik H10F (Δ) and Kennametal F285 (\*) carbides.

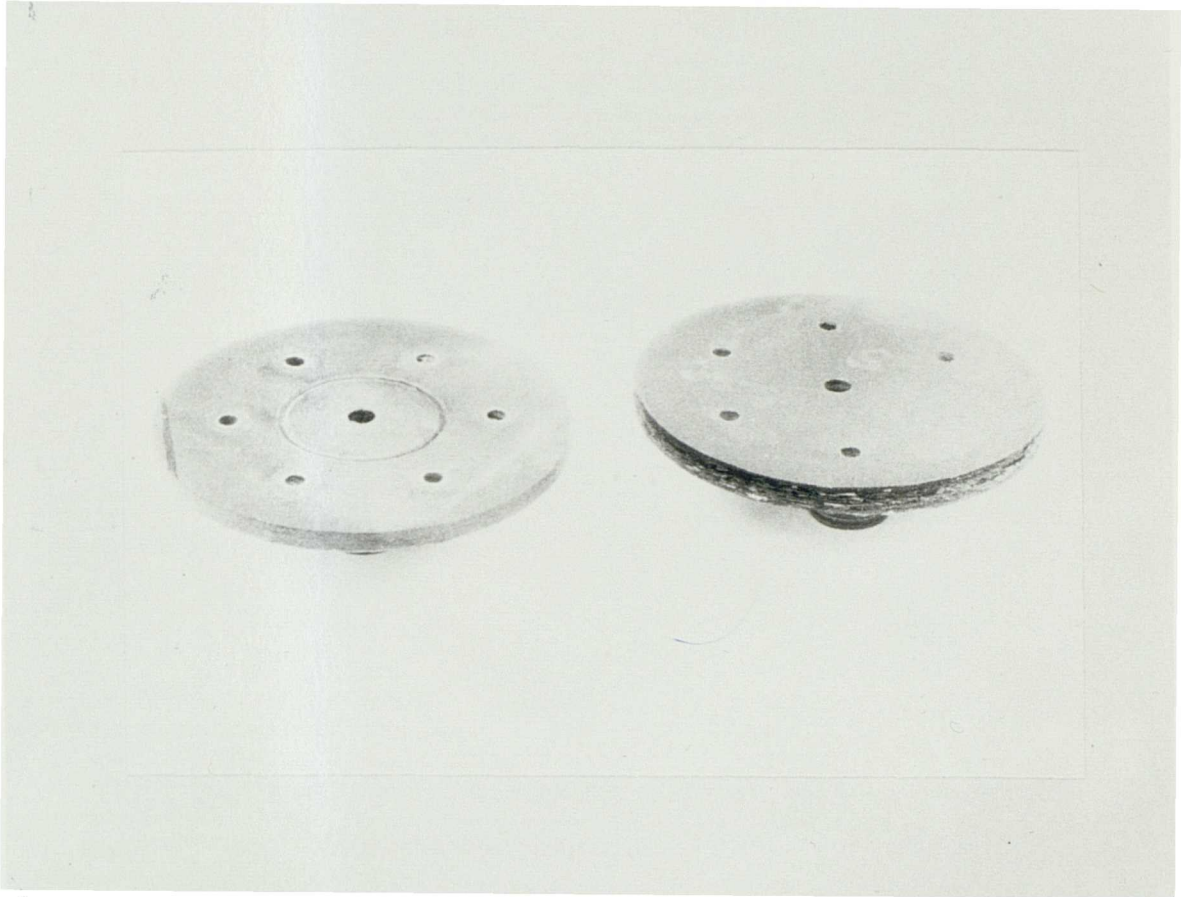


Fig. (92): Photograph showing comparison between a new CFC disc (left) and the delaminated CFC disk (right) after the Kearney and Trecker dry wear test.

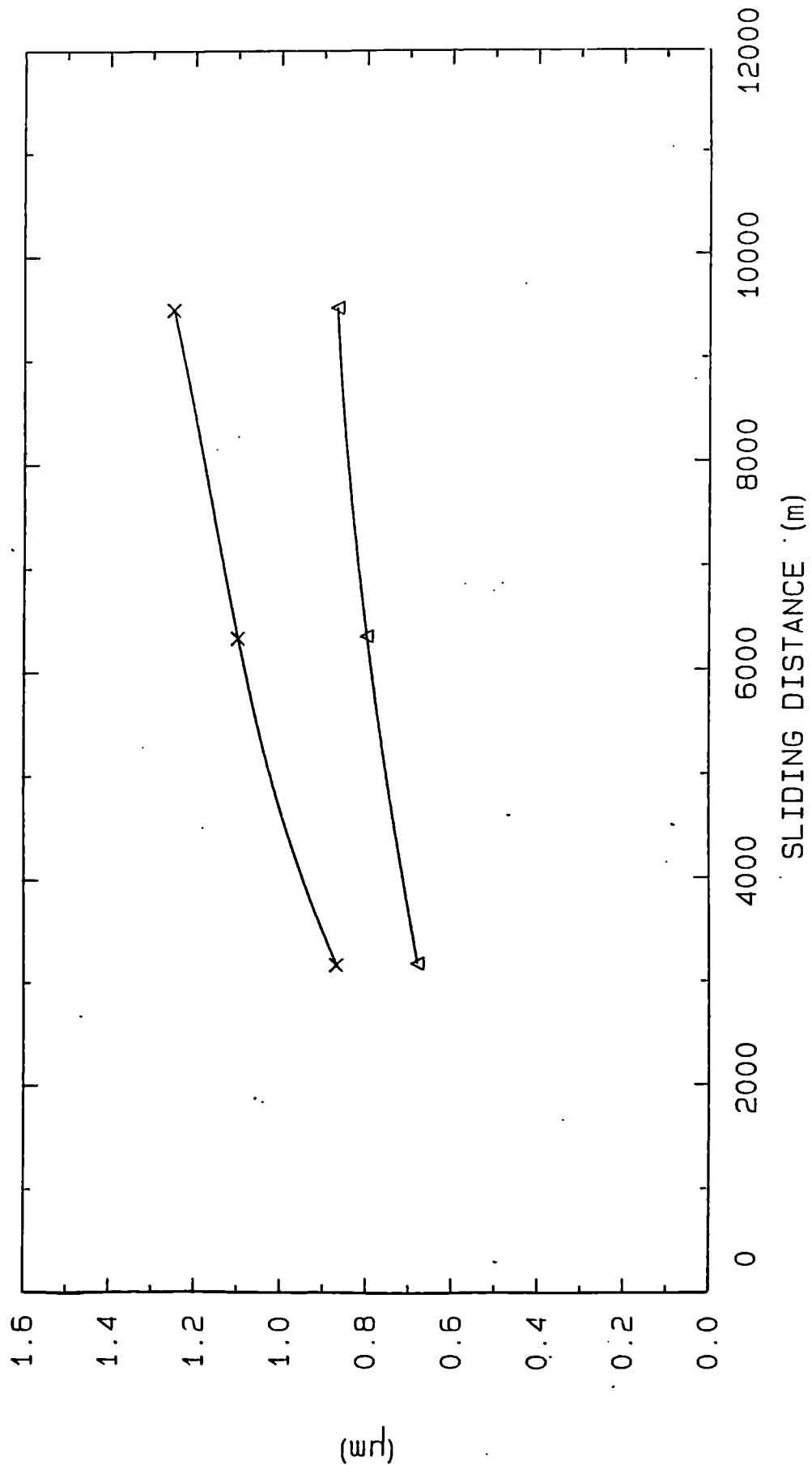


Fig. (93): Graph showing the wear scar dia. on Krupp THR/Sandvik H10F (x) and Kennametal F285 (Δ) specimens as a function of sliding dist. in the pin-on-disc sliding test.



Fig. (94): The incidence of cracks on the Krupp specimen developed during the pin-on-disc sliding test.

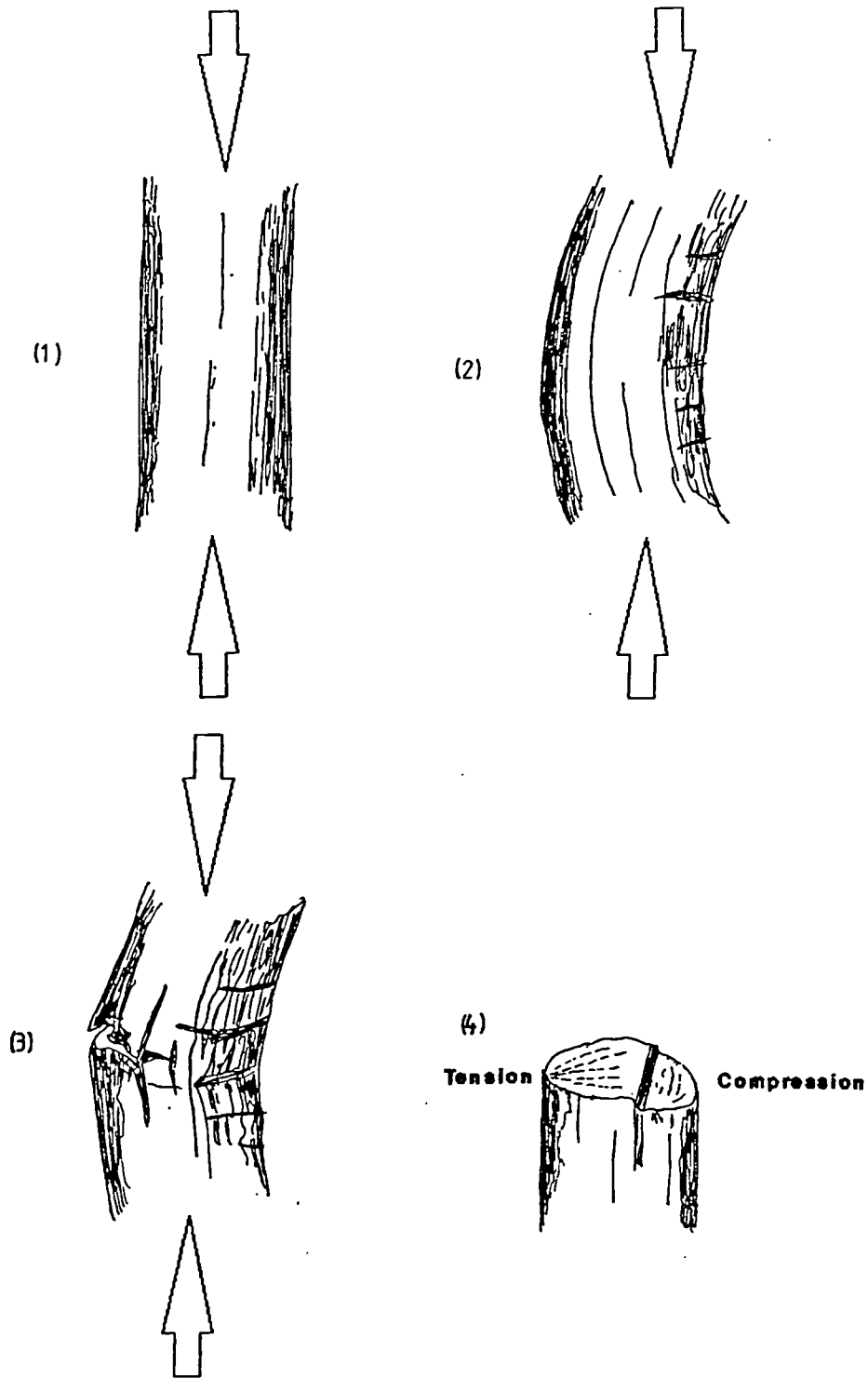


Fig.(96): Drawing showing the mechanism of bimodal failure of microbuckled  $-45^\circ$  carbon fibres in CFC holes.

Material	Spec. Gravity	Tens. Strength, GPa	Elastic Modulus, GPa	Spec. Strength, GPa	Spec. Modulus, GPa
Carbon-Epoxy (type-I)	1.6	0.93	213	0.58	133
Carbon-Epoxy (type-II)	1.5	1.62	148	1.01	92
Glass-Epoxy	1.9	1.31	41	0.69	22
Kevlar-Epoxy	1.45	1.38	58	0.95	40
Boron-Epoxy	2.0	1.49	224	0.73	110
Steel	7.8	0.99	207	0.13	27
Aluminum Alloy, 2014-T6	2.8	0.46	72	0.17	26
Titanium, Ti-6Al-4V	4.5	0.93	110	0.21	24
Carbon Fibre (type-I)	2.0	1.9	400	0.95	200
Carbon Fibre (type-II)	1.7	2.6	200	1.52	118
E-glass	2.54	2.6	84	0.98	33
S-glass	2.49	4.6	72	1.85	29
Kevlar	1.44	2.8	130	1.94	90
Boron	2.5	3.5	420	1.4	168

Table (1): The properties of various composite materials, metals and fibres in terms of specific strength and modulus [15].

	<b>CARBON</b>	<b>KEVLAR (ARAMID)</b>	<b>GLASS</b>
<b>MAJOR ADVANTAGES</b>	<ul style="list-style-type: none"> <li>■ High Specific Strength</li> <li>■ High Specific Modulus</li> <li>■ High Temp. Resistance</li> </ul>	<ul style="list-style-type: none"> <li>■ Tough, good impact resist.</li> <li>■ Light Weight</li> <li>■ Does not cause galvanic corrosion</li> </ul>	<ul style="list-style-type: none"> <li>■ High Strength</li> <li>■ High Temp. Resistance</li> <li>■ Does not cause galvan. Corrosion</li> <li>■ High Fatigue Limit</li> <li>■ Low Notch Sensitivity</li> </ul>
<b>DISADVANTAGES</b>	<ul style="list-style-type: none"> <li>■ Expensive</li> <li>■ Low Impact Resistance</li> <li>■ When in contact with metals and in presence of moisture, galvanic corrosion occurs</li> <li>■ Difficult to machine</li> </ul>	<ul style="list-style-type: none"> <li>■ Poor Compression Strength</li> <li>■ Poor Coupling to resins</li> <li>■ Absorbs Moisture</li> <li>■ Difficult to machine</li> </ul>	<ul style="list-style-type: none"> <li>■ High Density</li> <li>■ Low Stiffness</li> </ul>
<b>TYPICAL APPLICATIONS</b>	<ul style="list-style-type: none"> <li>■ High Performance Applications</li> </ul>	<ul style="list-style-type: none"> <li>■ Leading Edges</li> <li>■ Ballistic Protection</li> <li>■ Ropes</li> </ul>	<ul style="list-style-type: none"> <li>■ Mostly used in low tech. applications, housing appliances.</li> </ul>
<b>COST INDEX (1988)</b>	High (6-7)	Intermediate (3)	Low (1-2)

Table (2): A summary of the major advantages, disadvantages and typical applications of carbon, kevlar and glass fibres.

<b>PROPERTIES OF CARBON FIBRE COMPOSITE SYSTEM, ORIENTATION:0° 34% RESIN</b>	<b>XA-S/914 Epoxy (1st Generation)</b>	<b>T800/924C Epoxy (2nd Generation)</b>
Long. Tensile Strength (GPa)	1.85	2.3-2.4
Trans. Tensile Strength (GPa)	0.02	0.065
Long. Compressive Strength (GPa)	0.735	1.5
Trans. Comp. Strength (GPa)	0.14	-
Long. Youngs Modulus (GPa)	126	170
Trans. Youngs Modulus (GPa)	7.4	9.34
Torsional Modulus (GPa)	5.58	6.0
Shear Strength (GPa)	0.068	0.10
Poisson Ratio	0.28	0.34

Table (3): Important physical and mechanical properties of 1st generation (Ciba Geigy XA-S/914C) and 2nd generation (Ciba Geigy T800/924C) CFC [17,19,20].

<b>PROPERTIES OF CIBA GEIGY-924C, EPOXY SYSTEM</b>	<b>VALUE</b>
Matrix Softening Temperature (°C)	210
Tensile Strength (GPa)	0.066
Compressive Strength (GPa)	0.160-0.180
Tensile Modulus (GPa)	4.0
Compressive Modulus (GPa)	2.75
Flexural Modulus (GPa)	4.1
Flexural Strength (GPa)	0.140
Poisson Ratio	0.39-0.4
Water Absorption , 24 hours at 20°C (% by weight)	0.1-0.4

Table (4): Important physical and mechanical properties of ciba Geigy 924C epoxy matrix [19,20].

PROPERTIES OF CARBON FIBRE	T-300	T-700	T-800
Tensile Strength (GPa)	3.31	4.48	5.5
Compressive Strength (GPa)	2.88		8.0
Tensile Modulus (GPa)	228	248	295
Compressive Modulus (GPa)			267
Coefficient of Thermal Expansion, Long. (°C)	$-0.54 \times 10^{-6}$		$-0.2 \times 10^{-6}$
Coefficient of Thermal Expansion, Trans. (°C)			$35 \times 10^{-6}$
Thermal Conductivity ( $W m^{-1} \cdot K^{-1}$ )			$0.1 \times 10^{-6}$
Density ( $g/cm^3$ )	1.75	1.80	1.81
Diameter of fibre ( $\mu m$ )	7.01		5.5
Hardness (Could not be measured)*	N.A.	N.A.	N.A.

Table (5): Important physical and Mechanical properties of T-300, T-700 and T-800 carbon fibres [20,40\*,41].

DRILL	TYPE-1	TYPE-2	TYPE-3	TYPE-4
<b>Manufacturer</b>	Klenk GmbH	Gandtrack Ltd	Precision Twist Drill Co.	Klenk GmbH
<b>Address</b>	Mühlstraße 17, D-7959 Balzheim (Germany) Tel:07347 66-0	Wellington Mill, Greenfield Oldham OL3 7AF (UK) Tel:0457 873146	One Precision Plaza, Crystal lake, IL 60014 (USA)	Mühlstraße 17, D-7959 Balzheim (Germany) Tel:07347/ 66-0
<b>Catalogue No.</b>	Custom made to B.Ae., PTS 62.01.07	Custom made to B.Ae., PTS 62.01.07	Custom made to B.Ae., PTS 62.01.07	Catalogue No: 2000600
<b>Carbide Tip</b>	Brazed	Brazed	Brazed	Solid Carbide
<b>Tip Material</b>	Krupp THR	K20	C2	K10
<b>Diameter (mm)</b>	6.035	6.035	6.035	6.00
<b>Total Length (mm)</b>	91	91.5	94.65	66
<b>Flute Length (mm)</b>	56	58.5	60.65	28
<b>Point Angle (deg)</b>	125	116	118	118
<b>Body Helix Angle (deg)</b>	28	18	20	30
<b>Lip Relief Angle (deg)</b>	-	16	16	-
<b>Cost of 10 drills (£) Prices: 1990</b>	9.75	9.59	20.82	23.59
<b>Procurement Efficency</b>	Medium	Fast	Slow	Medium
<b>Regrind Accuracy (deg)</b>	± 0.25	± 0.25	± 0.25	± 0.25

Table (6): The specifications and related details about the four types of drills used in the present study.

**PHASE 1 - DRILL EVALUATION PROGRAMME**

**KLENK - GANDTRACK - PRECISION - SOLID CARBIDE**

TYPE	NO	Outer Corner Wear, mm (holes drilled)				Total Number of Holes Drilled	Penetration Distance (mm)	Plug Gauge Test	S.E.M. Results
		New Drill	Regrind 1	Regrind 2	Regrind 3				
KLENK	1	.198 (160)*	.259 (250)*	.21 (160)*	.19 (160)GF	730	7300	Failed	Damage was observed in the brazing but failure was non-catastrophic
	2	.193 (150)*	.279 (260)*	.178 (150)GF	GF	560	5600	Failed	
	3	.066 (30)	.076 (30)	.089 (30)	.061 (30)	120	1200	Passed	
	4	.071 (30)	.889 (30)	.086 (30)	.038 (20)GF	110	1100	Failed	
	5	.066 (30)	.081 (30)	.1 (30)	.055 (20) GF	110	1100	Failed	
GANDTRACK	1	.25 (220)*	.21 (190)*	.16 (130)GF	GF	540	5400	Failed	Same as above
	2	.177 (220)*	GF	GF	GF	220	2200	Failed	
	3	.066 (30)	.063 (30)	.076 (30)	.071 (30)	120	1200	Passed	
	4	.071 (30)	.084 (30)	.086 (30)	.094 (30)	120	1200	Passed	
	5	.076 (30)	.089 (30)	.076 (30)	.076 (30)	120	1200	Passed	
PRECISION	1	.20 (220)*	.11 (119)GF	GF	GF	339	3390	Failed	Same as above
	2	.198 (220)*	.14 (190)*	.13 (155)GF	GF	565	5650	Failed	
	3	.063 (30)	.063 (30)	.055 (30)	.068 (30)	120	1200	Passed	
	4	.063 (30)	.061 (30)	.063 (30)	.056 (30)	120	1200	Passed	
	5	.066 (30)	.061 (30)	.061 (30)	.056 (30)	120	1200	Passed	
SOLID CARBIDE	1	.152 (220)*	.127 (190)*	.27 (160)*	.114 (140)GF	710	7100	Failed	Not relevant
	2	.127 (220)*	.132 (190)*	.27 (135)*	.109 (160)GF	705	7050	Failed	
	3	.05 (30)	.05 (30)	.09 (30)	.0635 (30)	120	1200	Passed	
	4	.05 (30)	.055 (30)	.1 (30)	.08 (30)	120	1200	Passed	
	5	.05 (30)	.05 (30)	.105 (30)	.0635 (30)	120	1200	Passed	

NB GF : Gauge Failure  
\* : Flank Wear Failure

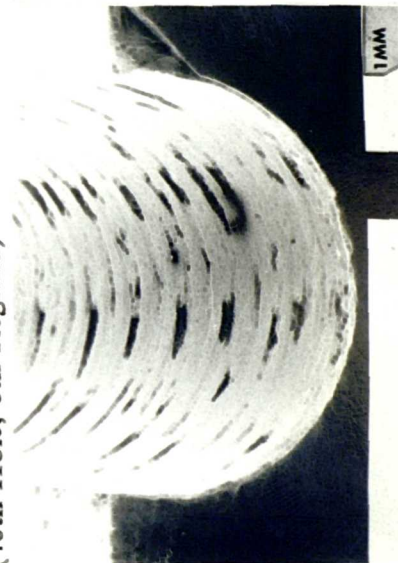
Table (7): Summary of drill evaluation, phase-1 test results.

**PHASE 2 - DETAILED STUDY OF PRECISION AND GANDTRACK DRILLS**

**Extended 40 Hole Regrind Cycle**

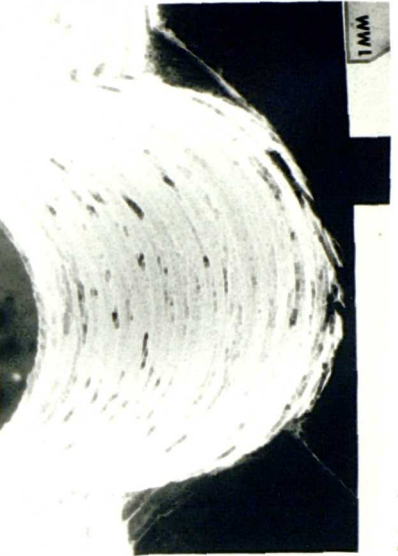
Type	Outer Corner	OUTER CORNER WEAR, mm										Total Holes Drilled	Penetration Distance (mm)			
		New Drill	Regrind 1	Regrind 2	Regrind 3	Regrind 4	Regrind 5	Regrind 6	Regrind 7	Regrind 8	Regrind 9					
PRECISION	A	.086	.071	.066	.071	.066	.066	.066	.071	.066	.066	.071	.066	.071	400	4000
	B	.071	.071	.071	.071	.071	.071	.071	.071	.076	.071	.071	.071	.071		
GANDTRACK	A	.081	.089	.093	.086	.091	.096	.086	.091	.096	.086	.086	.086	.086	280	2800
	B	.045	.04	.045	.038	.04	.04	.04	.04	.04	.04	.04	.04	.04		

**PRECISION HOLE QUALITY**  
(40th Hole, 6th Regrind)



Maximum Scar Depth = 0.180mm  
N.B. GF = Gauge Failure

**GANDTRACK HOLE QUALITY**  
(40th Hole, 6th Regrind)



Maximum Scar Depth = 0.120mm

Table (8): Summary of drill evaluation, phase-2 test results.

SPEED (rpm)		FEED (mm/rev)					
		.01	.025	.035	.05	.075	.1
2250	Thrust	100	148	160	170	200	220
	Torque	7.6	10	12	14.5	17	22
2500	Thrust	125	150	180	190	225	247
	Torque	8	12	13	15	20	24
2800	Thrust	-	160	190	220	240	275
	Torque	8	12	14	18	22	25
3000	Thrust	-	172	200	240	260	285
	Torque	8.5	13	14	19	22	26
3250	Thrust	150	185	215	225	-	-
	Torque	9	12	15	19	-	-

Table (9): Thrust force (N) and torque measurements (N-cm) for Klenk drills over a range of speeds and feeds.

SPEED (rpm)		FEED (mm/rev)					
		.01	.025	.035	.05	.075	.1
2250	Thrust	-	-	-	145	165	180
	Torque	28.5	-	-	20	-	50
2500	Thrust	125	150	-	165	195	225
	Torque	22	25	-	36	-	40
2800	Thrust	-	-	170	190	215	240
	Torque	20	27	31	33	37	48
3000	Thrust	-	-	180	200	235	255
	Torque	-	-	30	32	35	44
3250	Thrust	150	165	190	210	240	275
	Torque	-	22	29	33	35	44

Table (10): Thrust force (N) and torque measurements (N-cm) for Gandtrack drills over a range of speeds and feeds.

SPEED (rpm)		FEED (mm/rev)					
		.01	.025	.035	.05	.075	.1
2250	Thrust	205	-	230	250	290	320
	Torque	22	-	34	35	49	64
2500	Thrust	185	220	240	255	265	315
	Torque	22	31	33	39	57	59
2800	Thrust	120	160	165	184	212	235
	Torque	20	29	32	36	45	54
3000	Thrust	140	165	200	215	240	275
	Torque	-	-	30	36	45	52
3250	Thrust	158	175	210	235	253	295
	Torque	15	24	30	36	46	56

Table (11): Thrust force (N) and torque measurement (N-cm) for Carbide drills over a range of speeds and feeds.

SPEED (rpm)		FEED (mm/rev)					
		.01	.025	.035	.05	.075	.1
2250	Thrust	70	120	-	140	155	185
	Torque	26	34	34	-	45	52
2500	Thrust	105	125	-	160	180	210
	Torque	24	30	-	34	41	47
2800	Thrust	-	165	-	175	200	230
	Torque	20	29	31	32	33	47
3000	Thrust	-	170	-	180	220	240
	Torque	14	28	-	32	42	46
3250	Thrust	135	175	-	200	225	250
	Torque	18	22	-	30	40	42

Table (12): Thrust force (N) and torque measurement (N-cm) for Precision drills over a range of speeds and feeds.

<b>Fringe Order</b>	<b>Residual Strain (<math>\mu\text{m}/\text{m}</math>)</b>	<b>Residual Stress, MPa</b>	<b>Drill Type</b>
<b>Black</b>	0.0	0	
<b>Yellow</b>	210.15	8.62	
<b>Red</b>	420.3	17.25	
<b>1st Fringe</b>	630.50	25.8	Klenk
<b>Blue Green</b>	840.60	34.5	
<b>Yellow</b>	1050.75	43.1	Gandtrack /Carbide
<b>Red</b>	1261.0	51.7	
<b>2nd Fringe</b>	1261.0	51.7	Precision

Table (13): The residual strains and stresses generated by drilling during the birefringent photoelasticity test.

Parameter	Klenk	Gandtrack	Preci'n	Carbide	Equa'n
Force, P (N)	220	190	184	175	
Torque, T (N-mm)	180	330	360	320	
Length of Drill (mm)	91	91.5	94.65	66	
Effective Length of Drill, L (mm)	56	56.5	59.65	31	
Area, A (mm <sup>2</sup> )	10	12.95	15.39	15.3	
Polar Moment of Inertia, J, (mm <sup>4</sup> )	36.66	47.9	53.17	64.48	
Minimum Moment of Inertia, I, (mm <sup>2</sup> )	4.37	19.8	25.0	12.97	
Elastic Modulus, E (kN/mm <sup>2</sup> )	230	230	230	630	
Poisson Ratio, v	0.2	0.2	0.2	0.22	
Shear Modulus, G (kN/mm <sup>2</sup> )	95.8	95.8	95.8	258	$E / \{2(1 + v)\}$
Torsional Rigidity (kN/mm <sup>2</sup> )	3512	4589	5094	16636	J × G
Axial Deflection, (μmm)	5360	3600	3100	560	(PL) / (AE)
Critical Buckling Load, P <sub>c</sub> (N)	6471	28802	32836	171670	$20.19 (IE/L^2)$
Safety Margin	30	150	178	980	P <sub>c</sub> / P
Angular Deflection, (Deg.)	0.16	0.23	0.24	0.034	(TL) / (GJ)

Table (14): Summary of results of structural analysis of Klenk, Gandtrack, Precision and Solid Carbide drills.

## SUMMARY OF EVALUATION OF DRILLING TESTS ON CFC

	Outer Corner Wear (100 Holes)	Drill Life (Penet dist)	Hole Quality (Depth of pit)	Side Clearance	Residual Strain	Thrust	Torque	General Remarks
KLENK	Highest (.15mm)	ND	Highest (0.1mm)	Highest	Low	High (220N)	Low (180N-mm)	Unpredic. Life with best hole quality
GENDTRACK	High (.12mm)	High (2800mm)	High (0.12mm)	High	Medium	Medium (190N)	Medium (330N-mm)	Acceptable life with good hole quality
PRECISION	Medium (.1mm)	Highest (4000mm)	Low (0.18mm)	Low	Highest	Medium (175N)	High (320N-mm)	Maximum life with poor hole quality
CARBIDE	Low (0.8mm)	ND	Medium (0.15mm)	ND	High	Low (184N)	High (360N-mm)	Maximum life, fair hole quality, brittle and expensive

ND : Not determined

Table (15): Summary of Drill Evaluation Test Results.

<b>S/No</b>	<b>Krupp, THR (HV)</b>	<b>Sandvik, H10F (HV)</b>	<b>Kennametal, F285 (HV)</b>
1.	1610	1660	1733
2.	1596	1655	1738
3.	1520	1670	1708
4.	1610	1665	1738
5.	1564	1674	1708
<b>AVERAGE</b>	<b>1580</b>	<b>1665</b>	<b>1725</b>

Table (16): Results of the Vickers hardness test on the Krupp THR, Sandvik H10F and Kennametal F285 cemented carbides.

Carbide Material	Inden- tation corner	20 Newton Load	40 Newton Load	60 Newton Load	80 Newton Load
Krupp, THR ( $\mu\text{m}$ )	1	24	56	104	133
Krupp, THR ( $\mu\text{m}$ )	2	14	64	109	136
Krupp, THR ( $\mu\text{m}$ )	3	17	40	109	129
Krupp, THR ( $\mu\text{m}$ )	4	23	44	105	117
Sandvik, H10F ( $\mu\text{m}$ )	1	20	69	119	131
Sandvik, H10F ( $\mu\text{m}$ )	2	7	70	103	113
Sandvik, H10F ( $\mu\text{m}$ )	3	7	57	79	151
Sandvik, H10F ( $\mu\text{m}$ )	4	24	66	82	150
K'metal, F285 ( $\mu\text{m}$ )	1	62	147	283	355
K'metal, F285 ( $\mu\text{m}$ )	2	57	134	210	170
K'metal, F285 ( $\mu\text{m}$ )	3	66	140	150	200
K'metal, F285 ( $\mu\text{m}$ )	4	73	130	159	402

Table (17): The crack lengths at the four corners of diamond indentation made in the Krupp THR, Sandvik H10F and Kennametal F285 cemented carbide in the Palmqvist test.

MANUFACTURER	KRUPPS, THR	SANDVIK, H10F	KENNAMETAL, F-285
Hardness (HV)	1580	1665	1725
Carbide Grain Distribution	Non-uniform	Uniform	Uniform
M' structure	Coarse	Medium	Fine
Cobalt Layer Thickness ( $\mu\text{m}$ )	0.17	0.16	0.14
Grain Size ( $\mu\text{m}$ )	1.07	0.98	0.83
Palmqvist Fracture Resistance (kN/m)	1186	1186	681
Bulk Toughness ( $\text{J/m}^2$ )	221	221	133
Dia. of Wear Scar; Sliding Dist.: 8000 m ( $\mu\text{m}$ )	1.16	1.16	0.83

Table (18): Summary of Krupp THR, Sandvik H10F and Kennametal F-285 cemented carbides evaluation test results.

PROPERTY	KRUPP, THR	SANDVIK, H10F	KENNAMETAL, F-285
Hardness, (HV)	1450	1550-1650	1626
Compr. Strength (kN/mm <sup>2</sup> )	4.95	4.75	6.82
Density (g/cm <sup>3</sup> )	14.6	14.5	14.53
Youngs Modulus of Elasticity (kN/mm <sup>2</sup> )	590	580	580
Poisson Ratio	0.23	0.22	0.228
Ther. Conductivity (W/m <sup>°K</sup> )	70	120	68.2
Mean Coefficient of Thermal Expansion (/°C)	$5.3 \times 10^{-6}$	$5.2 \times 10^{-6}$	$5.8 \times 10^{-6}$
Grain Size ( $\mu$ )	-	0.6-0.8	less than 1
% of Cobalt	9	10	10
Trans. Rupture. Strength (N/mm <sup>2</sup> )	2350	2200	3105

Table (19): Important physical and mechanical properties of Krupp THR, Sandvik H10F and Kennametal F-285 Cemented Carbides as reported in the literature [79].

## Appendix 'A'

<b>AIRCRAFT</b>	<b>MANUFACTURER</b>	<b>APPLICATIONS</b>
<b>AV-8B</b>	B.Ae/McDonnell Douglas	Wing skin, front fuselage, horizontal tail skin, control surfaces, outrigger fairing and engine access cowling.
<b>F-16, Falcon</b>	General Dynamics	Horizontal and vertical tail skins, leading edge and rudder
<b>F/A-18, Hornet</b>	Northrop	Wing skin, horizontal and vertical wing skins, control surfaces, speed brakes, avionics bay door.
<b>B-1B</b>	Rockwell	Weapon bay door, wing flaps, avionics bay door, rotary launcher.
<b>Gripen</b>	Saab Scania	Canard wing, fin box, flight control surfaces and cowlings.
<b>B757 and 767</b>	Boeing	Wing skin, control surfaces, Fairings, undercarriage doors, cowlings
<b>A330 and 340</b>	Airbus	Floor panels, spoilers, fin/fuselage fairing, control surfaces, landing gear bay panel, tail bumper.
<b>Learjet 2100</b>	Learjet	"ALMOST ALL" of structure

# Specification

## 1 Scope

This Part of BS 328 specifies the requirements for the following types of twist drills for general engineering use:

- (a) parallel shank jobber series twist drills;
- (b) parallel shank stub series twist drills;
- (c) parallel shank long series twist drills;
- (d) parallel shank extra long series twist drills;
- (e) Morse taper shank twist drills;
- (f) Morse taper shank extra long twist drills.

Appendix A gives a method of test for the drills and appendix B contains summary tables of drill diameters in millimetres and inches (table 15) and flute and overall lengths (table-16) in the different series of drills.

NOTE. The titles of the publications referred to in this standard are listed on the inside back cover.

## 2 Definitions

For the purposes of this Part of BS 328 the following definitions apply.

### 2.1 Types of twist drill

**2.1.1 parallel shank jobber series twist drill.** A drill having two helical flutes and a parallel shank of approximately the same diameter as the cutting end.

**2.1.2 parallel shank stub series twist drill.** A shortened form of parallel shank jobber series twist drill, the reduction in length being in the flute length.

**2.1.3 parallel shank long series twist drill.** A lengthened form of the parallel shank jobber series twist drill, the increase in length being in the flute length.

**2.1.4 parallel shank extra long series twist drill.** A lengthened form of the parallel shank jobber series twist drill, longer than the long series, the increase in length being in the flute length.

**2.1.5 Morse taper shank twist drill.** A drill having two helical flutes and a standard Morse taper shank.

**2.1.6 Morse taper shank extra long twist drill.** A lengthened form of the Morse taper shank twist drill, the increase in length being in the flute length.

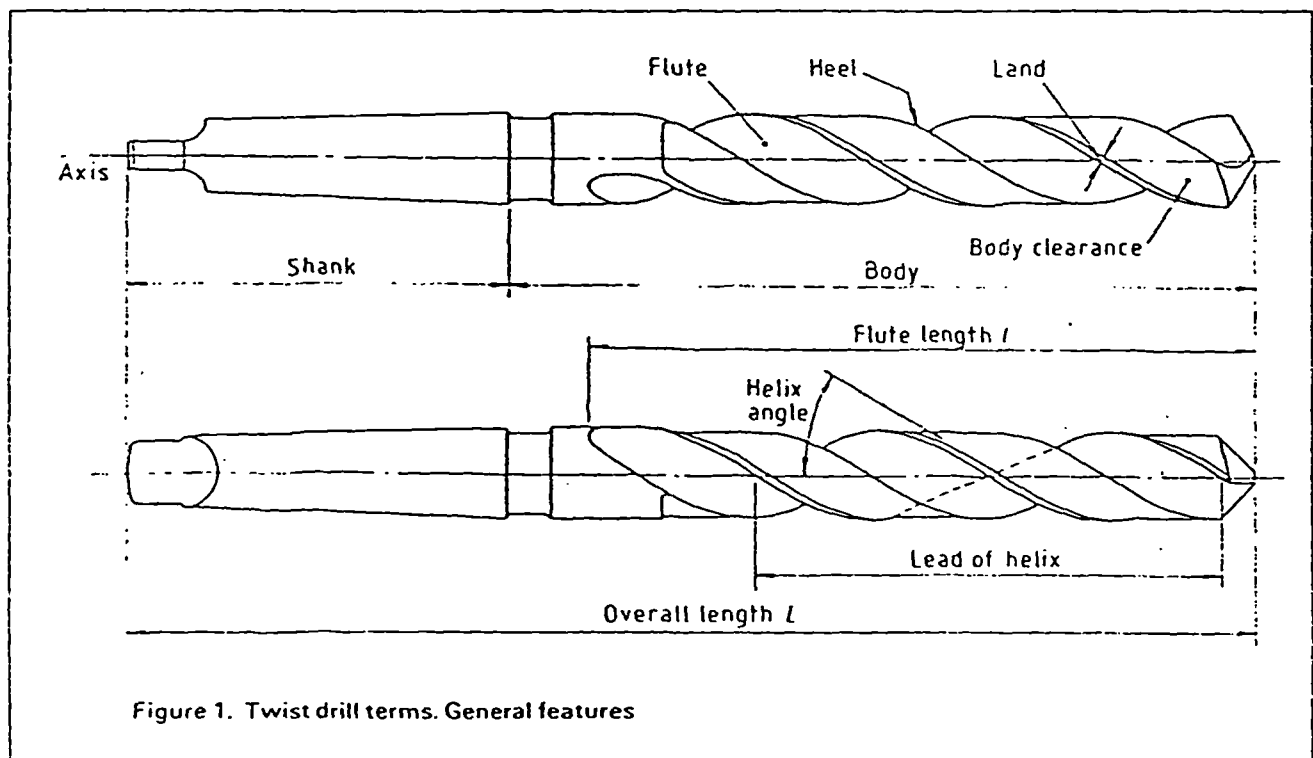


Figure 1. Twist drill terms. General features

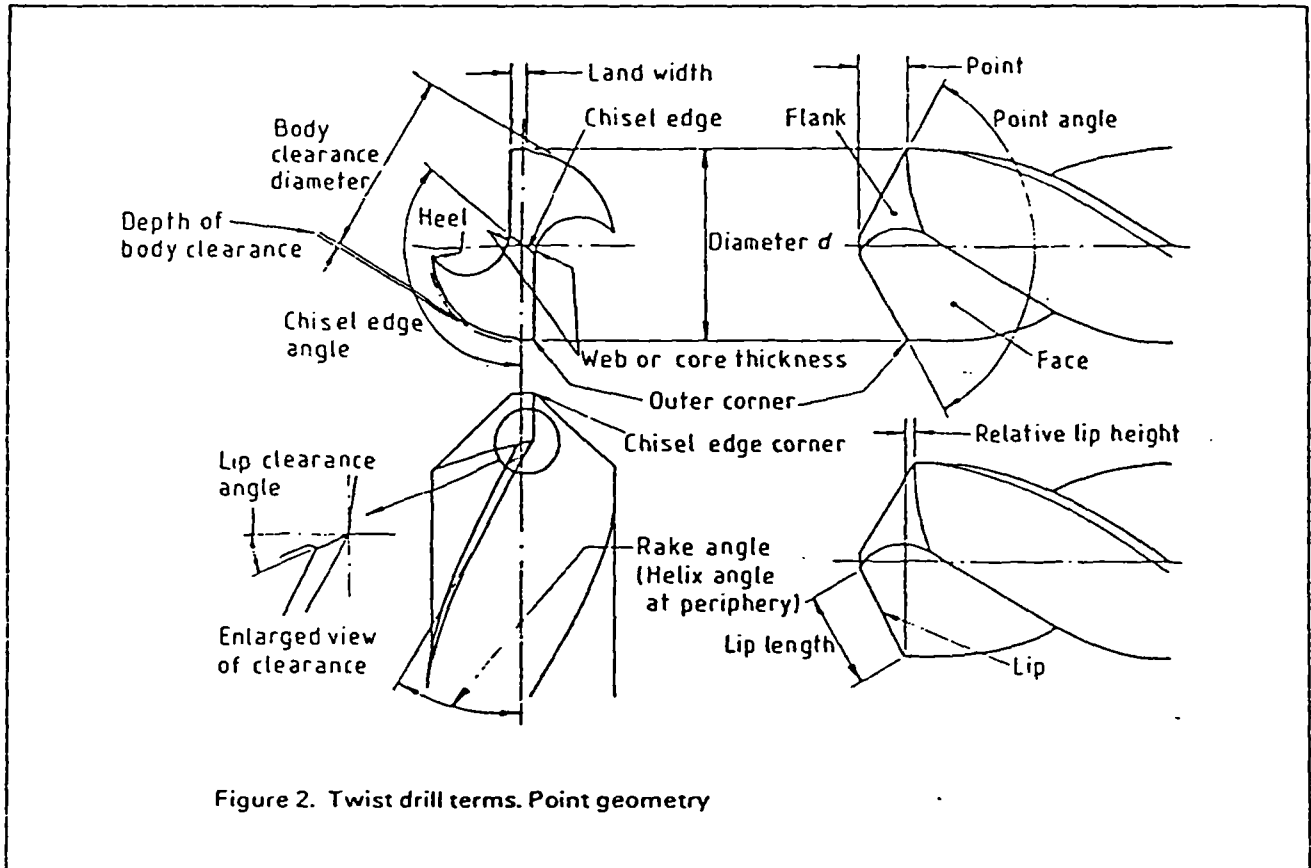


Figure 2. Twist drill terms. Point geometry

## 2.2 Other terms

2.2.1 axis. The longitudinal centre line.

NOTE See figure 1.

2.2.2 back taper (longitudinal clearance). The reduction in diameter per unit length of drill from the point towards the shank.

2.2.3 body. The portion of a drill extending from the extreme cutting end to the commencement of the shank (2.2.32).

NOTE. See figure 1.

2.2.4 body clearance. The portion of the body surface reduced in diameter to provide diametral clearance.

NOTE. See figure 1.

2.2.5 body clearance diameter. The diameter over that surface of the drill body situated behind the lands.

NOTE. See figure 2.

2.2.6 chisel edge. The edge formed by the intersection of the flanks.

NOTE. See figure 2.

2.2.7 chisel edge angle. The obtuse angle included by the chisel edge and a line from either outer corner to the corresponding end of the chisel edge, the angle being measured in a plane perpendicular to the drill axis.

NOTE See figure 2.

2.2.8 chisel edge corner. A corner formed by the intersection of a lip and the chisel edge.

NOTE. See figure 2.

2.2.9 depth of body clearance. The amount of diametral reduction per side to provide body clearance.

NOTE. See figure 2.

2.2.10 diameter,  $d$ . The measurement across the cylindrical lands at the outer corners of a drill.

NOTE. See figure 2.

2.2.11 face. The portion of the flute surface, adjacent to the lip, on which the chip impinges as it is cut from the work.

NOTE. See figure 2.

2.2.12 flank. One of the surfaces on a drill point that extends behind a lip to the following flute.

NOTE. See figure 2.

2.2.13 flutes. The grooves in the body of a drill that provide lips, permit the removal of chips and allow cutting fluid to reach the lips.

NOTE. See figure 1.

2.2.14 flute length,  $l$ . The axial length from the extreme end of the point to the termination of the flutes at the shank end of the body.

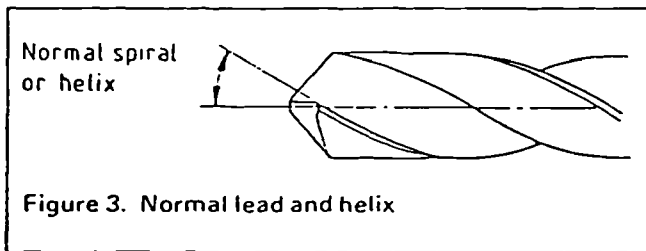
NOTE. See figure 1.

**2.2.15 heel.** The edge formed by the intersection of the flute surface and the body clearance.

NOTE. See figure 2.

**2.2.16 helix angle.** The angle between the leading edge of a land and the drill axis.

NOTE. See figure 3.



**2.2.17 lands.** The cylindrically-ground surfaces on the leading edges of the drill flutes.

NOTE. See figure 1.

**2.2.18 land width.** The width of the land measured at right angles to the flute helix.

NOTE. See figure 2

**2.2.19 lead of helix.** The distance measured parallel to the drill axis between corresponding points on the leading edge of a flute in one complete turn of the flute.

NOTE. See figure 1.

**2.2.20 left-hand cutting drill.** A drill that rotates in a clockwise direction when viewed on the point end of the drill.

**2.2.21 lip (cutting edge).** The edge formed by the intersection of a flank and a face.

NOTE. See figure 2.

**2.2.22 lip clearance angle.** The angle formed by a flank and a plane at right angles to the drill axis, normally measured at the periphery of the drill.

NOTE. See figure 2.

**2.2.23 lip length.** The minimum distance between the outer corner and the chisel edge corner of a lip.

NOTE. See figure 2.

**2.2.24 outer corner.** A corner formed by the intersection of a lip and the leading edge of a land.

NOTE. See figure 2.

**2.2.25 overall length,  $L$ .** The length over the extreme ends of the point and the shank.

NOTE. See figure 1.

**2.2.26 point.** The sharpened end of a drill, consisting of all that part of the drill that is shaped to produce lips, faces, flanks and a chisel edge

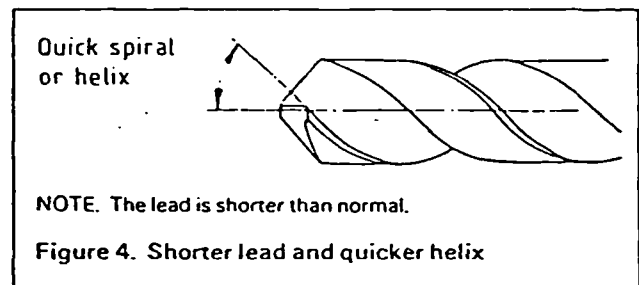
NOTE. See figure 2

**2.2.27 point angle.** The included angle of the cone formed by the lips.

NOTE. See figure 2.

**2.2.28 quick helix angle.** A helix angle that is larger in angular value (i.e. in number of degrees) than the normal helix angle, thereby shortening the lead of helix.

NOTE. See figure 4.



**2.2.29 rake angle.** The angle between a face and a line parallel to the drill axis.

NOTE 1. At the periphery of the drill the rake angle is equivalent to the helix angle.

NOTE 2. See figure 2.

**2.2.30 relative lip height.** The distance between two planes, perpendicular to the drill axis, each of which passes through an outer corner of the drill.

NOTE. See figure 2.

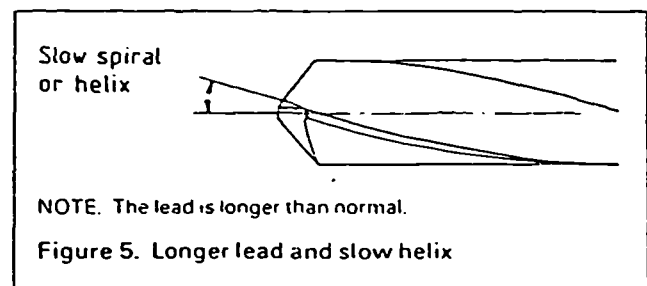
**2.2.31 right-hand cutting drill.** A drill that rotates in a counter-clockwise direction when viewed on the point end of the drill.

**2.2.32 shank.** The portion of a drill by which it is held and driven.

NOTE. See figure 1.

**2.2.33 slow helix angle.** A helix angle that is smaller in angular value (i.e. in number of degrees) than the normal helix angle, thereby lengthening the lead of helix.

NOTE. See figure 5.



**2.2.34 web (core).** The central portion of a drill situated between the roots of the flutes and extending from the point towards the shank.

NOTE 1. The point end of the web or core forms the chisel edge.

NOTE 2. See figure 2

2.2.35 web taper (core taper). The increase in the web or core thickness from the point of the drill to the shank end of the flutes.

2.2.36 web thickness (core thickness). The minimum dimension of the web or core measured at the point end of the drill.

NOTE. See figure 2.

### 3 Features of design

#### 3.1 General

Twist drills shall be supplied sharpened and ready for use.

#### 3.2 Flutes

The flutes shall be designed so that cutting lips are equal. The drills shall be provided with body clearance.

#### 3.3 Point

The point shall be ground to provide lip clearance.

NOTE. The included point angle should be approximately 118°, each lip being equally inclined to the axis of the drill.

#### 3.4 Back taper

Back taper shall be provided on nominal diameters of 6.35 mm or 0.25 in and larger from point to shank within the following limits:

(a) 6.35 mm diameter up to and including 40 mm diameter: 0.0005 mm to 0.001 mm per millimetre or 0.0005 in to 0.001 in per inch;

(b) over 40 mm: 0.0005 mm to 0.0015 mm per millimetre or 0.0005 in to 0.0015 in per inch.

NOTE. Below 6.35 mm or 0.25 in, back taper is not a requirement but may be provided

#### 3.5 Hand of cutting

Both right-hand and left-hand cutting drills are in conformity with this standard, but unless otherwise ordered, a right-hand cutting drill shall be supplied.

### 4 Marking

The marking shall be so applied and finished that it does not interfere with the secure holding of the drill.

NOTE. The drills should, whenever possible, be permanently, neatly and legibly marked, preferably by rolling, with the manufacturer's name or trade mark and the size of the drill. Additionally, drills made from high speed steel should, where practicable, be marked with the letters HSS.

### 5 Testing

5.1 Twist drills of 3 mm or  $\frac{1}{8}$  in diameter and above shall be tested in accordance with appendix A at the rate of 2%

per batch or two drills in the case of batches of less than 100, the drills being selected at random.

NOTE. Any tests on drills below 3 mm or  $\frac{1}{8}$  in diameter should be the subject of agreement between manufacturer and purchaser.

5.2 Each drill tested shall withstand the test in appendix A without seizing, choking or fusing and the points and lips shall be fit for further service on completion of the test.

5.3 If any of the drills tested do not comply with the requirements of 5.2, two further drills from the same batch shall be tested and if either fails, the batch represented shall be deemed not to comply with the requirements of this standard.

NOTE. The tests may be carried out at the manufacturer's premises or elsewhere as mutually agreed with the purchaser.

### 6 Dimensions

6.1 Preferred sizes of drills shall have the dimensions shown in tables 2, 4, 6, 8, 9 or 11. The flute lengths of Morse taper shank extra long twist drills shall be as given in table 12.

6.2 Non-preferred sizes shall have flute and overall lengths, and Morse taper shanks where applicable, in accordance with tables 3, 5, 7 or 10.

6.3 Shanks shall be either parallel without driving tenon as specified in tables 2 to 8 or of Morse taper as specified in tables 9 to 12. The dimensions of Morse taper shanks shall be in accordance with BS 1660.

### 7 Tolerances

7.1 The tolerance on the diameter,  $d$ , of a drill, as measured across the lands at the outer corners, shall be as shown in table 1 (i.e. h8 as specified in BS 4500 : Part 1).

7.2 The maximum value of each flute length and overall length shall be the value specified in tables 3, 5, 7 and 10 for the next larger sub-range of drill diameter. The minimum value of each flute and overall length shall be the value specified in tables 3, 5, 7 and 10 for the next smaller sub-range of drill diameter.

In the case of taper shank drills, if the next larger overall length is associated with a different taper shank from that of the length in question, the permissible upper limit shall be the next larger overall length reduced by the difference in the lengths of the taper shanks concerned; if the next smaller overall length is associated with a different taper shank from that of the length in question, the permissible lower limit shall be the next smaller overall length increased by the difference in the lengths of the taper shank concerned.

Table 1. Limits of tolerance on diameter

Diameter		Limits of tolerance h8*					
Over	Up to and including	Over	Up to and including	Upper	Lower	Upper	Lower
mm	mm	in	in	mm	mm	in	in
—	1	—	0.039 4	0	-0.014	0	-0.000 6
1	3	0.039 4	0.118 1	0	-0.014	0	-0.000 6
3	6	0.118 1	0.236 2	0	-0.018	0	-0.000 7
6	10	0.236 2	0.393 7	0	-0.022	0	-0.000 9
10	18	0.393 7	0.708 7	0	-0.027	0	-0.001 1
18	30	0.708 7	1.181 1	0	-0.033	0	-0.001 3
30	50	1.181 1	1.968 5	0	-0.039	0	-0.001 5
50	80	1.968 5	3.149 6	0	-0.046	0	-0.001 8
80	120	3.149 6	4.500	0	-0.054	0	-0.002 1

\* See BS 4500: Part 1.

```

1 OPEN "DATA" FOR OUTPUT AS FILE 1%
2 INPUT "FILE NAME",A$
3 PRINT #1,A$
4 CLOSE 1
5 OPEN A$ FOR OUTPUT AS FILE 1%
6 PRINT "HOLE MATRIX"
10 INPUT "DEVICE TO WHICH UNFORMATTED AND FORMATTED OUTPUT SHOULD GO",I
12 PRINT #1,D$
13 INPUT "METRIC OR IMPERIAL",Z1$
15 PRINT "FIRST HOLE CENTRE RELATIVE TO MACHINE DATUM POSITION"
20 INPUT "X DIMENSION";X1,"Y DIMENSION";Y1
50 PRINT #1,"NO01 G80 G90 M06"
55 INPUT "SPINDLE CW OR CCW";C$
56 INPUT "NUMBER OF HOLES TO BE DRILLED BEFORE INSPECTION",N2
60 C1$="CW"; C2$="CCW"
65 IF C$=C1$ GOTO 80
70 IF C$=C2$ GOTO 85
75 GOTO 55
80 PRINT #1,"NO02 M03 M00"; GOTO 90
85 PRINT #1,"NO02 M04 M00"
90 INPUT "COOLANT ON OR OFF";P$
95 P1$="ON"; P2$="OFF"
100 IF P$=P1$ GOTO 115
105 IF P$=P2$ GOTO 117
110 GOTO 90
115 PRINT #1,"NO03 M03"; N=4; GOTO 120
117 N=3
120 N1=1; INPUT "STOP NUMBER";S
125 INPUT "NUMBER OF ROWS";R1
130 INPUT "DISTANCE BETWEEN ROWS";Y2
132 INPUT "HOLE PITCH";X2
135 INPUT "ARE HOLES STAGGERED";T$
140 T1$="YES"; T2$="NO"
145 IF T$=T1$ GOTO 160
150 IF T$=T2$ GOTO 155
152 GOTO 135
155 INPUT "HOW MANY HOLES PER ROW";P1; GOTO 190
160 INPUT "INCREMENT BETWEEN FIRST HOLES IN ROWS 2 AND 1";X3
165 INPUT "HOW MANY HOLES IN FIRST ROW";P1
170 INPUT "HOW MANY HOLES IN SECOND ROW";P2
190 INPUT "DRILLING OR TAPPING";G$
195 G1$="DRILLING"; G2$="TAPPING"
200 IF G$=G1$ GOTO 215
205 IF G$=G2$ GOTO 220
210 GOTO 190
215 PRINT #1,"N",N;"G81";"S",S; GOTO 225
220 PRINT #1,"N",N;"G84";"S",S;
225 X=X1; Y=Y1
230 PRINT #1,"X",X;"Y",Y
235 IF T$=T2$ THEN 240 ELSE 315
240 FOR K=0 TO (R1-1)
245 N=N+1; N1=N1+1
250 Y=Y1+(Y2*X)
255 IF R=0 THEN X=X1+X2 ELSE X=X1
256 IF N1=N2 THEN GOSUB 500; GOTO 265
258 IF N1=1 THEN GOSUB 550; GOTO 265
260 PRINT #1,"N",N;"X",X;"Y",Y
265 FOR I=1 TO (P1-1)
267 IF K=0 AND I=1 THEN GOTO 285
270 N=N+1; N1=N1+1

```

```

275     X=X1+(X2*I)
276     IF N1=N2 THEN GOSUB 500 GOTO 285
277     IF N1=1 THEN GOSUB 550 GOTO 285
280     PRINT #1,"N",N;"X",X
285     NEXT I
290     NEXT R
295     N=N+1
300     PRINT #1,"N",N;"G80M00"
305     N=N+1
307     IF Z1$="IMPERIAL" THEN PRINT #1,"N",N;"XOYQF100M06" GOTO 312
310     PRINT #1,"N",N;"X0";"Y0";"F1000";"M06"
312     PRINT #1,"END" GOTO 460
315     FOR R=0 TO (R1-1) STEP 2
320     N=N+1 G N1=N1+1
325     Y=Y1+(Y2*R)
330     IF R=0 THEN X=X1+X2 ELSE X=X1
331     IF N1=N2 THEN GOSUB 500 GOTO 340
333     IF N1=1 THEN GOSUB 550 GOTO 340
335     PRINT #1,"N",N;"X",X;"Y",Y
340     FOR I=1 TO (P1-1)
345     IF R=0 AND I=1 THEN GOTO 365
350     N=N+1 G N1=N1+1
355     X=X1+(X2*I)
356     IF N1=N2 THEN GOSUB 500 GOTO 365
358     IF N1=1 THEN GOSUB 550 GOTO 365
360     PRINT #1,"N",N;"X",X
365     NEXT I
370     NEXT R
375     FOR R=1 TO (R1-1) STEP 2
380     N=N+1 G N1=N1+1
385     Y=Y1+(Y2*R)
390     X=X1+X3
391     IF N1=N2 THEN GOSUB 500 GOTO 400
393     IF N1=1 THEN GOSUB 550 GOTO 400
395     PRINT #1,"N",N;"X",X;"Y",Y
400     FOR I=1 TO (P2-1)
410     N=N+1 G N1=N1+1
415     X=X1+X3+(X2*I)
416     IF N1=N2 THEN GOSUB 500 GOTO 425
418     IF N1=1 THEN GOSUB 550 GOTO 425
420     PRINT #1,"N",N;"X",X
425     NEXT I
430     NEXT R
435     N=N+1
440     PRINT #1,"N",N;"G80M00"
445     N=N+1
450     IF Z1$="IMPERIAL" THEN PRINT #1,"N",N;"XOYQF100M06" GOTO 455
452     PRINT #1,"N",N;"XOYQF100M06"
455     PRINT #1,"END"
460     CLOSE 1%
465     CHAIN "DANDW"
470     GOTO 1000
500     PRINT #1,"N",N;"X",X;"Y",Y G N=N+1
505     PRINT #1,"N",N;"G80M00" G N=N+1 G N1=0
507     PRINT #1,"N",N;"M6"
510     RETURN
550     GOTO 560
560     PRINT #1,"N",N;"M03 M00" G N=N+1
562     IF P$=P2$ GOTO 566
564     PRINT #1,"N",N;"M0:" G N=N+1
566     IF G$="TAPPING" THEN GOTO 570
568     PRINT #1,"N",N;"G81X",X;"Y",Y;"S",S GOTO 580
570     PRINT #1,"N",N;"G84X",X;"Y",Y;"S",S
580     N=N+1 G RETURN
1000

```

```

5 A=0;B=0
6 G1=1;T1=0
8     GOTO 80
20 PRINT "THE WADKIN NC MACHINES AND PRODUCES A CONTROL TAPE"
30 INPUT "DSG OR WADKIN",Z$
40 Z1$="DSG";Z2$="WADKIN"
50 IF Z$=Z1$ GOTO 70
60 IF Z$=Z2$ GOTO 80 ELSE GOTO 30
70 Z1=1;PRINT "FOR DSG ONLY METRIC DIMENSIONS ARE ACCEPTABLE"
    GOTO 85
80 Z1=2
85 IF T1=1 GOTO 640
90 OPEN "DATA" FOR INPUT AS FILE 1%
92 INPUT #1,A$;CLOSE 1
94 OPEN A$ FOR INPUT AS FILE 1%;GOTO 110
100 PRINT A$;A=0;GOTO 120
110 INPUT #1,D$
120 INPUT #1,A$
130 Y%=LEN(A$);N=0;G=0;X=0;Y=0;S=0;F=0;M=0;Z=0;I=0;K=0;H=0;T=0
140 FOR I%=1% TO Y%
150 B$=MID(A$,I%,1%)
160 IF A$="END" GOTO 630
170 IF B$="N" GOTO 320
180 IF B$="H" GOTO 330
190 IF B$="G" GOTO 340
200 IF B$="Z" GOTO 360
210 IF B$="M" GOTO 370
220 IF B$="I" GOTO 390
230 IF B$="X" GOTO 400
240 IF B$="K" GOTO 410
250 IF B$="Y" GOTO 420
260 IF B$="T" GOTO 430
270 IF B$="S" GOTO 440
280 IF B$="F" GOTO 450
290
300 IF N=0 GOTO 460
302 GOTO 310
310 IF A=0 GOTO 120 ELSE GOTO 100
320 N=N+1;IF N=2 GOTO 470 ELSE GOTO 290
330 H=H+1;IF H=2 GOTO 560 ELSE GOTO 290
340 G=G+1;IF G=3 AND Z1=2 THEN GOTO 480
350 IF G=2 AND Z1=1 THEN GOTO 490 ELSE GOTO 290
360 Z=Z+1;IF Z=2 GOTO 570 ELSE GOTO 290
370 M=M+1;IF M=3 AND Z1=2 THEN GOTO 500
380 IF M=2 AND Z1=1 THEN GOTO 510 ELSE GOTO 290
390 I=I+1;IF I=2 GOTO 580 ELSE GOTO 290
400 X=X+1;IF X=2 GOTO 520 ELSE GOTO 290
410 K=K+1;IF K=2 GOTO 590 ELSE GOTO 290
420 Y=Y+1;IF Y=2 GOTO 530 ELSE GOTO 290
430 T=T+1;IF T=2 GOTO 600 ELSE GOTO 290
440 S=S+1;IF S=2 GOTO 540 ELSE GOTO 290
450 F=F+1;IF F=2 GOTO 550 ELSE GOTO 290
460 PRINT "ERROR;- NO N NUMBER";GOTO 302
470 GOSUB 610;PRINT "ONE N NUMBER";GOTO 290
480 GOSUB 610;PRINT "TWO G NUMBERS";GOTO 290
490 GOSUB 610;PRINT "ONE G NUMBER";GOTO 290
500 GOSUB 610;PRINT "TWO M NUMBERS";GOTO 290
510 GOSUB 610;PRINT "ONE M NUMBER";GOTO 290
520 GOSUB 610;PRINT "ONE X NUMBER";GOTO 290
530 GOSUB 610;PRINT "ONE Y NUMBER";GOTO 290

```

GOTO 625

```

540 GOSUB 610;PRINT "ONE S NUMBER";GOTO 290
550 GOSUB 610;PRINT "ONE F NUMBER";GOTO 290
560 GOSUB 610;PRINT "ONE H NUMBER";GOTO 290
570 GOSUB 610;PRINT "ONE Z NUMBER";GOTO 290
580 GOSUB 610;PRINT "ONE I NUMBER";GOTO 290
590 GOSUB 610;PRINT "ONE K NUMBER";GOTO 290
600 GOSUB 610;PRINT "ONE T NUMBER";GOTO 290
610 PRINT "ERROR;- MORE THAN ";
620 A=1;B=B+1;RETURN
625             NEXT IX
630 IF B>0 GOTO 2030
635 N1=0;CLOSE 1;OPEN A$ FOR INPUT AS FILE 1;
636     GOTO 680
637 INPUT #1,D$
640 INPUT "METRIC OR IMPERIAL",T$
650 T1$="METRIC";T2$="IMPERIAL";IF T1$=T$ GOTO 680
660 IF T2$=T$ GOTO 670 ELSE GOTO 640
670 T1=1;IF Z1=1 GOTO 70
675 GOTO 690
680 T1=2
690 OPEN "FODATA" FOR OUTPUT AS FILE 2;PRINT #2,D$
695 IF Z1=1 GOTO 1300
700 PRINT #2," ";B2$=""
710 INPUT #1,A$;Y%=LEN(A$);IF A$="END" GOTO 2050
715 FOR IX=1% TO Y%
720 B$=MID(A$,IX,1%);IF B$("<"N" GOTO 740
730 PRINT #2,B$;GOSUB 1050;GOSUB 1100;GOTO 750
740 NEXT IX
750 A=0
760 FOR IX=1% TO Y%
765 B$=MID(A$,IX,1%);IF B$("<"G" GOTO 780
770 PRINT #2,B$;A=A+1;GOSUB 1050;V=VAL(B$);GOSUB 1150
    IF A=2 GOTO 810
780 NEXT IX
785 IF A=0 GOTO 800
790 PRINT #2," ";GOTO 810
800 PRINT #2," ";
810 IF Y%=Z% GOTO 700
820 FOR IX=1% TO Y%;B$=MID(A$,IX,1%);IF B$("<"X" GOTO 840
830 PRINT #2,B$;GOSUB 1050;V=VAL(B$);GOSUB 1200;GOTO 860
840 NEXT IX
850 PRINT #2," ";
860 IF Y%=Z% GOTO 700
870 FOR IX=1% TO Y%;B$=MID(A$,IX,1%);IF B$("<"Y" GOTO 890
880 PRINT #2,B$;GOSUB 1050;V=VAL(B$);GOSUB 1200;GOTO 910
890 NEXT IX
900 PRINT #2," ";
910 IF Y%=Z% GOTO 700
920 FOR IX=1% TO Y%;B$=MID(A$,IX,1%);IF B$("<"S" GOTO 940
930 PRINT #2,B$;GOSUB 1050;V=VAL(B$);GOSUB 1150;GOTO 960
940 NEXT IX
950 PRINT #2," ";
960 IF Y%=Z% GOTO 700
970 FOR IX=1% TO Y%;B$=MID(A$,IX,1%);IF B$("<"I" GOTO 990
980 PRINT #2,B$;GOSUB 1050;V=VAL(B$);GOSUB 1250;GOTO 1010
990 NEXT IX
1000 PRINT #2," ";
1010 FOR IX=1% TO Y%;B$=MID(A$,IX,1%);IF B$("<"M" GOTO 1030
1020 PRINT #2,B$;GOSUB 1050;V=VAL(B$);GOSUB 1165
1030 NEXT IX;GOTO 700

```

```

1050 B2$=B2$+B$;B$=""
1060 IZ=IZ+1;B1$=MID(A$,IZ,1);B1=ASCII(B1$)
1070 IF B1>57 GOTO 1090
1075 IF B1<32 GOTO 1090
1080 B$=B$+B1$;B2$=B2$+B1$;Z%=LEN(B2$);GOTO 1060
1090 IZ=IZ-1;RETURN
1100 N1=N1+2;IF N1=1000 THEN N1=2
1110 IF N1>99 THEN PRINT #2 USING "### ",N1;GOTO 1140
1120 IF N1> 9 THEN PRINT #2 USING "0## ",N1;GOTO 1140
1130 PRINT #2 USING "00# ",N1;
1140 RETURN
1150 IF V>9 GOTO 1156
1153 PRINT #2 USING "0# ",V;GOTO 1160
1156 PRINT #2 USING "## ",V;
1160 RETURN
1165 IF V>9 GOTO 1175
1170 PRINT #2 USING "0#",V;GOTO 1180
1175 PRINT #2 USING "##",V;
1180 RETURN
1200 IF T1=1 GOTO 1230
1205 V=INT(100*V+0.5)/100
1210 PRINT #2 USING "#####.## ",V;
1220 RETURN
1230 PRINT #2 USING "###.#### ",V;
1240 RETURN
1250 IF T1=1 GOTO 1280
1260 PRINT #2 USING "#####.## ",V;
1270 RETURN
1280 PRINT #2 USING "###.### ",V;
1290 RETURN
1300 PRINT #2;B2$=""
1310 INPUT #1,A$;YZ%=LEN(A$);IF A$="END" GOTO 2050
1320 FOR IZ=1% TO YZ;B$=MID(A$,IZ,1);IF B$("<"N" GOTO 1340
1330 PRINT #2,B$;GOSUB 1050;GOSUB 1100;GOTO 1350
1340 NEXT IZ
1350 FOR IZ=1% TO YZ;B$=MID(A$,IZ,1);IF B$("<"G" GOTO 1370
1360 PRINT #2,B$;GOSUB 1050;V=VAL(B$);GOSUB 1150;GOTO 1415
1370 NEXT IZ
1375 GOTO 1410
1380 FOR IZ=1% TO YZ;B$=MID(A$,IZ,1);IF B$("<"H" GOTO 1400
1390 PRINT #2,B$;GOSUB 1050;V=VAL(B$);GOSUB 1910;GOTO 1405
1400 NEXT IZ
1402 GOTO 1430
1405 IF YZ=Z% GOTO 1300
1407 PRINT #2," ";GOTO 1630
1410 PRINT #2," ";GOTO 1420
1415 IF V=94 THEN G1=1
1416 IF V=33 THEN G1=3
1417 IF V=95 THEN G1=2
1418 IF V=36 THEN G1=4
1420 IF YZ=Z% GOTO 1300
1425 GOTO 1380
1430 FOR IZ=1% TO YZ;B$=MID(A$,IZ,1);IF B$("<"X" GOTO 1450
1440 PRINT #2,B$;GOSUB 1050;V=VAL(B$);GOSUB 1805;GOTO 1470
1450 NEXT IZ
1460 PRINT #2," ";
1470 IF YZ=Z% GOTO 1300
1480 FOR IZ=1% TO YZ;B$=MID(A$,IZ,1);IF B$("<"Z" GOTO 1500
1490 PRINT #2,B$;GOSUB 1050;V=VAL(B$);GOSUB 1805;GOTO 1500
1500 NEXT IZ

```

```

1510 PRINT #2," ";
1520 IF Y%=Z% GOTO 1300
1530 FOR I%=1% TO Y%:B$=MID(A$,I%,1%):IF B$("<"I" GOTO 1550
1540 PRINT #2,B$;:GOSUB 1050:V=VAL(B$):GOSUB 1805:GOTO 1570
1550 NEXT I%
1560 PRINT #2," ";
1570 IF Y%=Z% GOTO 1300
1580 FOR I%=1% TO Y%:B$=MID(A$,I%,1%):IF B$("<"K" GOTO 1600
1590 PRINT #2,B$;:GOSUB 1050:V=VAL(B$):GOSUB 1805:GOTO 1620
1600 NEXT I%
1610 PRINT #2," ";
1620 IF Y%=Z% GOTO 1300
1630 FOR I%=1% TO Y%:B$=MID(A$,I%,1%):IF B$("<"S" GOTO 1650
1640 PRINT #2,B$;:GOSUB 1050:V=VAL(B$):GOSUB 1910:GOTO 1670
1650 NEXT I%
1660 PRINT #2," ";
1670 IF Y%=Z% GOTO 1300
1680 FOR I%=1% TO Y%:B$=MID(A$,I%,1%):IF B$("<"T" GOTO 1700
1690 PRINT #2,B$;:GOSUB 1050:V=VAL(B$):GOSUB 1885:GOTO 1720
1700 NEXT I%
1710 PRINT #2," ";
1720 IF Y%=Z% GOTO 1300
1730 FOR I%=1% TO Y%:B$=MID(A$,I%,1%):IF B$("<"F" GOTO 1750
1740 PRINT #2,B$;:GOSUB 1050:V=VAL(B$):GOSUB 1930:GOTO 1770
1750 NEXT I%
1760 PRINT #2," ";
1770 IF Y%=Z% GOTO 1300
1780 FOR I%=1% TO Y%:B$=MID(A$,I%,1%):IF B$("<"M" GOTO 1800
1790 PRINT #2,B$;:GOSUB 1050:V=VAL(B$):GOSUB 1165
1800 NEXT I%:GOTO 1300
1805 IF V<0 GOTO 1845
1807 IF G1=3 GOTO 2000
1808 IF G1=4 GOTO 2040
1810 IF V>=1000 THEN PRINT #2 USING "####.### ",V;:GOTO 1880
1815 IF V>=100 THEN PRINT #2 USING "0###.### ",V;:GOTO 1880
1820 IF V>=10 THEN PRINT #2 USING "00##.### ",V;:GOTO 1880
1825 IF V>=1 THEN PRINT #2 USING "000#.### ",V;:GOTO 1880
1830 IF V>=0.1 THEN PRINT #2 USING "0000.### ",V;:GOTO 1880
1835 IF V>=0.01 THEN PRINT #2 USING "0000.0## ",V;:GOTO 1880
1840 PRINT #2 USING "0000.00# ",V;:GOTO 1880
1845 IF V<=-1000 THEN PRINT #2 USING "-####.### ",-V;:GOTO 1880
1850 IF V<=-100 THEN PRINT #2 USING "-0###.### ",-V;:GOTO 1880
1855 IF V<=-10 THEN PRINT #2 USING "-00##.### ",-V;:GOTO 1880
1860 IF V<=-1 THEN PRINT #2 USING "-000#.### ",-V;:GOTO 1880
1865 IF V<=-0.1 THEN PRINT #2 USING "-0000.### ",-V;:GOTO 1880
1870 IF V<=-0.01 THEN PRINT #2 USING "-0000.0## ",-V;:GOTO 1880
1875 PRINT #2 USING "-0000.00# ",-V;
1880 RETURN
1885 IF V>999 THEN PRINT #2 USING "#### ",V;:GOTO 1905
1887 IF V=0 THEN PRINT #2,"0000";:GOTO 1905
1890 IF V>99 THEN PRINT #2 USING "0### ",V;:GOTO 1905
1900 IF V<10 THEN PRINT #2 USING "0# ",V;:GOTO 1905
1902 PRINT #2 USING "0### ",90*INT(V/10)+V;
1905 RETURN
1910 IF V>99 THEN PRINT #2 USING "### ",V;:GOTO 1925
1915 IF V>9 THEN PRINT #2 USING "0## ",V;:GOTO 1925
1920 PRINT #2 USING "00# ",V;
1925 RETURN
1930 IF G1=2 GOTO 1955
1935 IF V>=1000 THEN PRINT #2 USING "#### ",V;:GOTO 1975

```

```

1940 IF V>=100 THEN PRINT #2 USING "0### ",V;GOTO 1975
1945 IF V>=10 THEN PRINT #2 USING "00## ",V;GOTO 1975
1950 PRINT #2 USING "000# ",V;GOTO 1975
1955 IF V>=1 THEN PRINT #2 USING "#.### ",V;GOTO 1975
1960 IF V>=0.1 THEN PRINT #2 USING "0.### ",V;GOTO 1975
1965 IF V>=0.01 THEN PRINT #2 USING "0.### ",V;GOTO 1975
1970 PRINT #2 USING "0.00# ",V;
1975 RETURN
2000 IF V>=10 THEN PRINT "THREAD PITCH TOO LARGE" GOTO 2080
2005 IF V>=1 THEN PRINT #2 USING "0#.####",V;GOTO 2035
2010 IF V>=0.1 THEN PRINT #2 USING "00.####",V;GOTO 2035
2015 IF V>=0.01 THEN PRINT #2 USING "00.0####",V;GOTO 2035
2020 IF V>=0.001 THEN PRINT #2 USING "00.00###",V;GOTO 2035
2025 IF V>=0.0001 THEN PRINT #2 USING "00.000##",V;GOTO 2035
2030 PRINT #2 USING "00.0000#",V;
2035 G1=0;RETURN
2040 IF V>=100 THEN PRINT "EXTENDED LEAD TOO LARGE" GOTO 2080
2041 IF V>=10 THEN PRINT #2 USING "0#.####",V;GOTO 2047
2042 IF V>=1 THEN PRINT #2 USING "00#.####",V;GOTO 2047
2043 IF V>=0.1 THEN PRINT #2 USING "000.####",V;GOTO 2047
2044 IF V>=0.01 THEN PRINT #2 USING "000.0###",V;GOTO 2047
2045 IF V>=0.001 THEN PRINT #2 USING "000.00##",V;GOTO 2047
2046 PRINT #2 USING "000.000#",V;
2047 G1=0;RETURN
2050 PRINT #2,"END"
2060 CLOSE 1,2
2070 CHAIN "FORM"
2080 END

```

```

2 OPEN "FODATA" FOR INPUT AS FILE 1%
5 INPUT #1,D$
6         GOTO 10
7         INPUT "PAPER TAPE?",B$
8         IF B$="YES" OR B$="NO" GOTO 10 ELSE GOTO 7
10 GOTO 25
25 PRINT "FORMATTED OUTPUT"
30         INPUT #1,A$
35         IF A$="END" GOTO 60
40 PRINT A$
50         GOTO 30
60         CLOSE 1%,2%
61 GOTO 70
62         IF B$="NO" GOTO 70
70 CHAIN "WADCON"

```

INPUT: WADKIN NC DRILL/MILL

FILE NAME ? PPG97.

HOLE MATRIX

DEVICE TO WHICH UNFORMATTED AND FORMATTED OUTPUT SHOULD GO ? KB

METRIC OR IMPERIAL ? METRIC

X DIMENSION ? 15

Y DIMENSION ? 15

SPINDLE CW OR CCW ? CW

NUMBER OF HOLES TO BE DRILLED BEFORE INSPECTION ? 10

COOLANT ON OR OFF ? OFF

STOP BAR NUMBER ? 1

NUMBER OF ROWS ? 11

DISTANCE BETWEEN ROWS ? 18

HOLE PITCH ? 18

ARE HOLES STAGGERED ? NO

HOW MANY HOLES PER ROW ? 20

DRILLING OR TAPPING ? DRILLING

```

1 OPEN "DATA" FOR INPUT AS FILE 1%
2 INPUT #1,A$
3 CLOSE 1
4 OPEN "FODATA" FOR INPUT AS FILE 2%
5 OPEN "WAD"+MID(A$,4%,3%) FOR OUTPUT AS FILE 1%
6 INPUT #2,A$
7 INPUT #2,A$
8 FOR I=1 TO 70
9 PRINT #1,CHR$(0);$NEXT I
10 INPUT #2%,A$
15 C$=""
20 Y%= LEN(A$)
40 FOR I%=1% TO Y%
50 B$=MID(A$,I%,1%)
80 IF B$="E" GOTO 305
90 IF B$=" " GOTO 292
95 IF B$="." GOTO 292
100 IF B$="F" GOTO 200
105 IF B$="G" GOTO 205
110 IF B$="M" GOTO 210
115 IF B$="N" GOTO 215
125 IF B$="S" GOTO 225
130 IF B$="X" GOTO 230
135 IF B$="Y" GOTO 235
140 IF B$="1" GOTO 240
145 IF B$="2" GOTO 245
150 IF B$="3" GOTO 250
155 IF B$="4" GOTO 255
160 IF B$="5" GOTO 260
165 IF B$="6" GOTO 265
170 IF B$="7" GOTO 270
175 IF B$="8" GOTO 275
180 IF B$="9" GOTO 280
185 IF B$="0" GOTO 285
187 IF B$="-" GOTO 287
200 C%=70;$GOTO 290
205 C%=71;$GOTO 290
210 C%=77;$GOTO 290
215 C%=78;$GOTO 290
225 C%=83;$GOTO 290
230 C%=88;$GOTO 290
235 C%=89;$GOTO 290
240 C%=49;$GOTO 290
245 C%=50;$GOTO 290
250 C%=51;$GOTO 290
255 C%=52;$GOTO 290
260 C%=53;$GOTO 290
265 C%=54;$GOTO 290
270 C%=55;$GOTO 290
275 C%=56;$GOTO 290
280 C%=57;$GOTO 290
285 C%=48;$GOTO 290
287 C%=45;$GOTO 290
290 C$=C$+CHR$(C%)
292 NEXT I%
293 D$=CHR$(13)
294 E$=CHR$(10)
297 PRINT #1, C$;D$;E$
300 GOTO 10
305 FOR I=1 TO 70
306 PRINT #1,CHR$(0);$NEXT I
307 CLOSE 1,2
310 END

```



N116	X	69.00				
N118	X	87.00				
N120	X	105.00				
N122	X	123.00				
N124	X	141.00				
N126	X	159.00				
N128	X	177.00	Y	51.00		
N130	G80					M00
N132						M06
N134						M03M00
N136	G81	X	195.00	Y	51.00	S01
N138		X	213.00			
N140		X	231.00			
N142		X	249.00			
N144		X	267.00			
N146		X	285.00			
N148		X	303.00			
N150		X	321.00			
N152		X	339.00			
N154		X	357.00	Y	51.00	
N156	G80					M00
N158						M06
N160						M03M00
N162	G81	X	15.00	Y	69.00	S01
N164		X	33.00			
N166		X	51.00			
N168		X	69.00			
N170		X	87.00			
N172		X	105.00			
N174		X	123.00			
N176		X	141.00			
N178		X	159.00			
N180		X	177.00	Y	69.00	
N182	G80					M00
N184						M06
N186						M03M00
N188	G81	X	195.00	Y	69.00	S01
N190		X	213.00			
N192		X	231.00			
N194		X	249.00			
N196		X	267.00			
N198		X	285.00			
N200		X	303.00			
N202		X	321.00			
N204		X	339.00			
N206		X	357.00	Y	69.00	
N208	G80					M00
N210						M06
N212						M03M00
N214	G81	X	15.00	Y	87.00	S01
N216		X	33.00			
N218		X	51.00			
N220		X	69.00			
N222		X	87.00			
N224		X	105.00			
N226		X	123.00			
N228		X	141.00			
N230		X	159.00			
N232		X	177.00	Y	87.00	
N234	G80					M00



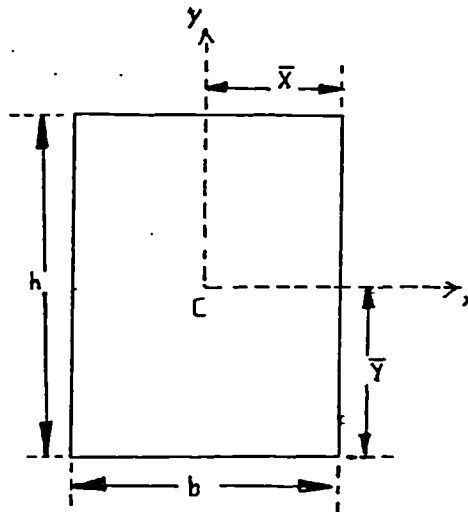
N356	X	303.00			
N358	X	321.00			
N360	X	339.00			
N362	X	357.00	Y	123.00	
N364					M00
N366					M06
N368					M03M00
N370	G01	X	15.00	Y	141.00 S01
N372		X	33.00		
N374		X	51.00		
N376		X	69.00		
N378		X	87.00		
N380		X	105.00		
N382		X	123.00		
N384		X	141.00		
N386		X	159.00		
N388		X	177.00	Y	141.00
N390	G01				M00
N392					M06
N394					M03M00
N396	G01	X	195.00	Y	141.00 S01
N398		X	213.00		
N400		X	231.00		
N402		X	249.00		
N404		X	267.00		
N406		X	285.00		
N408		X	303.00		
N410		X	321.00		
N412		X	339.00		
N414		X	357.00	Y	141.00
N416	G01				M00
N418					M06
N420					M03M00
N422	G01	X	15.00	Y	159.00 S01
N424		X	33.00		
N426		X	51.00		
N428		X	69.00		
N430		X	87.00		
N432		X	105.00		
N434		X	123.00		
N436		X	141.00		
N438		X	159.00		
N440		X	177.00	Y	159.00
N442	G01				M00
N444					M06
N446					M03M00
N448	G01	X	195.00	Y	159.00 S01
N450		X	213.00		
N452		X	231.00		
N454		X	249.00		
N456		X	267.00		
N458		X	285.00		
N460		X	303.00		
N462		X	321.00		
N464		X	339.00		
N466		X	357.00	Y	159.00
N468	G01				M00
N470					M06
N472					M03M00
N474	G01	X	15.00	Y	177.00 S01

N476	X	33.00				
N478	X	51.00				
N480	X	69.00				
N482	X	87.00				
N484	X	105.00				
N486	X	123.00				
N488	X	141.00				
N490	X	159.00				
N492	X	177.00	Y	177.00		
N494	G80					M00
N496						M06
N498						M03M00
N500	G81	X	195.00	Y	177.00	S01
N502		X	213.00			
N504		X	231.00			
N506		X	249.00			
N508		X	267.00			
N510		X	285.00			
N512		X	303.00			
N514		X	321.00			
N516		X	339.00			
N518		X	357.00	Y	177.00	
N520	G80					M00
N522						M06
N524						M03M00
N526	G81	X	15.00	Y	195.00	S01
N528		X	33.00			
N530		X	51.00			
N532		X	69.00			
N534		X	87.00			
N536		X	105.00			
N538		X	123.00			
N540		X	141.00			
N542		X	159.00			
N544		X	177.00	Y	195.00	
N546	G80					M00
N548						M06
N550						M03M00
N552	G81	X	195.00	Y	195.00	S01
N554		X	213.00			
N556		X	231.00			
N558		X	249.00			
N560		X	267.00			
N562		X	285.00			
N564		X	303.00			
N566		X	321.00			
N568		X	339.00			
N570		X	357.00	Y	195.00	
N572	G80					M00
N574						M06
N576	G80					M00
N578	X	0.00	Y	0.00	F 1000.00	M06
END						

## Appendix 'D'

### CALCULATION OF POLAR MOMENT OF INERTIA OF KLENK, GANDTRACK, PRECISION AND SOLID CARBIDE DRILLS

The polar moment of inertia,  $I_p$  is the summation of the moment of inertia about the X-axis and Y-axis. The moment of inertia of Klenk, Gandtrack, Precision and Solid Carbide drills was calculated by dividing the drill cross section into a number of rectangles and triangles. A good approximation has been made by careful selection of the best fit triangles and rectangles to the drill curves. The moment of inertia of a triangle around its axis on the centroid (C) as shown below is given by the following relation



$$\bar{x} = b/2$$

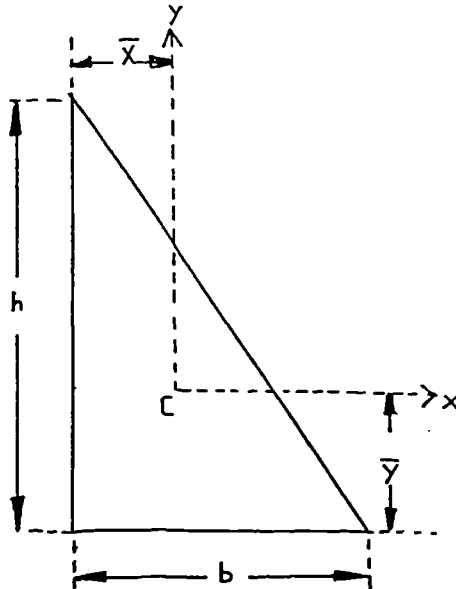
$$\bar{y} = h/2$$

$$\text{Area} = A = b h$$

$$I_x = \text{Moment of Inertia around X-axis} = (b h^3)/12$$

$$I_y = \text{Moment of Inertia around Y-axis} = (h b^3)/12$$

The moment of inertia of a right triangle around the x-axis ( $I_x$ ) and the y-axis ( $I_y$ ) passing through the centroid (C) is given by;



$$\bar{x} = b/3$$

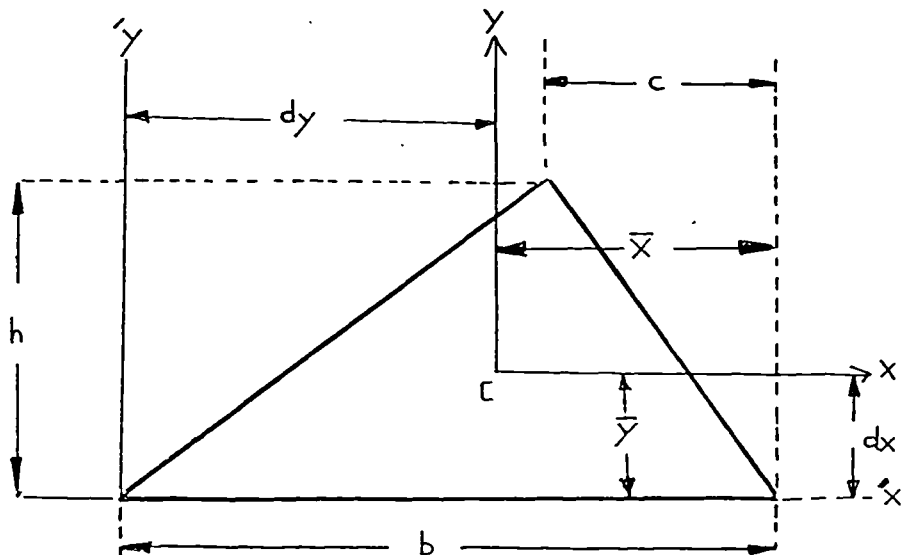
$$\bar{y} = h/3$$

$$\text{Area} = A = (b \times h)/2$$

$$I_x = (b h^3)/36$$

$$I_y = (h b^3)/36$$

The moment of inertia of any triangle around its axes passing through the centroid (C) is given by



$$x = (b + c)/3$$

$$y = h/3$$

$$A = (b \times h)/2$$

$$I_x = (b \times h^3)/36$$

$$I_y = \{b \times h \times (b^2 - b c + c^2)\} / 36$$

The moment of inertia around any other axis ( $I_{x'}$ ) can be calculated by

$$I_{x'} = I_x + A (d_x)^2$$

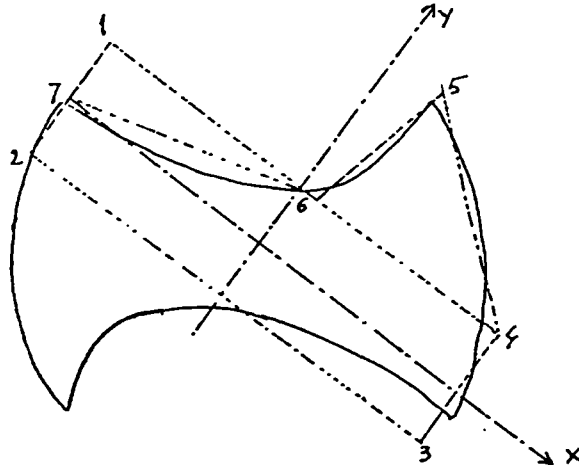
where  $d_x$  is the perpendicular distance between the area centroid from the  $x'$ - axis.

Similarly

$$I_{y'} = I_y + A (d_y)^2$$

where  $d_y$  is the perpendicular distance between the area centroid from the  $y'$ -axis.

POLAR MOMENT OF INERTIA OF THE GANDTRACK DRILL



$$I_p = \text{Polar Moment of Inertia of drill} = I_x + I_y$$

$$I_x = \text{Moment of Inertia around X-axis}$$

$$I_y = \text{Moment of Inertia around Y-axis}$$

$$(I_x)_{1234} = \text{Moment of Inertia of rectangle 1,2,3,4 around x-axis}$$

$$(I_x)_{456} = \text{Moment of Inertia of rectangle 4,5,6 around x-axis}$$

$$(I_x)_{167} = \text{Moment of Inertia of rectangle 1,6,7 around x-axis}$$

$$(I_y)_{1234} = \text{Moment of Inertia of rectangle 1,2,3,4 around Y-axis}$$

$$(I_y)_{456} = \text{Moment of Inertia of rectangle 4,5,6 around Y-axis}$$

$$(I_y)_{167} = \text{Moment of Inertia of rectangle 1,6,7 around Y-axis}$$

$$I_x = (I_x)_{1234} + 2(I_x)_{456} - 2(I_x)_{167}$$

$$I_x = 2.46 + 18.31 + 0.92 = 19.85$$

$$I_y = (I_y)_{1234} + 2(I_y)_{456} - 2(I_y)_{167}$$

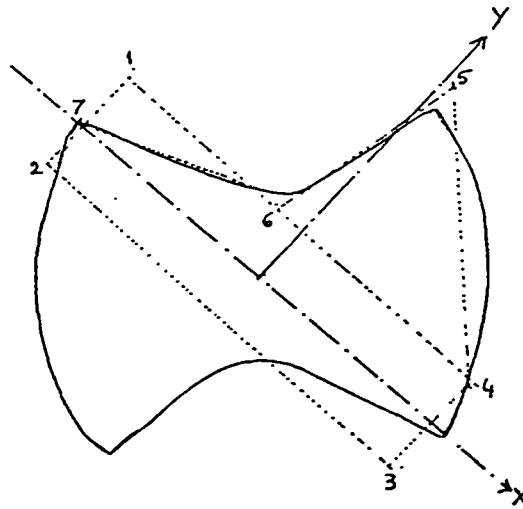
$$I_y = 30.6 + 10.98 - 13.5 = 28.08$$

$$I_p = I_x + I_y = 19.85 + 28.08 = 47.93 \text{ mm}^4$$

Polar Moment of Inertia of the Gandtrack Drill = 47.93 mm<sup>4</sup>

Minimum Moment of Inertia of the Gandtrack Drill = 19.85 mm<sup>4</sup>

## POLAR MOMENT OF INERTIA OF THE PRECISION DRILL



$$\begin{aligned} I_x &= (I_x)_{1234} + 2(I_x)_{456} - 2(I_x)_{167} \\ &= 1.68 + 27.24 + 0.91 = 28.01 \end{aligned}$$

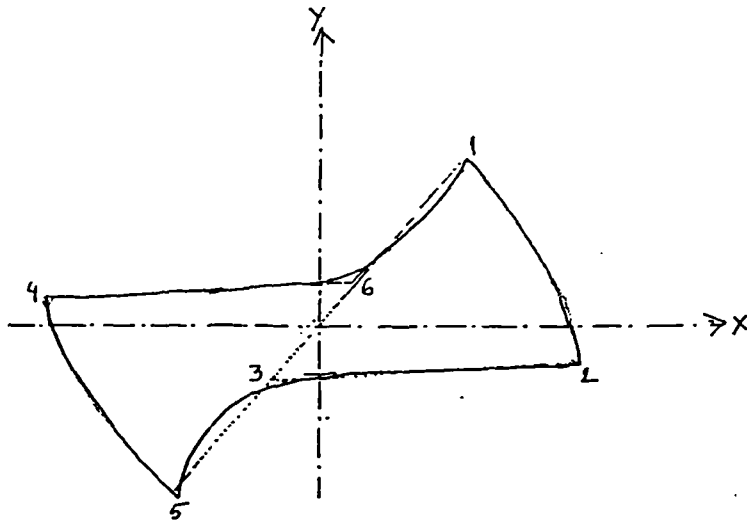
$$\begin{aligned} I_y &= (I_x)_{1234} + 2(I_x)_{456} - 2(I_x)_{167} \\ &= 27 + 11.9 + 13.74 = 25.16 \end{aligned}$$

$$I_p = I_x + I_y = 28.01 + 25.16 = 53.17$$

Polar moment of inertia of the Precision drill = 53.17 mm<sup>4</sup>

Minimum Moment of Inertia of the Precision drill = 25.16 mm<sup>4</sup>

**POLAR MOMENT OF INERTIA OF THE KLENK DRILL**



$$I_x = (I_x)_{123} + (I_x)_{456}$$

As  $(I_x)_{123} = (I_x)_{456}$

$$I_x = 2(I_x)$$

$$I_y = 4.37$$

$$I_y = (I_y)_{123} + (I_y)_{456}$$

As  $(I_y)_{123} = (I_y)_{456}$

$$I_y = 2(I_y)$$

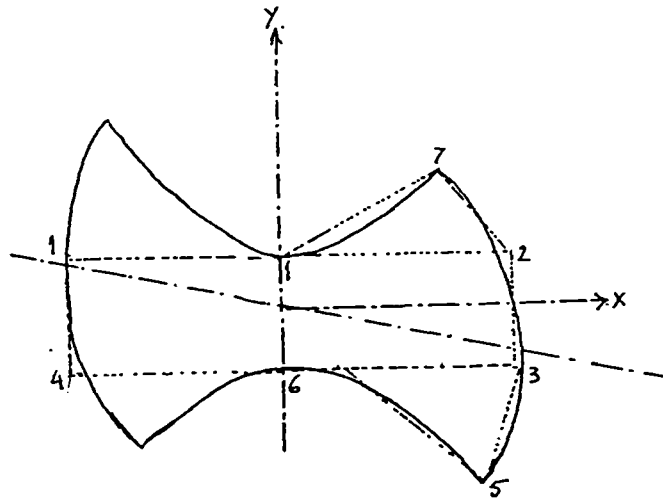
$$I_y = 32.29$$

$$I_p = I_x + I_y = 4.37 + 32.29 = 36.66$$

Polar moment of inertia of the Klenk drill =  $36.66 \text{ mm}^4$

Minimum Moment of Inertia of the Klenk drill =  $4.37 \text{ mm}^4$

## POLAR MOMENT OF INERTIA OF THE SOLID CARBIDE DRILLS



$$I_x = (I_x)_{1234} + 2(I_x)_{127} + 2(I_x)_{356}$$

$$I_x = 1.63 + 3.61 + 7.72 = 12.96$$

$$I_y = (I_y)_{1234} + 2(I_y)_{127} + 2(I_y)_{356}$$

$$I_y = 24.39 + 9.598 + 17.319 = 51.31$$

$$I_p = I_x + I_y = 12.96 + 51.31 = 64.48 \text{ mm}^4$$

Polar Moment of Inertia of the Solid Carbide Drill= 64.48 mm<sup>4</sup>

Minimum Moment of Inertia of the Solid Carbide Drill= 12.96 mm<sup>4</sup>

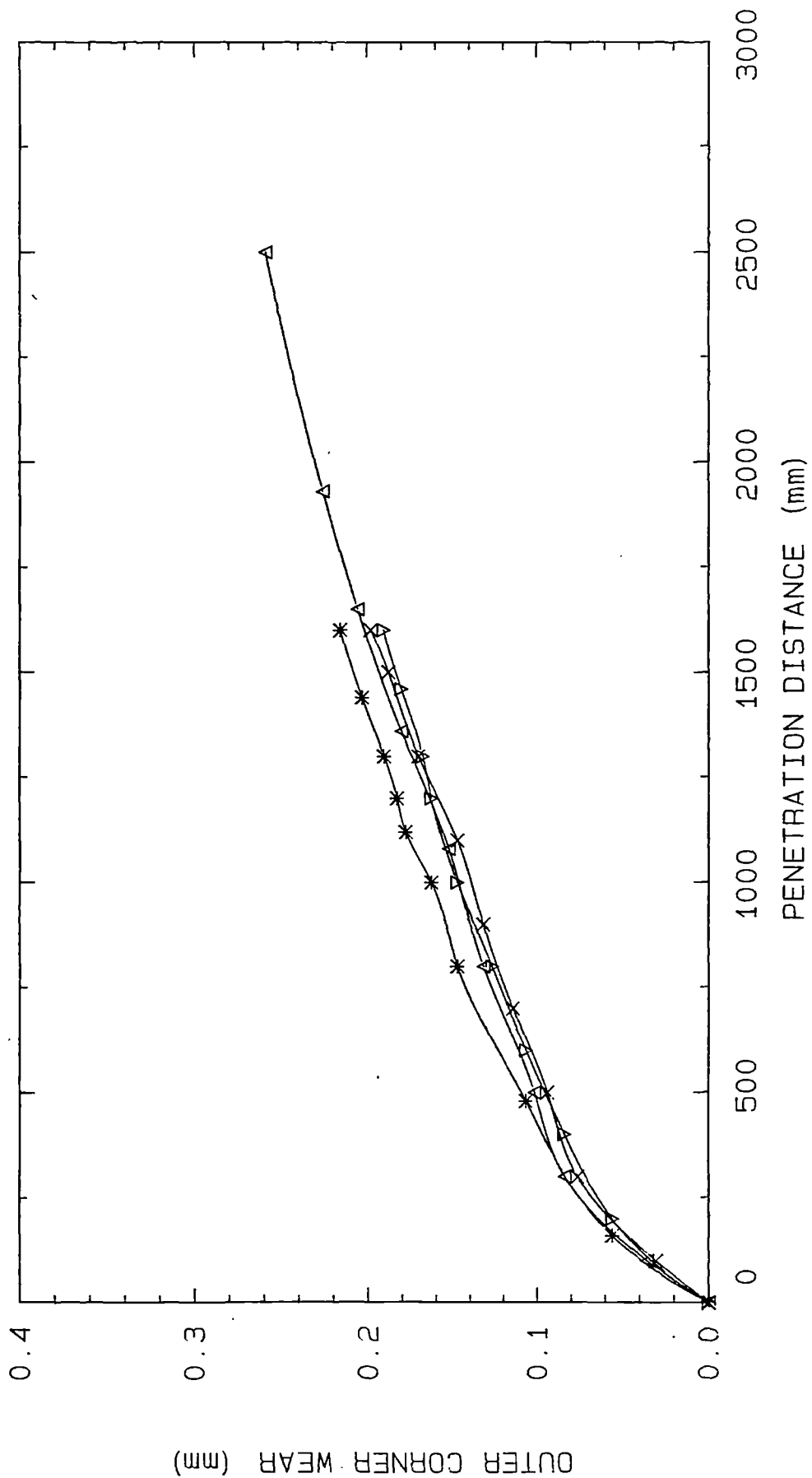
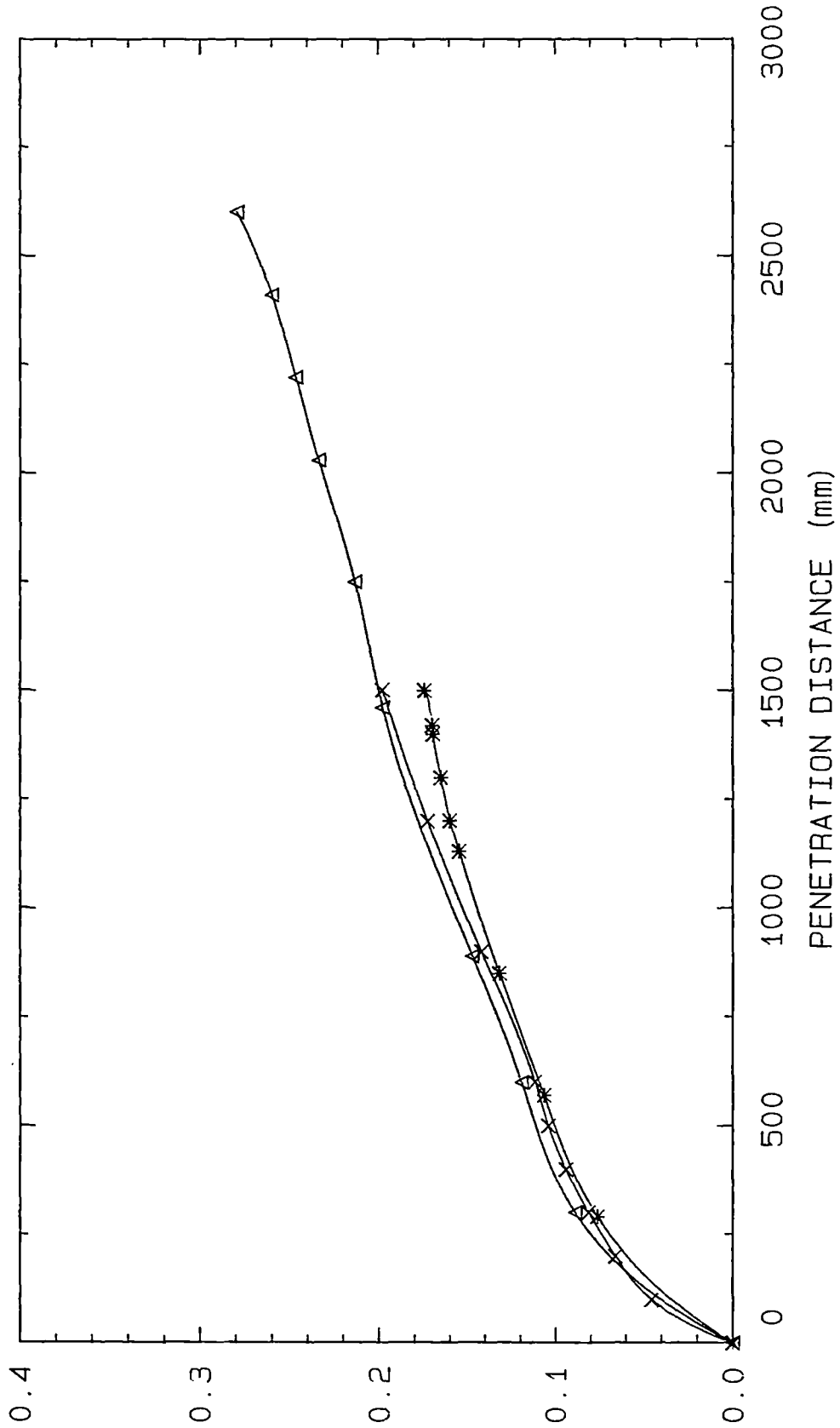


Fig. (1): The outer corner wear of the Klenk-1 drill in the first stage of drill testing;

New Drill: x, Regrind 1: Δ, Regrind 2: \*, Regrind 3: ∇.



OUTER CORNER WEAR (mm)

Fig. (2): The outer corner wear of the Klenk-2 drill in the first stage of drill testing;

New Drill: x, Regrind 1: Δ, Regrind 2: \*.

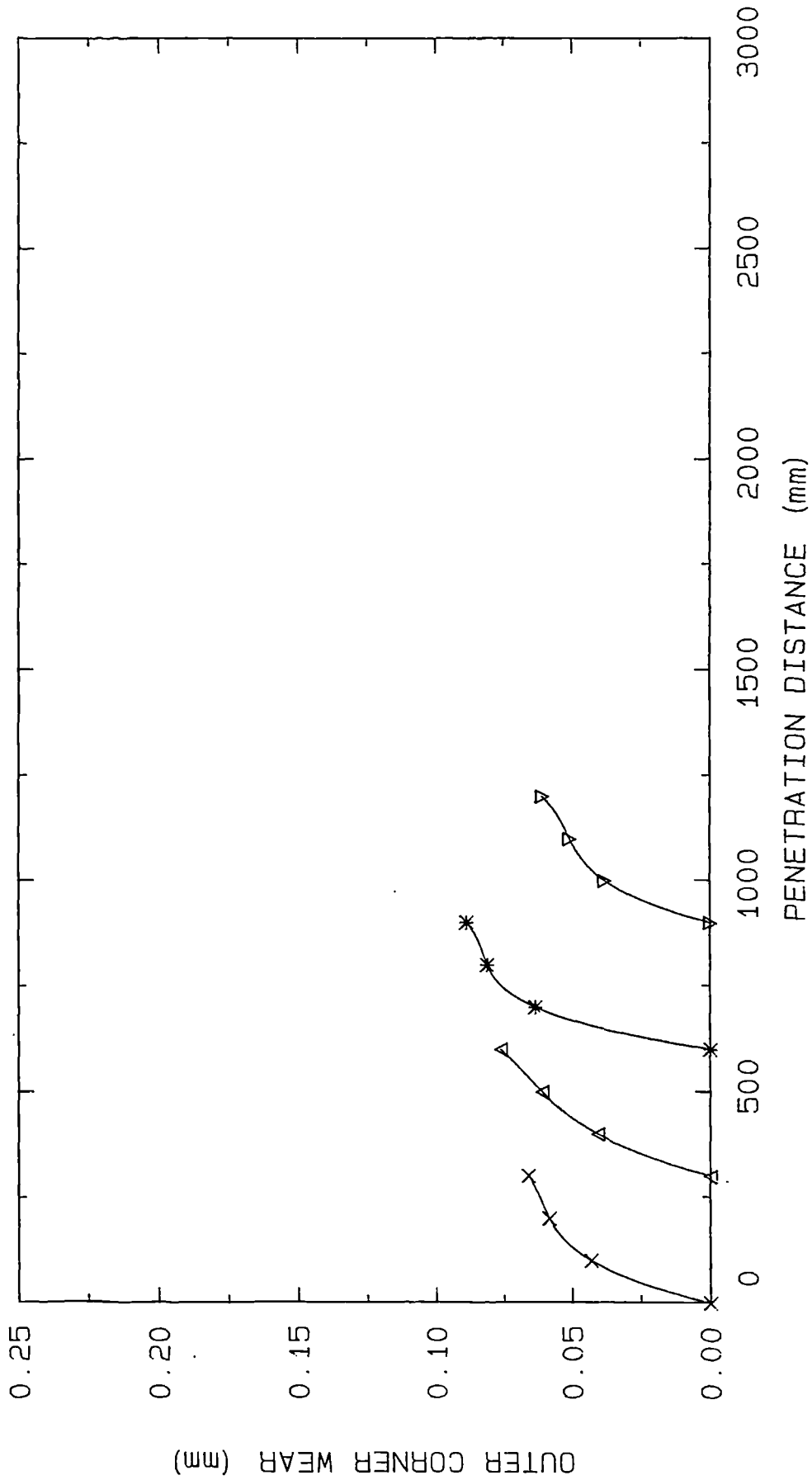


Fig. (3): The outer corner wear of the Klenk-3 drill in the first stage of drill testing;

New Drill: x, Regrind 1: Δ, Regrind 2: \*, Regrind 3: ▽.

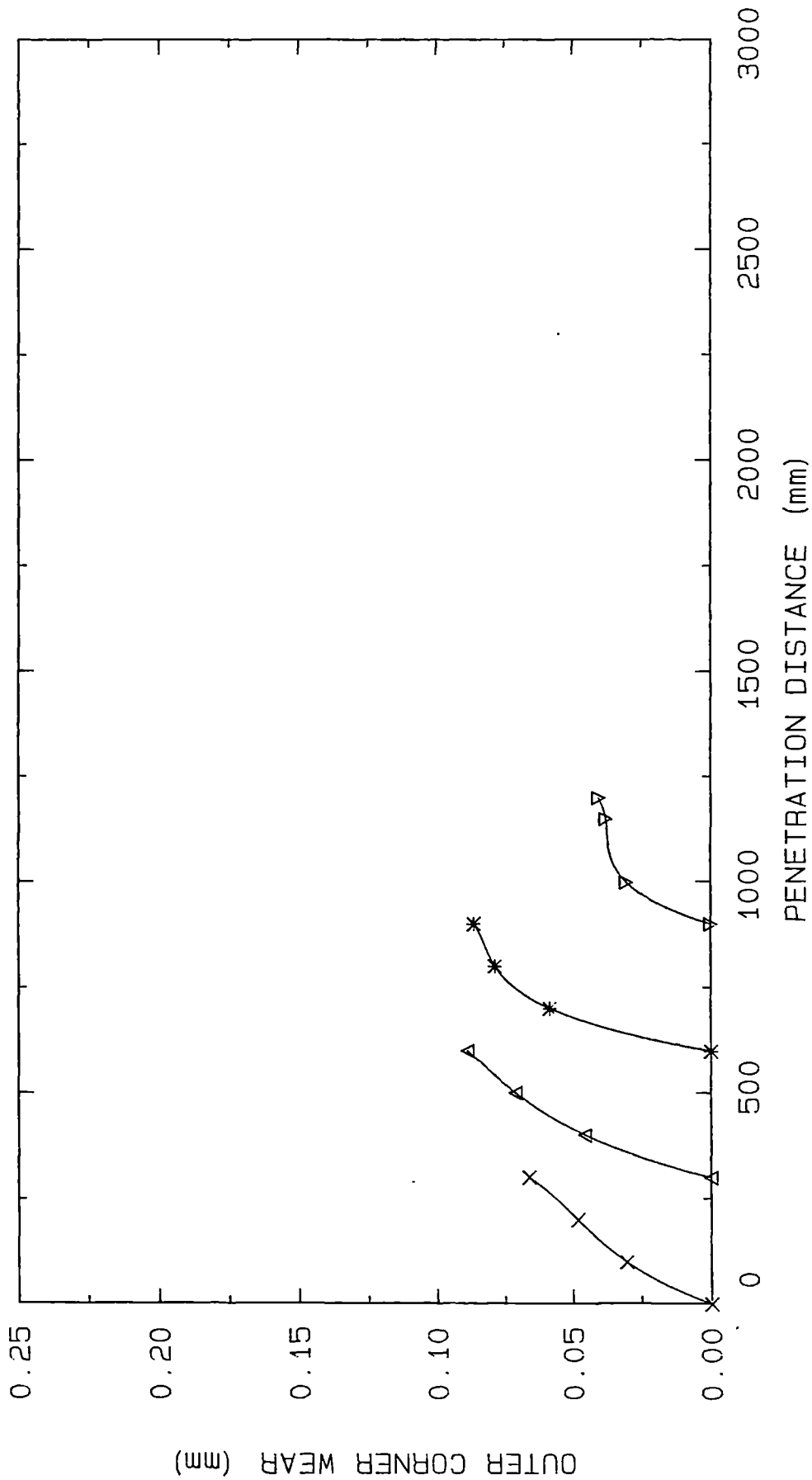


Fig. (4): The outer corner wear of the Klenk-4 drill in the first stage of drill testing;

New Drill: x, Regrind 1: Δ, Regrind 2: \*, Regrind 3: ▽.

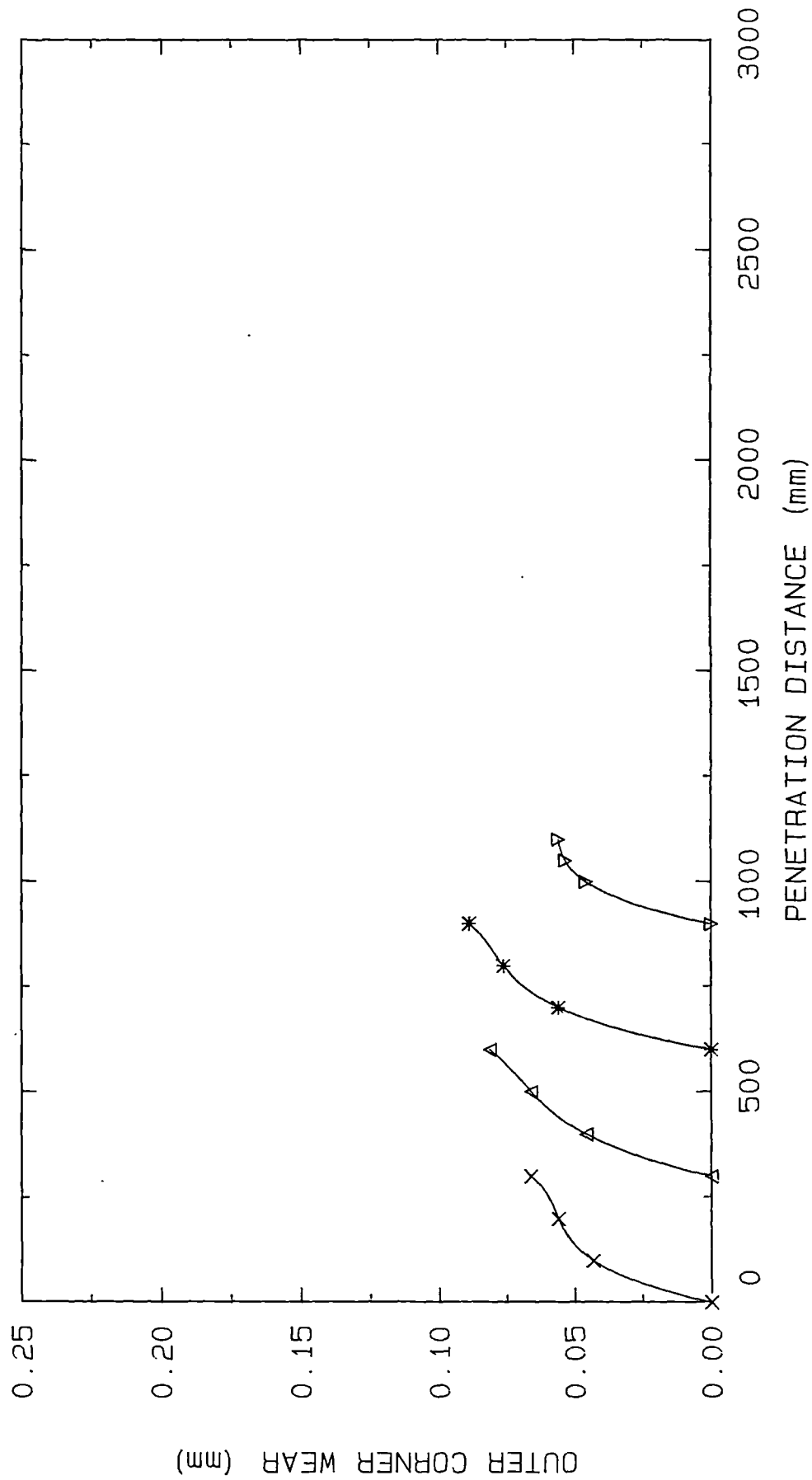


Fig. (5): The outer corner wear of the Klenk-5 drill in the first stage of drill testing;

New Drill: x, Regrind 1: Δ, Regrind 2: \*, Regrind 3: ▽.

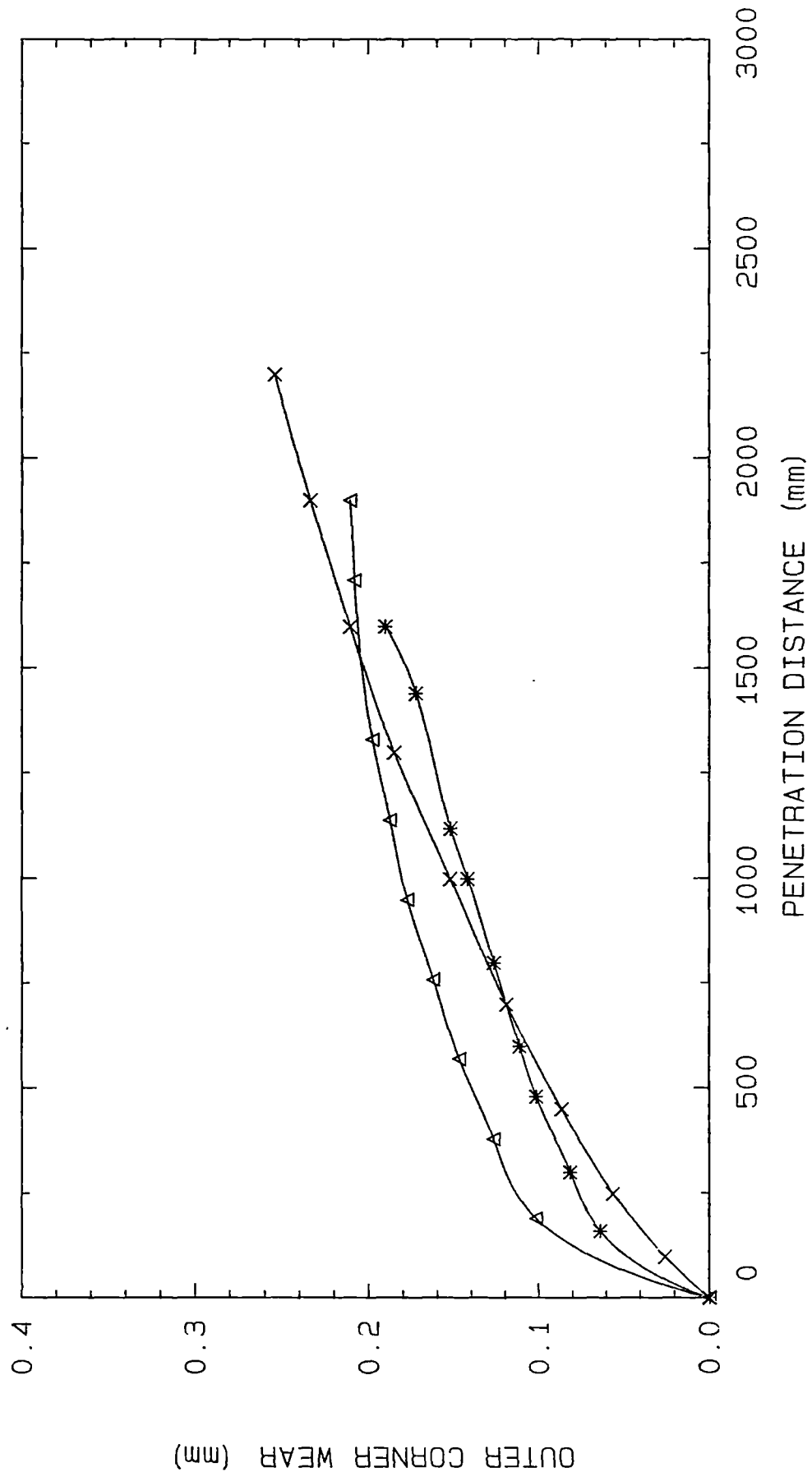


Fig. (6): The outer corner wear of the Gandtrack-1 drill in the first stage of drill testing;

New Drill: x, Regrind 1: Δ, Regrind 2: \*.

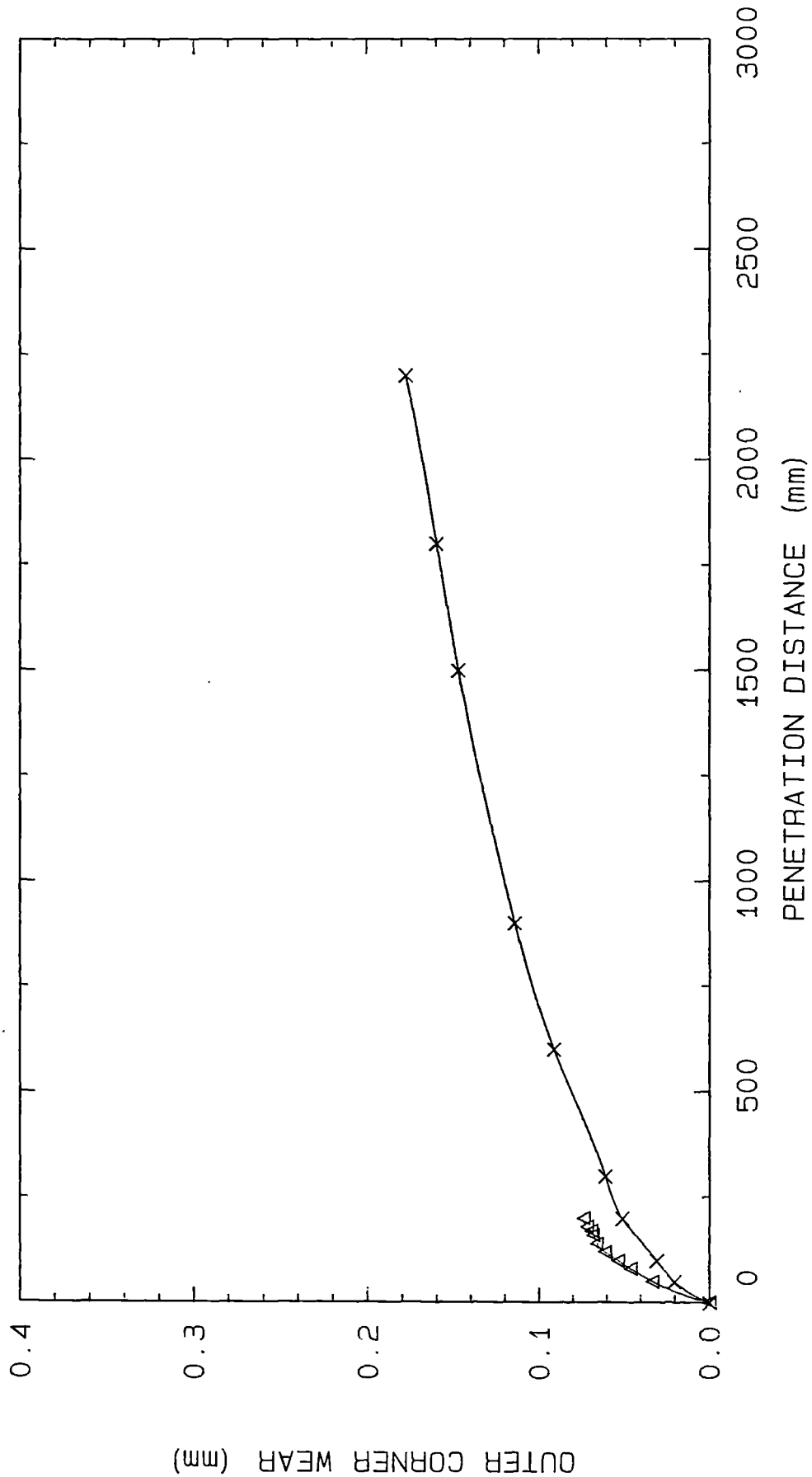


Fig. (7): The outer corner wear of the Gandtrack-2 drill in the first stage of drill testing;

New Drill: x, Regrind 1:

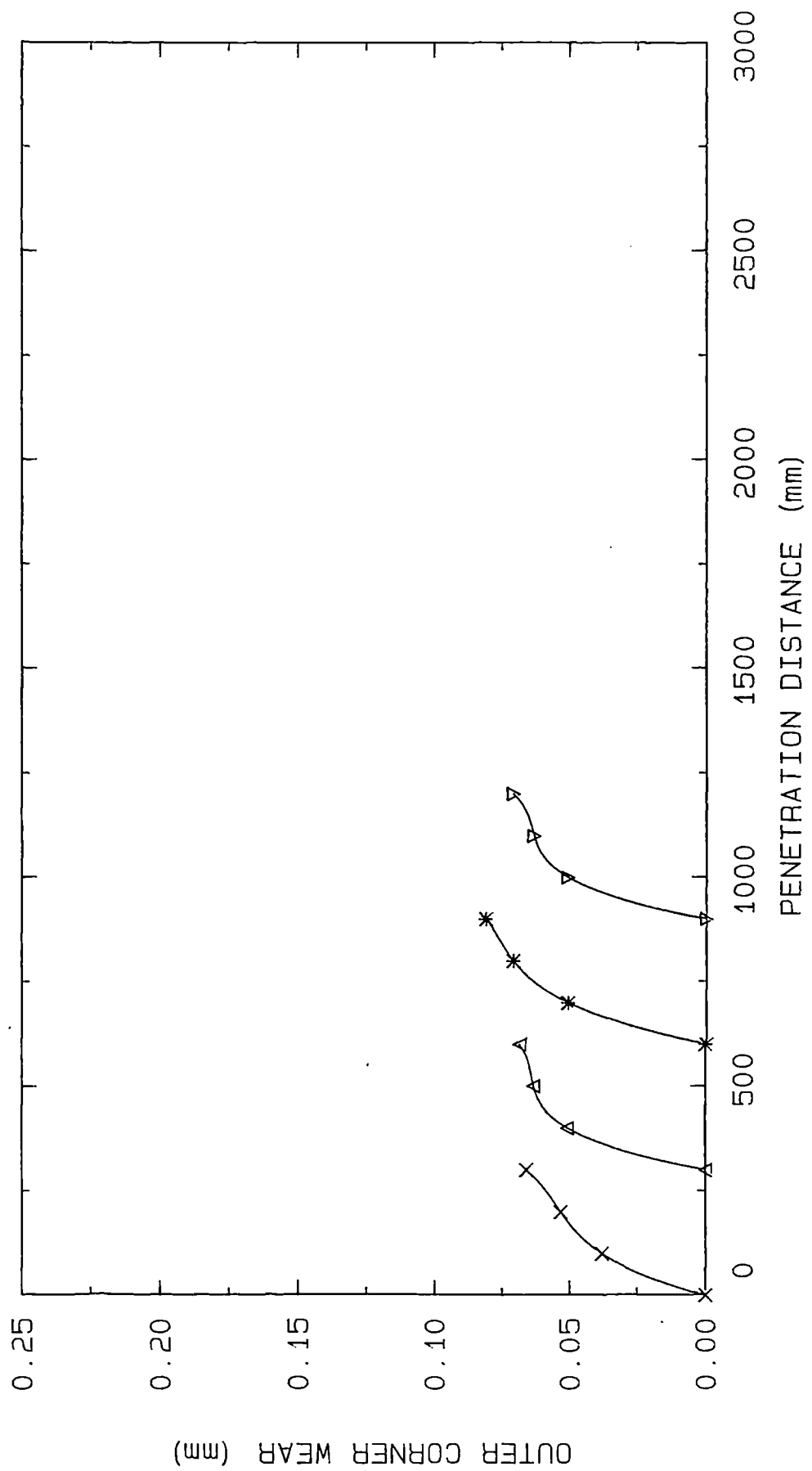


Fig. (8): The outer corner wear of the Gandtrack-3 drill in the first stage of drill testing;

New Drill: x, Regrind 1: Δ, Regrind 2: \*, Regrind 3: ▽.

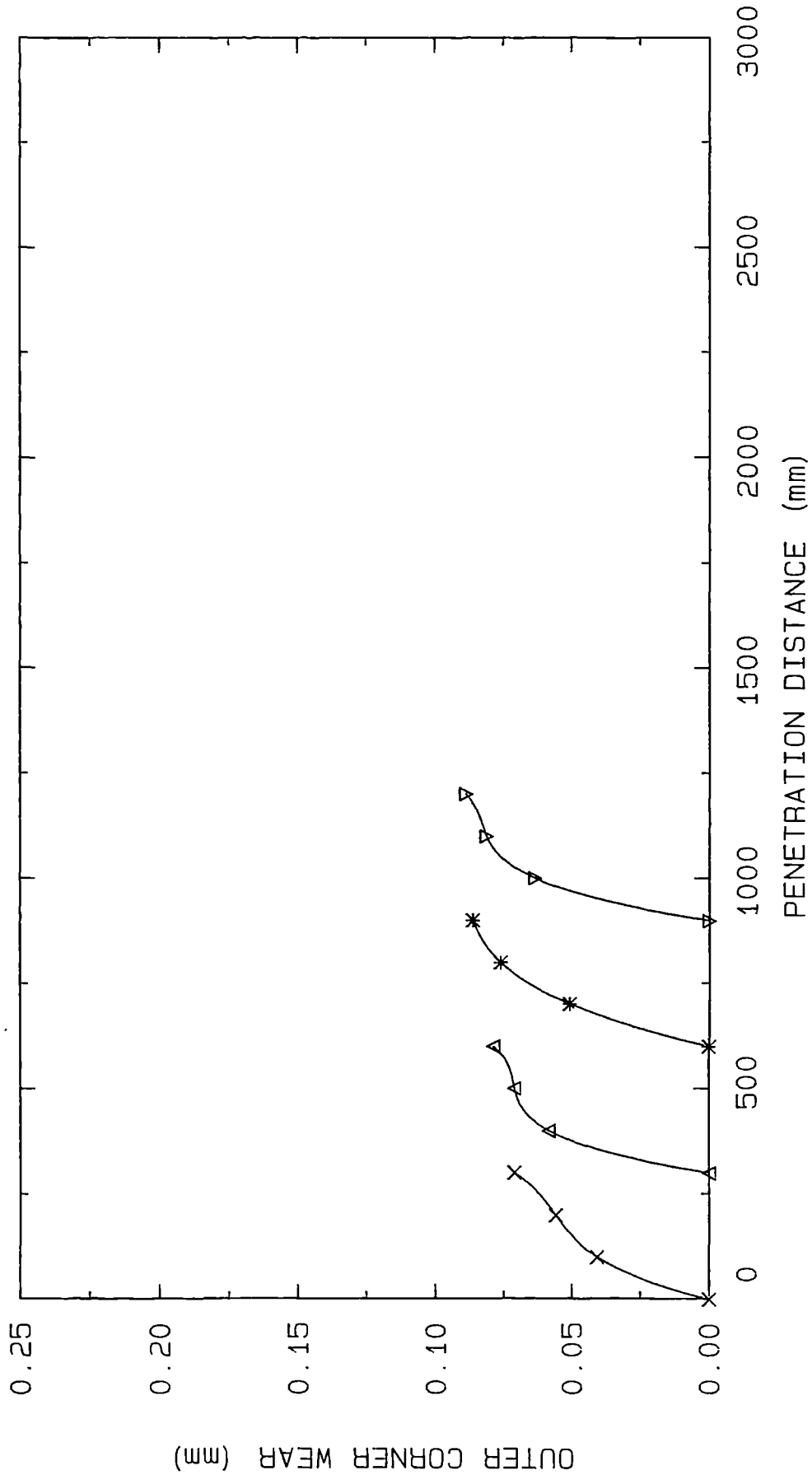


Fig. (9): The outer corner wear of the Gandtrack-4 drill in the first stage of drill testing;

New Drill: x, Regrind 1: Δ, Regrind 2: \*, Regrind 3: ▽.

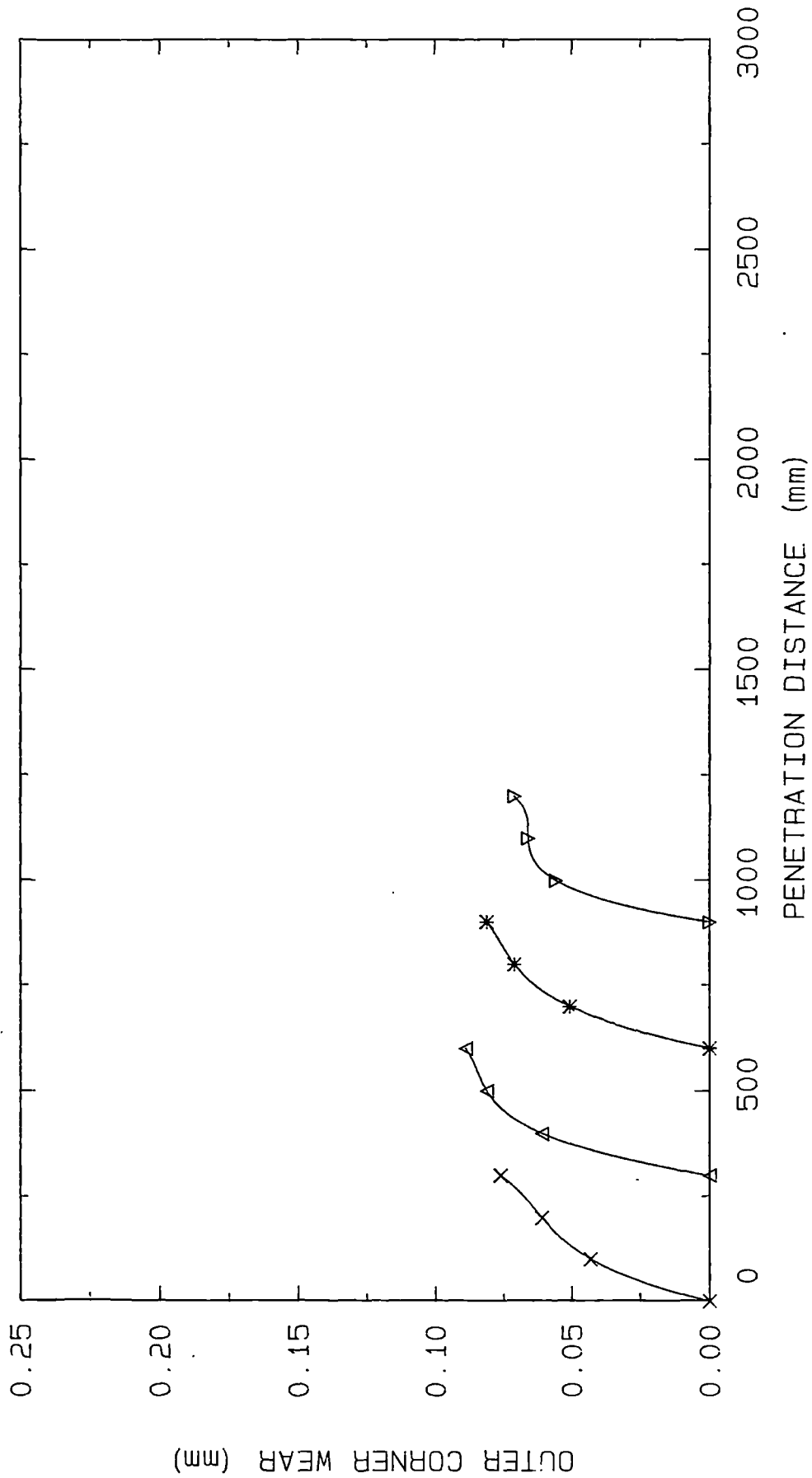
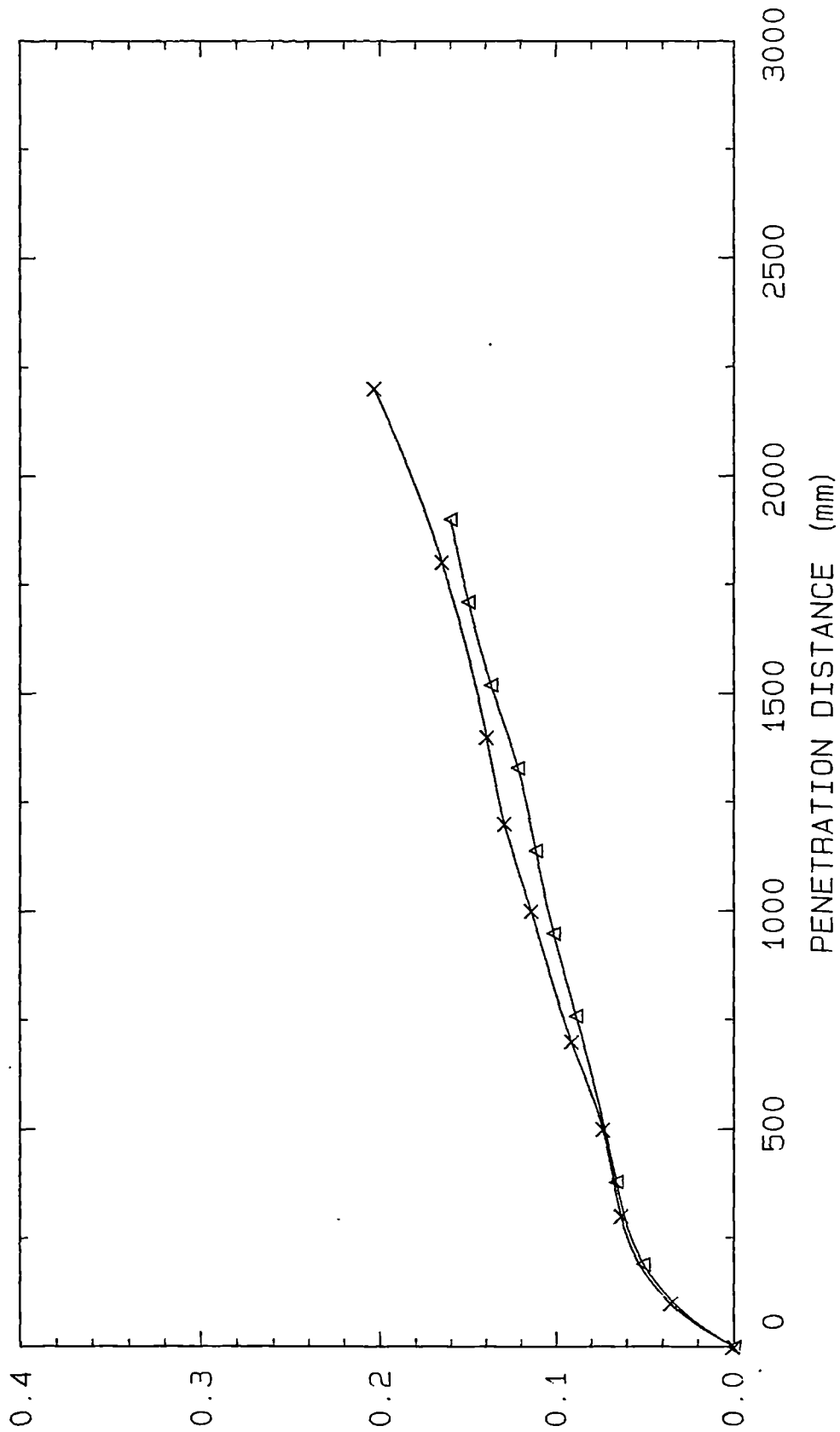


Fig. (10): The outer corner wear of the Gandtrack-5 drill in the first stage of drill testing;

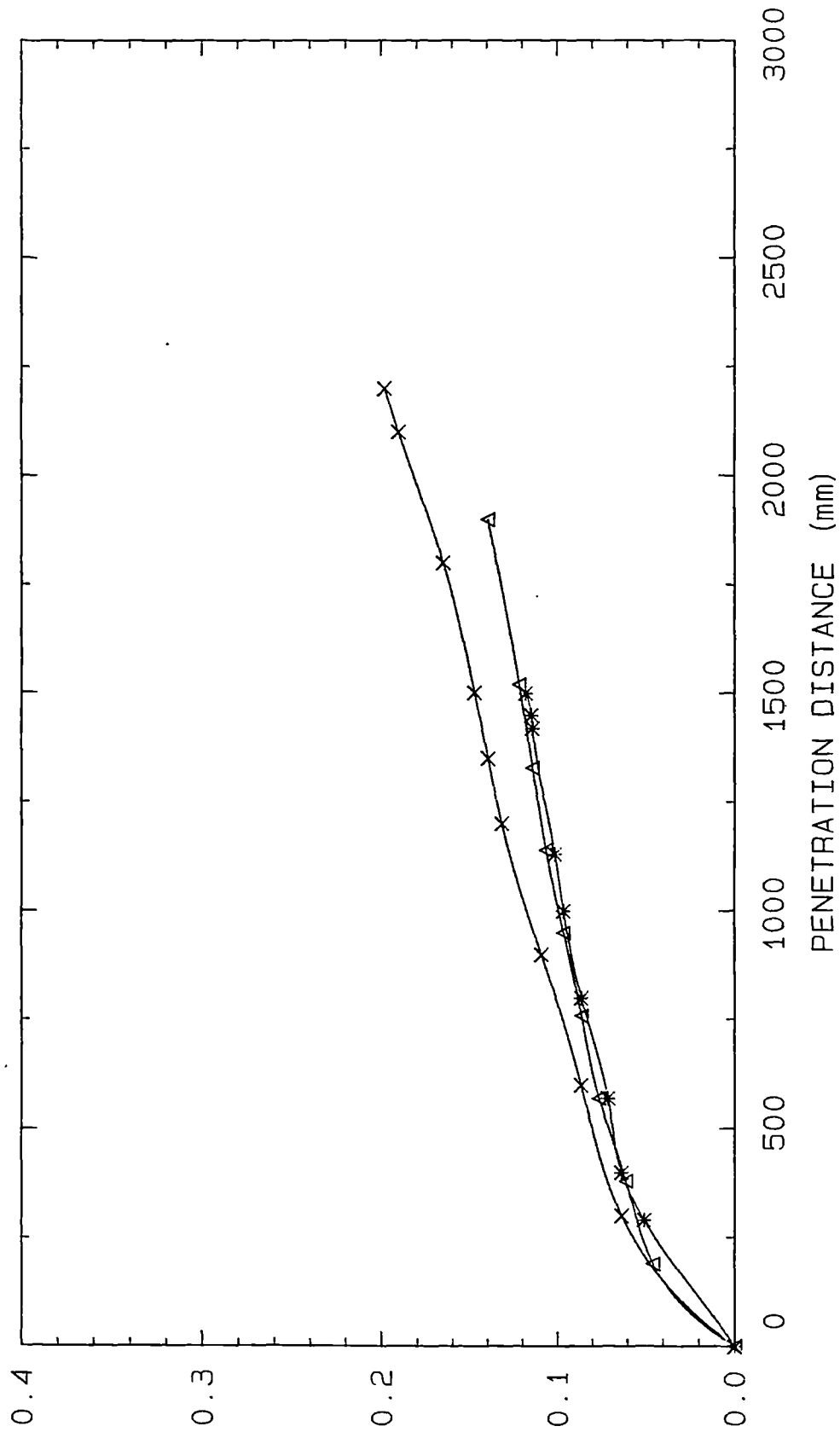
New Drill: x, Regrind 1: Δ, Regrind 2: \*, Regrind 3: ▽.



OUTER CORNER WEAR (mm)

Fig. (11): The outer corner wear of the Precision-1 drill in the first stage of drill testing;

New Drill: x, Regrind 1: Δ.



OUTER CORNER WEAR (mm)

Fig. (12): The outer corner wear of the Precision-2 drill in the first stage of drill testing;

New Drill: x, Regrind 1: Δ, Regrind 2: \*.

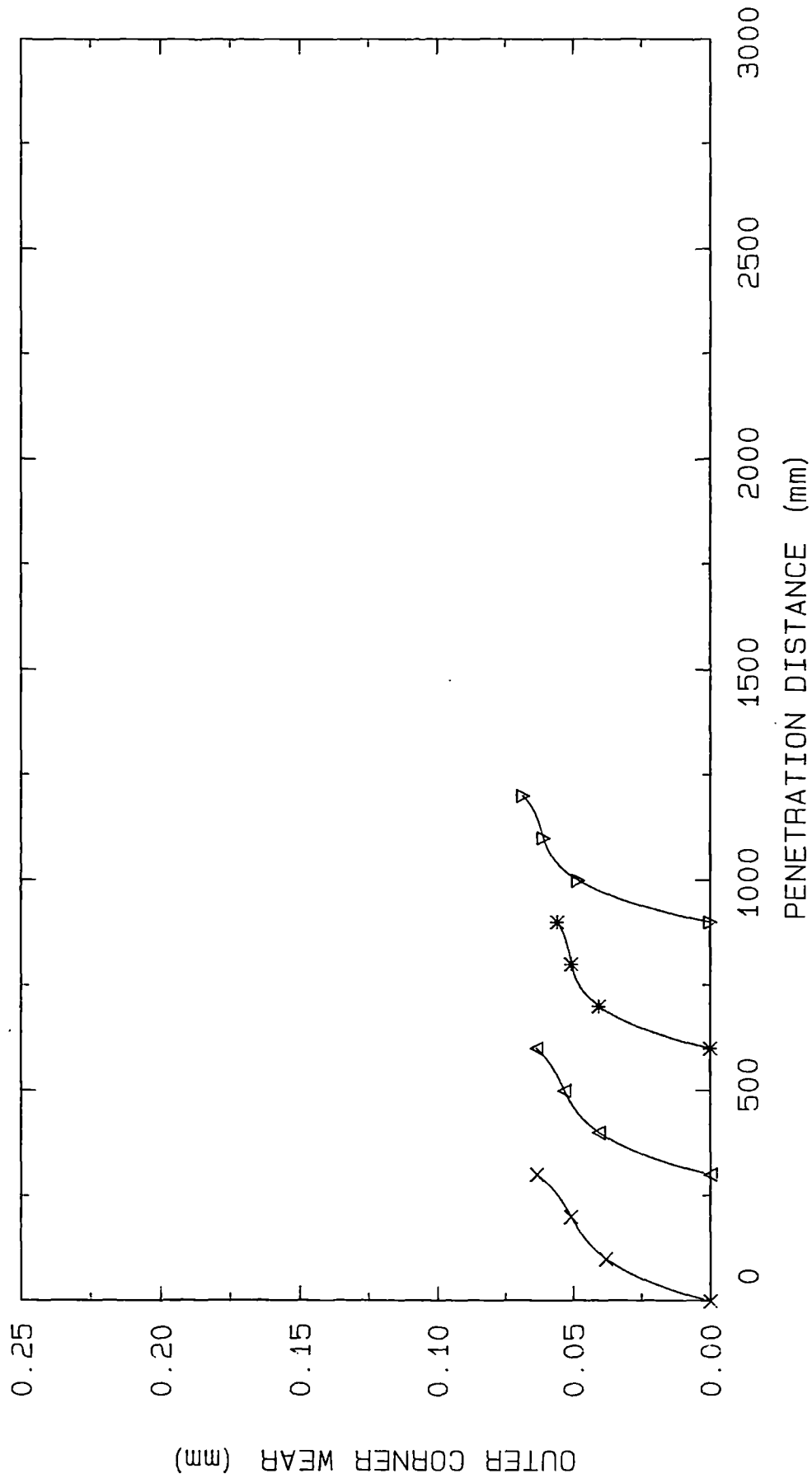


Fig. (13): The outer corner wear of the Precision-3 drill in the first stage of drill testing;

New Drill: x, Regrind 1: Δ, Regrind 2: \*, Regrind 3: ▽.

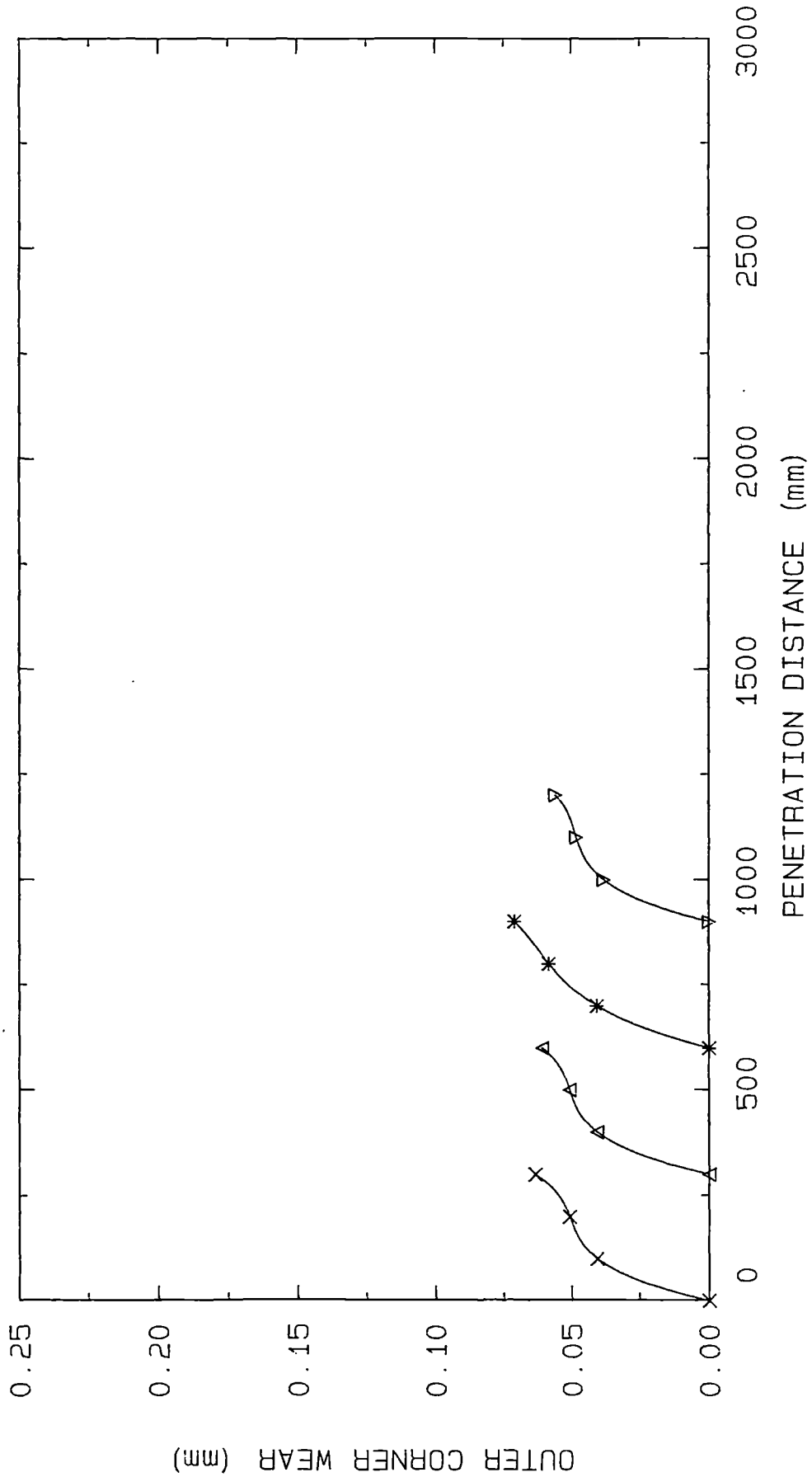


Fig. (14): The outer corner wear of the Precision-4 drill in the first stage of drill testing;

New Drill: x , Regrind 1: Δ, Regrind 2: \*, Regrind 3: ▽.

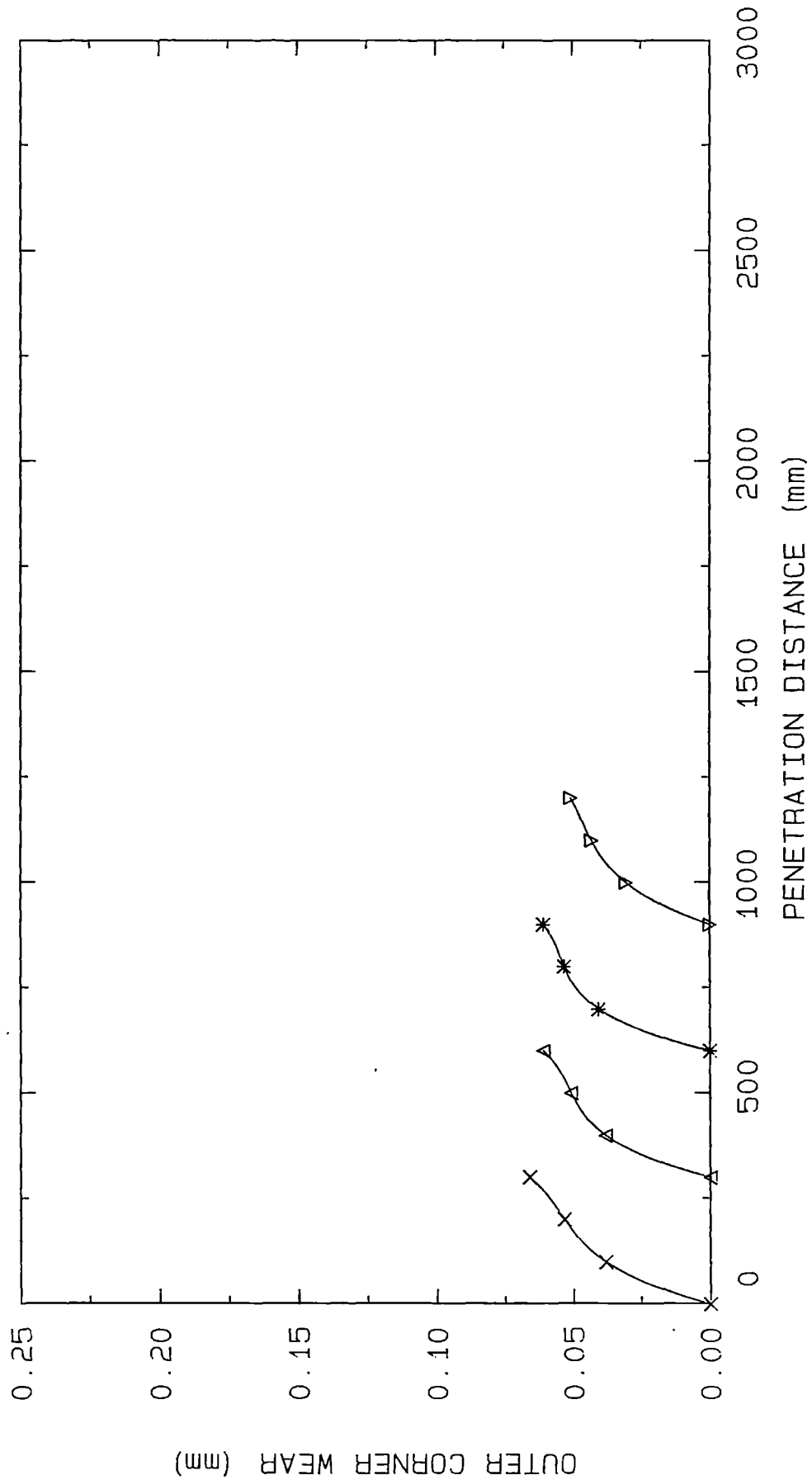


Fig. (15): The outer corner wear of the Precision-5 drill in the first stage of the drill testing;

New Drill: x, Regrind 1: Δ, Regrind 2: \*, Regrind 3: ▽.

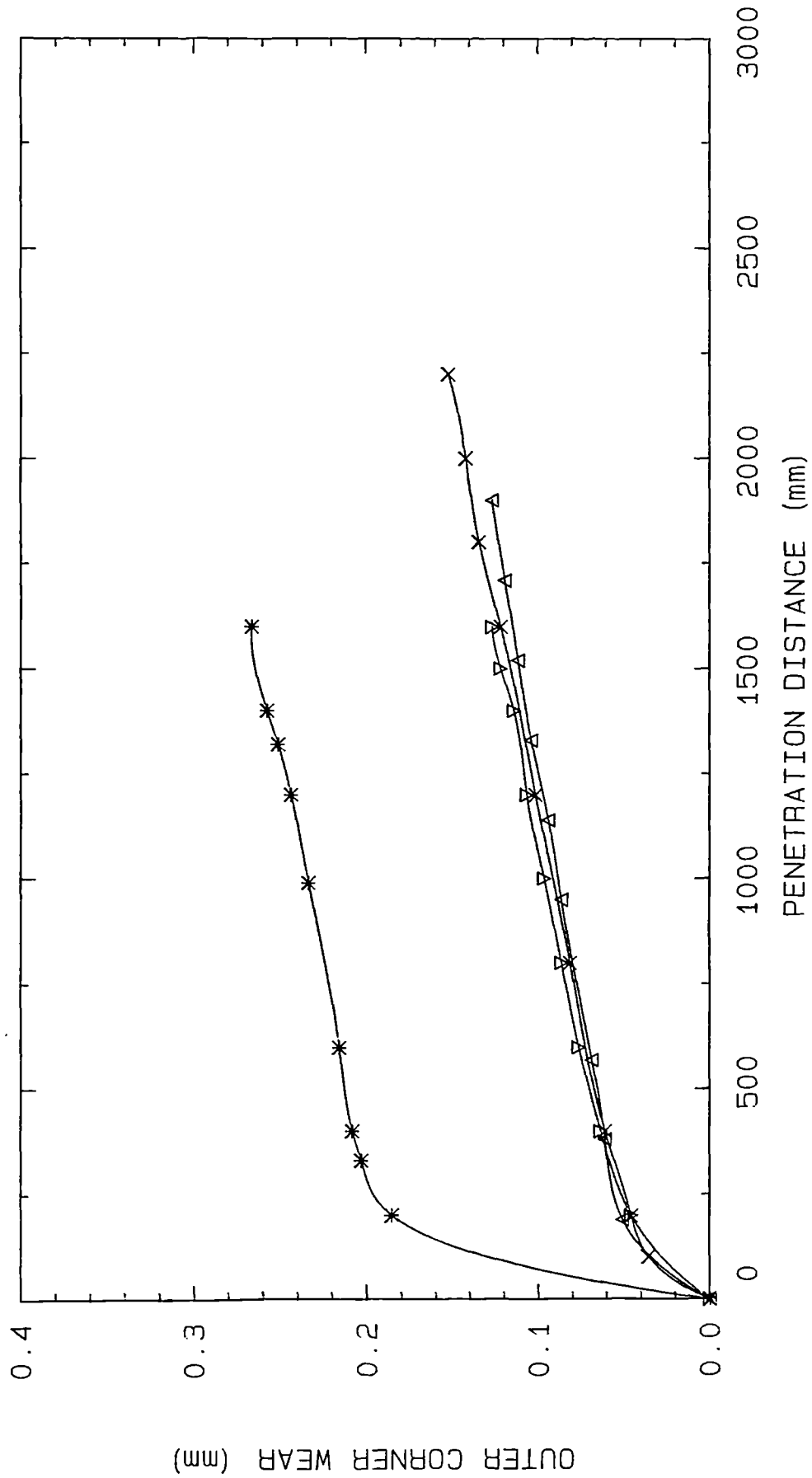
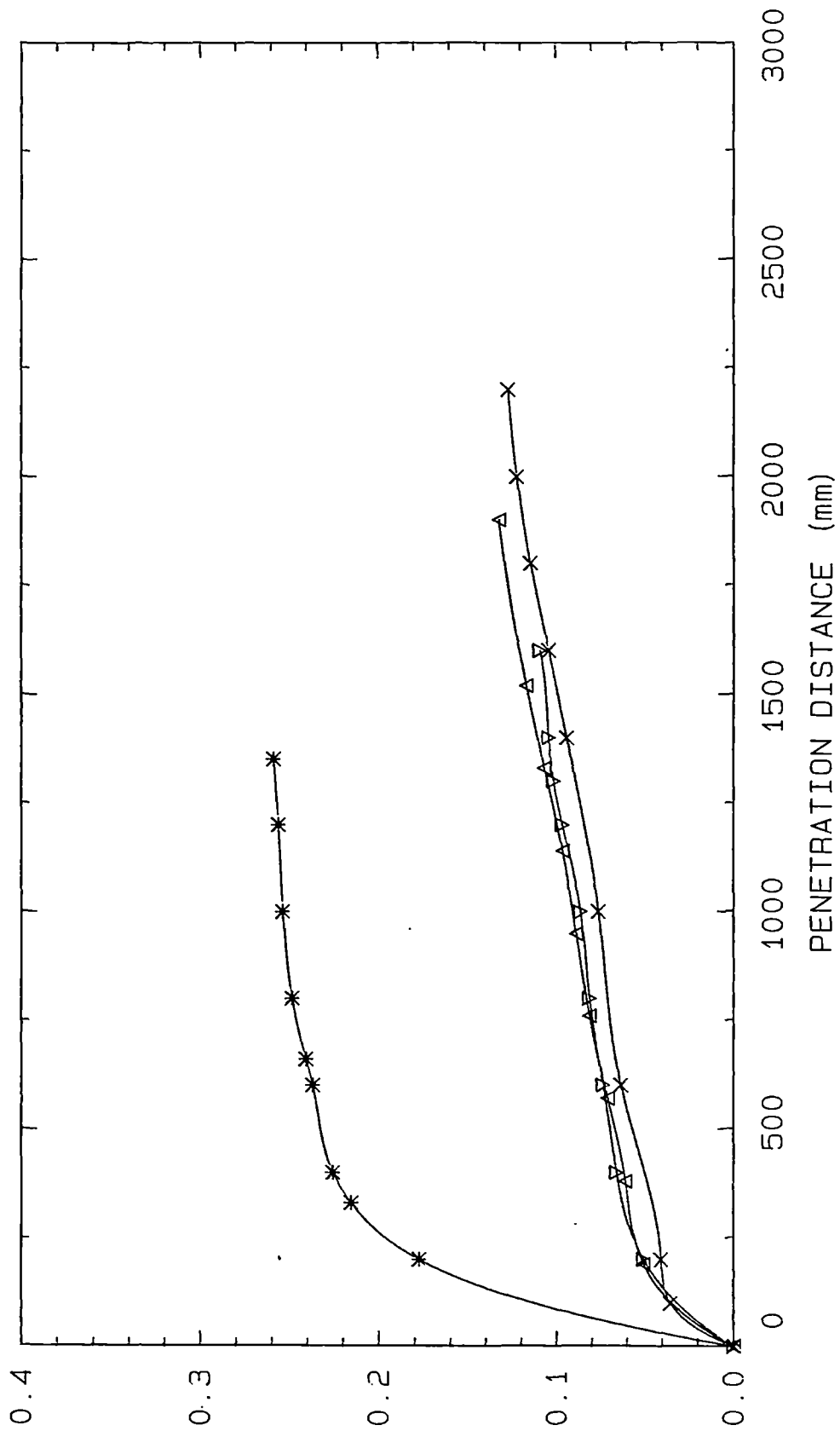


Fig. (16): The outer corner wear of the Carbide-1 drill in the first stage of the drill testing;

New Drill: x, Regrind 1: Δ, Regrind 2: \*, Regrind 3: ∇.



OUTER CORNER WEAR (mm)

Fig. (17): The outer corner wear of the Carbide-2 drill in the first stage of the drill testing;

New Drill: x, Regrind 1: Δ, Regrind 2: \*, Regrind 3: ∇.

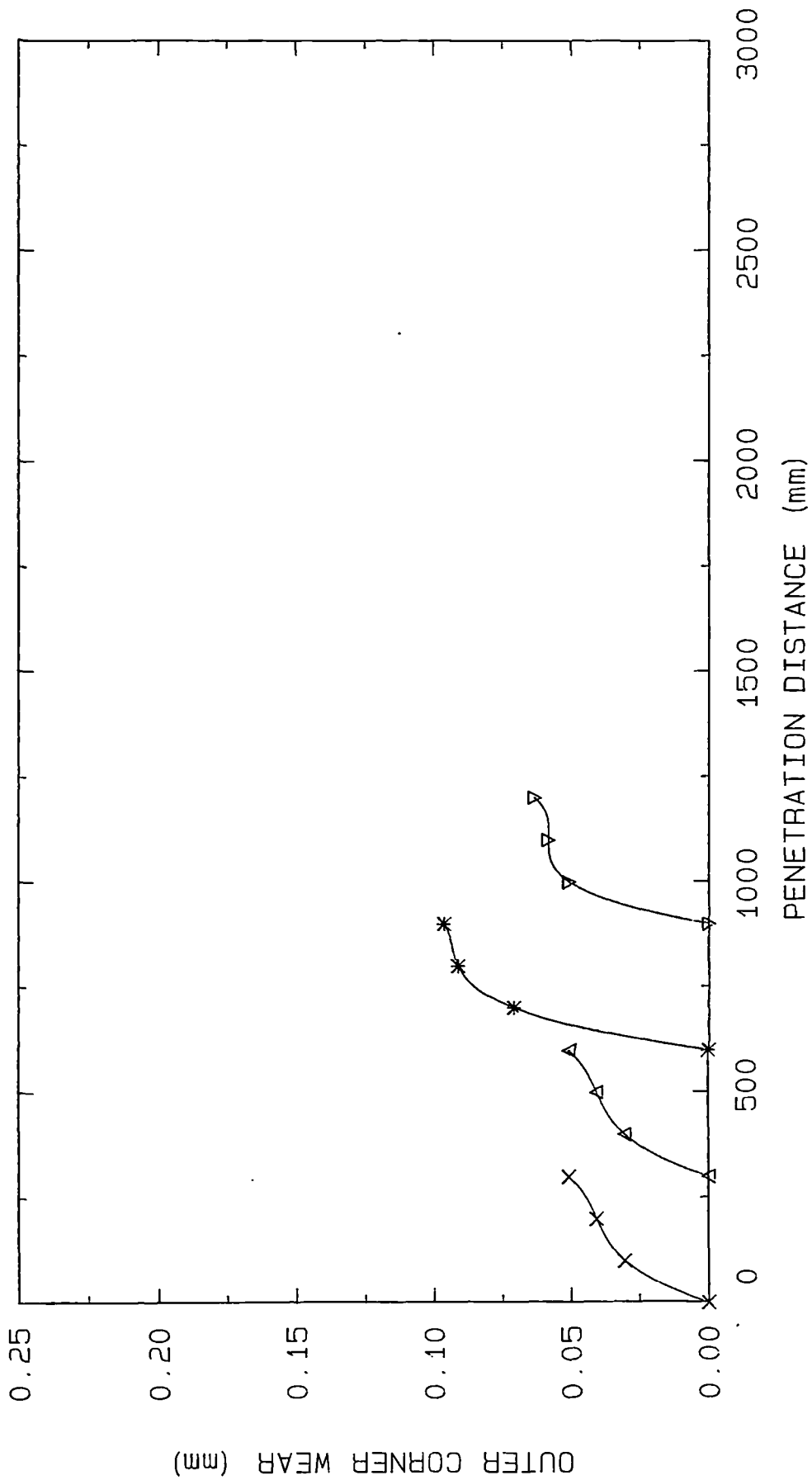


Fig. (18): The outer corner wear of the Carbide-3 drill in the first stage of the drill testing;

New Drill: x, Regrind 1: Δ, Regrind 2: \*, Regrind 3: ▽.

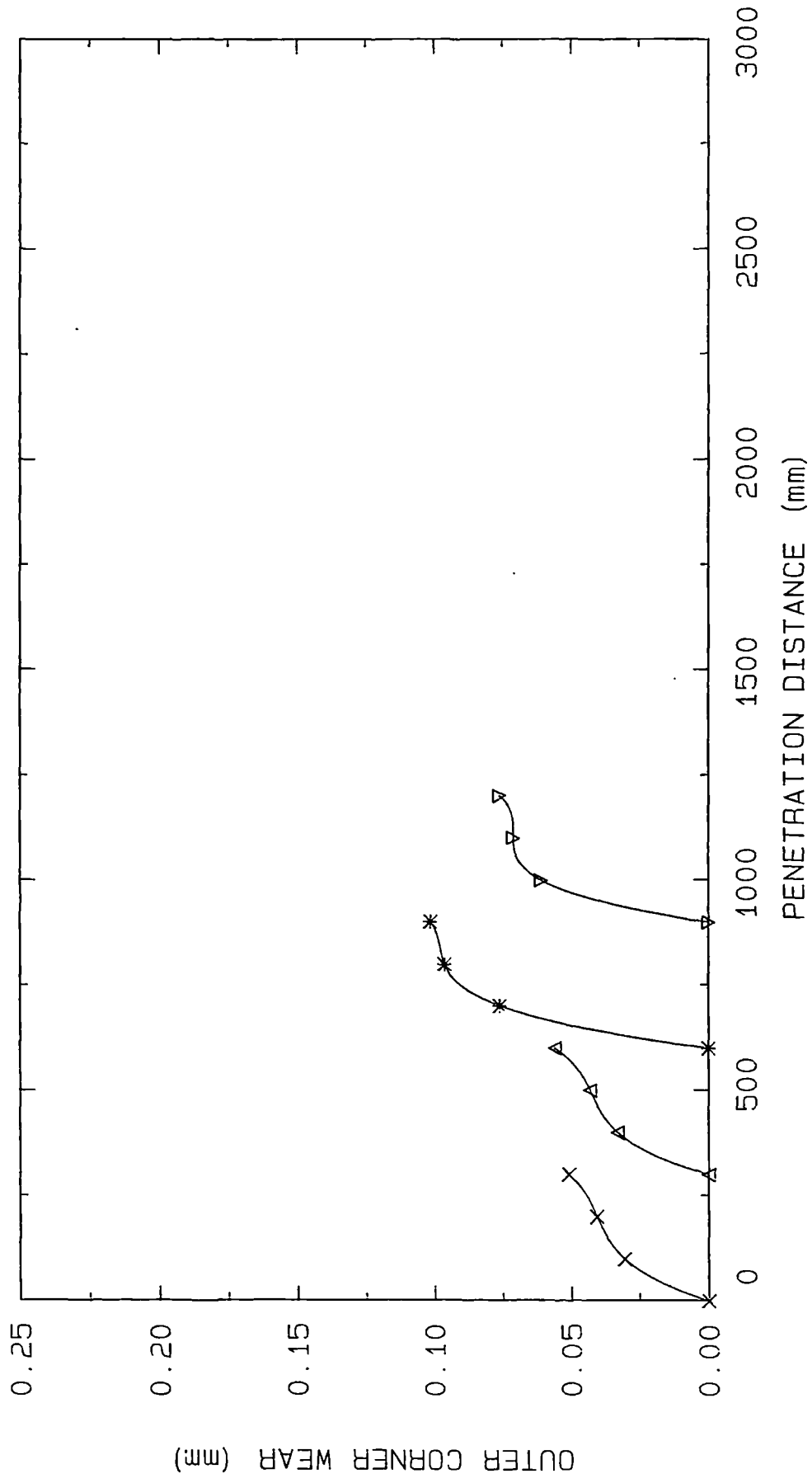


Fig. (19): The outer corner wear of the Carbide-4 drill in the first stage of the drill testing;  
 New Drill: x, Regrind 1: Δ, Regrind 2: \*, Regrind 3: ▽.

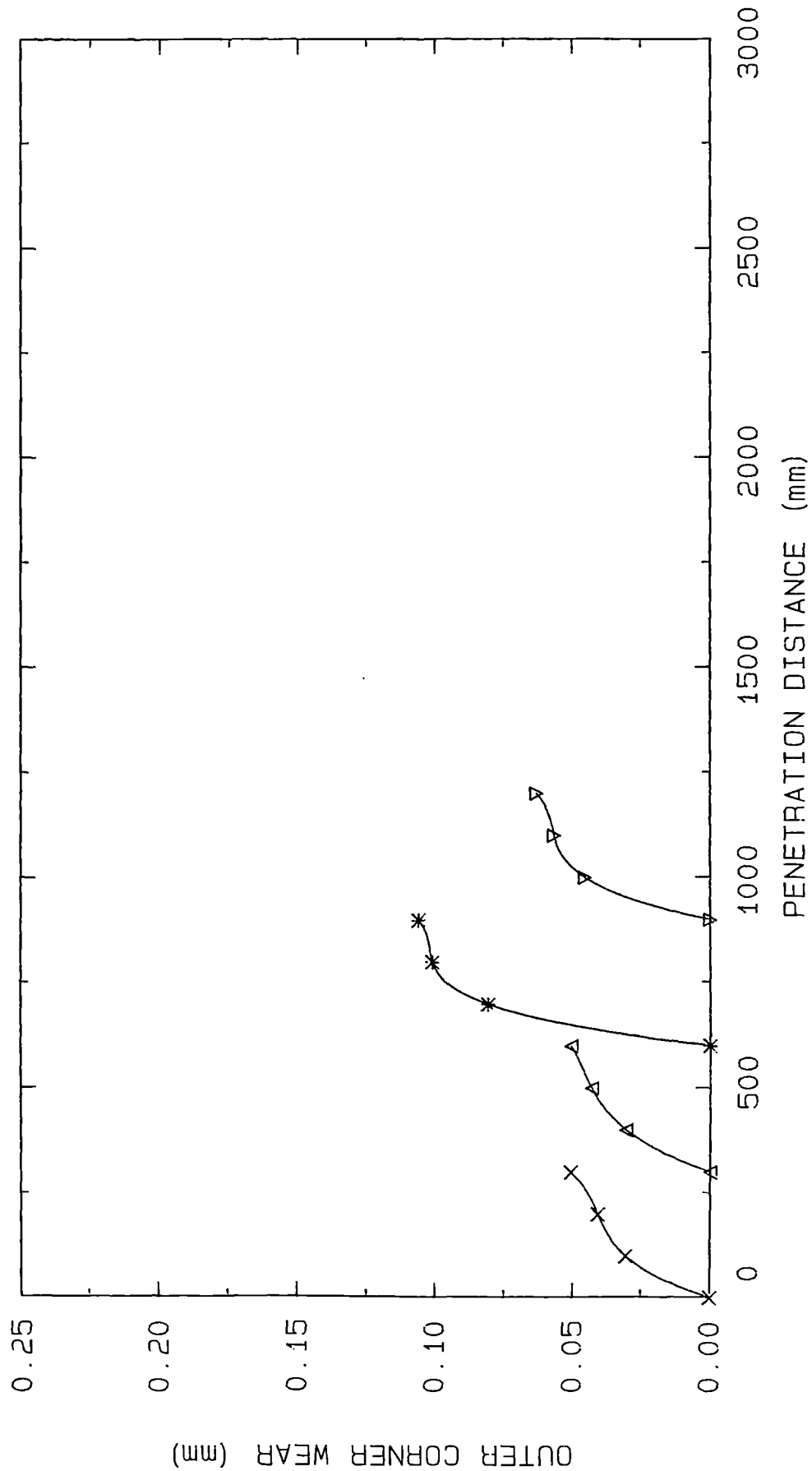


Fig. (20): The outer corner wear of the Carbide-5 drill in the first stage of the drill testing;  
 New Drill: x, Regrind 1: Δ, Regrind 2: \*, Regrind 3: ▽.